

DOCTORAL THESIS

Synthesis of Chiral Urea-based Macrocycles and their Application as Molecular Containers

Kamini Atindrakumar Mishra

TALLINN UNIVERSITY OF TECHNOLOGY
DOCTORAL THESIS
20/2022

**Synthesis of Chiral Urea-based
Macrocycles and their Application as
Molecular Containers**

KAMINI ATINDRAKUMAR MISHRA



TALLINN UNIVERSITY OF TECHNOLOGY
School of Science
Department of Chemistry and Biotechnology

This dissertation was accepted for the defence of the degree of Doctor of Philosophy in
Chemistry 04/05/2022

Supervisor: Prof. Riina Aav
School of Science
Tallinn University of Technology
Tallinn, Estonia

Opponents: Prof. Agnieszka Szumna
Institute of Organic Chemistry
Polish Academy of Sciences
Warsaw, Poland

Dr. Kerti Ausmees
Laboratory of Chemical Physics
National Institute of Chemical Physics and Biophysics
Tallinn, Estonia

Defence of the thesis: 07/06/2022, Tallinn

Declaration:

Hereby I declare that this doctoral thesis, my original investigation and achievement, submitted for the doctoral degree at Tallinn University of Technology has not been submitted for doctoral or equivalent academic degree.

Kamini A. Mishra

Signature



European Union
European Regional
Development Fund



Investing
in your future

Copyright: Kamini A. Mishra, 2022
ISSN 2585-6898 (publication)
ISBN 978-9949-83-831-8 (publication)
ISSN 2585-6901 (PDF)
ISBN 978-9949-83-832-5 (PDF)
Printed by Koopia Niini & Rauam

TALLINNA TEHNIKAÜLIKOOL
DOKTORITÖÖ
20/2022

Kiraalsete urea-põhiste molekulaarsete mahutite süntees ja rakendus

KAMINI ATINDRAKUMAR MISHRA



Contents

List of Publications	7
Author's Contribution to the Publications	7
Author's other Publications and Conference Presentations	8
Introduction	9
Abbreviations	11
1 Literature Overview	13
1.1 Supramolecular Chemistry and Macrocycles	13
1.2 Cucurbit[<i>n</i>]uril-type Hosts	15
1.2.1 Cucurbiturils: Synthesis and Mechanism	15
1.2.2 Synthetic Procedures for Functionalized Cucurbit[<i>n</i>]uril	17
1.2.3 Unsubstituted Hemicucurbit[<i>n</i>]urils and their Applications	18
1.3 Chirality Induction in CB-Type Hosts (Publication I)	20
1.3.1 Induction of Chirality in CB-Type Hosts from Achiral Building Blocks	22
1.3.2 Chirality Induction in CB-Type Hosts through Desymmetrization	24
1.3.3 Chirality Induction in CB-Type Hosts through Chiral Monomers	25
1.3.4 Chirality Induction in CBs through Complexation with Chiral Compounds	27
1.4 Cyclohexanohemicucurbit[<i>n</i>]urils	29
1.4.1 Synthesis and Mechanism	29
1.4.2 Complexation Studies of CycHC[<i>n</i>]	31
1.5 Solid-State Synthesis	33
1.5.1 Mechanochemistry	34
1.5.2 Synthesis of Macrocyclic Molecules by Mechanochemistry	35
1.5.3 Mechanochemical Approaches in Amidation Reactions	36
2 Motivation and Aim of the Present Work	38
3 Results and Discussions	39
3.1 (<i>R,R</i>)-Cyclohexanohemicucurbit[12]uril (Publication II)	39
3.1.1 Synthesis and Structural Characterization	39
3.2 CycHC[8] Inclusion Complexes with Heterocycles and its Application in SPE (Publication III)	44
3.2.1 ¹ H NMR and ITC Binding Studies in Solution	45
3.2.2 Selective Extraction of Sulfur Compounds from Water	47
3.3 Efficient Mechanochemical Synthesis of Amides (Publication IV)	49
3.3.1 Mechanochemical Formation of Challenging Amide Bonds	52
3.3.2 Functionalization of Biotin[6]uril	54
4 Conclusions	56
References	57
Acknowledgements	63
Abstract	64
Lühikokkuvõte	65
Appendix 1	67
Appendix 2	95

Appendix 3	101
Appendix 4	111
Curriculum vitae	126
Elulookirjeldus.....	127

List of Publications

The list of author's publications, on the basis of which the thesis has been prepared:

- I R. Aav, **K. A. Mishra**, 'The Breaking of Symmetry Leads to Chirality in Cucurbituril-Type Hosts'. *Symmetry*, **2018**, *10* (4), 98.
- II **K. A. Mishra**, J. Adamson, M. Öeren, S. Kaabel, M. Fomitšenko, R. Aav, 'Dynamic Chiral Cyclohexanohemicucurbit[12]uril'. *Chemical Communications*, **2020**, *56* (93), 14645–14648.
- III T. Shalima, **K. A. Mishra**, S. Kaabel, L. Ustrnul, S. Bartkova, K. Tõnsuaadu, I. Heinmaa, R. Aav, 'Cyclohexanohemicucurbit[8]uril Inclusion Complexes with Heterocycles and Selective Extraction of Sulfur Compounds from Water'. *Frontiers in Chemistry*, **2021**, *9*, 1036.
- IV T. Dalidovich, **K. A. Mishra**, T. Shalima, M. Kudrjašova, D. G. Kananovich, R. Aav, 'Mechanochemical Synthesis of Amides with Uronium-based Coupling Reagents: A Method for Hexa-amidation of Biotin[6]uril'. *ACS Sustainable Chemistry & Engineering*, **2020**, *8* (41), 15703–15715.

Author's Contribution to the Publications

Contributions to the publications in this thesis are:

- I The author analyzed all possible chiral guests used in binding studies with cucurbiturils as available from literature and participated in the preparation of the manuscript.
- II The author planned and conducted all synthetic experiments and prepared all samples for structure characterization and dynamic studies. The author participated in the final manuscript preparation and compiled the supporting information.
- III The author was involved in planning and executing the experiments. The author was responsible for a considerable portion of the solution-state binding as well as solid-state extraction studies. The author also participated in the final manuscript preparation and compiling of supporting information.
- IV The author was involved in planning and conducting synthetic experiments and contributed to the analytical parts. The author also participated in the manuscript preparation and compiling of supporting information.

Author's other Publications and Conference Presentations

Other publications

1. L. Ustrnul, T. Burankova, M. Öeren, K. Juhhimenko, J. Ilmarinen, K. Siilak, **K. A. Mishra**, R. Aav, 'Binding between Cyclohexanohemicucurbit[*n*]urils and Polar Organic Guests'. *Frontiers in Chemistry*, **2021**, *9*, 468.
2. M. Šakarašvili, L. Ustrnul, E. Suut, J. V. Nallaparaju, **K. A. Mishra**, N. Konrad, J. Adamson, V. Borovkov, R. Aav, 'Self-Assembly of Chiral Cyclohexanohemicucurbit[*n*]urils with Bis(Zn Porphyrin): Size, Shape, and Time-Dependent Binding'. *Molecules*, **2022**, *27* (3), 937.

Oral Presentations

1. 'Chiral Hemicucurbit[*n*]urils: their Synthesis, Post Functionalization and Application'. Scientific Conference of the Graduate School of Functional Materials and Technologies (GSFMT), Tartu, Estonia, 14.–15.06.2021.
2. 'Synthesis of Cyclohexanohemicucurbit[10-12]urils: Success and Difficulties in their Analysis'. Scientific Conference of the Graduate School of Functional Materials and Technologies (GSFMT), Tallinn, Estonia, 4.–5.02.2020.
3. 'Synthesis of Cyclohexanohemicucurbit[10-12]urils: Success and Difficulties in their Analysis'. SEMINAR Frontiers in Organic Synthesis, Tallinn, Estonia, 15.11.2019.
4. 'Synthesis of Cyclohexanohemicucurbit[10-12]urils: Success and Difficulties in their Analysis'. 4th From Molecular Modeling to Nano- and Biotechnology (MMNB 2018), Opole-Groszowice, Poland, 29.–31.08.2018.

Poster Presentations

1. '(*R,R*)-Cyclohexanohemicucurbit[12]uril'. 6th International Conference on Cucurbiturils (ICCB 2019), Athens, Ohio, USA, 21.–24.07.2019.
2. 'Toward the Synthesis of New Chiral Hemicucurbit[*n*]urils'. 14th International Symposium on Macrocyclic and Supramolecular Chemistry (ISMCS2019), Lecce, Italy, 2.–6.06.2019.
3. 'Synthesis of New Chiral Macrocyclic from (2*S*)-2,3-Diaminopropionic Acid'. Scientific Conference of the Graduate School of Functional Materials and Technologies (GSFMT), Tartu, Estonia, 4.–5.02.2019.
4. 'Synthesis of New Chiral Macrocyclic from (2*S*)-2,3-Diaminopropionic Acid'. 10th Balticum Organicum Syntheticum (BOS 2018), Tallinn, Estonia 1.–4.07.2018.
5. '(2*S*)-2,3-Diaminopropionic Acid-based Urea'. Scientific Conference of the Graduate School of Functional Materials and Technologies (GSFMT), Tallinn, Estonia, 7.–8.03.2018.
6. 'Large Chiral Cyclohexanohemicucurbit[*n*]urils'. 5th International Conference on Cucurbiturils (ICCB 2017), Brno, Czech Republic, 27.–30.06.2017.
7. 'Large Chiral Cyclohexanohemicucurbit[*n*]urils'. Scientific Conference of the Graduate School of Functional Materials and Technologies (GSFMT), Tartu, Estonia, 7.–8.03.2017.

Introduction

Supramolecular chemistry, defined as “chemistry beyond the bonds” by the Noble Laureate Prof. Jean-Marie Lehn,^[1] deals with the study of non-covalent interactions that influence molecular recognition between two or more molecular entities, called the host and the guest(s), and their self-assembly. These concepts have been especially influential in the design and construction of novel macrocyclic compounds for various applications.^[2]

The host molecule is very often a macrocycle, which is defined as a compound that connects at least 12 atoms in cycle. Macrocyclic compounds have found extensive applicability in medicinal chemistry due to their anti-cancer, anti-fungal, and immunosuppressive characteristics, and are now being intensively investigated for the development of novel therapeutic medications.^[3] Since they are capable of molecular recognition, macrocyclic compounds are of major importance in the field of supramolecular chemistry as host molecules, and they have also found applications in chemical sensors,^[4] chromatography,^[5,6] the capture of organic pollutants,^[7] and in the capture and storage of CO₂.^[8] Macrocycles are widely found in natural products.^[9]

The design and synthesis of new macrocyclic supramolecular hosts is challenging. Efforts directed to this area, however, represent a valuable investment of time, as optimal binding properties of a host molecule rely on a carefully designed guest binding site such as that offered by the cavity of a macrocycle. The formation of a macrocycle is challenging due to the final ring-closing step, also called macrocyclization. Lack of preorganization, several consecutive synthetic steps, high dilution conditions, and a high risk of forming a complex mixture of products result in a synthesis process that is generally tedious and low yielding. Notably, many of these challenges may be overcome by applying the technique of template-directed dynamic combinatorial chemistry (DCC),^[10] which yields a target macrocycle through oligomerization of simple building blocks. Furthermore, DCC can provide access to a wide range of supramolecular hosts through one-pot macrocyclization of modifiable building components, and the reaction-directing effect of templates.

One example of an oligomeric macrocycle is the pumpkin-shaped cucurbiturils^[11], known for their ability to form extremely strong complexes with alkylammonium guests (binding constants of up to $3 \times 10^{15} \text{ M}^{-1}$). Numerous cation-binding supramolecular hosts have been described, including crown ethers and cryptands, which initiated the field of supramolecular chemistry.^[1,12,13] The design of an anion-binding host, on the other hand, is very challenging, as strong binding of anions is more difficult, due to the competitive hydration of an anion, lower charge density compared to cations, and the presence of anions in a wide range of sizes and shapes. Hemicucurbiturils^[14,15] are novel anion-binding analogs of cucurbiturils. The hemicucurbituril family has shown potential for application in various fields including anion sensing,^[16,17] catalysis,^[18] chirality sensing,^[19–21] and selective transmembrane anion transport.^[22,23] Although the majority of known hemicucurbiturils are six-membered macrocycles with a cavity size appropriate for the inclusion of halide anions, novel larger homologs would enable varied guest selectivity and therefore new application possibilities.

The goal of the research presented in this thesis was to investigate novel methods for synthesizing new enantiopure hemicucurbiturils, as the number of available examples from the literature is very limited. The results presented in this thesis include an overview of various approaches for inducing chirality in cucurbituril-type hosts (**Publication I**), with

the aim of finding a solution for the synthesis and isolation of large-ring hemicucurbiturils. This overview is followed by a description of the synthesis, isolation, and conformational characterization of the largest substituted hemicucurbituril homolog known to date (**Publication II**), which had previously been detected only by mass-spectrometry analysis. Cyclohexanohemicucurbit[12]uril (cycHC[12]) consists of 12 monomers and resembles a concave octagon at 265 K as revealed by variable temperature (VT) ^1H -NMR and density functional theory (DFT) calculations and it has two temperature-dependent conformational flexibilities.

Although hemicucurbiturils have been reported to form inclusion complexes with anionic species, evidence that they do the same with electron-rich neutral molecules has not been reported. In this thesis, the binding capability of cyclohexanohemicucurbit[8]uril (cycHC[8]) to neutral heterocyclic guests was investigated, and the solid cycHC[8] was used as a reusable sorbent in the selective solid-phase extraction (SPE) of sulfur-containing heterocycles (**Publication III**).

Embedded functional groups in the core structure of macrocyclic compounds enable easy customization, which increases the application possibilities for this class of host molecules. **Publication IV** describes the development of a mechanochemical solid-state approach for the efficient formation of amide bonds from carboxylic acids and amines, which was used for the post-functionalization of a hemicucurbituril host – biotin[6]uril,^[24] and produced the derivatized product in a high yield and purity, respectively.

To summarize, the research described in this thesis analyzes the properties of chiral cucurbituril-type macrocycles and describes the synthesis, structural characteristics and temperature-based dynamics of the enantiopure cycHC[12] obtained. Additionally, the selective complex-formation capability of chiral enantiopure cycHC[8] with sulfur-containing neutral heterocycles in a polar solvent is described. Last but not least, the development of an energy-efficient and eco-friendly mechanochemical protocol for the synthesis of new hemicucurbiturils *via* post-functionalization is presented. The results of this thesis have been published in four peer-reviewed journals and were also presented at international conferences in Estonia, Czech Republic, Poland, Italy, and the United States.

Abbreviations

aq.	aqueous
bis- <i>ns</i> -CB	bis- <i>nor-seco</i> -cucurbituril
Boc	<i>tert</i> -butyloxycarbonyl
BU[<i>n</i>]	bambus[<i>n</i>]uril
CD	cyclodextrin (only in Figure 20, CD refers to circular dichroism)
CA[<i>n</i>]	calix[<i>n</i>]arene
CB[<i>n</i>]	cucurbit[<i>n</i>]uril
Cbz	benzyloxycarbonyl
CDI	<i>N,N'</i> -carbonyldiimidazole
cycHC[<i>n</i>]	cyclohexanohemicucurbit[<i>n</i>]uril
COMU	(1-cyano-2-ethoxy-2-oxoethylideneaminoxy)dimethylamino-morpholinocarbeniumhexafluorophosphate
DCC	dynamic covalent chemistry
DCL	dynamic combinatorial library
DFT	density functional theory
DIPEA	<i>N,N</i> ,-diisopropylethylamine
DMAP	4-dimethylaminopyridine
DMF	<i>N,N</i> -dimethylformamide
EDC	1-ethyl-3-(3-dimethylaminopropyl) carbodiimide
<i>ee</i>	enantiomeric excess
EIC	extracted ion current
eq.	equivalent
ESI-MS	electrospray ionization mass spectrometry
Fmoc	fluorenylmethyloxycarbonyl
HATU	1-[bis(dimethylamino)methylene]-1 <i>H</i> -1,2,3-triazolo[4,5- <i>b</i>]pyridinium-3-oxide hexafluorophosphate
HC[<i>n</i>]	hemicucurbit[<i>n</i>]uril
HOMO	highest occupied molecular orbital
HPLC	high-performance liquid chromatography
HRMS	high-resolution mass spectrometry
IBX	2-iodoxybenzoic acid
<i>i</i> -CB	<i>inverted</i> -cucurbituril
ICD	induced circular dichroism
<i>i-cis</i> -cycHC[6]	<i>inverted-cis</i> -cyclohexanohemicucurbit[6]uril
ITC	isothermal titration calorimetry
LAG	liquid-assisted grinding
LAP	leucine aminopeptidase
LUMO	lowest unoccupied molecular orbital
MDPP	dimethyldiazaperopyrenium
MESP	map of electrostatic potential
MPA	α -methoxyphenylacetic acid

MTPA	α -methoxy- α -trifluoromethylphenylacetic acid
n.d.	not determined
NMI	<i>N</i> -methylimidazole
NMR	nuclear magnetic resonance
<i>ns</i> -CB	<i>nor-seco</i> -cucurbituril
PG	protecting group
PA[<i>n</i>]	pillar[<i>n</i>]arene
RP	reverse phase
RT	room temperature
SILP	supported ionic liquid phase
SPE	solid-phase extraction
TCFH	<i>N,N,N',N'</i> -tetramethylchloroformamidinium hexafluorophosphate
TCT	2,4,6-trichloro-1,3,5-triazine
TGA	thermogravimetric analysis
<i>t</i> -CB	<i>twisted</i> -cucurbituril
PTSA	<i>p</i> -toluenesulfonic acid
UV	ultraviolet
VT-NMR	variable-temperature nuclear magnetic resonance
SC-XRD	single-crystal X-ray diffraction
%R	removal percentage
η (eta)	liquid-to-solid ratio ($\mu\text{l mg}^{-1}$) in a lag experiment

1 Literature Overview

1.1 Supramolecular Chemistry and Macrocycles

Supramolecular chemistry,^[1] since it was first proposed, has demonstrated its capability in the achievement of molecular recognition and self-assembly through weak and reversible non-covalent interactions. One branch of supramolecular chemistry deals with host-guest chemistry. The host-guest system is comprised of two fundamental units: 1) a macrocyclic host which acts as a larger molecule and 2) a suitable small guest. The host and guest interact through non-covalent reversible intermolecular forces, such as electrostatic interactions, hydrogen and halogen bonds, π - π interactions, van der Waals forces, and solvation effects. These interactions can vary in strength from 2 kJ mol⁻¹ for weak van der Waals forces to 300 kJ mol⁻¹ for strong ion-ion dipole electrostatic interactions.^[25] The implicated interacting region of the host and guest in these non-covalent interactions is referred to as the binding site. Crown ether, also referred to as the first-generation macrocyclic host molecule, was synthesized and characterized by Prof. C. J. Pedersen in 1967, and is considered the origin of the development of supramolecular chemistry. In 1987, Prof. D. J. Cram, J. M. Lehn, and C. J. Pedersen were jointly awarded the Nobel Prize in Chemistry for developing organic molecules with selective complexing capabilities that mimicked the selective complexation found in biological processes.^[1,12,13]

Following the initial success of cation-binding crown ether hosts, a broad range of organic macrocycles, such as cyclodextrins (CDs), calix[*n*]arenes (CAs), pillar[*n*]arenes (PAs), and cucurbit[*n*]urils (CBs), have been developed for binding a variety of guest molecules (Figure 1). These macrocycles display a combination of molecular recognition and complex-forming properties and have had a significant impact on supramolecular chemistry.^[26]

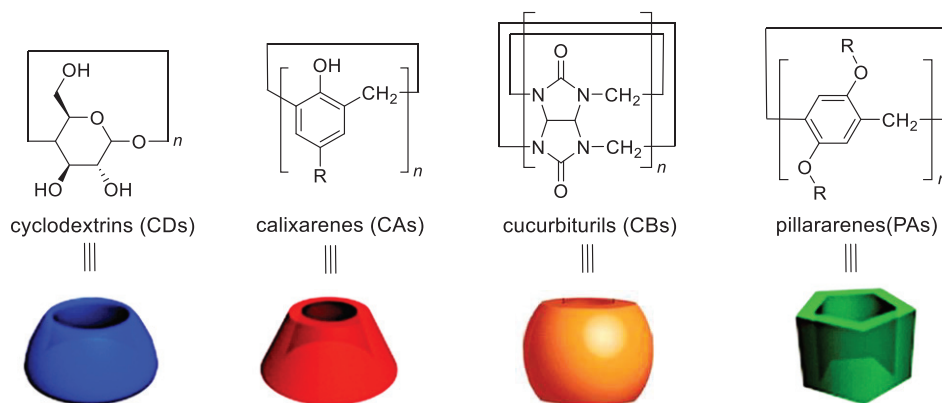


Figure 1. Structures of representative cation-binding macrocyclic hosts and cartoon depictions showing their cavity shapes.

In macrocycles, the interacting functional groups are preorganized into a convergent binding site which favors high host-guest binding affinity and the shape-selective association of guest molecules or ions.^[27] As a result, a number of supramolecular chemists have focused their efforts in developing new macrocyclic host molecules. Furthermore, dynamic molecules capable of adopting different shapes as a response to

external stimuli have fueled the development of molecular machines in supramolecular chemistry.^[28] The latter have also been recognized by the Nobel Prize Committee, when Jean-Pierre Sauvage, Sir J. Fraser Stoddart, and Bernard L. Feringa were awarded the Nobel Prize in Chemistry in 2016 for their design and synthesis of molecular machines.^[29] These investigators have developed molecules with controllable movements that can perform a task when energy is added.

Macrocycles are one of the pillars of this rapidly advancing field, as their structures contain confined spaces within their cavities, thereby offering controllable and directed patterns of interaction. For this reason, macrocycles with large cavities have attracted researcher's interest, as these structures can undergo significant and continuous conformational changes while retaining molecular integrity.^[30] Several macrocycles with significantly different conformations than their smaller counterparts have already been identified. The oligomeric macrocycles with small cavities usually have 4-6 monomers. For example, CDs containing more than 9 glucose units are referred to as large-ring CDs (LR-CDs)^[31] and depending on the number of glucose units in the ring, LR-CDs can adopt different conformations. They can assume either a helical folding arrangement *e.g.*, the 26-membered CD^[32] (Figure 2A) or adopt a conformation that resembles a concave polygon.^[31,33] Due to their high solubility and flexible conformation, several potential applications have been proposed for LR-CDs, including in the food industry and in drug formulations.^[34] Large pillar[*n*]arenes, where *n* = 8–10, also adopt concave polygon shapes, resulting in two cavities that can accommodate up to two guests (Figure 2B).^[35] Although calix[*n*]arenes with up to 90 phenolic subunits have been reported, *p*-tert-butylcalix[16]arene is the largest calix[*n*]arene of which the structure is known to date.^[36] It has the appearance of two Celtic torcs superimposed on top of each other. Cucurbit[*n*]urils exhibit remarkably high binding affinities as molecular hosts for large and diverse guests and have potential applications in various fields.^[37,38] CBs with up to 10 monomers display a tubular shape, whereas homologs with 13 or more monomers are locked in a twisted conformation (Figure 2C).^[39,40] There are also hemicucurbit[*n*]urils (HC[*n*]), a branch in the CB family, among which conformationally flexible HC[12] was the only known 12-membered macrocycle^[14] at the start of my PhD studies in 2016.

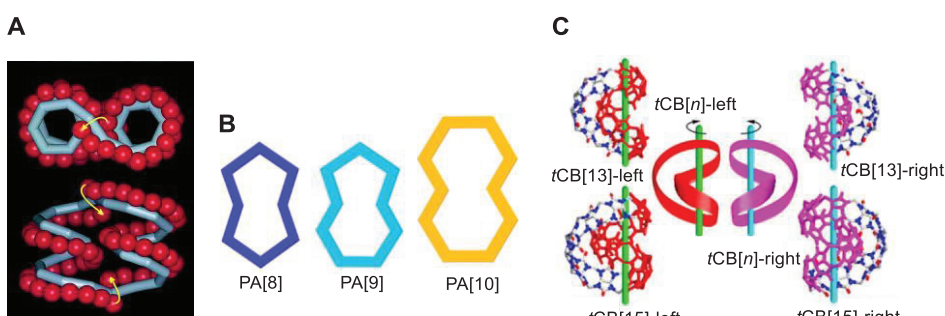


Figure 2. (A) Top and side views of a cyclodextrin (CD), composed of 26 monomers, and a schematic representation of the folding of the macrocycle into two left-handed single helices connected in the form of a “figure-eight.” Reprinted from ref.,^[32] Copyright (1999) National Academy of Sciences, U.S.A. (B) Cartoon representations of the structures corresponding to typical concave polygon-shaped pillar[*n*]arenes (*n* = 8–10). (C) Structures of *t*-CB[13 and 15], with a schematic representation of the axial chirality. Figure C is reprinted, from ref.^[39] with permission from the American Chemical Society.

The synthesis of new large macrocycles could have many advantages. For example, the larger cavity of these new macrocycles can accommodate larger organic guests such as larger hydrophobic drugs that could subsequently enhance their solubility in water. In addition, the synthesis of large chiral macrocycles could be useful in enhancing molecular recognition through selective host-guest interactions.

1.2 Cucurbit[n]uril-type Hosts

Cucurbituril (CB)-type hosts are macrocyclic compounds synthesized from glycoluril and formaldehyde under acidic conditions, in which the glycoluril moieties are connected through methylene bridges.^[41–43] The family of CB-type hosts can be broadly divided into two main branches: the double-bridged CBs, which mostly bind cations *via* interactions at their portals; and the single-bridged hemicucurbiturils (HCs), which bind anions in their cavity.^[41,44]

1.2.1 Cucurbiturils: Synthesis and Mechanism

In 1905, Behrend *et al.* reported the synthesis of the first cucurbit[n]uril from the condensation reaction of glycoluril and formaldehyde under acidic conditions.^[45] At that time, the chemical structure of the condensation product was unknown. Mock *et al.* revisited the synthesis of CBs in 1981 and were able to reveal the structure of this pumpkin-shaped cyclic molecule, as well as the reaction conditions that enabled the isolation of CB[6] in 70% yield (Figure 3).^[41]

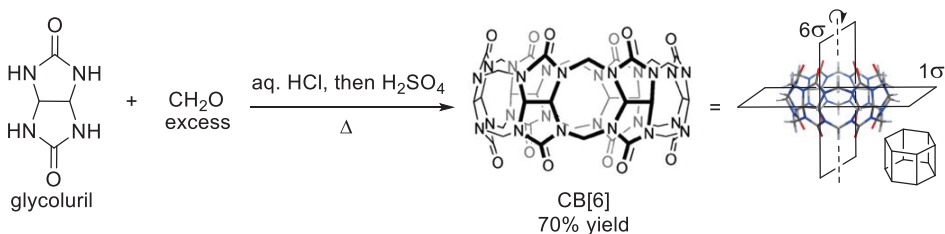


Figure 3. Synthesis of CB[6] by condensation of glycoluril and formaldehyde under acidic conditions and the structure of CB[6] with its 7 planes of symmetry is adapted, with permission, from Publication 1.

The molecular structure of CB[6] revealed the presence of seven planes of symmetry, including three vertical planes of symmetry passing through the urea oxygen, three vertical planes through the methylene bridges, and one horizontal plane which passes through the equator of the macrocycle (Figure 3). Although the synthesized structure was thoroughly described back in 1981, a complete understanding of the mechanism of CB[n] formation was not available, and the synthesis was considered to be an “enigmatic spontaneous synthesis”.^[41]

The mechanism of CB[n] formation, a step-growth cyclo-oligomerization, was elaborated by studies carried out in the research groups of Day^[43,46] and Isaacs.^[47,48] The first step in CB[n] synthesis is the acid-catalyzed condensation between two equivalents of formaldehyde and glycoluril, which results in the formation of diastereomeric *C*- and *S*-shaped dimers (Figure 4).^[49,50] Isaacs *et al.* studied the earliest stages of the mechanism of CB[n] formation, which includes interconversion of *C*-shaped and *S*-shaped methylene-bridged glycoluril dimers. Access to synthetic intermediates demonstrated that both *C*-shaped and *S*-shaped glycoluril dimers are the building blocks

for CB[n] derivatives.^[50,51] The C-shaped dimer is thermodynamically more stable than the S-shaped dimer by more than 2.25 kcal mol⁻¹, and the dimers are in constant equilibration.^[52] The C-shaped glycoluril oligomers are required for macrocyclization, since the S-shaped units are included in linear oligomeric ribbons. These conditions result in the formation of a mixture of oligomers varying in shape and size and exist in thermodynamic equilibrium. All the constituents of this reaction mixture are termed as members of the dynamic covalent library (DCL), and they continuously interconvert during the equilibrium process.

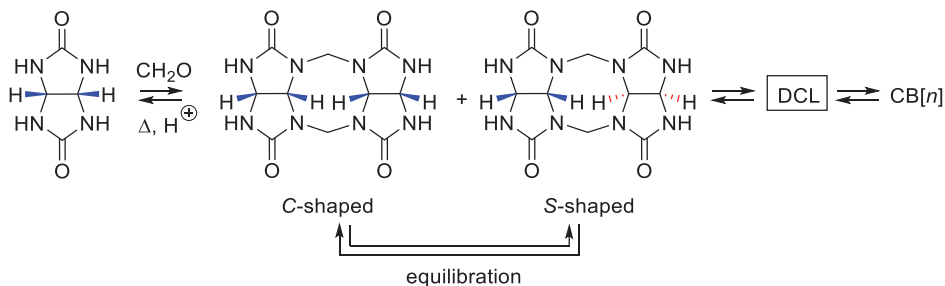


Figure 4. Reversible formation of CB[n] via C- and S-shaped dimers and longer oligomers included in the dynamic covalent library (DCL).

Day and co-workers described the initial polymer-forming steps, as well as the final cyclization stages of CB[n] formation and screened parameters (acid type and concentration, temperature, reactants concentration, and salt additive), that could influence the reaction outcome and determine the relative ratio of CBs formed.^[43] They found that a stronger acid in sufficient concentration and higher temperature speeds up the reaction rate but did not show any influence on product distribution. The concentration of the starting reactant played a crucial role in product distribution. A lower glycoluril concentration induced cyclization, resulting in small cycles, whereas a higher glycoluril concentration favored the formation of larger rings. Salt additives were explored as templates. In general, the role of the template in chemical reactions is to organize an assembly of molecules, smaller subunits, or atoms in an ordered manner that favors the formation of a specific product from a mixture with multiple possibilities. In some cases, the template also stabilizes one product through complexation. Templates often contribute to the selectivity of macrocyclization reactions; therefore, it was assumed that cations of alkali metals might influence the product distribution. In the case of CBs, the role of alkali metals as templates in the polymerization of glycoluril units into a single product other than CB[6] has not been fully clarified.^[43]

Day^[43] and Isaacs^[48] both showed that smaller CB[5]–CB[7] macrocycles are thermodynamically more stable, whereas CB[8] could be converted into smaller analogs when boiled in concentrated HCl to give a mixture of CB[5–8]. Isaacs *et al.* found that condensation of glycoluril with less than 2 equivalents of formaldehyde leads to a series of C-shaped glycoluril oligomers (from dimers to hexamers) and *nor-sec*-CB[n] (achiral *ns*-CB[6] and bis-*ns*-CB[10], as well as racemic (±)-bis-*ns*-CB[6]).^[53] *Nor-seco* (*ns*) cucurbiturils differ from their parent CBs by one or two missing methylene bridges. Product resubmission experiments using these isolated intermediates further confirmed the step-growth mechanism. Isaacs and Kim reported the isolation of diastereomeric CB[n], also known as *inverted*-CB[n] (*i*-CB[n]), in which one monomer is in the inverted configuration and a single pair of methine C-H groups points into the central cavity.

It was found that the *i*-CB[6] and *i*-CB[7] isolated were kinetic intermediates and could be converted to thermodynamically more favorable CBs by heating in HCl. Thus, confirming the reversibility of the reaction steps in the proposed mechanism.^[47,54]

The impact of CBs on the development of supramolecular chemistry has grown due to the discovery of different-sized cyclic homologs (CB[5]-CB[8] and CB[10]), several substituted derivatives, acyclic CB analogs, and single-bridged anion-binding analogs, as shown in Figure 5.

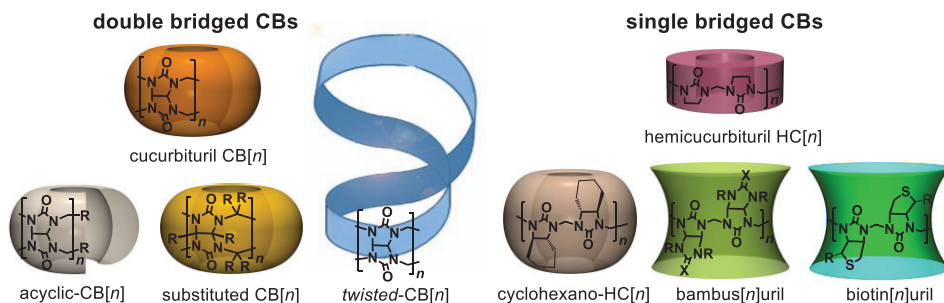


Figure 5. Cucurbit[*n*]uril-type hosts. Reprinted, with permission, from **Publication I**.

1.2.2 Synthetic Procedures for Functionalized Cucurbit[*n*]uril

The development of synthetic routes for synthesizing modified CB[*n*]s has undoubtedly played a significant role in broadening their application in several areas.^[55] In principle, there are three strategies for synthesizing functionalized CBs. The first approach is to start with a substituted glycoluril monomer and react it with formaldehyde. In 1992, the Nobel laureate Prof. F. Stoddart and co-workers reported the first modified CB[*n*]. His group synthesized the fully equatorially methylated CB[5] (Me₁₀CB[5]) from dimethyl glycoluril (Figure 6A).^[56] The first approach can also be employed by taking a mixture of monomers or oligomers with different substituents in the polymerization reaction. However, this approach can generate a very complicated mixture of isomeric products due to the similarities in their thermodynamic stability. In 2002, Nakamura reported the synthesis of diphenylCB[6], the first CB[*n*] derivative formed from a mixture of glycoluril monomers, by combining five equivalents of unsubstituted glycoluril and one equivalent of diphenyl glycoluril (Figure 6B).^[57] The second method involved reacting glycoluril or oligomers with modified aldehydes, which would introduce the corresponding substituents at the methylene bridge of CB[*n*]. The Šindelář research group reported the synthesis of the first monofunctionalized CB[6] at the methylene bridge position by reacting glycoluril, formaldehyde, and substituted aldehyde (3-phenylpropionaldehyde) in an equimolar ratio (Figure 6C).^[58] The third method involved inserting reactive functional groups directly into already synthesized macrocycles in a post-functionalization step. Kim,^[59] as well as Ouari and Bardelang,^[60] reported the direct oxidative conditions for the functionalization of CB[*n*]s (Figure 6D). Although this approach of producing functionalized CB[*n*] has only been accomplished through hydroxylation of CB[*n*], the resulting product has found numerous applications, including the construction of various supramolecular systems, such as artificial ion channels, polymers, vesicles, and many others.^[61]

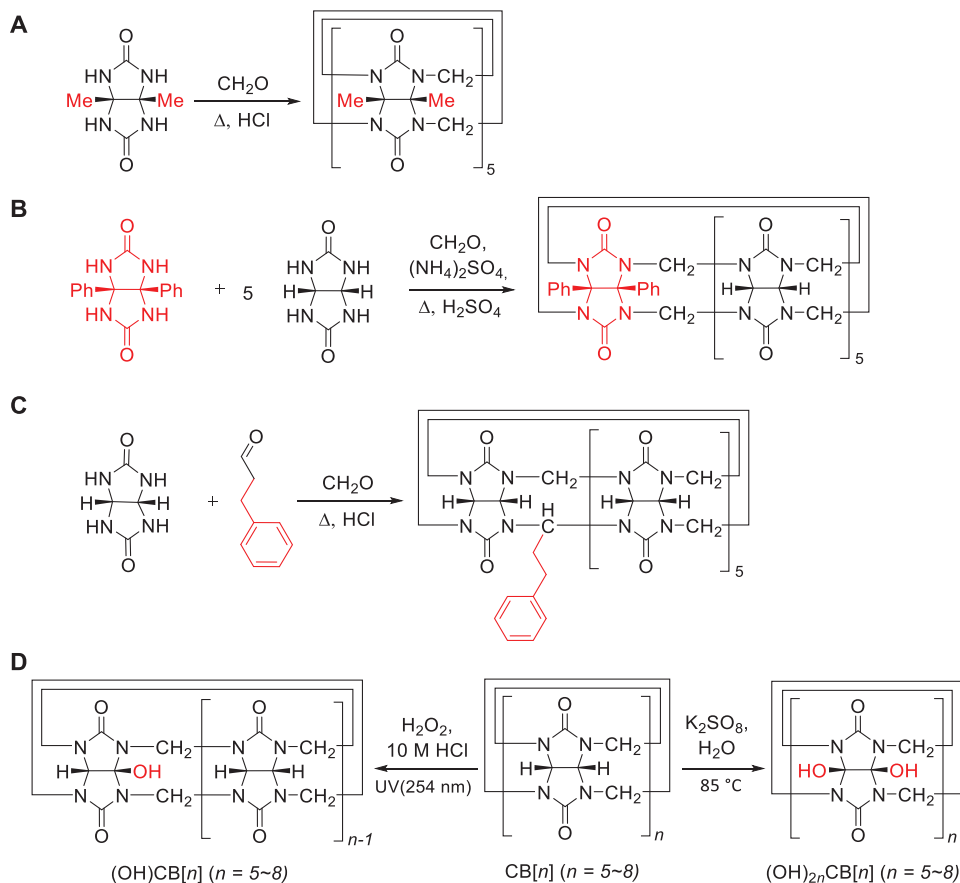


Figure 6. Representative synthetic approaches toward cucurbit[n]uril derivatives: (A) from substituted monomer,^[56] (B) from a mixture of monomers,^[57] (C) from substituted aldehyde,^[58] and (D) post-functionalization of CBs.^[59,60]

1.2.3 Unsubstituted Hemicucurbit[n]urils and their Applications

In 2004, Miyahara^[44] and co-workers reported the synthesis of the first hemicucurbituril (HC) members of the cucurbituril family. By reacting an equimolar amount of ethylene urea and 37% formalin in 4 M HCl for 30 minutes at room temperature, Miyahara synthesized the first structurally simple members of HCs. HC[6], a six-membered cyclic compound, was precipitated as an HCl adduct with a 94% yield from the reaction mixture (Figure 7). They also reported that heating the same starting reaction mixture at 55 °C for 3 hours and changing the concentration to 1 M HCl would yield 93% of HC[12].

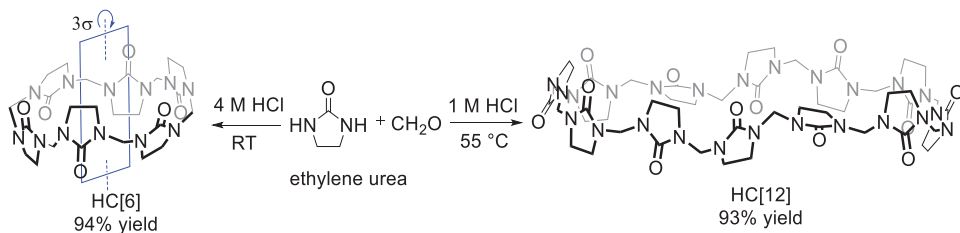


Figure 7. Synthesis of HCs using ethylene urea.^[44]

These new macrocycles were viewed as CBs when cut in half along their equator and hence were named hemicucurbiturils.^[14] Unlike CBs, in which the glycoluril is connected through two methylene bridges, the ethylene urea-based monomeric unit in HCs is connected by single methylene bridges, enabling the monomer to rotate freely and acquire alternate conformations arranged in a “zig-zag” pattern. As a result, they have fewer planes of symmetry in their structure than their parent CBs. (Figure 7). Furthermore, the hydrogen atoms are pointing inside the HC macrocycle creating a hydrophobic cavity (Figure 8). This situation, along with alternate conformations of monomers, results in HCs having very different binding properties compared to CBs. While CBs prefer to bind cations, HCs form host-guest complexes with anions.

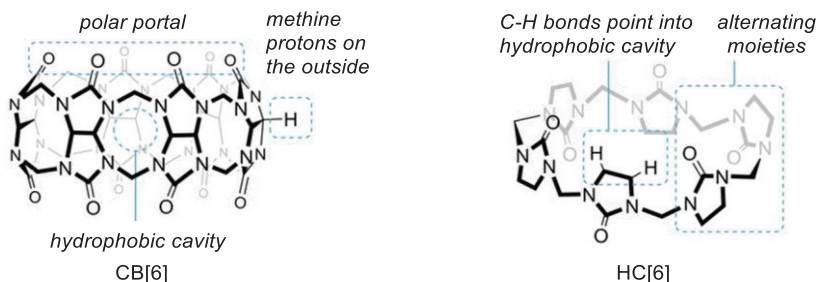


Figure 8. Structures of CB[6] and HC[6] highlighting characteristic structural features. Reprinted, with permission, from ref.^[14].

During complex-formation with HCs, several C-H...anion interactions are possible. For example, chaotropic anions^[14,62] are preferably bound to HCs, as these anions prefer to bind to hydrophobic surfaces and do not provide strong hydrogen bonding with protonic solvents. HC[6] can interact with anions like SCN⁻, and I⁻.^[63] In addition to anion-binding capability, HCs have electron-rich carbonyl groups that interact with transition metal cations.^[64] HC[6] forms a 1:1 complex with phenazine HCl salt, whereas HC[12] is capable of forming a 1:2 complex with the two molecules of the same salt.^[65] This is likely because of the more flexible structure of HC[12], as well as its larger cavity compared to HC[6]. Whereas HC[6] has good solubility in organic solvents like chloroform and methanol, it is scarcely soluble in water. It was found that the solubility of HC[6] in aqueous media can be enhanced from 0.03 mg/L to 250 mg/L upon binding to thiocyanate.^[63]

HC[6] was found to act as a supramolecular catalyst in various organic reactions (Figure 9); for example, CB[6] catalyzes the esterification of conjugated carboxylic acids (Figure 9A),^[18] as well as the aerobic oxidation of furan, 2-methyl furan and thiophene in water (Figure 9B).^[66] Although HC[12] did not show similar catalytic activity as that of HC[6], both compounds have been utilized to recognize amine- and Schiff-base substituted phenols.^[67,68] Tao's group reported that HC[6] shows chemoselectivity toward the oxidation of hydroxybenzyl alcohols to aldehydes by 2-iodoxybenzoic acid (IBX) without over-oxidation (Figure 9C).^[69] Both HC[6] and HC[12] have been used in the liquid-liquid extraction of amino-esters of serine, cysteine, phenylalanine, leucine, and valine from an aqueous phase into chloroform.^[70] Kurane *et al.* reported the synthesis of a HC[6] supported ionic liquids phase (HC[6]SILP) palladium catalyst that can catalyze cross-coupling of various aryl halides with different sodium alkoxides (Figure 9D).^[71]

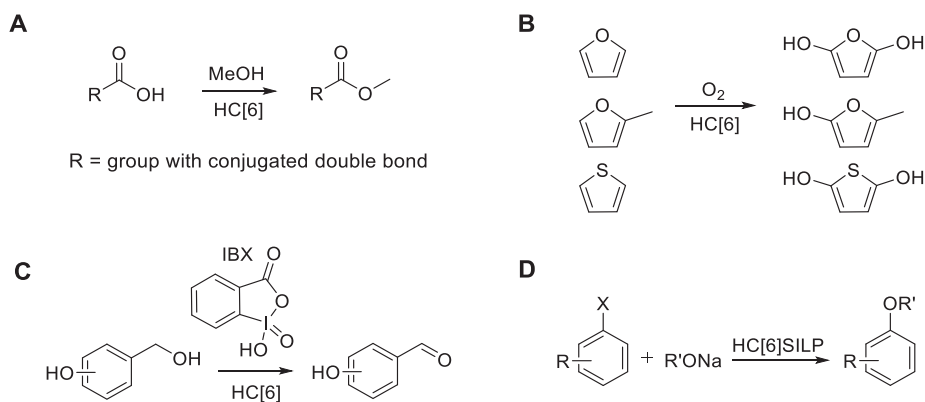


Figure 9. Reactions catalyzed by HC[6]: (A) esterification of conjugated carboxylic acids,^[18] (B) aerobic oxidation of different heterocycles,^[66] (C) chemo-selective oxidation of benzyl alcohols to aldehydes,^[69] and (D) cross-coupling of aryl halides with alcoholates.^[71]

The synthesis and outstanding applications of HC[6] and HC[12] laid the groundwork for developing novel HC members, and several substituted HCs have been developed since then.^[14,15,72]

Though the synthesized achiral HCs showed several applications, they lacked chiral properties. Nevertheless, chiral members of cucurbituril-type hosts exist and will be discussed in the next section.

1.3 Chirality Induction in CB-Type Hosts (Publication I)

Chirality is the geometrical property of three-dimensional objects that are non-superposable on their mirror image. Such objects that do not have any reflective symmetry elements (rotation-reflection axis S_n , a mirror plane σ , center of inversion i) are called chiral or dissymmetric molecules. Chirality is a unique feature in nature, and the number of naturally occurring chiral molecules is large and possesses vast structural diversity. For example, majority of naturally occurring biological molecules (e.g., sugars, amino acids, RNA, DNA and proteins) are chiral and comprised of a single enantiomer. Chiral cyclic molecules (macrocycles) are important compounds that can provide a broad range of functionality and stereochemical interactions in a conformationally restricted manner. Many examples of naturally occurring macrocycles, as well as their synthetic derivatives, have been successfully used by the pharmaceutical industry.^[73] For example, Erythromycin A is used as an antibiotic, Epothilone B is an anti-cancer agent, and Cyclosporin A is a drug with immunosuppressive properties (Figure 10).

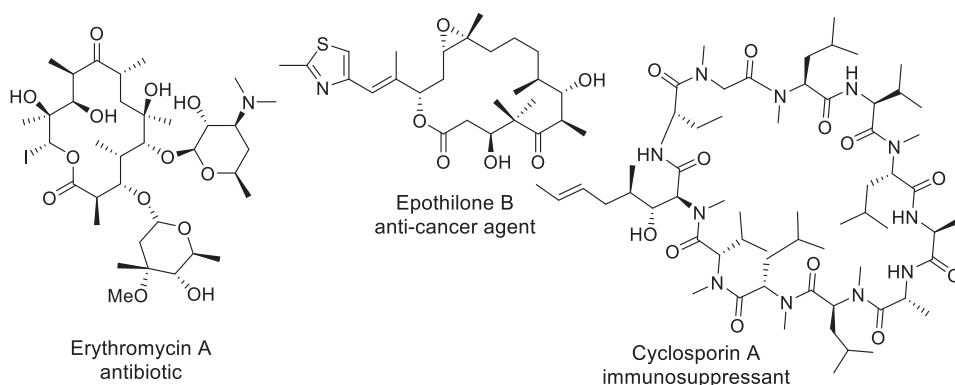


Figure 10. Structures of Erythromycin A, Epothilone B, and Cyclosporin A.^[73]

Currently, more than half of pharmaceuticals in use are chiral molecules, and nearly 90% of the latest drugs are marketed as racemates consisting of an equimolar amount of two enantiomers.^[74] However, it is well-known that only one enantiomer is responsible for pharmacological activity. A historically well-known example is thalidomide (used in the late 1950s until 1961) in which the *R*-enantiomer was solely responsible for the drug's therapeutic effect while the corresponding *S*-enantiomer was teratogenic and caused serious fetal malformations.^[75] To avoid such undesirable effects due to the biological activity of enantiomers, in 1992, The United States Food and Drug Administration (FDA) imposed strict guidelines^[76] that promoted the development of new chiral drugs as single enantiomer formulations. These regulations have had a major impact on the development of new analytical methods for monitoring chirality in drug development. Reliable and efficient chiral separation techniques are crucial for monitoring enantioselective synthesis, checking the racemization process, verifying enantiomeric purity, and conducting pharmacokinetic studies. Intriguingly, chiral macrocycles have found applications in enantioselective recognition and enantiomeric separation techniques.^[77,78] In addition to naturally occurring macrocycles (e.g., cyclodextrins and macrocyclic antibiotics)^[78], several fascinating synthetic chiral macrocycles derived from crown ethers^[79] (e.g., (+)-(18-crown-6)-2,3,11,12-tetracarboxylic acid, with point chirality, shown in Figure 11), have been used as chiral selector in separation of enantiomers. In addition, BINOL-based macrocycles^[80] (with axial chirality) and more recently reported inherently chiral calixarene (*P*-(+)-catechol[4]arene^[81] with helical chirality) illustrated in Figure 11 have been utilized in sensing of chiral carboxylates and ammonium salts respectively.

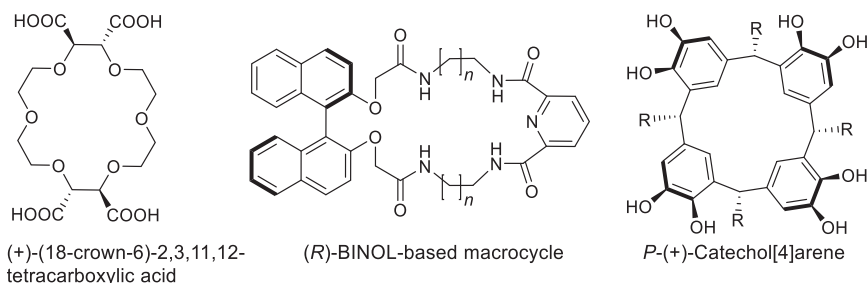


Figure 11. Structures of selected macrocycles directly (or their derivatives) used in various chiral discrimination processes and separation techniques.^[79–81]

CB-type hosts have often shown high selectivity in binding^[82] and can enhance the solubility of pharmaceuticals.^[83] Moreover, the efficient hosts for both cationic and anionic guests that are derived from the CB family offer a great opportunity for multifaceted applications. Although the majority of CBs and HCs are made from achiral monomers, nevertheless, there are several ways of inducing chirality in CB-type hosts, which will be reviewed in sections 1.3.1-1.3.4. Application of these methods would create chiral CB-type hosts that could expand the use of these compounds for supramolecular studies in a chiral environment.

1.3.1 Induction of Chirality in CB-Type Hosts from Achiral Building Blocks

Isaacs and co-workers isolated new derivatives of CBs, including *ns*-CB[6], (\pm)-bis-*ns*-CB[6], and bis-*ns*-CB[10].^[53] The chiral host (\pm)-bis-*ns*-CB[6] has a cross-connection between the two trimeric glycoluril units, and due to this, the symmetry plane in this molecule was lost (Figure 12). Because the macrocycle was formed in an achiral medium, it was isolated as a racemic mixture. The host (\pm)-bis-*ns*-CB[6] is the first chiral member isolated in the CB family and showed similar binding characteristics as that of CB[6]. Isaacs *et. al* investigated the binding behavior of (\pm)-bis-*ns*-CB[6] toward several enantiomerically pure and racemic guests (Figure 12) by NMR in D₂O.^[84]

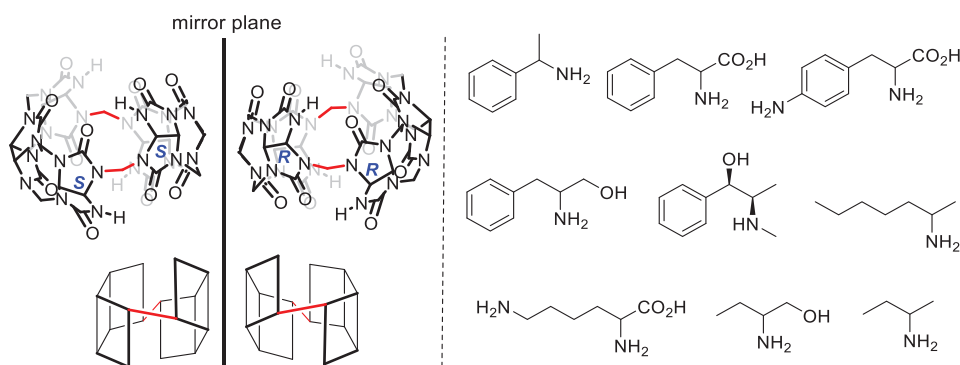


Figure 12. (*R,R*) and (*S,S*) enantiomer of (\pm)-bis-*ns*-CB[6] and chiral guests, the binding characteristics of which were studied with (\pm)-bis-*nor-seco*-CB[6]. Adapted with permission from **Publication I**.

If an enantiomerically pure guest forms a complex with a racemic host, then a mixture of two diastereomeric complexes is formed. In such situations, NMR can be used to differentiate between two diastereomers, resulting in two sets of signals. However, if the racemic host and guest are mixed, then similarly two diastereomers will be formed, although they will be racemic. Because simple NMR measurements cannot distinguish between enantiomerically pure and racemic complexes, their NMR spectra are expected to be identical. Isaacs noticed that the situation with (\pm)-bis-*ns*-CB[6] was not as simple as expected, and that the ratio of the diastereomeric host-guest complex was affected by the enantiomeric purity of the guest. It was speculated that aggregation of one or both of the chiral entities used in the studies may have affected the NMR signals.^[85] Isaac found that the binding dynamics of (\pm)-bis-*ns*-CB[6] was dependent on the structure of the guest molecule, because in the presence of aromatic amines, the separation of signals due to slow guest exchange was observed on the NMR timescale. In contrast, the NMR peaks were only slightly broadened upon complexation

with aliphatic guests, pointing toward the association-dissociation process occurring during the experimental measurements at room temperature.

Isaacs *et al.* demonstrated that chirality can be induced in acyclic CBs due to helical folding^[86]. It is surprising, for example, how a very small change in the structure of the oligomer, such as a single turn of the face of the glycoluril and disconnection of one methylene bridge, can affect the geometry of the molecule. The acyclic 10-membered oligomer, also known as a (\pm)-glycoluril decamer (Figure 13), for example, has no plane of symmetry, and the two pentamers are connected by a single bond. The absence of one methylene bridge in the (\pm)-glycoluril decamer turns all glycoluril CH carbon atoms stereogenic, which induced its crystallization in a helical conformation. Since this compound was formed in achiral media, two opposite-hand helices were formed in a 1:1 ratio. According to my knowledge, no binding studies with chiral guests using a (\pm)-glycoluril decamer have been published to date.

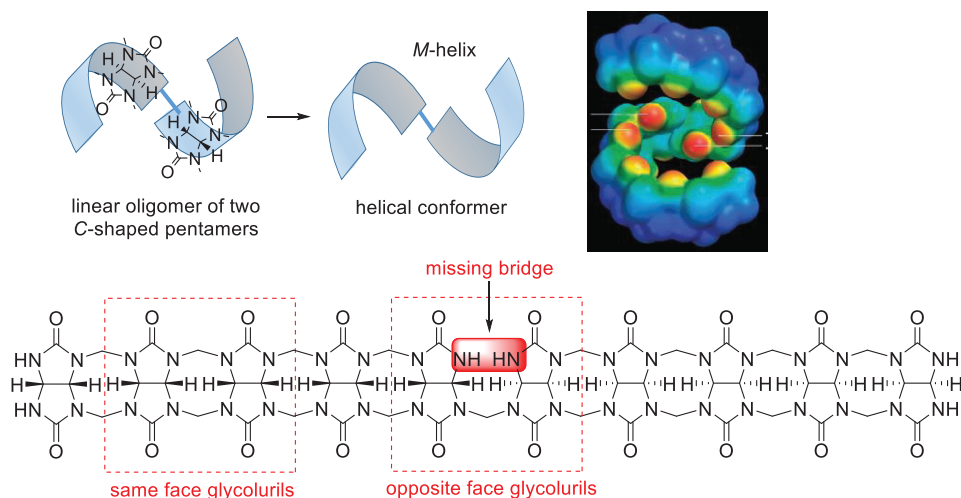


Figure 13. Map of the electronic potential of a single enantiomer of the (\pm)-glycoluril decamer in the shape of an M-helix and its structure. Adapted with permission from **Publication I**.

Twisted-CB[n] (*t*-CB[*n*]) are a unique sub-class of CBs that possess chirality, despite the absence of stereocenters in the monomeric units. These *twisted*-CBs possess axial chirality. The crystal structure of *t*-CB[14] revealed a helical conformation for this CB and hence the name *twisted*-CB[14] was given.^[40] Currently, there are three known CBs with 13, 14, and 15 glycoluril units in their structure that have a helical conformation (Figure 14).^[39,40,87] These *t*-CB[13], *t*-CB[14], and *t*-CB[15] compounds were isolated in 3%, 0.2%, and 0.6% yields, respectively, revealing the challenging synthesis of *t*-CB[*n*]. Moreover, these macrocycles have a 360° twist in their oligomer belt. As a result, they do not have a normal cavity like most CBs. The direction of this twist defines the resulting stereochemistry of the macrocycle. Because the *t*-CB[13-15] belt is made up of glycoluril units linked together through the same face, the helical conformation is locked into these macrocyclic structures.^[88] Surprisingly, in aqueous solution without any guest, *t*-CB[14] behaves like a normal cucurbituril. However, complexation studies revealed the unique binding ability of *t*-CB[14].^[89] For example, complexation studies of *t*-CB[14] in solution showed that a larger 1,8-octyldiammonium guest binds in a 1:1 stoichiometry and with a K_a value of $7.9 \times 10^6 \text{ M}^{-1}$, similar to that of CB[8]. However, binding with a small 1,4-butylammonium guest molecule takes place in a 1:2 stoichiometry, with a K_a

value of $1.9 \times 10^8 \text{ M}^{-1}$ and $2.9 \times 10^6 \text{ M}^{-1}$. This observation clearly shows that *t*-CB[14] has two distinct binding compartments, and that these compartments are flexible.

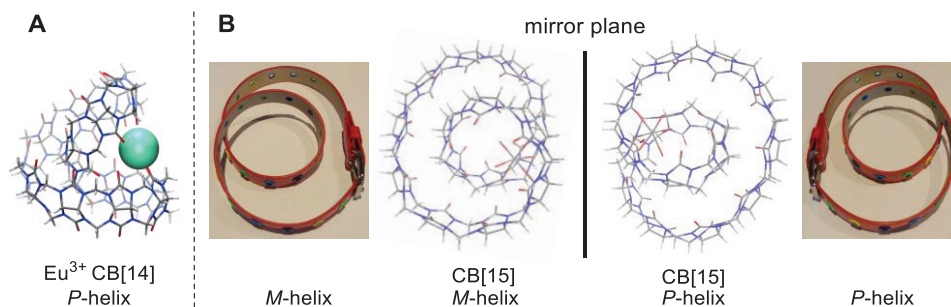


Figure 14. (A) (Eu^{3+} -CB[14]) side view of P-helix; (B) top view of (Cd^{2+} -CB[15]) in M- and P-helical conformations formed in the same crystal and an illustration of these helical configurations with a belt. Figures A and B are reprinted with permission from **Publication 1**.

1.3.2 Chirality Induction in CB-Type Hosts through Desymmetrization

Isaac *et al.* developed a new class of CB-type molecules and called them acyclic CBs.^[90] This work was inspired by glycoluril's C-letter-shaped conformation and their ability to bind guests through electrostatic interactions with the glycoluril carbonyl group. Acyclic CB-type hosts can become chiral on desymmetrization. Isaac and co-workers reported a synthetic approach for functionalizing acyclic CB oligomers with aromatic groups containing enantiopure substituents (Figure 15A). These groups were introduced at the terminal end of acyclic CBs to allow further functionalization of the core structure and to provide UV-active properties. The synthetic method produced enantiopure acyclic CBs. Complexation studies of these acyclic CBs showed a poor level of enantioselectivity with the chiral guests investigated, which is most likely due to the distant location of chiral centers from the binding site of the tetramer where the actual complexation takes place.^[90] Isaacs also reported the synthesis of a series of CB[7] derivatives by introducing one functionalized monomer into its core and connecting it through an amide-bond linker with chiral biotin.^[91] This functionalized CB[7] enabled efficient delivery of the anti-cancer drug oxaliplatin to cancer cells.

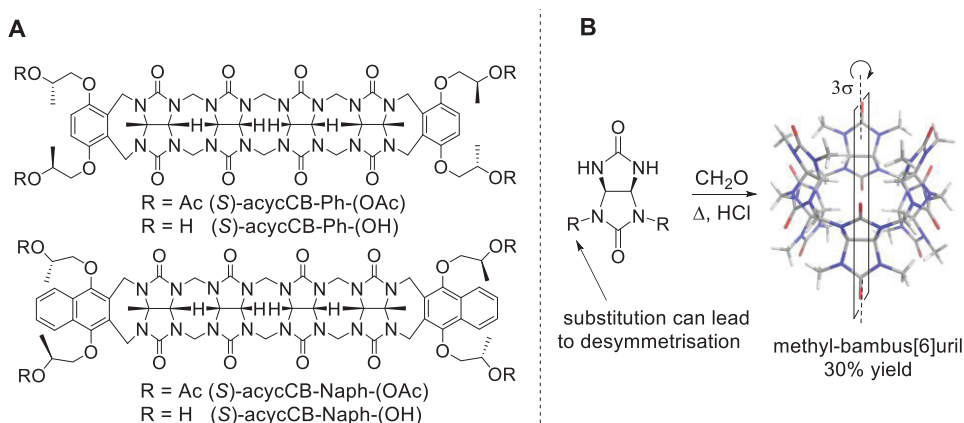


Figure 15. (A) Enantiopure acyclic CBs. (B) Crystal structure of achiral methyl-bambus[6]uril and its monomer ($\text{R} = \text{Me}$, 2,4-dimethylglycoluril). Figure B is adapted with permission from **Publication 1**.

In 2010, Šindelář and co-workers reported the synthesis of the first bambus[*n*]uril (BU[*n*]).^[92] BUs are a sub-class of the single-bridged CB family and are synthesized from achiral monomers. BUs consist of the same monomeric units as the parent CB, however, due to the *N*-substituents on one of the cyclic urea nitrogens, macrocyclization takes place *via* another urea cycle. These macrocycles are the most widely investigated single-bridge CB members, and several analogs have been synthesized to date that are comprised of achiral monomers.^[15] For example, the BU[*n*]^[92] shown in Figure 15B was reported to be synthesized from 2,4-dimethylglycoluril, resulting in an achiral product with a 30% isolated yield. It can be envisioned that a non-equivalent R-substituent of glycolurils would lead to desymmetrization in the structure and create stereogenic centers at the carbon atoms in the fused cycles. In this way, the formation of chiral BU[*n*] would be possible. Such an example can be found in work by Rivollier *et. al.*^[93] The latter reported synthesis of the first monofunctionalized BU[4], heptaallyl(2-hept-en-1-yl)bambus[4]uril, in two steps. The synthesis involved the formation of a symmetrical four-membered BU from diallyl glycoluril, followed by post-functionalization in one of the monomeric units (Figure 16), which afforded a racemic mixture of monofunctionalized BU[4].

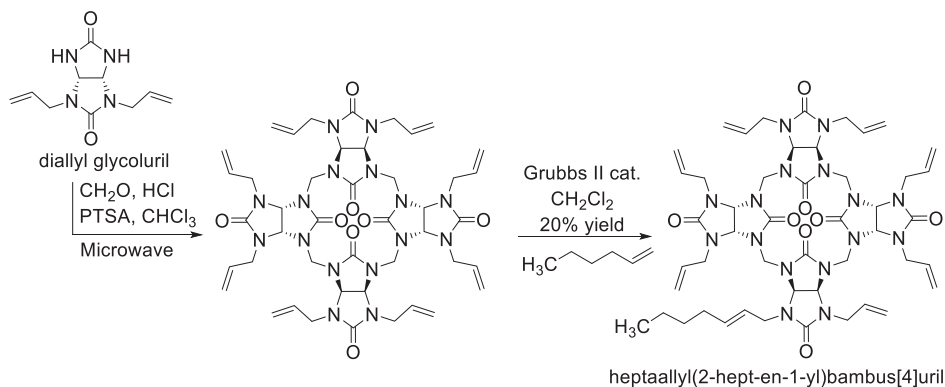


Figure 16. Synthesis of heptaallyl(2-hept-en-1-yl)bambus[4]uril from diallyl glycoluril.^[93]

1.3.3 Chirality Induction in CB-Type Hosts through Chiral Monomers

Chiral CB-type hosts can be obtained in a single step using enantiomerically pure monomeric units for macrocyclization reactions. Riina Aav and co-workers reported the synthesis of several enantiopure substituted HCs. For example, enantiomerically pure (*S,S*)- or (*R,R*)-cyclohexano-hemicucurbit[6,8]urils (cycHC)^[19,94] were derived from enantiopure cyclohexa-1,2-diylurea (Figure 17A). The synthesis of these macrocycles and their specific binding properties will be discussed in section 1.4.1-1.4.2. Pittelkow *et al.* published the synthesis of biotin[6]uril from the chiral and water-soluble compound biotin (vitamin B₇) (Figure 17B).^[24]

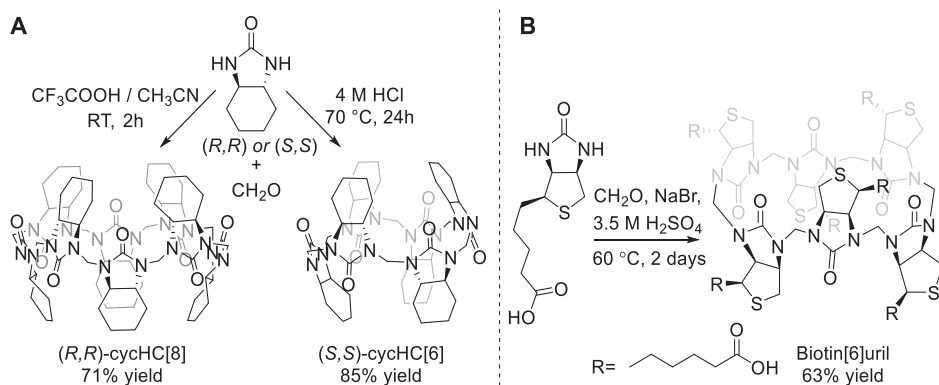


Figure 17. (A) Structures of cyclohexa-1,2-diyurea and enantiopure cycHCs. (B) Structure of biotin and biotin[6]juril.

In 2018, Šindelář and co-workers synthesized and isolated the first enantiomerically pure BU[6]s (Figure 18).^[20] The synthetic approach started from the enantiopure amine, (S)-1-phenylethylamine, and resulted in a mixture of diastereomeric glycolurils. These diastereomers were separated and converted into the corresponding enantiopure (S,R,S)-BU[6] and (S,S,R)-BU[6]. These BUs formed a supramolecular complex with a range of chiral alkyl carboxylates guests *via* C-H \cdots O $_2$ C-R and showed good enantioselectivity for some of the carboxylates investigated; for example, the K_R/K_S ratio for methoxymandelic acid was 3. The same research group further synthesized new derivatives of enantiopure BU[6]s^[21] bearing ester functional groups in the para position of the benzylic substituents. These bambusuril showed higher enantioselectivity for the same set of chiral carboxylate guests under investigation when compared to enantiomerically pure BUs (illustrated in Figure 18) without any ester functionality.

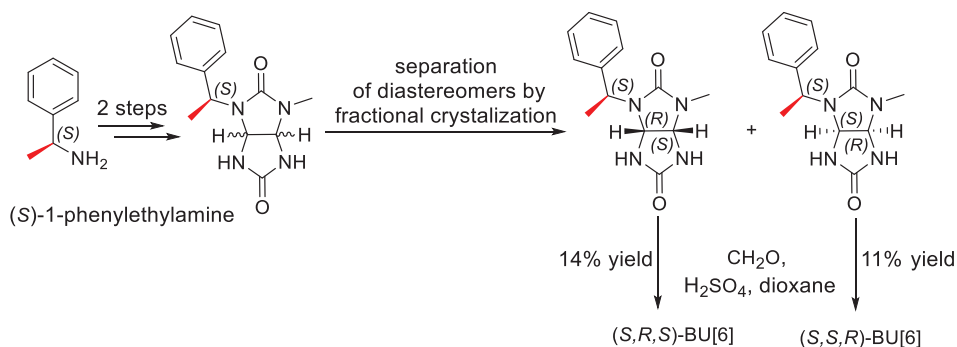


Figure 18. Synthetic approach toward enantiomerically pure bambus[6]jurils.^[20]

Two years later, the same research group (Šindelář) reported the synthesis of another monofunctionalized derivative of BU[6] by introducing one premodified racemic monomeric unit into subsequent macrocyclization reactions, which led to the formation of racemic macrocycles.^[95] The introduction of the carboxylate functional group ($\text{R} = -(\text{CH}_2)_4\text{COOH}$), facilitated a covalent connection of BU[6] with crown ethers, giving rise to diatopic receptors for salt extraction from water into the organic phase. In the example provided, desymmetrized glycoluril (colored in red, Figure 19) was chiral and employed as racemate in later macrocyclization reactions.

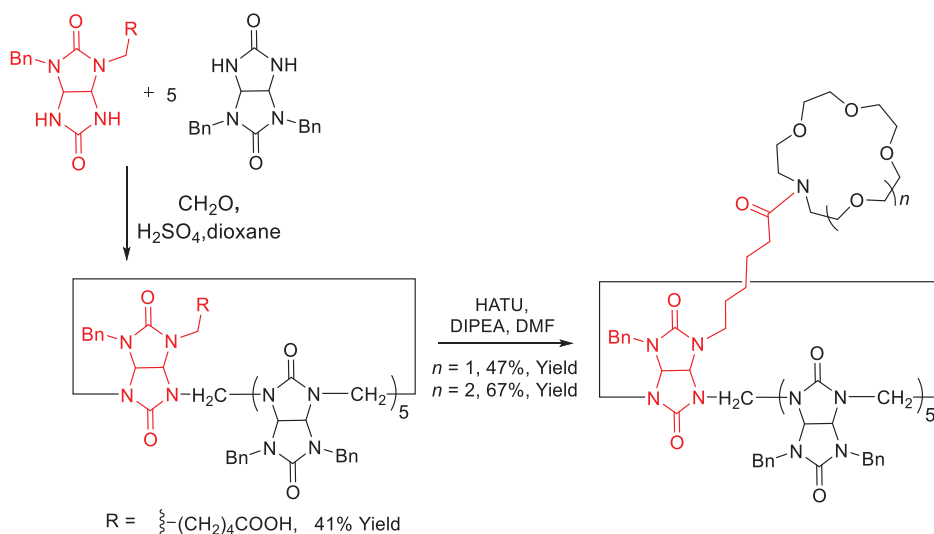


Figure 19. Post-functionalization of bambus[6]uril synthesized from premodified monomeric units.^[95]

1.3.4 Chirality Induction in CBs through Complexation with Chiral Compounds

Upon complexation with an enantiomerically pure guest, the entire host-guest complex becomes chiral. Such supramolecular complexes can be used for the further induction of chirality or enantiodiscrimination.^[96] One of the most reliable methods for detecting chirality in such systems is circular dichroism spectroscopy. Circular dichroism is an absorption spectroscopy technique based on the differential absorption of left and right circularly polarized light by optically active chiral molecules. Biedermann and Nau developed a versatile method that could determine the micromolar concentration of water-soluble chiral analytes, such as amino acids, peptides, and aromatic drugs, through the induced circular dichroism (ICD) effect in the near-UV or visible region.^[97] The sensor developed consisted of CB[8], acting as a host and a fluorescent dye, such as dimethyldiazaperopyrenium (MDPP), which served as a signaling unit (Figure 20A). The addition of the achiral host-dye receptor, to enantiomerically enriched analytes, results in the formation of a chiral host-dye-analyte complex that induces strong ICD signals.

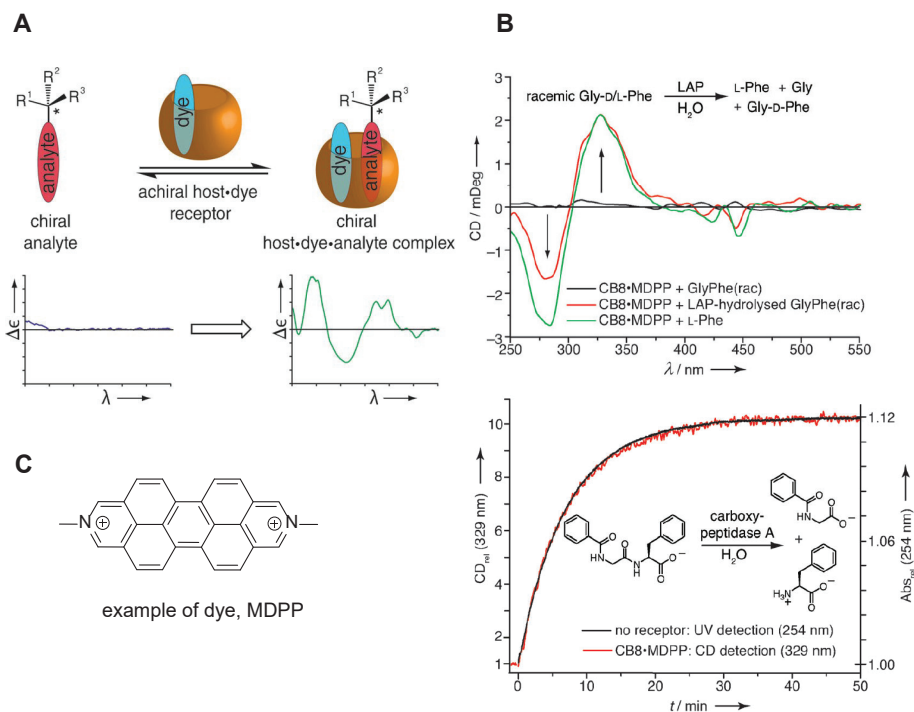


Figure 20. (A) Principle of the supramolecular chirality sensing system with CB[8]. (B) Examples of the application of this sensing system: (top) Circular dichroism spectra of CB[8]·MDPP (20 μM) in the presence of racemic Gly-D/L-Phe, before and after its enzymatic hydrolysis by leucine aminopeptidase (LAP) at pH 7.8; (bottom) kinetic trace for the hydrolysis of Hippuryl-Phe (160 μM) by carboxypeptidase A at pH 7.8. The reaction progress was monitored by circular dichroism (329 nm) in the presence of MDPP@CB8 (20 μM, red line) and, as a control, directly by UV-Visible spectroscopy (254 nm, black line). In this Figure, CD refers to circular dichroism. (C) Structure of MDPP (dimethyldiazaperopyrenium). Figures A and B are reprinted from ref.,^[97] with permission from Wiley and Sons.

For example, the method developed was used to follow enzymatic digestion of racemic glycyl-phenylalanine dipeptide (Gly-D/L-Phe) where only the Gly-L-Phe enantiomer is hydrolyzed to form L-phenylalanine, whereas the Gly-D-Phe dipeptide remains intact. The binding constant of L-Phe ($450 \times 10^3 \text{ M}^{-1}$) to supramolecular sensor MDPP@CB[8] is much higher than that of Gly-D-Phe ($7 \times 10^3 \text{ M}^{-1}$) dipeptide and, therefore, the {L-Phe·MDPP@CB[8]} complex is mainly formed. The formation of L-Phe can be sensed through the ICD signal of the ternary complex (Figure 20B, top). The developed method was capable of monitoring the hydrolysis kinetics of Hippuryl-phenylalanine dipeptide. The kinetics determined with the ICD signal of the CB[8]-sensor, corresponded with the conventionally measured UV-outcome (Figure 20B, bottom). However, by using the first method one can instantly monitor the enantioselectivity of the reaction and assign an absolute configuration to the product.

According to the literature on the solid-state characteristics of CBs, there are few examples of CBs that, while complexing with achiral guests, spontaneously resolve into a helical structure during crystallization.^[98–100] This situation gives rise to chiral crystals that are equally likely to be right-handed or left-handed. Kim and co-workers were the first to report a helical structure that formed upon the complexation of the achiral guest

with CB[6].^[101] Later, along with several achiral polyrotaxanes from CB[6], another helical racemic polyrotaxane was reported by Kim's group.^[102] The research was further explored by Tao and co-workers who reported the formation of a pair of homochiral 1-D-helical coordination polymers of CB[5] with lanthanide cation (Dy^{3+}) upon crystallization in the presence of an achiral hydroquinone guest.^[103]

To conclude, various methods of chirality induction in cucurbituril-type compounds have been investigated in the past, which has led to new opportunities for the scientific community to explore novel chiral macrocycles in further studies and applications.

1.4 Cyclohexanohemicucurbit[*n*]urils

1.4.1 Synthesis and Mechanism

Cyclohexanohemicucurbiturils (cycHCs) are oligomeric products formed in acid-catalyzed condensation reactions between cyclohexa-1,2-diylurea (monomer **1**) and paraformaldehyde (Figure 21). The reaction begins with the protonation of paraformaldehyde. The nucleophilic nitrogen of monomer **1** then attacks the electrophilic carbon atom of activated paraformaldehyde resulting in the formation of intermediate **i**, which is followed by deprotonation and protonation steps, and the subsequent removal of water, to form an iminium intermediate **iv**. The electrophilic carbon atom in this high-energy iminium intermediate **iv** is attacked by the nucleophilic nitrogen of another monomer **1**, from the reaction media, to form **v**. The deprotonation of intermediate **v** results in the formation of a dimer **vi** consisting of an acylaminal linkage, *i.e.*, the methylene bridge between two monomers. Yoo and Kang carried out detailed studies on the formation of hemicucurbituril and proposed that the rate-determining step in the synthesis was the formation of the iminium intermediate.^[104] Continuous formation of acylaminal linkages *via* step-growth produces oligomers of various lengths. Under acidic conditions, the acylaminal linkage is unstable, *i.e.*, it can hydrolyze back to produce the monomer and aldehyde, which makes the oligomerization reaction reversible. Thus, a DCL of oligomers and cycHC[*n*] is formed during the synthesis of cycHC[*n*]. DCL consists of all intermediates in this reaction. The equilibrium between the DCL members is based on continuous and reversible reactions of oligomer chain growth, oligomer to macrocycle formation, and macrocycle stabilization. For the reaction to result in a macrocycle, the oligomer chain–macrocycle equilibrium must promote the formation of a cyclic product. An anionic template, either from acid or salt additives, was found to influence the conformational preorganization of oligomers and to drive the reaction toward the formation of macrocycles of suitable size.^[94] For example, the formation of cycHC[8] was observed in the presence of acids that, on dissociation, formed suitably sized anionic templates, such as formic acid or trifluoroacetic acid, whereas cycHC[6] was precipitated from a 4 M aqueous HCl solution.^[19,94] In both cases, conjugate anions of corresponding acids served as template for the respective macrocyclization.

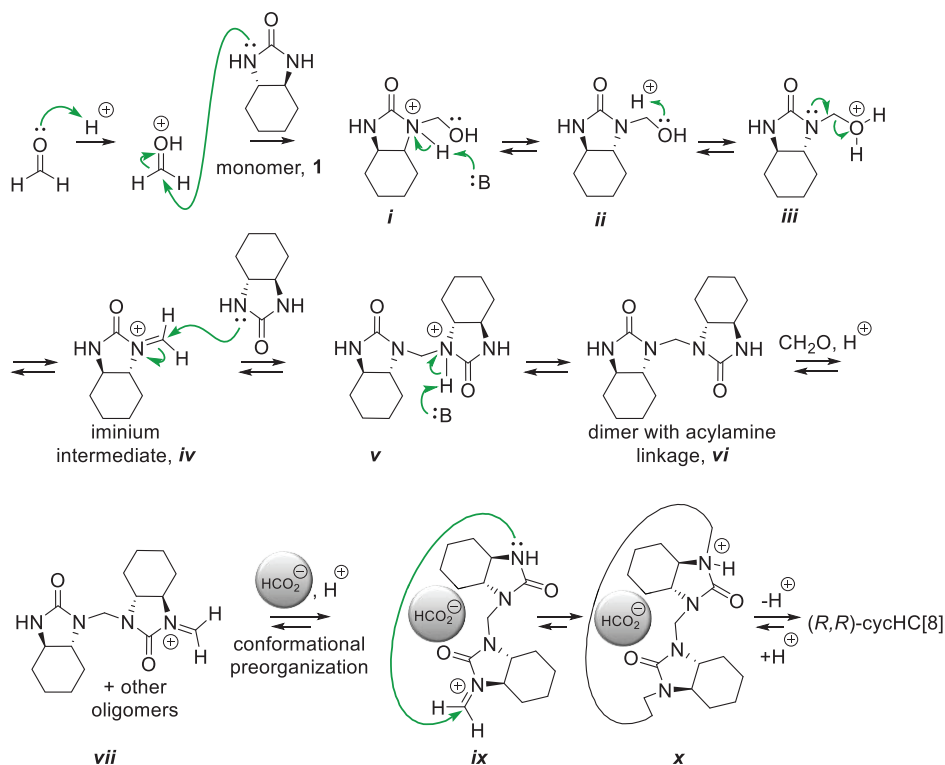


Figure 21. The proposed reaction mechanism for the synthesis of (cyc)HCs, illustrated with the example of (R,R)-cycHC[8] synthesis from the monomer (R,R)-cyclohexa-1,2-diyurea **1**, proceeding through the dynamic covalent library (DCL), and templated by HCO_2^- .

The dynamic nature of the system was also characterized by testing the transformation between two differently sized cycHC[n].^[94] To study the reversible macrocyclization of cycHCs, the course of the cycHC[8] formation reaction from the cycHC[6] macrocycle was monitored (Figure 22).

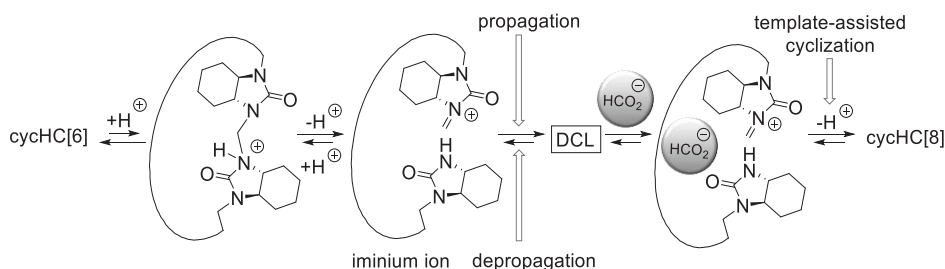


Figure 22. Template effect on the equilibrium between cycHC[6] and cycHC[8].^[94]

The transformation proceeds through key steps, including first protonation of cycHC[6] in an acidic media, which cleaves the methylene bridge and produces the reactive iminium ion. Propagation and depropagation reactions result in different sizes of oligomeric cyclic and acyclic intermediates that form DCL. These oligomers can combine to form a homolog of the original macrocycle if a suitable template is present. It was determined that cycHC[6] was converted to the eight-membered cycHC[8] in the

presence of formic acid or trifluoroacetic acid. Furthermore, using the classical CB synthetic path, it was possible to transform cycHC[8] into cycHC[6] in the presence of a halide template from HCl. The reaction rate for the cycHC[*n*] synthesis was found to be dependent on acid strength and proceeds faster in organic acids.^[94] In the presence of trifluoroacetic acid, cycHC[6] was selectively transformed into cycHC[8] at a rate 10 times faster than in presence of formic acid, and resulted in a 71% yield of isolated product. However, under similar conditions, the rate of formation of cycHC[8] from the monomer was found to be slower. This observation was likely due to the need for an additional acid-promoted monomer and formaldehyde condensation step.

CycHC[6] can be synthesized from enantiomerically pure *trans*-monomer or *meso-cis*-monomer. The dynamic nature of the methylene bridge was also observed when the first *inverted-cis*-cyclohexanohemicucurbit[6]uril (*i-cis*-cycHC[6]) was isolated as a thermodynamically unfavorable reaction product from the heating of *cis*-cyclohexa-1,2-diylurea and paraformaldehyde.^[105] The product was isolated with a yield of 33% of *i-cis*-cycHC[6] and 60% of *cis*-cycHC[6], respectively, with the possibility of shifting the equilibrium toward the synthesis of the latter simply by increasing the concentration of HCl in the reaction mixture.

1.4.2 Complexation Studies of CycHC[*n*]

The diffusion NMR technique is an important analytical tool for determining the properties of supramolecular systems in solution, including host-guest complexes. The technique can be used to study self-association, aggregation, and intermolecular interactions, as well as for calculating the association constants (K_a) of a complex. Successive complexation studies performed by diffusion NMR in CDCl₃ has shown the ability of the (*R,R*)-cycHC[6] and (*R,R*)-cycHC[8] to form complexes with carboxylic acids. The comparative results of the complexation of (*R,R*)-cycHC[6] and (*R,R*)-cycHC[8] are outlined in Table 1.

Table 1. Association constants K_a (M^{-1}) of carboxylic acids with (*R,R*)-cycHC[6] and (*R,R*)-cycHC[8] in 1:1 mixtures in CDCl₃.^[19]

Entry	Guest	CycHC[6], K_a	CycHC[8], K_a ^b
1	CH ₃ COOH	8.0 ± 0.5 ^a	17 ± 2
2	HCOOH	97 ± 1 ^b	72.6 ± 0.5
3	CF ₃ COOH	21 (±3) × 10 ³	29(±1) × 10 ³
4	<i>R</i> -MPA	27.2 ± 0.8 ^a	27.0 ± 0.5
5	<i>S</i> -MPA	20.1 ± 0.2 ^a	53 ± 3
6	<i>R</i> -MTPA	n.d.	3.3 (±0.1) × 10 ²
7	<i>S</i> -MTPA	n.d.	3.0 (±0.1) × 10 ²

^aAssociation constants from ref.^[19], ^bAssociation constants from ref.^[94], n.d.- not determined.

The association constants of acetic, formic, and trifluoroacetic acids were in agreement with the order of their acidity for both (*R,R*)-cycHC[6] and (*R,R*)-cycHC[8] hosts (Table 1, entries 1-3). In a similar manner to simple carboxylic acids, complexation with the more acidic α -methoxy- α -trifluoromethylphenylacetic acid (MTPA) was stronger than that with α -methoxyphenylacetic acid (MPA) (Table 1, entries 4-7). The two *R*-handed hosts, (*R,R*)-cycHC[6] and (*R,R*)-cycHC[8], showed opposite preferences for the two enantiomers of MPA, with the *R*-handed cycHC[8] showing

approximately double the affinity for *S*-MPA as opposed to *R*-MPA. The (*R,R*)-cycHC[6] showed a preference for binding (*R*)-MPA, and (*R,R*)-cycHC[8] a preference for (*S*)-MPA, with a $K_{(R)}/K_{(S)}$ value of 1.4 and K_S/K_R of 2.0, respectively. This finding demonstrated that (*R,R*)-cycHC[8] was capable of forming complexes enantioselectively.

As cycHCs are synthesized in polar media using the approach of anion templating, the binding of inorganic anions to cycHC[8] is expected.^[106] Comprehensive studies with various anions (e.g., SbF_6^- , $\text{PF}_6^- > \text{BF}_4^-$, CF_3SO_3^- , and AcO^-) have revealed a preference for cycHC[8] to bind large symmetrical anions and to form 1:1 complexes. Binding affinity is strongly influenced by factors such as size, shape, and charge distribution of the anion. Thus, the large SbF_6^- anion, which matched the size and shape of the octahedral cavity of cycHC[8] was the most tightly bound guest, with the highest binding constant $2.5 \pm 0.7 \times 10^5$. Furthermore, the complexation study of *i-cis*-cycHC[6] by $^1\text{H-NMR}$ confirmed the formation of external complex with CF_3COOH and an assumed stoichiometry of 2:1 (acid : *i-cis*-cycHC[6]).^[105] The position of the guest was determined by following the influence of the guest on the chemical shift of inner and outer protons of *i-cis*-cycHC[6]. The studies highlighted the dependence of the association constant on the geometry and size of the host, as well as highlighting the superiority of these multifunctional macrocycles over their monomeric counterparts. In 2019, the binding capability of cycHC[6] and cycHC[8] in forming external complexes with zinc(II) porphyrin in chlorinated solvents was reported.^[107] The binding was characterized by coordination to the carbonyl group from the outer surface of the cycHC[*n*]. In 2021, a thorough investigation into the binding studies of cycHCs in chlorinated solvents revealed that only guests capable of hydrogen bonding exhibited signs of complex-formation through the carbonyl group of cycHCs, which broadened the scope of guest molecules studied.^[108]

Computational studies on the frontier molecular orbitals and electrostatic potential of cycHCs have facilitated the understanding and prediction of its complex-forming properties.^[109] DFT studies have shown that the highest occupied molecular orbital (HOMO) of cycHC[6] and cycHC[8] is located on the heteroatoms of the cycHCs, whereas the lowest unoccupied molecular orbital (LUMO) for the respective cycHC was found to be inside the cavity (Figures 23A and 23B). This observation elucidated the binding of electron-rich guests inside the cycHCs. The map of electrostatic potential (MESP) for (*S,S*)-cycHC[6] identified the most electron negative region (red areas) on the oxygen atoms and the most electron-deficient region (blue region) on the methylene bridges and in the core of the cyclohexyl group (Figure 23C). These findings confirmed that cycHCs can complex an anion within the electron-deficient cavity of the macrocycle, whereas non-dissociated acids prefer to bind from outside the macrocycle, *via* acidic protons, to the oxygen atoms of cycHCs.

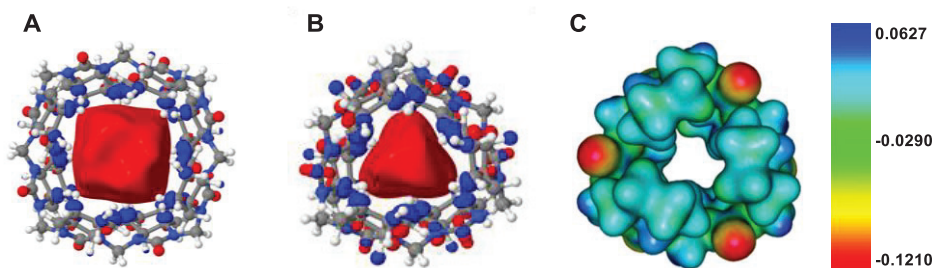


Figure 23. Electronic structures of LUMO of: (A) *(R,R)*-cycHC[8] and (B) *(S,S)*-cycHC[6]. (C) MESP for *(S,S)*-cycHC[6]. Figure A is reprinted with permission from **Publication II**. Figures B and C are reprinted with permission from ref.^[109]

1.5 Solid-State Synthesis

Solution-based traditional syntheses are extremely useful methods that have been used by chemists to synthesize a variety of both natural and synthetic molecular scaffolds.^[73,110] However, when it comes to the formation of macrocycles, such synthetic strategies are often associated with certain disadvantages, including the use of substantial amounts of solvents to inhibit intermolecular polymerization reactions and enhance intramolecular cyclization.^[111] The need for high dilution leads to the generation of significant solvent waste, which is an environmental hazard. Therefore, the development of new, more sustainable methods for chemical synthesis has a positive outlook.^[112] However, not all supramolecular hosts require high dilution synthetic techniques, and a few examples reported in section 1.5.2 were synthesized in solvent-free macrocyclization processes. Such solvent-free covalent interactions can be triggered by various sources of energy, for example, mechanochemical treatment,^[113] microwave^[114] and UV-radiation,^[115] or by ultrasound.^[116] The term *solvent-free reactions*, as used in this thesis, refers to those in which no bulk solvent is used. The solvent-free synthetic approach has many advantages such as:^[117,118]

- Avoiding bulk solvents encourages reaction conditions that are environmentally friendly and sustainable.
- Solvent-free reactions can proceed faster due to high concentrations of reactant, lead to high or quantitative yields, minimize purification steps and diminish the generation of by-products. Therefore, solvent-free reactions can offer a feasible scale-up of the synthetic process.
- Solid-state syntheses can enable access to products that are difficult or even impossible to achieve with a solvent-based approach.
- Solvent-free reactions can expand the access of available reactants to insoluble starting materials and the use of grinding/auxiliary agents to obtain the desired product.

1.5.1 Mechanochemistry

Recent advances in mechanochemistry and its related fields have established solvent-free reactions as environmentally friendly tools to perform chemical transformations efficiently.^[113,117,119,120] Mechanochemistry, which is common in inorganic and chemical metallurgy, is a rapidly growing field that has evolved into a valuable tool in organic, organometallic, and material science, as well as supramolecular chemistry.^[118,121,122]

The first mechanochemical reactions were performed using a mortar and pestle (Figure 24A), and it was the first time that manual grinding was used for chemical system activation.^[123] However, this approach has several inherent limitations which influence the chemical reaction during manual grinding, including limited reproducibility owing to the experimenter's strength and grinding control, poor reporting of reaction parameters, for example, temperature, humidity, or the nature of the grinding assembly, and scale-up constraints, as well as safety issues. The use of ball-milling techniques employing an electronic automated ball mill has replaced traditional manual grinding in research laboratories, and because it enables control of parameters such as frequency of shaking and milling duration, it has assured experiment reproducibility. Furthermore, with milling machines such as the shaker mill (Figure 24D), the sample is enclosed in safe cylindrical jars charged with ball bearing(s) (Figure 24C) and shaken at a fixed frequency (Figure 24B), that substantially minimizes the experimenter's exposure to potentially harmful chemicals.

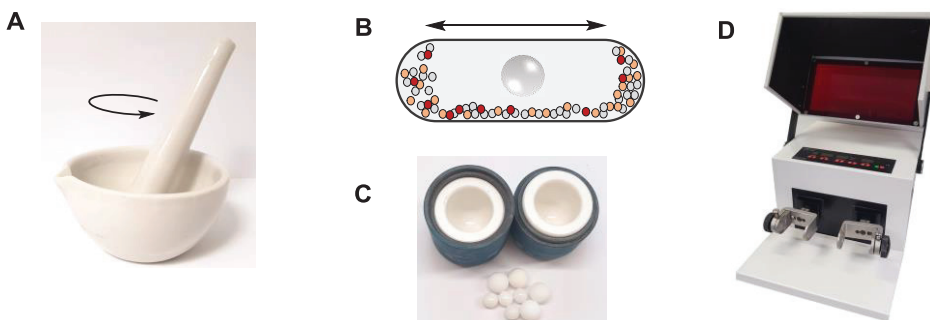


Figure 24. Mechanical agitation (A) by mortar and pestle and (B) in a jar of a shaker mill. (C) Zirconium oxide milling jars with ball bearings and (D) a shaker mill.

Mechanochemical reactions can be performed in solvent-free conditions called as neat grinding or the reaction condition can be modified by adding a small amount of liquid to the grinding mixture, known as liquid-assisted grinding (LAG). The ratio of the volume of liquid (μl) added to the amount of solid present (mg) is denoted as η ($\mu\text{l mg}^{-1}$).^[119] A value of $\eta = 0 \mu\text{l mg}^{-1}$ generally corresponds to neat grinding, however in a typical LAG process, η is usually between 0 and 1.

The examples in this overview will provide a brief insight into the diverse macrocycles that have been synthesized mechanochemically. Novel mechanochemical methods used by various research groups in the syntheses of amide and peptides are also included as examples, which can be used to develop new functionalized macrocycles, hence expanding the list of possible macrocyclic structures for supramolecular applications.

1.5.2 Synthesis of Macrocylic Molecules by Mechanochemistry

In 2019, Aav and Friščić reported the first mechanochemical synthesis of cycHC[*n*] under solvent-free conditions through the anion templating effect of DCC (Figure 25).^[124] The aging process was used to complement the synthesis, which is a low-energy input solid-state technique in which the solid is held at an elevated temperature and the chemical reaction is allowed to progress to drive the formation of the macrocycle through the DCL. The synthesis was achieved by mechanochemical milling of a 1:1 mixture of (*R,R*)-cyclohexa-1,2-diylurea **1** and paraformaldehyde in the presence of a catalytic amount of concentrated HCl, followed by aging at an elevated temperature. This process resulted in the formation of a six-membered macrocycle cycHC[6] in a yield of 95%. When ClO₄⁻ from HClO₄ was used as the anion template, an eight-membered macrocycle cycHC[8] was formed with a 99% yield.

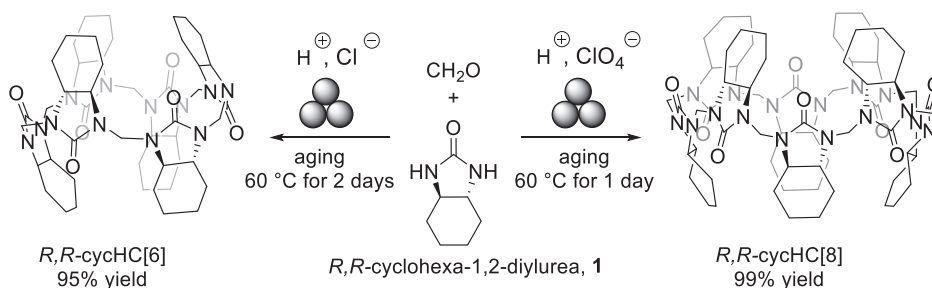


Figure 25. Anion templated solid-state synthesis of cycHC[*n*] involving liquid-assisted grinding (LAG) and aging.^[124]

Since the introduction of the ball-milling technique for constructing macrocyclic structures, several groups have adopted and used it to investigate the potential of mechanochemistry in the synthesis of a variety of macrocyclic molecules that are either impossible or difficult to obtain by the solution method. For example, Severin and co-workers reported the mechanochemical synthesis of an elegant, macro bicyclic cage-like nanostructure with a multicomponent polycondensation reaction (Figure 26).^[125]

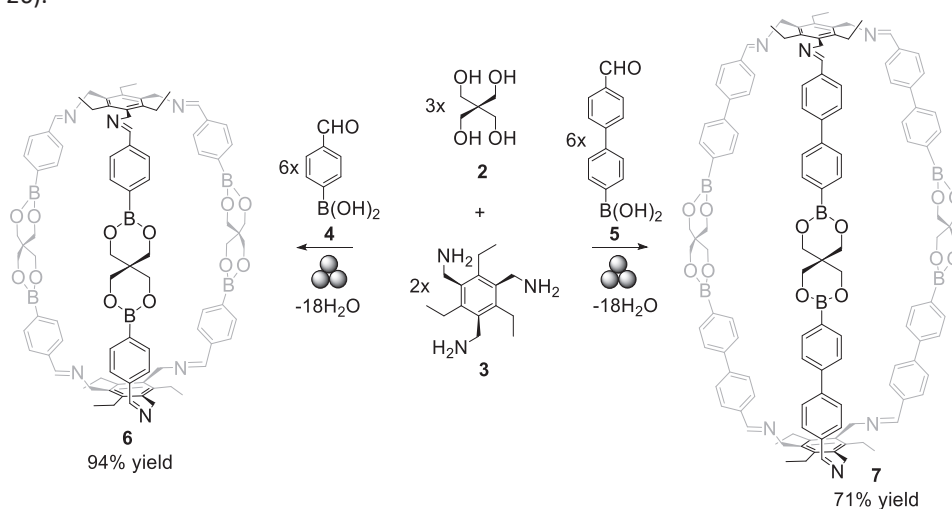


Figure 26. Synthesis of the boronic ester cages **6** and **7** by multicomponent polycondensation reactions in a ball mill.^[125]

The cages **6** and **7** were synthesized from the condensation reaction of pentaerythritol **2**, 1,3,5-tris(aminomethyl)-2,4,6-triethylbenzene **3** and either of the rigid linkers 4-formylphenylboronic acid **4** or 4-(4-formylphenyl)phenylboronic acid **5**. Under the ball-milling conditions, the respective one-pot condensation resulted in 94% of cage **6** or 71% of **7**. The resulting yields surpassed the solution-based synthesis which gave up to 56% of **6** and <40% of the larger cage **7** that was contaminated with a substantial amount of an incomplete condensation product.

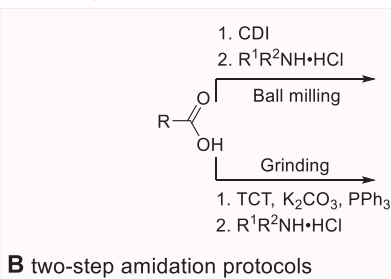
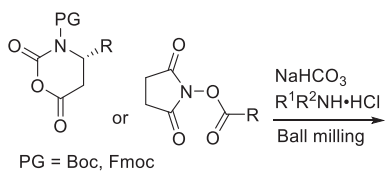
Recent investigations have demonstrated that CB[6] and its functionalized derivatives can be synthesized mechanochemically with a yield of 75-95% and a selectivity of >95%.^[126] Thus, a clean and more efficient procedure for the synthesis of CB compounds was proposed. For example, the method developed was useful for the synthesis of methyl-substituted CB[6] with a high yield (95%) that was otherwise difficult to achieve directly, with traditional synthetic methods resulting in only a 16% overall isolated yield.^[56]

A recent review, published in 2019, provides a comprehensive overview of mechanochemistry in the formation of supramolecular receptors and the mechanochemical strategies used in this area, such as subcomponent self-assembly, dynamic covalent chemistry, and supramolecular catalysis.^[127]

1.5.3 Mechanochemical Approaches in Amidation Reactions

Amide bond formation is among the most important conversions in organic chemistry and is widely applied in the synthesis of active pharmaceutical ingredients.^[128] Hence, it is not surprising that the synthesis of amide and peptide bonds has become one of the major interests in mechanochemical studies. The most commonly used traditional approaches for the synthesis of amide bonds are associated with certain limitations; for example, harsh reaction conditions, large volumes of organic solvents, long reaction times, a limited substrate scope and the low-atom economy of amide-bond coupling reagents, all of which have substantial environmental and safety drawbacks.^[129,130] Recent advances in mechanochemistry and its related fields have established solvent-free reactions as an environmentally sustainable approach for performing amide-bond chemical transformations (Figure 27).^[131–133] For example, straightforward and high-yielding amidation reactions have been carried out mechanochemically from various preactivated carboxylic acid derivatives (Figure 27A), such as *N*-carboxyanhydrides,^[134,135] *N*-hydroxysuccinimide esters,^[136] and *N*-acyl benzotriazoles.^[137] Another fast and efficient synthetic protocol for amides and dipeptide has been developed through the in-situ activation of carboxylic acids. These reactions are carried out in two steps, with the first step activating the carboxylic acid and the second step facilitating the activated acid to react with amine. Using these protocols, *N*-acyl imidazoles^[138] and acyloxytriazine esters^[139] have been produced mechanochemically from carboxylic acids activated with either *N,N'*-carbonyldiimidazole (CDI), or 2,4,6-trichloro-1,3,5-triazine (TCT) with a catalytic amount of triphenyl phosphine (PPh₃), before reacting with amines (Figure 27B).

A one-step amidation of preactivated carboxylic acids



C mechanoenzymatic strategy

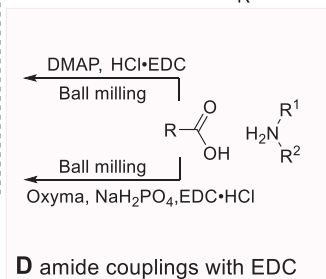
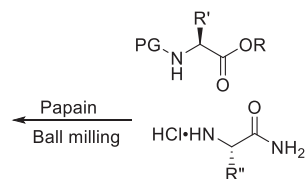


Figure 27. An overview of a mechanochemical approach to the synthesis of amides and peptides: (A) one-step amidation protocol for preactivated carboxylic acid,^[134–137] (B) two-step amidation protocols,^[138,139] (C) mechanoenzymatic strategy,^[140–142] and (D) amide coupling using EDC.^[143,144]

Compatibility between enzyme-based biocatalysts and mechanochemical techniques has been demonstrated in the synthesis of amide linkage in peptides. Under solvent-free conditions, papain enzyme, for example, has been shown to catalyze the formation of peptides from the corresponding amino acid building blocks (Figure 27C).^[140–142] Moreover, the biocatalyst remained stable and remarkably effective at mediating the synthesis of peptides and amides, despite the mechanical stress experienced inside the ball mill during the milling process.

Efforts have been made for the direct coupling of amines with carboxylic acid by using environmentally friendly coupling reagents. It was reported that 1-ethyl-3-(3-dimethylaminopropyl)carbodiimide (EDC)-mediated coupling eliminates the need to pre-activate reactants, allowing for the synthesis of amides and dipeptides in a single step with short reaction times and good yields after following a simple workup protocol (Figure 27D).^[143,144]

2 Motivation and Aim of the Present Work

Significant progress has been achieved in the synthesis of CB[*n*]-type hosts and their derivatives in the last two decades, with a focus on enhancing the synthesis, isolation, and purification of each of the CB[*n*] family members. The widespread interest in CBs has led to a range of applications, such as in nanoparticle-based sensors,^[145] as potent drug delivery agents,^[146] and as supramolecular reaction vessels in photocatalytic cycloaddition reactions.^[147] The key driving force behind these expanding applications is the remarkably strong binding ability of CBs and the isolation of new members of CBs with high solubility in water. Applications of HCs have been limited by the small size of the available hosts.^[14,15] To broaden the application of HCs, a high-yielding, scalable synthesis of higher family members (*n*>6) with a flexible conformation and providing a large cavity for the inclusion of several guest molecules is required. For this purpose, the effects of templating agents have been studied, with mixed results to date; nevertheless, further research in this area is needed. The primary factor regarding CB[*n*]-type hosts is their efficient synthesis followed by separation and purification. A crucial pathway toward high-purity hosts is the development of new and efficient synthetic methods. cycHC[8], being a unique 8-membered hemicucurbituril, did extend the range of bound guests to larger chaotropic anions, but the larger internal dimensions could also enable the binding of small organic molecules, an area that has not yet been explored. Post-functionalization of macrocycles could lead to faster discovery of new hosts, and solid-state methods can provide an efficient and environmentally benign approach for functionalizing poorly soluble or insoluble macrocycles, as observed in the synthesis of the hexa-amide biotin[6]uril. Furthermore, the application of HCs in chiral recognition is restricted for achiral derivatives, and more research is needed to synthesize new chiral family members. If such approaches are developed, we can certainly expect a wide range of rich and diverse HC[*n*] chemistry in the future. Thus, there is still room for further improvement in the synthetic methodology and understanding of the properties of new macrocycles for their further applications. Therefore, the main aims of the present work were to:

- Investigate templating agents for the synthesis of a larger chiral homolog of cycHC[*n*], and isolate and characterize its structure to predict its binding properties for future studies.
- Broaden the scope of application of cycHC[8] and investigate its binding capability with neutral heterocyclic guests to apply cycHC[8] in solid-phase extractions as a sorbent.
- Develop an environmentally friendly solid-state approach for the efficient synthesis of amides, and apply the synthetic methodology thus developed in the synthesis of uniformly substituted biotin[6]uril.

3 Results and Discussions

The results described in this thesis are based on four publications. Details from the first paper are incorporated in the literature section and provide an overview of the different approaches for obtaining chiral cucurbituril-type compounds based on the published data (**Publication I**). The second paper covers the synthesis, structural characterization, and temperature-based dynamics of cyclohexanohemicucurbit[12]uril (cycHC[12]) (**Publication II**). The third paper focuses on the supramolecular properties of cyclohexanohemicucurbit[8]uril (cycHC[8]), and describes its capability of selectively binding neutral guests in polar media and its application in solid-phase extraction of sulfur-containing heterocycles from water (**Publication III**). The fourth paper describes the development of an environmentally friendly and novel solid-state approach to the synthesis of amide bonds and its application for the post-functionalization of biotin[6]uril (**Publication IV**).

3.1 (*R,R*)-Cyclohexanohemicucurbit[12]uril (Publication II)

3.1.1 Synthesis and Structural Characterization

The first chiral HC synthesized was enantiomerically pure cycHC[6].^[19] Synthesis of biotin[6]uril,^[24] and more recently chiral bambus[*n*]urils,^[20,21,95,148] have further expanded the HC family. Only 4-membered^[93,149,150] or 6-membered^[15,17,19–21,24,44,93,149–151] macrocycles have been isolated as substituted HCs, with the exception of cycHCs,^[94,124] in which the reaction could be steered to the 8-membered product through templating. Formation of even larger macrocycles have been recorded by mass-spectrometry, as members of the DCL in cycHC^[152] and norbornaHC^[151] synthesis; however, only the non-chiral unsubstituted HC[12]^[44] was isolated. HC[12] was shown to be flexible, in contrast to the rigid structure of the smaller macrocycles. Thus, the motivation was to synthesize large chiral cycHC host molecules displaying flexible conformations and large cavities for the inclusion of several guest molecules.

Based on the available information discussed in the literature section 1.4.1 and 1.5.2, it has been established that the size of the templating anion plays a key role in directing the size of the cycHCs formed; thus, we can hypothesize, that a larger template will lead to the formation of larger cycHCs. Anionic templates may be introduced to the reaction mixture as the conjugate anion of the acid used, or within a salt that is used in combination with a non-templating acid. In the presence of pentafluoropropionic acid, traces of homologs larger than cycHC[8] have been already identified, implying the capability of fluorinated acids to generate larger cycHCs.^[152] Although the larger cycHC[*n*] (*n* = 10, 11, 12) were identified in the crude reaction mixture by UV-HPLC, they were not isolated. The focus of the research included in this thesis was to synthesize and isolate the larger cycHC[*n*] homolog, *i.e.*, the 12-membered cycHC[12]. Interconversion of macrocycles, previously shown for the template-driven transformation of cycHC[6] to cycHC[8] and *vice versa*,^[94] was chosen as the reaction setup for the isolation of cycHC[12]. Namely, different acids (Table 2) were screened for the interconversion of cycHC[8] to cycHC[12] (Figure 28A), with the dissociated anions from these acids serving as templates. The choice of acids was primarily influenced by two factors: acid strength (*pKa* value), which is required to protonate the starting macrocycle, that further triggers the ring-opening for the propagation stage, and the size of the conjugated anion produced during dissociation, which would drive the reaction toward cyHC[12]

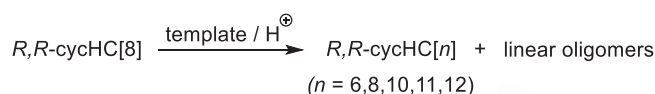
formation. In some reactions, either CH₃CN or a non-templating weaker acid (CH₃COOH) was used as solvent or as co-acid (Table 3).

Table 2. Acids screened for interconversion of macrocycle cycHC[8] into cycHC[12].

Acid	pK_a^*	Length of conjugated anion (Å) [#]
3,5-bis(trifluoromethyl)benzoic acid	3.34±0.10	9.88
CF ₃ CF ₂ CF ₂ COOH	0.37±0.10	9.03
CBr ₃ COOH	0.22±0.10	7.47
Cl ₃ CCOOH	0.09±0.18	7.19
CF ₃ CF ₂ COOH	0.38±0.10	7.01
F ₂ ClCCOOH	0.21±0.10	6.72
CHCl ₂ COOH	1.37±0.10	6.01

* pK_a values for the acids were calculated using Advanced Chemistry Development (ACD/Labs) Software V11.02 (©1994-2021 ACD/Labs) at 25 °C. [#]The lengths of the conjugated acids were calculated using Mercury software and the van der Waals radii^[153] of the associated atoms, as shown in Figure 28B.

A



B example of template size measurement:

calculation:
 Size of conjugated anion
 = Distance measured between F-O
 + van der Waals radii for F atom
 + van der Waals radii for O atom
 = 6.04 Å + 1.47 Å + 1.52 = 9.03 Å

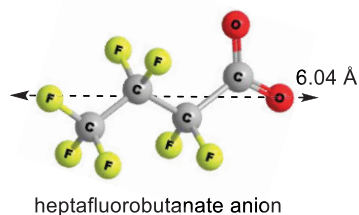


Figure 28. (A) Re-macrocyclization of cycHC[8] to cycHC[12]. (B) Example of determination of the size of the conjugated anion (Table 2) for the sketched heptafluorobutanate anion.

The first screening of the reaction conditions (Table 3) was carried out with the help of students Oliver Paberits and Karin Kreekman under the supervision of Dr. Sandra Kaabel. RP-HPLC analysis showed that anionic templates from weaker organic acids, e.g., 3,5-bis(trifluoromethyl)benzoic acid, did not lead to the formation of larger cycHC[*n*]s (Table 3, entry 1). However, in the presence of α -halogenated acetic, propionic, or butyric acids formation of larger cycHC[*n*]s ($n = 10, 11, 12$) could be observed (Table 3, entries 2-9), although not all of these reactions showed the formation of cycHC[12]. The latter was formed in the presence of CCl₃COOH, CF₃CF₂COOH, or CF₃CF₂CF₂COOH (Table 3, entries 2, 3, 5, 6 and 7). While DCL was generated the most quickly in the pure perfluorinated acids (Table 3, entries 2 and 6), consuming most of cycHC[8] and forming cycHC[6] and larger homologs, the amount of cycHC[12] was largest when CF₃CF₂CF₂COOH was diluted with a weaker co-acid (Table 3, entry 3).

Table 3. Representative examples from screened reaction conditions^a for transforming (*R,R*)-cycHC[8] to (*R,R*)-cycHC[12].

Entry	Acid (eq.)	Eq. of acid to cycHC[8]	Solvent/ Co-acid	Time (h)	Amount of cycHC[8] left (%)	Estimated yield of cycHC[<i>n</i>] (%) for the cycHC [6] : [10] : [11] : [12]
1	<i>m</i> -Ph(CF ₃) ₂ COOH(<i>s</i>)	100	CH ₃ CN	24	83	0.0 : 0.0 : 0.0 : 0.0
2	CF ₃ CF ₂ CF ₂ COOH(<i>l</i>)	150	-	7	14	10 : 5.0 : 8.0 : 2.0
3	CF ₃ CF ₂ CF ₂ COOH(<i>l</i>)	150	CH ₃ COOH	2	20	32 : 3.4 : 5.0 : 4.4
4	CBr ₃ COOH(<i>s</i>)	150	CH ₃ COOH	24	16	5.0 : 3.0 : 1.1 : 0.0
5	Cl ₃ CCOOH(<i>s</i>)	150	CH ₃ COOH	24	25	4.3 : 1.8 : 2.0 : 1.1
6	CF ₃ CF ₂ COOH(<i>l</i>)	300	-	51	7.6	7.5 : 2.0 : 3.2 : 2.4
7	CF ₃ CF ₂ COOH(<i>l</i>)	100	CH ₃ CN	5	39	7.0 : 4.0 : 3.0 : 2.0
8	F ₂ ClCCOOH(<i>l</i>)	150	CH ₃ CN	42	77	3.8 : 3.5 : 2.2 : 0.0
9	CHCl ₂ COOH(<i>l</i>)	300	-	1.5	27	1.8 : 0.0 : 2.7 : 0.0

^aGeneral screening conditions: To 4.3–4.6 mg of cycHC[8] was added the acid-solvent mixture listed in the table, with concentrations in the range of 0.01-0.05 M, and stirred. The crude reaction mixture was analyzed by RP-HPLC after the time indicated in Table 3. The estimated HPLC yields outlined in Table 3, column 7 were quantified using the calibration graph for cycHC[8] according to the published procedure.^[154] In table 3, column 2, subscripts (*s*) and (*l*) refers to the solid and liquid states of the acids used in the screened reactions, respectively.

While none of the tested conditions gave cycHC[12] as the major product, we chose the conditions from Table 3, entry 3 for the large-scale reaction and isolation of cycHC[12]. In the larger scale reaction, the 1.69 g of cycHC[8] in acetic and heptafluorobutyric acids was converted to a mixture of products during two hours at room temperature. The RP-HPLC-UV chromatogram from the reaction mixture (Figure 29A) revealed the formation of a mixture of cycHC[*n*], *n* = 6, 8, 10, 11, 12 homologs, which was confirmed by mass-spectrometric analysis.

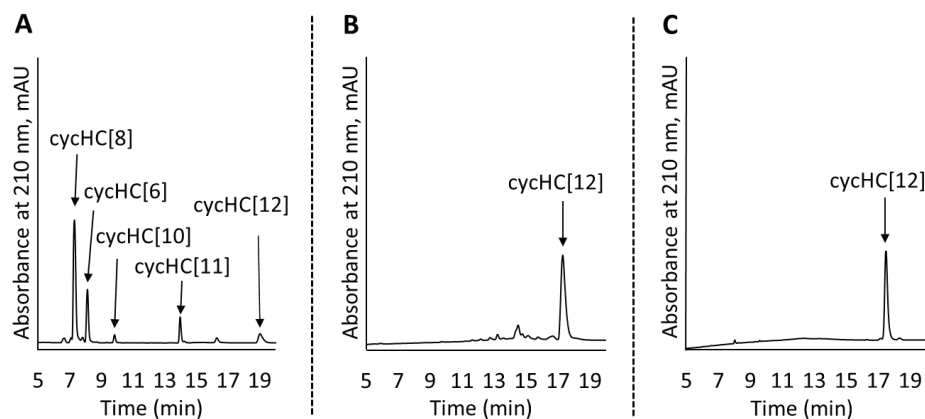


Figure 29. HPLC-UV chromatogram measured at 210 nm: (A) crude reaction mixture, (B) cycHC[12] after purification by RP column chromatography, and (C) cycHC[12] after additional purification by normal phase column chromatography.

The crude product was purified first by reverse-phase column chromatography. This purification resulted in a fraction containing mainly a mixture of oligomers, which are difficult to observe by HPLC-UV due to their low absorption^[154] and poor ionization

ability in electrospray ionization mass spectrometry (ESI-MS), along with another fraction containing mainly macrocycles. From the latter, 17 mg (1%) of cycHC[12] was isolated and was confirmed by HRMS. RP-HPLC-UV chromatogram (Figure 29B) and NMR analysis revealed that the isolated macrocycle was still contaminated with oligomers; therefore, to obtain cycHC[12] in an analytically pure grade, the isolated product was repurified using normal column chromatography (Figure 29C).

The methylene bridges in cycHCs can be either in *syn* or *anti* configurations due to the alternating orientations of the cyclohexano-monomers in HCs (Figure 30A). The *syn* and *anti* configurations define the mutual orientation of the bridges, and its nearest neighboring cyclohexano-carbon skeleton. *Syn* bridges are those that point in the same direction as the cyclohexano skeleton, while those pointing in the opposite direction are referred to as *anti* (Figure 30A). Smaller chiral homologs of cycHCs are known to adopt a barrel-shaped conformation with distinct *syn* or *anti* oriented bridges in a 1:1 ratio as observed in their NMR analysis.^[19,94] The new chiral cycHC[12] macrocycle was initially expected to have similarly a regular 12-gon conformation, which would also result in a 1:1 ratio of *syn*- or *anti*-oriented bridges. To understand the conformational landscape of cycHC[12], NMR experiments were conducted in the 800 MHz NMR spectrometer by Dr. Jasper Adamson. Unlike smaller chiral homologs of cycHCs, the NMR study of the isolated cycHC[12] in toluene at 265 K did not support a highly symmetric structure. The experimental 1D NMR spectra of cycHC[12] revealed the presence of three types of non-equal urea groups (α , β , and γ) and four types of methylene bridges (B1, B2, B3, and B4) (Figure 30B). This finding pointed towards the existence of two perpendicular axes of C_2 symmetry that divide the structure into four symmetry-related parts (Figure 30C). These structural features, supported by NMR data, suggest a concave polygon conformation, with two methylene bridges flipped towards the center of the cavity.

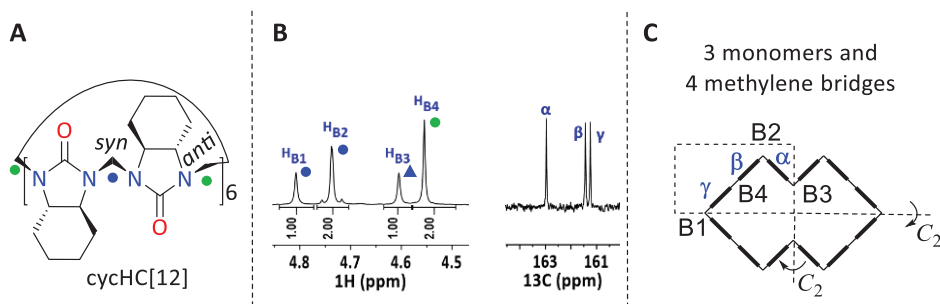


Figure 30. (A) Chemical structure of cycHC[12] based on smaller chiral homologs. (B) NMR spectra of cycHC[12] bridge protons H_{B1} – H_{B4} (left) and carbonyl carbons (right) in toluene- d_8 . (C) Symmetry elements of cycHC[12] and the position of symmetry non-related monomers (α , β , γ).

A variable temperature (VT) 800 MHz ¹H-NMR experiment in toluene- d_8 was performed to investigate the conformational dynamics of cycHC[12]. At a temperature of 265 K, the macrocycle adopted a concave octagonal shape. At elevated temperatures, two dynamic exchange processes took place. The first dynamic exchange, called the “bridge flip”, was observed when the temperature was raised from 265 K to 308 K (Figure 31A). The best way to explain this bridge flip motion is to consider it as a flip of the B3 bridge outwards and the B4 bridge inwards, which simultaneously exchanges the magnetic environment of the B1 and B2 bridge moieties. As a result, the B3 bridges turn around to face outward and take the original position of the B4 bridges, and *vice versa*.

During this process the distance between opposing carbons at the B4 methylene bridges is reduced from 18 Å to 7 Å, whereas the distance between carbon atoms of the B3 bridges is increased. At temperatures above 308 K, a second dynamic exchange known as the “monomer flip” was observed, which was hypothesized to be due to the free rotation of the monomers (Figure 31B). As a result of the free rotation of urea monomers, the magnetic environment of *syn*- and *anti*-configurations, as well as the inwards and outwards orientations of bridges, are averaged.

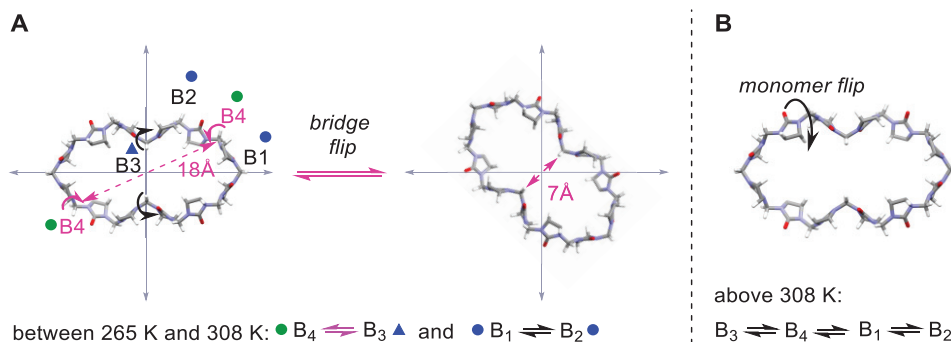


Figure 31. (A) Representation of the cycHC[12] bridge flip mechanism. Dotted arrows denote bridge moieties that move in reference to the center of the macrocycle. The conformational flip is indicated by curved arrow. Blue and green dots represent *syn*- and *anti*-configurations of the bridges, respectively. The triangle represents the bridges pointing inside the cavity. (B) Representation of the monomer flip at higher temperatures at which all bridge signals undergo NMR chemical exchange. Cyclohexano groups are omitted from the structure for clarity. Figures are adopted, with permission from **Publication II**.

Dr. Mario Ören carried out computational studies of cycHC[12] which contributed to a deeper understanding of the cycHC[12] formation, an improved prediction for the preferred concave octagonal conformation, and ultimately an explanation for its low-yielding synthesis. The rotation of the two methylene bridges in cycHC[12] into the cavity induced a conformational change, which collapsed the cavity of the macrocycle. Furthermore, this conformational change strongly affected the localization of the frontier orbitals as shown in Figure 32, thereby concentrating the LUMO on the urea monomers rather than inside the cavity as in the case of cycHC[8] and all smaller HCs,^[109,155] as described in section 1.4.2.

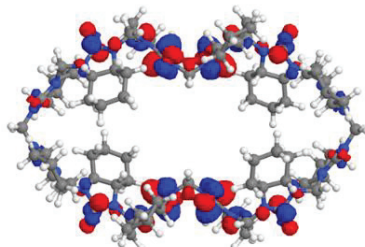


Figure 32. Electronic structure of LUMO of cycHC[12] in the concave octagon conformation. Reprinted with permission from **Publication II**.

The absence of the cavity-centered electron-deficient LUMO orbital, which underpins the ability of cycHC[6] and cycHC[8] to bind anions, suggests that cycHC[12] neither binds nor templates the screened anions (Table 3). Thus, it was proposed that the synthesis of cycHC[12] from heptafluorobutyric acid was not a product of template-directed synthesis.

To conclude, cycHC[12] was synthesized, isolated, and characterized by DFT and VT-NMR analysis which revealed that cycHC[12] possesses a concave octagon conformation at 265 K and adapts its structure in response to external stimuli. Because these temperature-dependent dynamic processes have not been observed for the cycHC[8]^[94] macrocycle due to its small size, we propose that the dynamic characteristics of cycHC[12] will enable it to bind larger species and adjust its structure for the guest molecule.

3.2 CycHC[8] Inclusion Complexes with Heterocycles and its Application in SPE (Publication III)

cycHC[*n*] (*n* = 6, 8) binds anions^[106,109] in their cavity in protic solvents. In aprotic solvents, they are capable of forming external complexes with Lewis and carboxylic acids.^[19,107] Although there are several examples of cucurbiturils efficiently binding neutral guests in aqueous media,^[156] only a limited amount of research on the binding of neutral guests, especially heterocycles, by single-bridged cucurbiturils in solution has been previously reported, which was the underlying motivation for the present research.

For this study, a series of suitably sized 5- and 6-membered *S*-, *O*-, and *N*-heterocyclic guests **8-20** (Figure 33) were chosen as they have a higher electron density compared to that of hydrocarbons and may fit into the cavity of eight-membered cycHC[8]. The neutral guest binding properties of cycHC[8] were therefore studied by different analytical methods, including single-crystal X-ray diffraction analysis (SC-XRD), ¹H NMR, isothermal titration calorimetry (ITC), solid-state NMR, and thermogravimetric analysis (TGA).

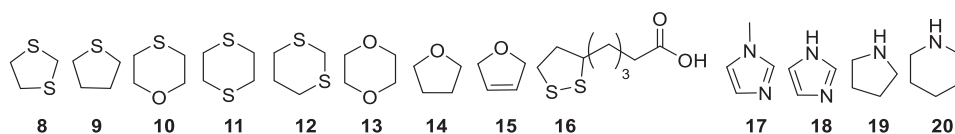


Figure 33. Scope of the neutral guests investigated (from left to right): 1,3-dithiolane **8**, tetrahydrothiophene **9**, 1,4-thioxane **10**, 1,4-dithiane **11**, 1,3-dithiane **12**, 1,4-dioxane **13**, tetrahydrofuran **14**, 2,5-dihydrofuran **15**, α -lipoic acid **16**, *N*-methylimidazole **17**, imidazole **18**, pyrrolidine **19**, and piperidine **20**.

Single crystals were obtained by Dr. Sandra Kaabel from a methanol solution of cycHC[8] in the presence of 60 molar equivalents of 5- and 6- membered heterocycles, 1,3-dithiolane **8**, 1,4-thioxane **10**, 1,4-dioxane **13**, tetrahydrofuran **14**, and 2,5-dihydrofuran **15**, respectively. SC-XRD analysis of these crystals revealed that cycHC[8] can bind neutral guests in their hydrophobic pocket and form a 1:1 inclusion complex. This finding was the first evidence of the binding of any neutral guest within the cycHC[8] cavity. The *N*-containing heterocycles, pyrrolidine **19**, and piperidine **20**, and the largest investigated guest, α -lipoic acid **16**, did not yield crystals of inclusion complexes with cycHC[8].

3.2.1 ¹H NMR and ITC Binding Studies in Solution

The host-guest complex was studied in a 3mM CD₃OD solution of the host cycHC[8] upon addition of 60 equivalents of the neutral guest. The study was carried out for guests **8-18** and the inclusion complex formation was followed by the chemical shift change of cycHC[8] proton H_{2ax}. This proton is positioned inside the cavity which becomes magnetically deshielded upon binding with the electron-rich guest. The change in cycHC[8] chemical shifts in the presence of 1,3-dithiolane **8** is illustrated in Figure 34 and summarized in Table 4 for all the guests screened.

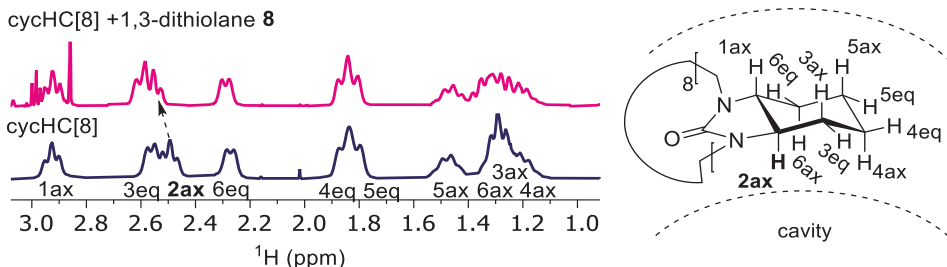
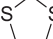
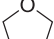
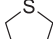
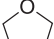
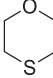
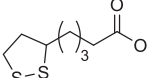
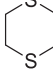
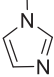
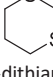
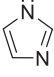
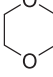


Figure 34. ¹H NMR of cycHC[8] with 60 eq. of 1,3-dithiolane **8** (left) in CD₃OD and structure of cycHC[8] with numbered atoms (right).

Table 4. Screening of guest binding in CD₃OD based on the ¹H NMR chemical shift change ($\Delta\delta$) of H_{2ax} signal of 3 mM cycHC[8] upon addition of 60 eq. of heterocycles.

Entry	Guest	$\Delta\delta$ (H _{2ax} , ppm)	Entry	Guest	$\Delta\delta$ (H _{2ax} , ppm)
1	 1,3-dithiolane 8	0.064	7	 tetrahydrofuran 14	0.006
2	 tetrahydrothiophene 9	0.048	8	 2,5-dihydrofuran 15	–
3	 1,4-thioxane 10	0.030	9	 α -lipoic acid 16 ^b	n.d. ^a
4	 1,4-dithiane 11	0.028	10	 N-methylimidazole 17 ^b	–
5	 1,3-dithiane 12	0.013	11	 imidazole 18 ^b	–
6	 1,4-dioxane 13	0.012			

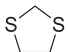
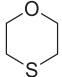
^aGuest signals overlapped with cycHC[8] H_{2ax} ¹H NMR signal. ^bMeasured by Tatsiana Shalima

Sulfur-containing five-membered heterocycles 1,3-dithiolane **8** and tetrahydrothiophene **9** (Table 4, entries 1 and 2) caused a larger chemical shift change compared to that of the six-membered heterocycles; 1,4-thioxane **10**, 1,4-dithiane **11**, 1,3-dithiane **12** and 1,4-dioxane **13** (Table 4, entries 3–6). This observation can be explained by a higher affinity and a larger population of complexed species formed with five-membered sulfur-heterocycles 1,3-dithiolane **8** (Table 4, entry 1). It is vital to note that the affinity as determined here is based on the magnitude of the chemical shift change, under the assumption that it is proportionate to the population of complexed species, which remains true with respect to comparable guest molecules. 1,3-dithiolane **8** induced the most prominent shift in the H_{2ax} signal of cycHC[8] among all the compounds studied. A negligible shift was observed for tetrahydrofuran **14** (Table 4, entry 7), while no shift was observed for 2,5-dihydrofuran **15** and *N*-heterocycles, *N*-methylimidazole **17**, and imidazole **18** (Table 4, entries 8, 10, and 11). Due to the overlapping of α -lipoic acid **16** signals with the characteristic cycHC[8] signal, the binding of this molecule was not evaluated by ¹H NMR (Table 4, entry 9).

The binding of 1,3-dithiolane **8**, 1,4-thioxane **10**, and 1,4-dioxane **13** were further evaluated by ¹H NMR titration. The observed differences in guest binding to cycHC[8] appeared to be dependent on the hydrophobicity of the guests, which is determined based on the partition coefficients (logP) of the respective guest. The guest binding in methanol followed the order of logP values, and the results were in agreement with our screening studies (see details in **Publication III**). The strongest degree of binding was observed for 1,3-dithiolane **8** followed by 1,4-thioxane **10** and 1,4-dioxane **13**, with values of $K = 7.9 \pm 0.2 \text{ M}^{-1}$, $2.18 \pm 0.04 \text{ M}^{-1}$, and $1.77 \pm 0.04 \text{ M}^{-1}$, respectively. The association constants were determined by Dr. Sandra Kaabel and Tatsiana Shalima with a one-to-one binding model.

To determine the thermodynamic parameters for the binding of guests 1,3-dithiolane **8**, 1,4-thioxane **10**, and 1,4-dioxane **13**, isothermal titration calorimetry (ITC) experiments were performed with the assistance of Dr. Lukaš Ustrnul. The results are shown in (Table 5).

Table 5. Thermodynamic parameters from ITC experiments for the complexation of guests 1,3-dithiolane **8**, 1,4-thioxane **10**, and 1,4-dioxane **13** with cycHC[8] for the 1:1 binding model. All energy values are given in kJ/mol.

Entry	Guest	Solvent	ΔH°	$-T\Delta S^\circ$	ΔG°	K_a, M^{-1}
1		CH ₃ OH	-9.8 ± 0.6	3.6	-6.2	13.1 ± 0.8
2	1,3-dithiolane 8	CH ₃ OH:H ₂ O (50:50)	-20.4 ± 0.9	10.2	-10.2	65.6 ± 2.5
3		CH ₃ OH	-13.7 ± 1.2	11.4	-2.3	2.5 ± 0.2
4	1,4-thioxane 10	CH ₃ OH:H ₂ O (50:50)	-42.9 ± 3.9	39.6	-3.3	3.7 ± 0.3

The binding of 1,4-dioxane **13** to cycHC[8] in methanol was too weak to be determined by ITC; however, the K values for sulfur-heterocycles 1,3-dithiolane **8** and 1,4-thioxane **10** were in agreement with NMR data showing the strongest binding for the guest 1,3-dithiolane **8** (Table 5, entries 1 and 3). The binding of both guests in methanol was found to be enthalpically favorable and entropically unfavorable. A similar binding character was also observed upon the binding of chaotropic anions to cycHC[8] in

protonic media.^[106] Although chaotropy is mainly attributed to ionic species, chaotrope-like organic molecules have been identified in studies of crystalline hydrates.^[157] It has also been reported that chaotropic character is most strongly exhibited in aqueous media, and higher solvent polarity can enhance binding to the hydrophobic guest.^[62] Therefore, we further studied the binding of 1,3-dithiolane **8** and 1,4-thioxane **10** in a mixture of CH₃OH:H₂O. The binding of guests with cycHC[8] was indeed enhanced in the presence of water, with the association constant of 1,3-dithiolane **8** increasing from 13 M⁻¹ in CH₃OH to a value of 66 M⁻¹ in the 1:1 CH₃OH:H₂O (50:50) mixture (Table 5, entries 1 and 2). For the bulkier and less hydrophobic guest 1,4-thioxane **10**, the observed increase in the association constant was smaller (Table 5, entries 3 and 4). In the presence of water, the binding enthalpy increased dramatically, as did the entropic penalty for both guests (Table 5). Due to the very low water solubility of cycHC[8], a quantitative study of the binding thermodynamics of these guests in pure water was not feasible.

3.2.2 Selective Extraction of Sulfur Compounds from Water

The solution-state studies revealed that cycHC[8] binds selectively to guest 1,3-dithiolane **8**, and the binding efficiency is enhanced in the presence of water. The next task was to determine if cycHC[8] could be used as a solid sorbent for the selective removal of sulfur-containing heterocycles from water. It was also of interest to evaluate whether the inclusion complex-forming ability of cycHC[8] influences the sorption of heterocycles. For this purpose, the extraction experiments were performed in parallel with the 6-membered homolog (cycHC[6]) of cycHC[8]. Since cycHC[6] is made up of the same monomeric units as those of cycHC[8], its outer surface hydrophobic properties are very similar, but its cavity is much smaller (35 Å³),^[94] and therefore cannot accommodate the heterocycle studied. This critical knowledge served to differentiate between external physisorption and inclusion complex formation during extraction.

In addition, since the sorbent's textural properties, such as particle size and surface area, are critical for binding efficacy, the macrocyclic hosts were milled to obtain finer powders prior to the extraction experiments. The Brunauer-Emmett-Teller (BET) analysis of milled cycHC[*n*] by using N₂ adsorption-desorption (determined by Dr. Mai Uibu) revealed that the available surface area for both macrocycles cycHC[6] and cycHC[8] was very similar, with values of 6.03 m²/g and 9.02 m²/g, respectively. Based on this sorbent material analysis, cycHC[*n*] homologs were expected to have similar extraction efficiencies if the adsorption was solely dependent on the available surface area.

Solid-phase extraction (SPE) was performed for heterocycles 1,3-dithiolane **8**, 1,4-thioxane **10**, 1,4-dioxane **13**, α -lipoic acid **16**, by stirring the solid cycHC[*n*] sorbent in an aqueous solution of the respective guest. The change in guest concentration was analyzed after extraction and was assumed to be equal to the amount of host-guest complex formed. The extraction experiments were performed together with Tatsiana Shalima, and the extraction results are shown in Figure 35A. CycHC[*n*] showed negligible removal of the *O*-containing heterocycle 1,4-dioxane **14**, and only 5% of it was extracted using cycHC[8], whereas cycHC[6] was inefficient in this case. The use of cycHC[8] for SPE resulted in the efficient removal of *S*-containing heterocycles 1,3-dithiolane **8** (78%) and the moderate removal of 1,4-thioxane **10** (25%). CycHC[6] was found to be significantly less efficient at removing these guests, at 16% for 1,3-dithiolane **8** and only 3% for 1,4-thioxane **10**. In comparison to the removal of 1,3-dithiolane **8**, the results from the extraction of the larger and more hydrophobic α -lipoic acid **16** showed smaller

differences between binding to cycHC[6] and cycHC[8], respectively (%R values were 16% and 78% for 1,3-dithiolane **8** and 46% and 74% for α -lipoic acid **16**, respectively). This relatively small selectivity difference indicated a very different character for α -lipoic acid **16** binding to cycHCs, compared to that of 1,3-dithiolane **8**. With the aid of solid-state NMR spectroscopy (measured by Ivo Heinmaa), it was revealed that the interaction between α -lipoic acid **16** and cycHC[*n*]s occurs from the outside surface of the macrocycles, while 1,3-dithiolane **8** forms an inclusion complex with cycHC[8] (see details in **Publication III**).

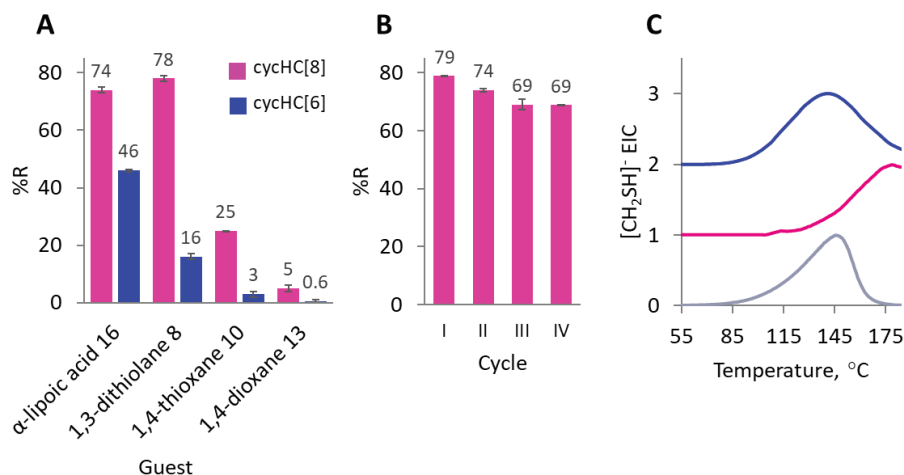


Figure 35. (A) %R exhibited by cycHC[8] and cycHC[6] (pink and dark blue) in water. (B) %R exhibited by cycHC[8] throughout repeated extraction cycles of guest 1,3-dithiolane **8**. In Figures 35A and 35B, %R is the amount of guest extracted in % from their aqueous solution by the respective cycHC[*n*], and the error bars represent the standard deviation between parallel experiments ($n \geq 2$). (C) Extracted ion current (EIC) of 1,3-dithiolane **8** fragment in TGA: 1 – pure 1,3-dithiolane **8**, 2 – cycHC[8] after extraction of 1,3-dithiolane **8**, and 3 – cycHC[6] after extraction of 1,3-dithiolane **8**.

As the reusability of sorbent content is a critical feature of SPE, it was shown that cycHC[8] can be reused after binding to guest 1,3-dithiolane **8**. For at least four cycles, a quick washing and drying process followed by milling enabled the surface of the sorbent to be reactivated for potential reuse, with no noticeable loss in binding efficiency (Figure 35B).

The formation of inclusion complexes in the cycHC[8] sorbent after SPE of 1,3-dithiolane **8** was further confirmed by thermogravimetric analysis (TGA). The TGA analysis of cycHC[*n*] sorbents enriched with 1,3-dithiolane **8** during extraction in parallel with pure 1,3-dithiolane **8** were performed by Dr. Kaia Tõnsuaadu, and the extracted ion current chromatograms are shown in Figure 35C. The TGA profile of pure 1,3-dithiolane **8** showed that at a certain temperature, it started to decompose, thereby releasing volatile degradation products. Formation of the 1,3-dithiolane **8** fragmentation product with $m/z = 47$, corresponding to $[\text{CH}_2\text{SH}]^-$, was detected by TGA combined with mass spectroscopy. The evolution profiles for pure 1,3-dithiolane **8** and its complex with cycHC[6] were similar. The decomposition products were released within the same temperature range, producing maximum ion current at 148 °C and 138 °C, respectively. Whereas, the complex with cycHC[8] released the characteristic degradation product at a significantly higher temperature at 189 °C. This observation suggests that 1,3-dithiolane **8**

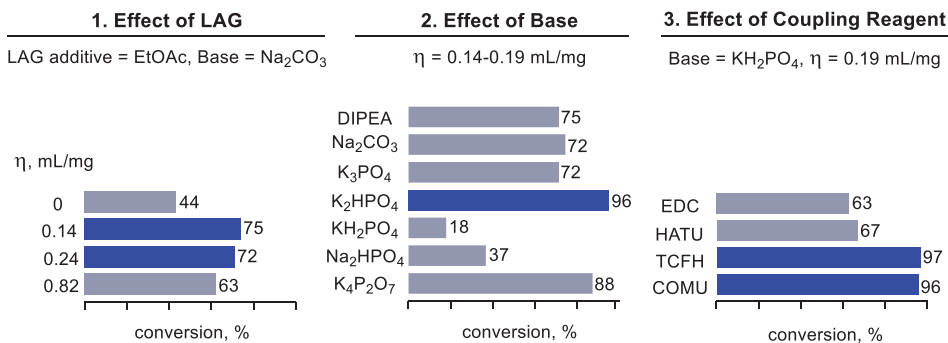
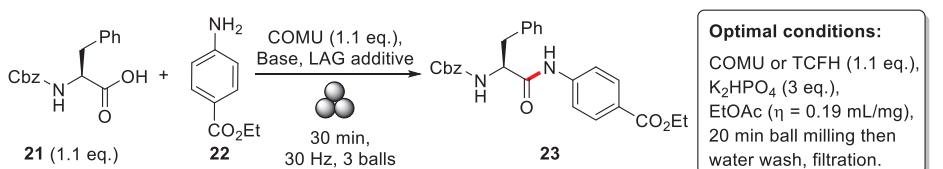
was encapsulated into the cycHC[8] cavity during the extraction procedure, which resulted in a higher affinity toward this guest.

To summarize, it was shown that in addition to binding anionic species, cycHC[8] can form inclusion complexes with suitably sized neutral heterocycles in a polar solvent and can be used as a sorbent for the selective removal of neutral hydrophobic sulfur-containing heterocyclic compounds from aqueous solutions. Because the solid macrocyclic host is reusable, we propose that it can have applications in the development of selective solid-phase extraction systems or can be employed in the selective removal of pollutants and other target compounds from water, based on molecular recognition properties.

3.3 Efficient Mechanochemical Synthesis of Amides (Publication IV)

Fine-tuning of macrocyclic structure could aid in exploring the potential of the synthesized macrocycles.^[20] Developing an efficient reaction protocol for the post-modification of these macrocycles may open new possibilities in a variety of fields. For example, mechanochemistry has proven to be an efficient method for the synthesis of cucurbituril,^[126] cycHC[6], and cycHC[8].^[124] This section addresses the development of a high-yield mechanochemical protocol for the direct synthesis of various amides from carboxylic acids and amines, with the use of uronium-type amide coupling reagents such as (1-cyano-2-ethoxy-2-oxoethylideneaminoxy)dimethylaminomorpholinocarbenium hexafluorophosphate (COMU) and *N,N,N',N'*-tetramethylchloroformamidinium hexafluorophosphate (TCFH). This section discusses how this novel approach can be used to synthesize functionalized biotin[6]uril through post-derivatization. My contribution to this work was in the substrate development, as indicated in Figure 37 (not marked with an asterisk), as well as in section 3.3.1, which gives an overview of the efficiency of screened coupling conditions in the synthesis of amide **33**.

The mechanochemical synthesis of amide bonds, using a one-step approach, was attempted based on the significant contribution of various research groups in developing the mechanochemical amidation protocols summarized in section 1.5.3. The extensive optimization studies were performed by Tatsiana Dalidovich. For these studies, the amide coupling of Cbz-protected L-phenylalanine **21** and ethyl 4-aminobenzoate (benzocaine, **22**), mediated by COMU was chosen as a model reaction (Figure 36). Optimization studies suggested that the reaction yield of amide **23** is influenced by three critical parameters, including the amide coupling reagent, base, and the quantity of liquid additive (LAG) used to assist the milling (see details in **Publication IV**). An overview of the results is outlined in Figure 36. After achieving these results, the optimal experimental procedure was formulated as follows: COMU or TFCH (1.1 eq.) as coupling reagents; K₂HPO₄ (3 eq.) as the base; ethyl acetate as the LAG additive, and a milling period of 20 minutes. Because all by-products in the synthesis of amide **23** were water-soluble, a simple water wash, followed by filtration, led to the isolation of pure amide **23** with a 96% yield in high stereochemical purity (>99% *ee*).



Structures of uronium-type coupling reagents used in optimization studies:

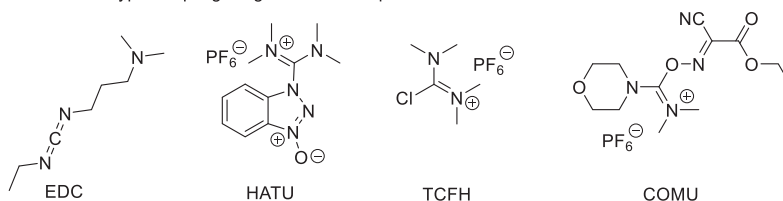


Figure 36. Overview of results from optimization studies for the synthesis of **23** and the chemical structures of the uronium-type coupling reagents. Adapted with permission from **Publication IV**.

With the optimal conditions in hand, we subsequently investigated the scope of the mechanochemical protocol with various amine and acid coupling partners possessing structural diversity in the starting materials. The results are summarized in Figure 37.

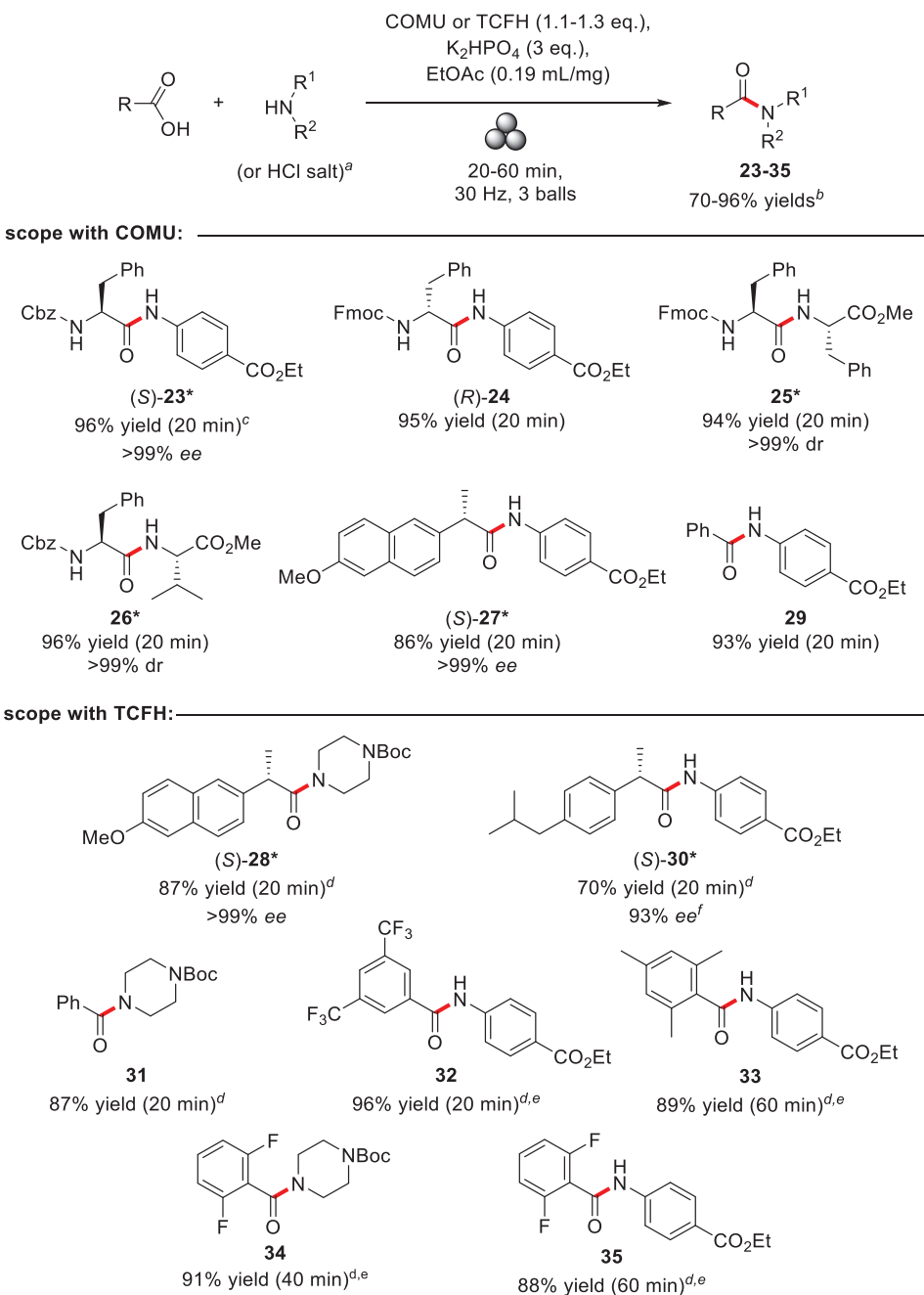
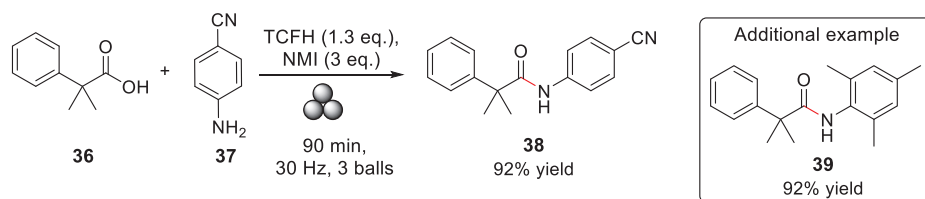


Figure 37. Substrate scope for mechanochemical amidation with COMU/ K_2HPO_4 and TCFH/ K_2HPO_4 systems. ^aAmine hydrochloride salt was used for the preparation of peptides **25** and **26**. ^bYields of isolated products. ^cObtained in 92% yield and >99% ee with TCFH. ^dIsolated by column chromatography. ^eWith 1.3 eq. of TCFH. ^f94% ee with COMU. *Synthesized by Tatsiana Dalidovich. Figure 37 is adapted with permission from **Publication IV**.

In addition to *N*- and *C*-protected amino acids, the substrate scope included various pharmaceutically relevant starting materials, such as (*S*)-naproxen, (*S*)-ibuprofen, benzocaine **22**, and *N*-Boc-protected piperazine. Similar to the Cbz-protected amide (*S*)-**23** described in detail in Figure 36, the Fmoc-protected analog of (*R*)-**24** was obtained in a high 95% yield under COMU-mediated reaction conditions. Following the same protocol, dipeptides **25** and **26**, which possess sterically hindered amino acid (phenylalanine and valine) components, were also synthesized efficiently, without showing any signs of epimerization of the stereocenters, and each resulting in 94% and 96% yields. The amide product (*S*)-**27** was obtained from (*S*)-(+)-6-methoxy- α -methyl-2-naphthaleneacetic acid (*S*)-naproxen with a high yield (86%) and remarkable stereochemical purity (>99% *ee*). This was likewise true for the TCFH-mediated reaction, which displayed strong reactivity and just a minor amount of epimerization for (*S*)-**28**. Amidation of (*S*)-ibuprofen (98% *ee*), on the other hand, yielded (*S*)-**30** with a slightly decreased enantiomeric purity (93% *ee*). Immediately after milling, crude amides **30**, **31**, and **34** appeared as oils and required chromatographic isolation. Even though the coupling of benzoic acid with benzocaine **22** went smoothly under the COMU-mediated procedure, yielding amide **29** in a 93% yield after 20 minutes of milling time, sterically hindered 2,4,6-trimethylbenzoic acid mesiotic acid **40** required TCFH as a coupling reagent to provide 89% of the target amide **33** after a longer milling time of 60 minutes. A decline in reactivity was also observed for 2,6-difluorobenzoic acid, which yielded amides **34** and **35** in reactions with *N*-Boc piperazine and low-nucleophilic amine **22** after milling times of 40 and 60 minutes, respectively. The coupling of the same amines with benzoic acid and 3,5-bis(trifluoromethyl)benzoic acid, on the other hand, proceeded smoothly and produced amides **31** and **32** with excellent yields and quick reaction times.

3.3.1 Mechanochemical Formation of Challenging Amide Bonds

To check the efficiency of the mechanochemical amidation protocols toward more challenging amide bond syntheses, the coupling of electron-deficient 4-aminobenzonitrile **37** with sterically hindered 2-methyl-2-phenylpropanoic acid **36** was executed. The optimization studies revealed the inefficiency of COMU and TCFH for the synthesis of amide product **38** (see details in **Publication IV**). Beutner *et al.*^[158] recently reported that combining TCFH and the *N*-methylimidazole (NMI) reagent produced high yields of amide **38** from a solution-state synthesis. Similarly, to our surprise, the same reagent combination resulted in a high yield of **38** (92%) (Figure 38). Following the same protocol, amide **39** was also obtained with a 92% yield. Thus, the high yields of amide **38** and **39** were achieved in an efficient reaction time of 1.5 hours, compared to a solution-based reaction that took 21 hours to produce amide **38**.^[158] Figure 38 illustrates the reaction mechanism involved in the activation of carboxylic acid by TCFH in the formation of amide **38** and **39**. According to the proposed reaction mechanism,^[158] in the first step TCFH and NMI react rapidly to form adduct *i*. The carboxylate anion from **36**, formed after deprotonation by the organic base NMI, attacks the adduct *i* to generate the unstable *O*-acyl (tetramethyl) isouronium salt *ii*. Another molecule of NMI from the reaction mixture attacks the intermediate *ii*, forming the highly reactive *C*-acyl imidazolium intermediate *iii* and releasing a stoichiometric amount of tetramethyl urea. The addition of amine **37** to acyl imidazolium *iii* produces amide **38** and simultaneously releases NMI, which scavenges the proton released from *iv* during C-N bond formation.



Mechanism:

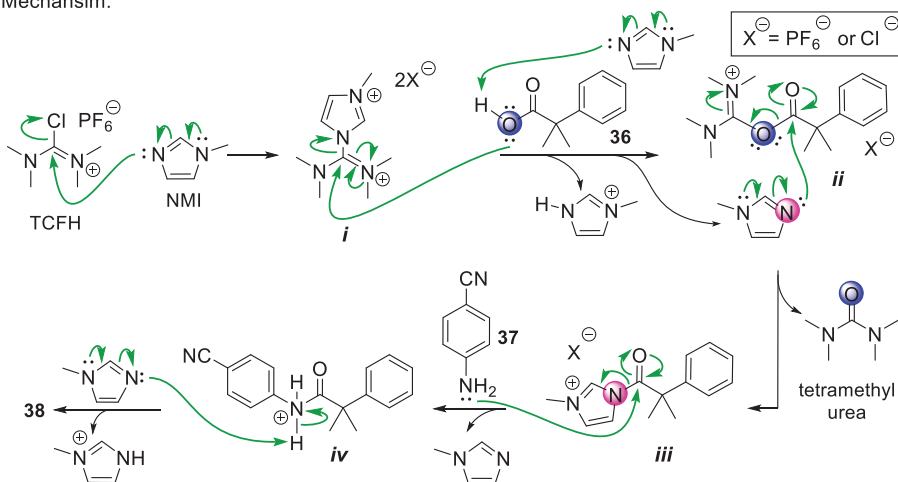
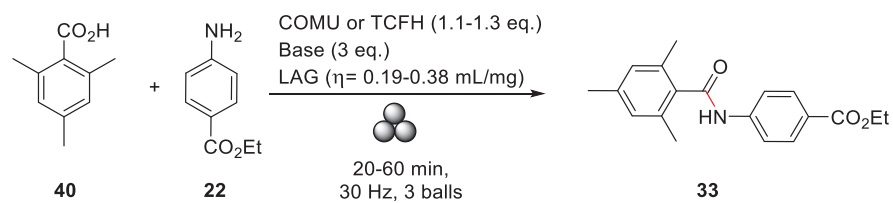


Figure 38. TCFH-NMI mediated mechanochemical amidation protocol for the synthesis of challenging amide products **38** and **39**. The reaction mechanism of TCFH-NMI is clarified using the synthesis of amide **38** from sterically hindered carboxylic acid **36** and poor nucleophilic amine **37**. Amide **38** and **39** were synthesized by Tatsiana Dalidovich.

Surprisingly, the highly reactive combination of NMI and TCFH reagents that had been investigated in the case of amide **38** and **39** resulted in only 22% yield of amide **33**. (Table 6, entry 1). The coupling reagent TCFH with K_2HPO_4 as a base, on the other hand, demonstrated remarkable efficiency in the formation of amide **33**, resulting in 92% conversion after 40 minutes of milling (Table 6, entry 2). The conversion was found to be further increased with a small excess (1.3 eq.) of TCFH and a longer milling time of 60 minutes (Table 6, entry 3). Under these conditions, 89% of amide **33** was obtained after chromatographic purification, which was needed to separate the mesitoic anhydride impurity. The COMU-mediated procedure provided only 22% of the target amide **33** (Table 6, entry 4), with no further change, even after a longer milling period (up to 60 minutes).

Table 6. Optimization of reaction conditions in the synthesis of amide **33**.



Entry	Coupling reagent	Base ^b	LAG (η)	Conversion by ¹ H NMR, % ^a		
				20 min	40 min	60 min
1	TCFH (1.3 eq.)	NMI ^c	NMI (0.38)	18	-	18
2	TCFH (1.1eq.)	K ₂ HPO ₄	EtOAc (0.19)	90	92	-
3	TCFH (1.3 eq.)	K ₂ HPO ₄	EtOAc (0.19)	95	-	99
4	COMU (1.1eq.)	K ₂ HPO ₄	EtOAc (0.19)	22	22	24

^aConversion of **22** into **33** was determined by ¹H NMR (characteristic signals of aromatic protons from starting benzocaine **22** at δ 6.64 and product **33** at δ 7.54-7.48 were integrated and recalculated into conversion). ^b3 eq. of base was used. ^c1.1 eq. of amine **22** was used. For details see **Publication IV**.

To understand the inefficiency of the TCFH/NMI reagent in producing **33**, Dr. Dmitry G. Kananovich performed the coupling reaction for amide **33** in solution-state (Figure 39). The reaction resulted in only 10% of the corresponding amide product, while 78% of mesitoic acid **40** was transformed into the inert imidazolium derivative **41**. We proposed that the inert nature of **41** is due to the steric shielding of its carbonyl group by the neighboring mesityl and imidazolyl moieties from both sides, which prevents the attack of nucleophile **22** along the Bürgi–Dunitz trajectory.

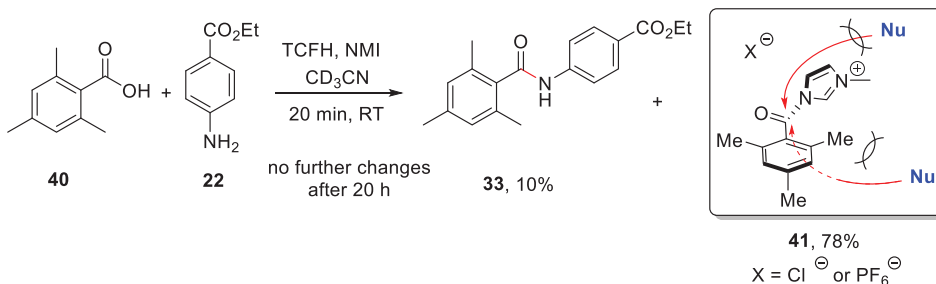


Figure 39. Synthesis of amide **33** in a solution-state, and the lowest energy conformer of imidazolium intermediate **41** with a sterically shielded carbonyl group.

3.3.2 Functionalization of Biotin[6]uril

As part of the ongoing efforts of the research presented in this thesis to develop new chiral supramolecular receptors, we further investigated the application of the mechanochemical protocol for the uniform derivatization of macrocycle biotin[6]uril. Biotin[6]uril is an enantiopure hemicucurbituril that has six carboxylic functionalities. Coupling these functionalities with various amines could provide easy access to a library of chiral functionalized macrocyclic receptors. Although the amide coupling of biotin[6]uril appears simple, the full amidation is challenging, as the reaction proceeds in

six consecutive steps. For example, if a reaction generates a 97% yield during each step, then the fully functionalized product would be produced in only $(0.97)^6 \cdot 100\% = 83\%$ yield, and the rest of the generated material would contain a mixture of under functionalized macrocycles. The resultant complex reaction mixture would require further chromatographic purification, which is time-consuming, labor-intensive, and inefficient in terms of mass. Tatsiana Dalidovich conducted extensive optimization experiments to synthesize hexa-amide **43** by coupling biotin[6]uril with the methyl ester of L-phenylalanine **42** used as the HCl salt (see details in **Publication IV**). Under the optimal conditions outlined in Figure 40, the required hexa-amide product **43** was obtained in 80% yield with 99% HPLC purity after a simple water wash followed by a simple purification protocol (filtration of chloroform solution *via* Celite® followed by precipitation with hexane from the EtOAc solution).

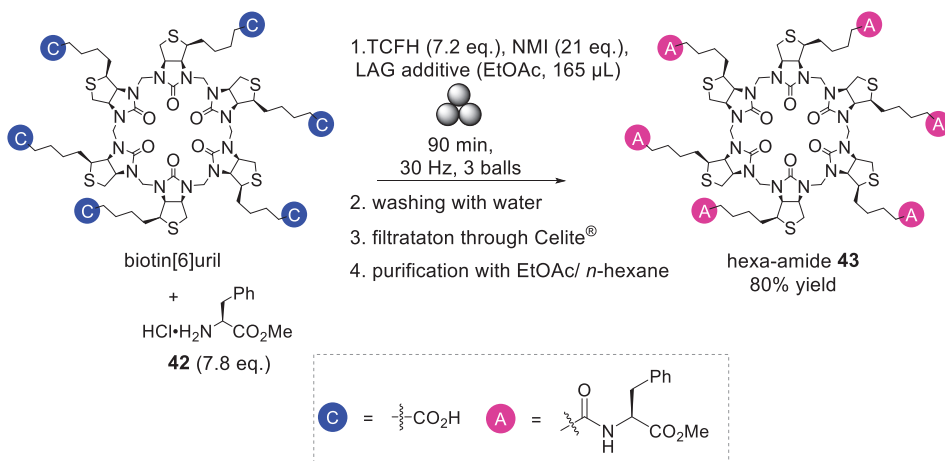


Figure 40. Amide coupling of biotin[6]uril via six-fold amidation with L-phenylalanine methyl ester (**42**).

To conclude, we have developed an efficient method to access the direct synthesis of amides from carboxylic acids and amines. The method utilizes uronium-based green coupling reagents such as COMU and TCFH and inexpensive non-toxic inorganic base K₂HPO₄. Using the conditions developed, challenging amide bonds between sterically hindered carboxylic acids and low-nucleophilic amines were efficiently formed in a short reaction time within the TCFH/K₂HPO₄ and TCFH/NMI system. The reaction procedure demonstrated characteristic features, including fast reaction rate, high yield, and simple isolation procedures for the solid products. In contrast to solution-based synthesis, the reaction is carried out under solvent-free conditions, which avoids wasting large volumes of solvent and greatly reduces various safety risks. The full amidation of biotin[6]uril was difficult to achieve, but with the use of a very reactive coupling reagent (TCFH/NMI) in combination with a longer reaction time and suitable LAG additive (EtOAc), a high yield and purity of hexa-amide **43** was obtained.

4 Conclusions

The state-of-the-art in the field of supramolecular chemistry is empowered by macrocycles functioning as selective host molecules, and there is a need for novel macrocycles with new properties. In this thesis, an overview of the cucurbituril-type host, including hemicucurbiturils, their synthesis, functionalization, and application, is presented. Options for promoting chirality induction during the synthesis of macrocycles from achiral and chiral monomers and *via* complexation with various guests are discussed. Additionally, solvent-free synthesis *via* mechanochemistry is described in this thesis and the literature overview.

The research covered in this thesis focuses on the synthesis of new chiral hemicucurbiturils and a study of their properties. The first enantiomerically pure 12-membered chiral cyclohexanohemicucurbituril (*R,R*)-cycHC[12], which is the largest substituted HC homolog to date, was synthesized and isolated by column chromatography with an overall yield of 1%. The structure of the isolated cycHC[12] resembles a concave octagon and displays a unique temperature-dependent conformation that has not been observed in previously known smaller HC derivatives.

Binding studies of cycHC[8] in methanol and methanol-water systems revealed the formation of an inclusion complex with compatibly sized 5- and 6-membered heterocycles, respectively. This complexation was favored in the presence of water and resembled the binding of chaotropic anion in water. Furthermore, cycHC[8] served as a solid sorbent for selective SPE of sulfur-containing heterocycles from their aqueous solution, and the reusability of the solid sorbent was also confirmed. During SPE, the selective nature of cycHC[8] towards five-membered sulfur-heterocycles was driven by inclusion-complex formation.

An efficient mechanochemical protocol for the direct synthesis of amide products from carboxylic acid and amines was investigated. The developed method used a simple isolation procedure for solid amide products that eliminated several drawbacks associated with a solution-based procedure. The established reaction protocol produced excellent yields of amide products after a short reaction time and was effective for the synthesis of a wide range of amides, namely *N*- and *C*-protected amino acids, peptides, and racemization-prone acids. The TCFH/ K_2HPO_4 and TCFH/NMI systems resulted in the rapid formation of amide bonds with challenging coupling components, such as sterically hindered carboxylic acids and poor nucleophilic amines. Most importantly, the new approach enabled post-derivatization of the polyfunctionalized substrate biotin[6]uril. The use of the highly reactive coupling reagent (TCFH/NMI), longer milling times (typically 90 minutes), and appropriate LAG (EtOAc) produced fully functionalized hexa-amide derivative of biotin[6]uril in high yield with high purity.

To summarize, the research described in this thesis led to the first largest chiral hemicucurbituril cycHC[12] and amide functionalized biotin[6]uril, as well as producing, for the first time, inclusion complexes with neutral organic heterocycles, enabling the application of cycHC[8] as a sorbent material for 5-membered sulfur-heterocycles. Therefore, the results in this thesis contribute to the expanding scope of knowledge in the field of hemicucurbiturils and supramolecular chemistry, which may lead to the development of new receptors and adsorbent materials.

References

- [1] J.-M. Lehn, *Angew. Chem. Int. Ed.* **1988**, *27*, 89–112.
- [2] J.-M. Lehn, *Angew. Chem. Int. Ed.* **2015**, *54*, 3276–3289.
- [3] J. Mallinson, I. Collins, *Future Med. Chem.* **2012**, *4*, 1409–1438.
- [4] D. Wu, A. C. Sedgwick, T. Gunnlaugsson, E. U. Akkaya, J. Yoon, T. D. James, *Chem. Soc. Rev.* **2017**, *46*, 7105–7123.
- [5] R. Mohammadzadeh Kakhki, *J. Incl. Phenom. Macrocycl. Chem.* **2013**, *75*, 11–22.
- [6] N. Morin-Crini, S. Fourmentin, É. Fenyvesi, E. Lichtfouse, G. Torri, M. Fourmentin, G. Crini, *Environ. Chem. Lett.* **2021**, *19*, 2581–2617.
- [7] X. Ji, H. Wang, H. Wang, T. Zhao, Z. A. Page, N. M. Khashab, J. L. Sessler, *Angew. Chem. Int. Ed.* **2020**, *59*, 23402–23412.
- [8] S. Kumar, M. Y. Wani, C. T. Arranja, J. de A. e Silva, B. Avula, A. J. F. N. Sobral, *J. Mater. Chem. A* **2015**, *3*, 19615–19637.
- [9] A. T. Frank, N. S. Farina, N. Sawwan, O. R. Wauchope, M. Qi, E. M. Brzostowska, W. Chan, F. W. Grasso, P. Haberfield, A. Greer, *Mol Divers* **2007**, *11*, 115–118.
- [10] S. J. Rowan, S. J. Cantrill, G. R. L. Cousins, J. K. M. Sanders, J. F. Stoddart, *Angew. Chem. Int. Ed.* **2002**, *41*, 898–952.
- [11] K. I. Assaf, W. M. Nau, *Chem. Soc. Rev.* **2014**, *44*, 394–418.
- [12] C. J. Pedersen, *Angew. Chem. Int. Ed.* **1988**, *27*, 1021–1027.
- [13] D. J. Cram, *Angew. Chem. Int. Ed.* **1988**, *27*, 1009–1020.
- [14] N. N. Andersen, M. Lisbjerg, K. Eriksen, M. Pittelkow, *Isr. J. Chem.* **2018**, *58*, 435–448.
- [15] T. Lizal, V. Sindelar, *Isr. J. Chem.* **2018**, *58*, 326–333.
- [16] V. Havel, M. A. Yawer, V. Sindelar, *Chem. Commun.* **2015**, *51*, 4666–4669.
- [17] M. A. Yawer, V. Havel, V. Sindelar, *Angew. Chem. Int. Ed.* **2015**, *54*, 276–279.
- [18] H. Cong, T. Yamato, X. Feng, Z. Tao, *J. Mol. Catal. Chem.* **2012**, *365*, 181–185.
- [19] R. Aav, E. Shmatova, I. Reile, M. Borissova, F. Topić, K. Rissanen, *Org. Lett.* **2013**, *15*, 3786–3789.
- [20] J. Sokolov, V. Šindelář, *Chem. Eur. J.* **2018**, *24*, 15482–15485.
- [21] J. Sokolov, A. Štefek, V. Šindelář, *ChemPlusChem* **2020**, *85*, 1307–1314.
- [22] M. Lisbjerg, H. Valkenier, B. M. Jessen, H. Al-Kerdi, A. P. Davis, M. Pittelkow, *J. Am. Chem. Soc.* **2015**, *137*, 4948–4951.
- [23] C. Lang, A. Mohite, X. Deng, F. Yang, Z. Dong, J. Xu, J. Liu, E. Keinan, O. Reany, *Chem. Commun.* **2017**, *53*, 7557–7560.
- [24] M. Lisbjerg, B. M. Jessen, B. Rasmussen, B. E. Nielsen, A. Ø. Madsen, M. Pittelkow, *Chem. Sci.* **2014**, *5*, 2647–2650.
- [25] J. W. Steed, D. R. Turner, K. Wallace, *Core Concepts in Supramolecular Chemistry and Nanochemistry*, John Wiley And Sons, Ltd, **2007**.
- [26] Z. Liu, S. K. M. Nalluri, J. F. Stoddart, *Chem. Soc. Rev.* **2017**, *46*, 2459–2478.
- [27] D. J. Cram, *Angew. Chem. Int. Ed.* **1986**, *25*, 1039–1057.
- [28] V. Balzani, A. Credi, F. M. Raymo, J. F. Stoddart, *Angew. Chem. Int. Ed.* **2000**, *39*, 3348–3391.

- [29] J.-P. Sauvage, S. J. F. Stoddart, B. L. Feringa, Nobel prize. Available online: http://www.nobelprize.org/nobel_prizes/chemistry/laureates/2016 (accessed on 9 April 2022).
- [30] L. Cronin, P. A. McGregor, S. Parsons, S. Teat, R. O. Gould, V. A. White, N. J. Long, N. Robertson, *Inorg. Chem.* **2004**, *43*, 8023–8029.
- [31] W. Saenger, J. Jacob, K. Gessler, T. Steiner, D. Hoffmann, H. Sanbe, K. Koizumi, S. M. Smith, T. Takaha, *Chem. Rev.* **1998**, *98*, 1787–1802.
- [32] K. Gessler, I. Usón, T. Takaha, N. Krauss, S. M. Smith, S. Okada, G. M. Sheldrick, W. Saenger, *PNAS* **1999**, *96*, 4246–4251.
- [33] K. Harata, T. Endo, H. Ueda, T. Nagai, *Supramol. Chem* **1998**, *9*, 143–150.
- [34] K. L. Larsen, *J. Incl. Phenom. Macrocycl. Chem.* **2002**, *43*, 1–13.
- [35] X.-B. Hu, Z. Chen, L. Chen, L. Zhang, J.-L. Hou, Z.-T. Li, *Chem. Commun.* **2012**, *48*, 10999–11001.
- [36] C. Bavoux, R. Baudry, I. Dumazet-Bonnamour, R. Lamartine, M. Perrin, *J. Incl. Phenom. Macrocycl. Chem.* **2001**, *40*, 221–224.
- [37] S. J. Barrow, S. Kasera, M. J. Rowland, J. del Barrio, O. A. Scherman, *Chem. Rev.* **2015**, *115*, 12320–12406.
- [38] R.-C. Mutihac, A. A. Bunaciu, H.-J. Buschmann, L. Mutihac, *J. Incl. Phenom. Macrocycl. Chem.* **2020**, *98*, 137–148.
- [39] Q. Li, S.-C. Qiu, J. Zhang, K. Chen, Y. Huang, X. Xiao, Y. Zhang, F. Li, Y.-Q. Zhang, S.-F. Xue, Q.-J. Zhu, Z. Tao, L. F. Lindoy, G. Wei, *Org. Lett.* **2016**, *18*, 4020–4023.
- [40] X.-J. Cheng, L.-L. Liang, K. Chen, N.-N. Ji, X. Xiao, J.-X. Zhang, Y.-Q. Zhang, S.-F. Xue, Q.-J. Zhu, X.-L. Ni, Z. Tao, *Angew. Chem. Int. Ed.* **2013**, *52*, 7252–7255.
- [41] W. A. Freeman, W. L. Mock, N. Y. Shih, *J. Am. Chem. Soc.* **1981**, *103*, 7367–7368.
- [42] J. Kim, I.-S. Jung, S.-Y. Kim, E. Lee, J.-K. Kang, S. Sakamoto, K. Yamaguchi, K. Kim, *J. Am. Chem. Soc.* **2000**, *122*, 540–541.
- [43] A. Day, A. P. Arnold, R. J. Blanch, B. Snushall, *J. Org. Chem.* **2001**, *66*, 8094–8100.
- [44] Y. Miyahara, K. Goto, M. Oka, T. Inazu, *Angew. Chem. Int. Ed.* **2004**, *116*, 5129–5132.
- [45] R. Behrend, E. Meyer, F. Rusche, *Justus Liebigs Ann. Chem.* **1905**, *339*, 1–37.
- [46] A. I. Day, R. J. Blanch, A. Coe, A. P. Arnold, *J. Incl. Phenom. Macrocycl. Chem.* **2016**, *43*, 247–250.
- [47] S. Liu, K. Kim, L. Isaacs, *J. Org. Chem.* **2007**, *72*, 6840–6847.
- [48] W.-H. Huang, P. Y. Zavalij, L. Isaacs, *J. Am. Chem. Soc.* **2008**, *130*, 8446–8454.
- [49] R. Aav, S. Kaabel, M. Fomitšenko, M. Chapter - 3.08 Cucurbiturils: Synthesis, Structures, Formation Mechanisms, and Nomenclature. In *Comprehensive Supramolecular Chemistry II*; Elsevier, **2017**, *3*, 203–220.
- [50] A. Chakraborty, A. Wu, D. Witt, J. Lagona, J. C. Fettinger, L. Isaacs, *J. Am. Chem. Soc.* **2002**, *124*, 8297–8306.
- [51] A. Wu, A. Chakraborty, D. Witt, J. Lagona, F. Damkaci, M. A. Ofori, J. K. Chiles, J. C. Fettinger, L. Isaacs, *J. Org. Chem.* **2002**, *67*, 5817–5830.
- [52] L. Isaacs, *Chem. Commun.* **2009**, 619–629.
- [53] W.-H. Huang, P. Y. Zavalij, L. Isaacs, *J. Am. Chem. Soc.* **2008**, *130*, 8446–8454.

- [54] L. Isaacs, S.-K. Park, S. Liu, Y. H. Ko, N. Selvapalam, Y. Kim, H. Kim, P. Y. Zavalij, G.-H. Kim, H.-S. Lee, K. Kim, *J. Am. Chem. Soc.* **2005**, *127*, 18000–18001.
- [55] H. Cong, X. L. Ni, X. Xiao, Y. Huang, Q.-J. Zhu, S.-F. Xue, Z. Tao, L. F. Lindoy, G. Wei, *Org. Biomol. Chem.* **2016**, *14*, 4335–4364.
- [56] A. Flinn, G. C. Hough, J. F. Stoddart, D. J. Williams, *Angew. Chem. Int. Ed.* **1992**, *31*, 1475–1477.
- [57] H. Isobe, S. Sato, E. Nakamura, *Org. Lett.* **2002**, *4*, 1287–1289.
- [58] L. Gilberg, M. S. A. Khan, M. Enderesova, V. Sindelar, *Org. Lett.* **2014**, *16*, 2446–2449.
- [59] S. Y. Jon, N. Selvapalam, D. H. Oh, J.-K. Kang, S.-Y. Kim, Y. J. Jeon, J. W. Lee, K. Kim, *J. Am. Chem. Soc.* **2003**, *125*, 10186–10187.
- [60] M. M. Ayhan, H. Karoui, M. Hardy, A. Rockenbauer, L. Charles, R. Rosas, K. Udachin, P. Tordo, D. Bardelang, O. Ouari, *J. Am. Chem. Soc.* **2015**, *137*, 10238–10245.
- [61] R. H. Gao, L. X. Chen, K. Chen, Z. Tao, X. Xiao, *Coord. Chem. Rev.* **2017**, *348*, 1–24.
- [62] K. I. Assaf, W. M. Nau, *Angew. Chem. Int. Ed.* **2018**, *57*, 13968–13981.
- [63] H.-J. Buschmann, E. Cleve, E. Schollmeyer, *Inorg. Chem. Commun.* **2005**, *8*, 125–127.
- [64] H.-J. Buschmann, A. Zielesny, E. Schollmeyer, *J. Incl. Phenom. Macrocycl. Chem.* **2006**, *54*, 181–185.
- [65] D.-D. Xiang, Q.-X. Geng, H. Cong, Z. Tao, T. Yamato, *Supramol. Chem.* **2015**, *27*, 37–43.
- [66] H. Cong, T. Yamato, Z. Tao, *J. Mol. Catal. A: Chem.* **2013**, *379*, 287–293.
- [67] X.-Y. Jin, F. Wang, H. Cong, Z. Tao, *J. Incl. Phenom. Macrocycl. Chem.* **2016**, *86*, 249–254.
- [68] X.-Y. Jin, F. Wang, H. Cong, Z. Tao, *J. Incl. Phenom. Macrocycl. Chem.* **2016**, *86*, 241–248.
- [69] H. Cong, T. Yamato, Z. Tao, *New J. Chem.* **2013**, *37*, 3778–3783.
- [70] E. I. Cucolea, H.-J. Buschmann, L. Mutihac, *Supramol. Chem.* **2016**, *28*, 727–732.
- [71] R. Kurane, P. Bansode, S. Khanapure, D. Kale, R. Salunkhe, G. Rashinkar, *Catal. Lett.* **2016**, *146*, 2485–2494.
- [72] V. Šindelář, T. Lízal, Chapter - 20 Hemicucurbiturils. *In Cucurbiturils and Related Macrocycles*; The Royal Society of Chemistry, **2020**, 527–545.
- [73] X. Yu, D. Sun, *Molecules* **2013**, *18*, 6230–6268.
- [74] L. A. Nguyen, H. He, C. Pham-Huy, *Int J Biomed Sci* **2006**, *2*, 85–100.
- [75] J. H. Kim, A. R. Scialli, *Toxicol. Sci.* **2011**, *122*, 1–6.
- [76] Development of New Stereoisomeric Drugs. Available online: <https://www.fda.gov/regulatory-information/search-fda-guidance-documents/development-new-stereoisomeric-drugs> (accessed on 9 April 2022).
- [77] X. Liang, W. Liang, P. Jin, H. Wang, W. Wu, C. Yang, *Chemosensors* **2021**, *9*, 279.
- [78] G. Gübitz, M. G. Schmid, *Mol. Biotechnol.* **2006**, *32*, 159–179.
- [79] M. H. Hyun, *Chirality* **2015**, *27*, 576–588.
- [80] A. Tyszka-Gumkowska, G. Pikus, J. Jurczak, *Molecules* **2019**, *24*, 2635.

- [81] S. J. Nemat, H. Jędrzejewska, A. Prescimone, A. Szumna, K. Tiefenbacher, *Org. Lett.* **2020**, *22*, 5506–5510.
- [82] S. Liu, C. Ruspic, P. Mukhopadhyay, S. Chakrabarti, P. Y. Zavalij, L. Isaacs, *J. Am. Chem. Soc.* **2005**, *127*, 15959–15967.
- [83] D. Das, K. I. Assaf, W. M. Nau, *Front. Chem.* **2019**, *7*, 619.
- [84] W.-H. Huang, P. Y. Zavalij, L. Isaacs, *Angew. Chem. Int. Ed.* **2007**, *46*, 7425–7427.
- [85] L. Kozerski, P. E. Hansen, *J. Phys. Org. Chem.* **1991**, *4*, 58–66.
- [86] W.-H. Huang, P. Y. Zavalij, L. Isaacs, *Org. Lett.* **2009**, *11*, 3918–3921.
- [87] S.-C. Qiu, K. Chen, Y. Wang, Z.-Y. Hua, F. Li, Y. Huang, Z. Tao, Y.-J. Zhang, G. Wei, *Inorg. Chem. Commun.* **2017**, *86*, 49–53.
- [88] R. Herges, *Chem. Rev.* **2006**, *106*, 4820–4842.
- [89] Q. Li, S.-C. Qiu, K. Chen, Y. Zhang, R. Wang, Y. Huang, Z. Tao, Q.-J. Zhu, J.-X. Liu, *Chem. Commun.* **2016**, *52*, 2589–2592.
- [90] X. Lu, L. Isaacs, *Org. Lett.* **2015**, *17*, 4038–4041.
- [91] L. Cao, G. Hettiarachchi, V. Briken, L. Isaacs, *Angew. Chem. Int. Ed.* **2013**, *52*, 12033–12037.
- [92] S. Jan, N. Marek, S. Vladimir, *Angew. Chem. Int. Ed.* **2010**, *49*, 2378–2381.
- [93] J. Rivollier, P. Thuéry, M.-P. Heck, *Org. Lett.* **2013**, *15*, 480–483.
- [94] E. Prigorchenko, M. Öeren, S. Kaabel, M. Fomitšenko, I. Reile, I. Järving, T. Tamm, F. Topić, K. Rissanen, R. Aav, *Chem. Commun.* **2015**, *51*, 10921–10924.
- [95] K. Maršálek, V. Šindelář, *Org. Lett.* **2020**, *22*, 1633–1637.
- [96] G. A. Hembury, V. V. Borovkov, Y. Inoue, *Chem. Rev.* **2008**, *108*, 1–73.
- [97] F. Biedermann, W. M. Nau, *Angew. Chem. Int. Ed.* **2014**, *53*, 5694–5699.
- [98] W. L. Leong, J. J. Vittal, *Chem. Rev.* **2011**, *111*, 688–764.
- [99] X.-L. Ni, X. Xiao, H. Cong, L.-L. Liang, K. Cheng, X.-J. Cheng, N.-N. Ji, Q.-J. Zhu, S.-F. Xue, Z. Tao, *Chem. Soc. Rev.* **2013**, *42*, 9480–9508.
- [100] X.-L. Ni, X. Xiao, H. Cong, Q.-J. Zhu, S.-F. Xue, Z. Tao, *Acc. Chem. Res.* **2014**, *47*, 1386–1395.
- [101] D. Whang, K. Kim, *J. Am. Chem. Soc.* **1997**, *119*, 451–452.
- [102] K.-M. Park, D. Whang, E. Lee, J. Heo, K. Kim, *Chem. Eur. J.* **2002**, *8*, 498–508.
- [103] K. Chen, Y.-F. Hu, X. Xiao, S.-F. Xue, Z. Tao, Y.-Q. Zhang, Q.-J. Zhu, J.-X. Liu, *RSC Adv.* **2012**, *2*, 3217–3220.
- [104] I. K. Yoo, Y. K. Kang, *Chem. Phys. Lett.* **2017**, *669*, 92–98.
- [105] E. Prigorchenko, S. Kaabel, T. Narva, A. Baškir, M. Fomitšenko, J. Adamson, I. Järving, K. Rissanen, T. Tamm, R. Aav, *Chem. Commun.* **2019**, *55*, 9307–9310.
- [106] S. Kaabel, J. Adamson, F. Topić, A. Kiesilä, E. Kalenius, M. Öeren, M. Reimund, E. Prigorchenko, A. Löökene, H. J. Reich, K. Rissanen, R. Aav, *Chem. Sci.* **2017**, *8*, 2184–2190.
- [107] L. Ustrnul, S. Kaabel, T. Burankova, J. Martõnova, J. Adamson, N. Konrad, P. Burk, V. Borovkov, R. Aav, *Chem. Commun.* **2019**, *55*, 14434–14437.
- [108] L. Ustrnul, T. Burankova, M. Öeren, K. Juhhimenko, J. Ilmarinen, K. Siilak, K. A. Mishra, R. Aav, *Front. Chem.* **2021**, *9*, 468.

- [109] M. Öeren, E. Shmatova, T. Tamm, R. Aav, *Phys. Chem. Chem. Phys.* **2014**, *16*, 19198–19205.
- [110] G. Zhang, M. Mastalerz, *J. Incl. Phenom. Macrocycl. Chem.* **2014**, *43*, 1934–1947.
- [111] V. Martí-Centelles, M. D. Pandey, M. I. Burguete, S. V. Luis, *Chem. Rev.* **2015**, *115*, 8736–8834.
- [112] J. C. Collins, K. James, *Med. Chem. Commun.* **2012**, *3*, 1489–1495.
- [113] S. L. James, C. J. Adams, C. Bolm, D. Braga, P. Collier, T. Friščić, F. Grepioni, K. D. M. Harris, G. Hyett, W. Jones, A. Krebs, J. Mack, L. Maini, A. G. Orpen, I. P. Parkin, W. C. Shearouse, J. W. Steed, D. C. Waddell, *Chem. Soc. Rev.* **2012**, *41*, 413–447.
- [114] R. S. Varma, *Green Chem.* **1999**, *1*, 43–55.
- [115] L. R. MacGillivray, G. S. Papaefstathiou, T. Friščić, T. D. Hamilton, D.-K. Bučar, Q. Chu, D. B. Varshney, I. G. Georgiev, *Acc. Chem. Res.* **2008**, *41*, 280–291.
- [116] T. Kimura, Chapter 7 - Application of Ultrasound to Organic Synthesis. *In Sonochemistry and the Acoustic Bubble*; Elsevier, **2015**, 171–186.
- [117] J.-L. Do, T. Friščić, *ACS Cent. Sci.* **2017**, *3*, 13–19.
- [118] J. L. Howard, Q. Cao, D. L. Browne, *Chem. Sci.* **2018**, *9*, 3080–3094.
- [119] J.-L. Do, T. Friščić, *Synlett* **2017**, *28*, 2066–2092.
- [120] J. G. Hernández, C. Bolm, *J. Org. Chem.* **2017**, *82*, 4007–4019.
- [121] T. Friščić, *Chem. Soc. Rev.* **2012**, *41*, 3493–3510.
- [122] D. Tan, T. Friščić, *Eur. J. Org. Chem.* **2018**, *2018*, 18–33.
- [123] L. Takacs, *Chem. Soc. Rev.* **2013**, *42*, 7649–7659.
- [124] S. Kaabel, R. S. Stein, M. Fomitschenko, I. Järving, T. Friščić, R. Aav, *J. Incl. Phenom. Macrocycl. Chem.* **2019**, *58*, 6230–6234.
- [125] B. İçli, N. Christinat, J. Tönnemann, C. Schüttler, R. Scopelliti, K. Severin, *J. Am. Chem. Soc.* **2009**, *131*, 3154–3155.
- [126] W. Xu, C. Li, *High Perform. Polym.* **2021**, *33*, 509–518.
- [127] A. Bose, P. Mal, *Beilstein J. Org. Chem.* **2019**, *15*, 881–900.
- [128] P. Ertl, E. Altmann, J. M. McKenna, *J. Med. Chem.* **2020**, *63*, 8408–8418.
- [129] D. S. MacMillan, J. Murray, H. F. Sneddon, C. Jamieson, A. J. B. Watson, *Green Chem.* **2013**, *15*, 596–600.
- [130] M. T. Sabatini, Lee. T. Boulton, H. F. Sneddon, T. D. Sheppard, *Nat. Catal.* **2019**, *2*, 10–17.
- [131] D. Margetić, V. Štrukil, Chapter 3 - Carbon–Nitrogen Bond-Formation Reactions. *In Mechanochemical Organic Synthesis*; Elsevier, **2016**, 141–233.
- [132] G. Kaupp, J. Schmeyers, J. Boy, *Tetrahedron* **2000**, *56*, 6899–6911.
- [133] Q. Cao, D. E. Crawford, C. Shi, S. L. James, *Angew. Chem. Int. Ed.* **2020**, *59*, 4478–4483.
- [134] V. Declerck, P. Nun, J. Martinez, F. Lamaty, *Angew. Chem. Int. Ed.* **2009**, *48*, 9318–9321.
- [135] J. G. Hernández, E. Juaristi, *J. Org. Chem.* **2010**, *75*, 7107–7111.
- [136] J. Bonnamour, T.-X. Métro, J. Martinez, F. Lamaty, *Green Chem.* **2013**, *15*, 1116–1120.

- [137] L. Gonnet, T. Tintillier, N. Venturini, L. Konnert, J.-F. Hernandez, F. Lamaty, G. Laconde, J. Martinez, E. Colacino, *ACS Sustainable Chem. Eng.* **2017**, *5*, 2936–2941.
- [138] T.-X. Métro, J. Bonnamour, T. Reidon, J. Sarpoulet, J. Martinez, F. Lamaty, *Chem. Commun.* **2012**, *48*, 11781–11783.
- [139] C. Duangkamol, S. Jaita, S. Wangngae, W. Phakhodee, M. Pattarawarapan, *RSC Adv.* **2015**, *5*, 52624–52628.
- [140] J. G. Hernández, K. J. Ardila-Fierro, D. Crawford, S. L. James, C. Bolm, *Green Chem.* **2017**, *19*, 2620–2625.
- [141] K. J. Ardila-Fierro, D. E. Crawford, A. Körner, S. L. James, C. Bolm, J. G. Hernández, *Green Chem.* **2018**, *20*, 1262–1269.
- [142] C. Bolm, J. G. Hernández, *ChemSusChem* **2018**, *11*, 1410–1420.
- [143] V. Štrukil, B. Bartolec, T. Portada, I. Đilović, I. Halasz, D. Margetić, *Chem. Commun.* **2012**, *48*, 12100–12102.
- [144] V. Porte, M. Thioloy, T. Pigoux, T.-X. Métro, J. Martinez, F. Lamaty, *Eur. J. Org. Chem.* **2016**, *2016*, 3505–3508.
- [145] R. W. Taylor, T.-C. Lee, O. A. Scherman, R. Esteban, J. Aizpurua, F. M. Huang, J. J. Baumberg, S. Mahajan, *ACS Nano* **2011**, *5*, 3878–3887.
- [146] S. Walker, R. Oun, F. J. McInnes, N. J. Wheate, *Isr. J. Chem.* **2011**, *51*, 616–624.
- [147] M. Pattabiraman, J. Sivaguru, V. Ramamurthy, *Isr. J. Chem.* **2018**, *58*, 264–275.
- [148] A. R. Mohite, O. Reany, *J. Org. Chem.* **2020**, *85*, 9190–9200.
- [149] V. Havel, J. Svec, M. Wimmerova, M. Dusek, M. Pojarova, V. Sindelar, *Org. Lett.* **2011**, *13*, 4000–4003.
- [150] O. Reany, A. Mohite, E. Keinan, *Isr. J. Chem.* **2018**, *58*, 449–460.
- [151] T. Fiala, V. Sindelar, *Synlett* **2013**, *24*, 2443–2445.
- [152] M. Fomitšenko, E. Shmatova, M. Öeren, I. Järving, R. Aav, *Supramol. Chem.* **2014**, *26*, 698–703.
- [153] A. Bondi, *J. Phys. Chem.* **1964**, *68*, 441–451.
- [154] M. Fomitšenko, A. Peterson, I. Reile, H. Cong, S. Kaabel, E. Prigorchenko, I. Järving, R. Aav, *New J. Chem.* **2017**, *41*, 2490–2497.
- [155] T. F. G. G. Cova, S. C. C. Nunes, A. J. M. Valente, T. M. V. D. Pinho e Melo, A. A. C. C. Pais, *J. Mol. Liq.* **2017**, *242*, 640–652.
- [156] M. Florea, W. M. Nau, *Angew. Chem. Int. Ed.* **2011**, *50*, 9338–9342.
- [157] Ł. Dobrzycki, P. Socha, A. Ciesielski, R. Boese, M. K. Cyrański, *Cryst. Growth Des.* **2019**, *19*, 1005–1020.
- [158] G. L. Beutner, I. S. Young, M. L. Davies, M. R. Hickey, H. Park, J. M. Stevens, Q. Ye, *Org. Lett.* **2018**, *20*, 4218–4222.

Acknowledgements

The work presented in this thesis was conducted within the Department of Chemistry and Biotechnology of Tallinn University of Technology (TalTech). I would like to express my gratitude for the financial supports that made this research possible, the Estonian Ministry of Education and Research (PUT692 and PRG399), the CoE in Molecular Cell Engineering (2014–2020.4.01.15–0013), the European Union H2020-FETOPEN grant 828779 (INITIO), the the ASTRA “TUT Institutional Development Programme for 2016-2022”, Graduate School of Functional Materials and Technologies (2014 – 2020.4.01.16 – 0032), and the ESF Dora Programs.

I am extremely grateful to my supervisor, Prof. Riina Aav, for her scientific guidance, continuous support, and patience during my PhD studies. You provided me with the opportunity to gain a thorough understanding of the exciting world of chemistry and assisted me in growing not only professionally in science, but also as a strong individual who I am today. I will be forever thankful for your kindness, valuable suggestions, and unwavering faith in me over the years.

This thesis was accomplished by the generous support and assistance of many people, and I would like to express my sincere appreciation to all of them.

I would like to express my great appreciation to all the co-workers and collaborators who have contributed to publications and helped me with my research. Many thanks to Dr. Dzmitry G. Kananovich, Dr. Lukaš Ustrnul, Dr. Sandra Kaabel, Dr. Maria Fomitšenko, Tatsiana Dalidovich, and Tatsiana Shalima for your excellent teamwork, and your contribution to this thesis is deeply appreciated. I wish to thank Dr. Jasper Adamson and Dr. Marina Kudrjašova for sharing your professional experience and kind assistance with NMR analysis and Dr. Mario Öeren for his help with computational chemistry. I also wish to thank Dr. Aleksander-Mati Müürisepp for helping with IR analysis and Kaia Tõnsuaadu for TG analysis.

I feel privileged to express my heartfelt gratitude to Prof. Anil. V. Karnik for introducing me to the world of asymmetric synthesis and for his exemplary guidance, patience as well as joyful time in the lab during my master’s studies.

I wish to thank the departmental faculty members and dear fourth-floor colleagues especially Dr. Kristin Erkman and Dr. Dmitri Trubitsõn for all their help and for creating a friendly atmosphere, as well as for giving me a sense of belonging over these years.

I am sincerely thankful to Dr. Victor Borovkov, Dr. Elena Prigorchenko, Dr. Anna Cowart, Marko, Kristjan, Jevgenija, Nele, and Jagadeesh for the fruitful discussions at the group seminars. I wish to thank Marek Kõllo for being by my side since the beginning of my PhD studies, assisting me in settling into the lab, supporting me with chemistry and technical skills, and for all the interesting discussions and pleasant working environment in the lab.

Special thanks to Dr. Maksim Ošeka for reviewing my thesis and providing valuable comments.

I express my wholehearted thanks to my family and dear friends for their unconditional love, support, and timely encouragement despite the long distance between us. I will be forever grateful to my mother, Nirmala Mishra, for providing me with the motivation and strength to explore new interests and follow my destiny. I thank and extend my love to Hemant Singh, my husband for being the constant source of joy and inspiration during my studies.

Abstract

Synthesis of Chiral Urea-based Macrocycles and their Application as Molecular Containers

The continuously emerging demand for macrocyclic receptors with interacting functional groups directed into a binding pocket has fueled the growth and development of cucurbituril chemistry. This thesis describes the synthesis, functionalization, and binding properties of cucurbituril-type hosts. The literature overview introduces various classes of macrocyclic hosts that have shown extraordinary application in supramolecular studies due to their unique binding properties. This overview is followed by an introduction to large-ring macrocycles. These are important host molecules, which possess flexible cavities that enable them to adapt the cavity in response to guest molecules. A brief overview of the literature concerning the different approaches towards induction of chirality in cucurbituril-type hosts is described with suitable examples. This section is followed by an introduction to cyclohexanohemicucurbiturils, with a description of their synthesis, mechanisms of formation, and specific binding properties. A comprehensive introduction to the field of mechanochemical synthesis is also provided, along with applications in the synthesis of solvent-free macrocyclic structures, as well as various amides and peptides. The results and discussion section of this thesis are divided into four subsections. The first subsection describes the various protocols for developing new chiral cucurbituril-type hosts by introducing an element of chirality into the core of the macrocyclic structure. Examples from published data are thoroughly reviewed and discussed in the literature section of this thesis. In the second subsection, the synthesis, isolation, and characterization of the largest substituted hemicucurbituril, *i.e.*, cycHC[12], is discussed. The conformational analysis supported by VT-NMR revealed a distinctive feature of this enantiomerically pure host with its ability to show temperature-dependent dynamics, such as bridge flip and monomer flip, which is absent in other smaller counterparts. The third section presents the binding behavior of cyclohexanohemicucurbit[8]uril (cycHC[8]) toward neutral heterocycles, characterized by single-crystal X-ray diffraction analysis (SC-XRD), ¹H NMR, isothermal titration calorimetry (ITC), solid-state ¹³C NMR, and thermogravimetry techniques. These studies revealed the formation of an enthalpy-driven 1:1 complex in solution. Binding strength was observed to increase in the presence of water, which allowed for the development of sorption conditions by the solid cycHC[8], which acts as sorbent material for the selective removal of sulfur-heterocycles from water. Additionally, a greener synthetic procedure for cucurbituril-type hosts was developed in order to avoid use of large excesses of solvent and chromatographic purification steps. This mechanochemical approach is discussed in section 3.3 and describes an efficient and environmentally friendly one-pot protocol that can be used to derivatize biotin[6]uril, a member of the hemicucurbituril family, as well as to synthesize amides and peptides.

Current research provides a good foundation for the synthesis of sorbents and chiral receptors for applications in environmental, pharmaceutical, and materials science.

Lühikokkuvõte

Kiraalsete urea-põhiste molekulaarsete mahutite süntees ja rakendus

Supramolekulaarne keemia rakendab kontrollitult üksikute molekulide omadust olla vastasmõjus teiste molekulide või ioonidega. Hea kontrolli molekulide vaheliste interaktsioonide tekkeks annavad makrotsüklid. Viimased on molekulid, kus enam kui 12 aatomit on ringiks ühendatud ja nende sisemusse moodustub kindla kuju ja suurusega õõnsus. Funktsionaalrühmade kindel paigutus makrotsükli struktuuris tagab selektiivsekomplekseerumise külalismolekuliga.

Käesoleva doktoritöö kirjanduse ülevaade kirjeldab oligomeerseid kukurbituriili tüüpi makrotsükleid, nende hulgas hemikukurbituriile, nende sünteesi, funktsionaliseerimist ja rakendamist. Kirjeldatakse käelisuse indutseerimist nimetatud makrotsükklitesse, lähtudes sünteesil akiraalsetest või kiraalsetest monomeeridest, või saavutatakse käelisuus komplekseerumisel kiraalsete külalismolekulidega. Lisaks antakse ülevaade kiiresti arenevast ja keskkonnasõbralikust sünteesimeetodist – lahustivabast mehhanokeemiast.

Eksperimentaalse töö käigus otsiti meetodeid uute käeliste hemikukurbituriilide sünteesiks. Sünteesiti ja eraldati kõrge puhtusega käeline 12-ühikuline tsükloheksanohemikukurbituriil – *R,R*-cycHC[12], ning kirjeldati selle molekuli õõnsuse konformatsiooni sõltuvust temperatuurist. Sellist dünaamilist sõltuvust temperatuurist, kus makrotsükli konformatsiooni muutus toob kaasa aatomite vahelise kauguse muutuse kuni 1 nm, ning samas säilib õõnsuse olemasolu, pole varem hemikukurbituriilide puhul kirjeldatud. Seega avardati arusaama hemikukurbituriilide omadustest. Uuriti ka 8-ühikulise hemikukurbituriili – cycHC[8] komplekseerumist ning leiti, et tekivad selektiivselt sulgühendid ehk kompleksid, kus külalismolekul on seotud makrotsükli õõnsusesse. Nimelt seonduvad cycHC[8] õõnsusesse 5- ja 6-lülilised heterotsüklid, sest cycHC[8] õõnsus on oma suuruse ja elektroonsete omaduste tõttu sobiv nende ühenditega vastasmõjude tekkeks. Tugevaim interaktsioon cycHC[8] õõnsuses tekkis 5-ühikulise väävel-heterotsükliga 1,3-ditiolaaniga, ning sulgkompleksi teke tõestati tahke faasi tuumamagnetresonantsi ja termogravimeetrilise analüüsi abil. CycHC[8] rakendati selektiivseks väävel-heterotsükli eraldamiseks veest tahke-faasi ekstraktsioonil ja näidati, et cycHC[8] on korduvkasutatav sorbent.

Lisaks töötati välja efektiivne meetod amiidide sünteesiks aktiveerimata karboksüülhapetest ja amiinidest. Süntees teostati tahkes faasis mehhaanilise aktivatsiooni abil kuulveskis ning välditi orgaaniliste lahustite kasutust. Sünteesiti kõrge saagise ja lühikese reaktsiooniajaga amiide nii kaitstud amino- kui karboksüülrühmaga aminohapetest, peptiididest kui ka labiilse stereokeemilise tsentriga karboksüülhapetest. Samuti leiti tingimused, mis andsid häid tulemusi reaktsioonides madala nukleofiilsusega amiinide ja steeriliselt takistatud karboksüülhapetega. Kõige märkimisväärsem on aga see, et uue meetodiga õnnestus sünteesida kõrge puhtuse ja saagisega uus funktsionaliseeritud hemikukurbituriil – biotiin[6]uriili heksaamiid.

Kokkuvõtteks käesoleva doktoritöö raames leiti meetodid kahe uue kiraalse hemikukurbituriili saamiseks (cycHC[12] ja biotiin[6]uriil heksaamiid) ning laiendati hemikukurbituriilide rakendust, kirjeldades cycHC[12] konformatsioonilist dünaamikat ja väävel-heterotsükli komplekseerumist cycHC[8]-ga tahke-vedelik piirpinnal.

Seega antud töö tulemused kasvatasid teadmisi supramolekulaarse keemia vallas, mis on vajalik uute ja selektiivsete retseptorite ning sorbentmaterjalide loomisel, ning on rakendatavad keskkonna-, farmaatsia- ja materjaliteaduses.

Appendix 1

Publication I

R. Aav, **K. A. Mishra**, 'The Breaking of Symmetry Leads to Chirality in Cucurbituril-Type Hosts'. *Symmetry*, **2018**, *10* (4), 98.

Reprinted with permission from MDPI Open Access License Agreement rules.

Review

The Breaking of Symmetry Leads to Chirality in Cucurbituril-Type Hosts

Riina Aav *  and Kamini A. Mishra 

Department of Chemistry and Biotechnology, School of Science, Tallinn University of Technology, Akadeemia tee 15, 12618 Tallinn, Estonia; kamish@ttu.ee

* Correspondence: riina.aav@ttu.ee; Tel.: +372-620-4365

Received: 2 February 2018; Accepted: 30 March 2018; Published: 5 April 2018



Abstract: Cucurbituril-type hosts are highly symmetric, but there are means to break their symmetry. This review will present examples from three directions of induction of chirality in or by cucurbituril-type hosts: first, through the incorporation of stereogenic elements into host molecules; second, through complexation with achiral guests, which leads to axial supramolecular chirality and helical structures; third, through the formation of complexes with chiral guests in multi-molecule complexes and induction of supramolecular chirality. In addition, a list of chiral guests used in binding studies with cucurbiturils is collected. We would envision that encouraged by the outlined examples of outstanding applications of chiral cucurbituril-supramolecular systems, the boundaries of chiral applications of cucurbiturils would be widened.

Keywords: cucurbiturils; hemicucurbiturils; chirality; supramolecular chirality; symmetry breaking; helices

1. Introduction

Cucurbituril (CB)-type hosts are oligomeric compounds, where cyclic urea monomers are connected through methylene bridges. Core CBs are double-bridged macrocycles, which are made from glycoluril and formaldehyde [1–4]. Further on, the family has enlarged [5–7]. One can divide CBs into two main branches: the double-bridged and single-bridged CBs (Figure 1). All CBs have hydrophobic cavities, but electronic binding properties are different for single- and double-bridged CBs. Double-bridged CBs bind cations at the portals and single-bridged CBs anions in their cavity. All single-bridged CBs can be viewed as derivatives of hemicucurbiturils (HCs). HCs are formed in condensation of ethylene urea and formaldehyde, and cyclohexano-HC, bambusurils and biotinuril all contain linked ethylene urea moieties in their structures.

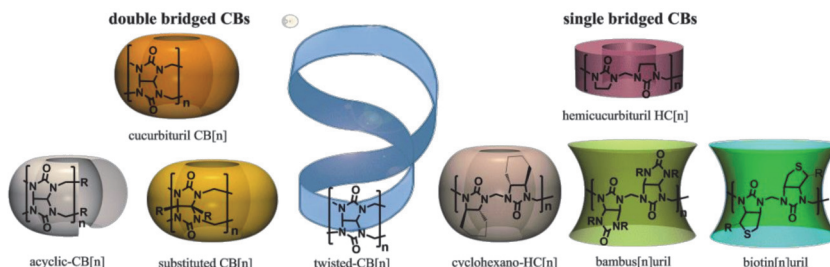


Figure 1. Cucurbituril-type hosts. CB, cucurbituril; HC, hemicucurbituril.

CB chemistry has been reviewed from various aspects [5–28], though so far, only one focused on the chirality of CBs [29]. CB-type hosts are very symmetric, but there are means to break this symmetry. This review will present examples from three directions of inducing chirality in CB chemistry: first, through the incorporation of stereogenic elements into the structure of CBs, through stereogenic atoms and helices; second, through complexation with achiral guests, which leads to axial supramolecular chirality in the helical structures; third, through the formation of complexes with chiral guests in multi-molecule complexes and induction of supramolecular chirality. In addition, a list of chiral guests that have been used in studies with CB-type hosts is collected.

2. Chiral Cucurbituril-Type Hosts

In general, the structures of core cucurbiturils are very symmetric. The CB[6] has seven planes of symmetry, as shown in Figure 2. Three vertical planes of symmetry pass through urea oxygens and three vertical planes through methylene bridges; additionally, one horizontal plane goes through the equator of the macrocycle.

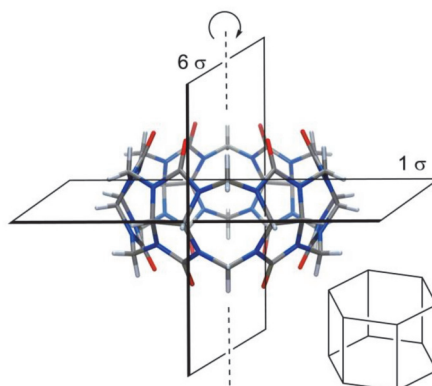


Figure 2. CB[6] and its planes of symmetry.

Because of these symmetry planes, neither substitution at a single methylene bridge nor at hydrogens of monomers by achiral groups will lead to chirality in the CB. To induce chirality, one must make changes at least at two methylene bridges in a way that disrupts all symmetry planes. In (\pm) -bis-*nor-seco*-CB[6] (Figure 3A), two methylene bridges are missing and trimeric glycolurils are connected in a diagonal fashion. Because of this, all glycoluril CH carbons become stereogenic, and as there are no symmetry planes, the macrocycle is chiral. Of course, if such a compound is formed in an achiral medium, then equal amounts of enantiomers are produced [30].

Isaacs et al. investigated the formation of host–guest complexes of (\pm) -bis-*nor-seco*-CB[6] in D₂O with a number of chiral compounds (Figure 3B) [30]. Intriguingly, differences in NMR signals were noted while complexes were formed from enantiopure or racemic guests with (\pm) -bis-*nor-seco*-CB. This observation is clear evidence of the formation of different supramolecular complexes. In a simple system, when one host enantiomer forms a complex with an enantiomerically pure guest, a single enantiomerically pure complex is formed. If an enantiomerically pure guest complexes with the chiral racemic host, then a mixture of two diastereomeric and enantiomerically pure complexes will be formed. By ¹H-NMR spectroscopy, one can distinguish diastereomers, and therefore, two sets of signals can appear. Now, if both chiral compounds would be mixed as racemates, then the same two diastereomeric complexes will be formed, just racemic complexes. By a simple NMR measurement, one cannot see the difference between enantiomerically pure and racemic complexes; therefore, the NMR spectra are expected to be the same. The situation with (\pm) -bis-*nor-seco*-CB[6] is not that simple. Isaacs et al. noted that the ratio of diastereomeric host–guest complexes is influenced by the guest stereoisomeric

purity. The reasons for these observations were not disclosed, but the aggregation of one or both chiral entities used in the study might have influenced the NMR signals [31,32]. Binding dynamics were dependent on the structure of the guest, as NMR spectra of (\pm)-bis-*nor-seco*-CB[6] showed increased complexity and multiplicity in the presence of an aromatic chiral guest, referring to binding where guests are not exchanged on the NMR timescale. On the other hand, NMR peaks became very broad upon complexation with aliphatic guests, referring to association-dissociation during the measurement at room temperature.

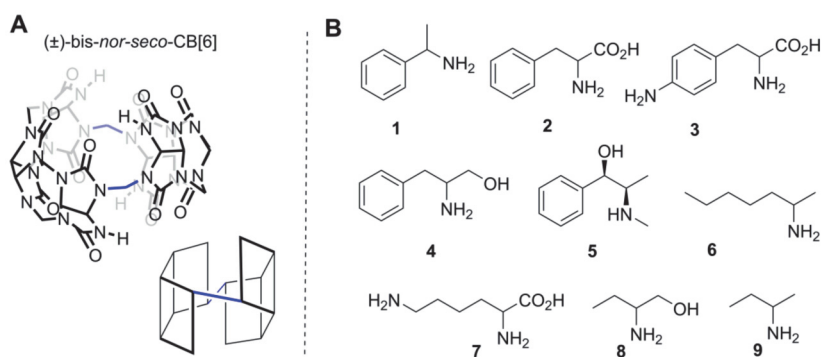


Figure 3. (A) One enantiomer of (\pm)-bis-*nor-seco*-CB[6]; (B) chiral guest whose binding was studied with (\pm)-bis-*nor-seco*-CB[6].

According to our knowledge, only a few chiral compounds have been isolated to date from the condensation reaction between glycoluril and formaldehyde, the abovementioned (\pm)-bis-*nor-seco*-CB[6] and acyclic 10-membered oligomer [33] (Figure 4), which have stereogenic atoms and twisted-CBs [34–36], which possess axial chirality (Figure 6). In the acyclic 10-membered oligomer, two pentamers are connected to each other through a single bond with no plane of symmetry.

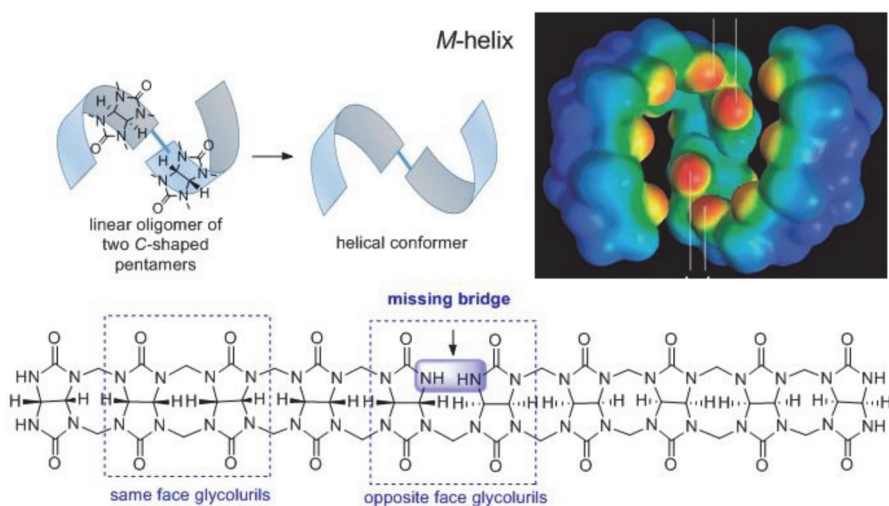


Figure 4. Map of electronic potential of a single enantiomer of the (\pm)-glycoluril decamer in the shape of an *M*-helix (adopted with permission from [33]) and its structure.

It is remarkable how a very small change in the structure of the oligomer, like the single turn of the face of the glycoluril and disconnection of one methylene bridge, can affect the geometry of the molecule. Oligomers, where same face glycolurils are linked, have a C-letter-shaped conformation, and they are achiral and can form a macrocycle. Absence of one methylene bridge in (\pm)-glycoluril decamer turns all glycoluril CH carbon atoms stereogenic, which induced its crystallization in a helical conformation. As this compound was formed in an achiral medium, two opposite-handed helices were formed in a ratio of 1:1 [33]. Binding with chiral guests was not probed with (\pm)-glycoluril decamer.

C-letter-shaped conformation of glycoluril oligomers and their ability to bind guest through electrostatic interactions with glycoluril carbonyl groups encouraged Isaacs to develop a new branch type of CB-type molecules, the acyclic CBs. To enrich oligomer structure with sites for additional functionalization and to add UV-active properties, Isaacs used substituted aromatic groups at the terminus of acyclic CBs. The structures of chiral and enantiopure acyclic CBs are shown in Figure 5A [37].

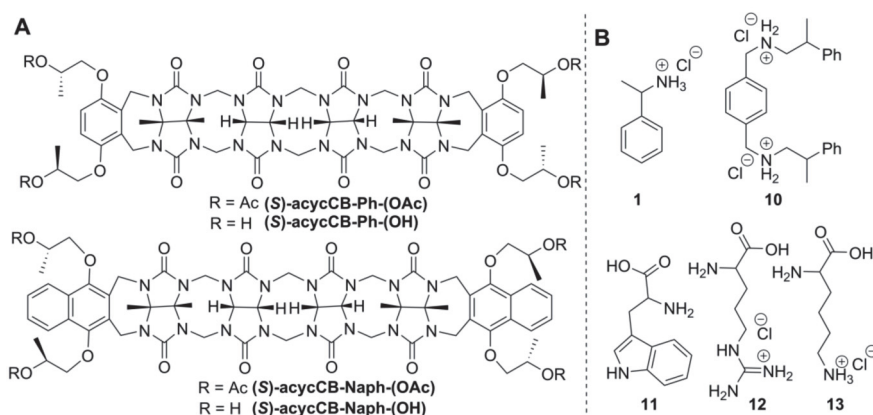


Figure 5. (A) Chiral acyclic CBs; (B) chiral guests, whose binding was studied with acyclic CBs [37].

Chiral acyclic CBs showed binding with ammonium-functionalized guest (Figure 5B) in acetic acid buffer at pH 5.5, and association constants were found to be in range of 10^3 – 10^6 M^{-1} . Small enantioselectivity in the binding of opposite enantiomers was also detected. The ratio of association constants for binding the (*S*)-**1** over (*R*)-**1** the $K_{(S)}/K_{(R)}$ was 1.3 for binding with (*S*)-acycCB-Ph-(OAc). Unfortunately, the binding of guest **1** to host (*S*)-acycCB-Ph-(OH) and guest **10** to both chiral acyclic CBs (*S*)-acycCB-Ph-(OAc) and (*S*)-acycCB-Ph-(OH) gave very close $K_{(S)}$ and $K_{(R)}$ values, and as the differences in measured K values were in the range of the measurement uncertainty, one can conclude that enantiodiscrimination is either absent or very small. The hosts (*S*)-acycCB-Naph-(OAc) and (*S*)-acycCB-Naph-(OH) were also able to bind cationic guests, but association constants could not be determined.

Isaacs has also developed a synthesis of functionalized CBs through macrocyclization of glycoluril hexamer and substituted glycoluril. By this strategy, amino acids and biotin were linked covalently to CBs, and efficient uptake of Oxaliplatin by cancer cells was achieved [38]. Recently, a polymeric biomaterial was prepared from glucose-based polymer: dextran and covalently-bound acyclic CB. This sugar-based chiral polymer was used for encapsulation of antitumor drugs, and its chiral properties were not investigated [39].

Apart from the listed CBs, which incorporate stereogenic centers in their structure, there is a special sub-class of CBs, which do not have stereocenters, but are still chiral. These are twisted CBs with axial chirality. The crystal structure of CB[14] revealed helical conformations of this CB, and therefore, the name *twisted*-CB[14] [34,35] was given (Figure 6). Currently there are three known CBs with 13,

14 and 15 glycolurils in their structures that have a helical conformation (Figure 6). Twisted CBs have a 360° turn in their oligomer belt, and the direction of this turn defines the stereochemistry of the macrocycle. Helical conformation is locked into the macrocyclic structure. One should mention that, in *twisted*-CB[13–15]s [34,36], the belt is formed so that all glycoluril monomers have the same faces linked next to each other, so these are not Möbius band [40]. Curiously, in aqueous solution, without any guests, *twisted*-CB[14] looks like normal cucurbituril, having only three signals in its $^1\text{H-NMR}$. Despite that, complexation studies of *twisted*-CB[14] in solution showed binding of a 1,8-octyldiammonium in a 1:1 stoichiometry, similarly to CB[8], with a K_a of $7.9 \times 10^6 \text{ M}^{-1}$, and smaller 1,4-butyldiammonium guest binds in a 1:2 ratio, with K_a values of $1.9 \times 10^8 \text{ M}^{-1}$ and $2.9 \times 10^6 \text{ M}^{-1}$, indicating clearly that *twisted*-CB[14] has two separate binding compartments and that these compartments are adaptable [41].

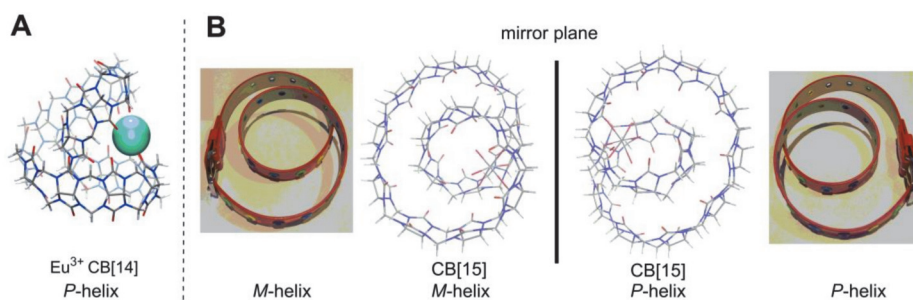


Figure 6. (A) ($\text{Eu}^{3+}\cdot\text{CB}[14]$) side view of *P*-helix [34]; (B) top view of ($\text{Cd}^{2+}\cdot\text{CB}[15]$) in *M*- and *P*-helical conformations formed in the same crystal [36] and illustration of these helix configurations with a belt.

Single-bridged CB-type macrocycles (Figure 1), the hemicucurbiturils [6,42] (HC), also have high symmetry like most CBs. The structure of an unsubstituted six-membered HC is shown in Figure 7. The monomers of HC are positioned in a “zig-zag” manner; therefore, HCs have fewer planes of symmetry in their structure than the parent CBs. Six-membered unsubstituted HC (Figure 7) and substituted HCs, which are formed from achiral monomers (Figure 8A), have three planes of symmetry.

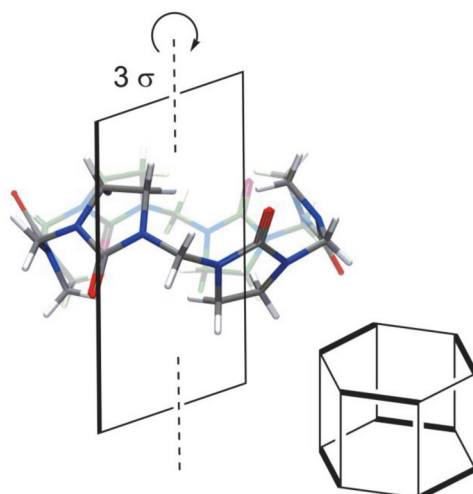


Figure 7. Hemicucurbit[6]uril [42] and its planes of symmetry.

Bambusurils [22,43] are a sub-class of single-bridged CBs that are made of achiral monomers (Figure 8B). One can see that nonequivalent R-substituents at glycolurils would lead to desymmetrization and creation of stereogenic centers at carbons of fused cycles. In this way, the formation of chiral bambusurils would be feasible.

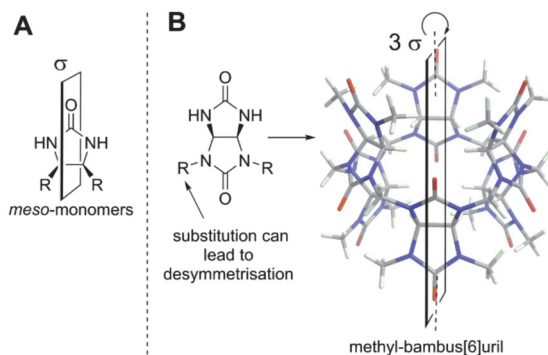


Figure 8. (A) The general structure of achiral substituted ethylene urea; (B) crystal structure of achiral methyl-bambus[6]uril [43] and its monomer.

Very interesting desymmetrization was achieved in azabambusuril [23,44] (Figure 9): substitution of a sulfur atom in symmetric thiobambusurils with an alkylimine moiety leads to the loss of all symmetry planes in this macrocycle.

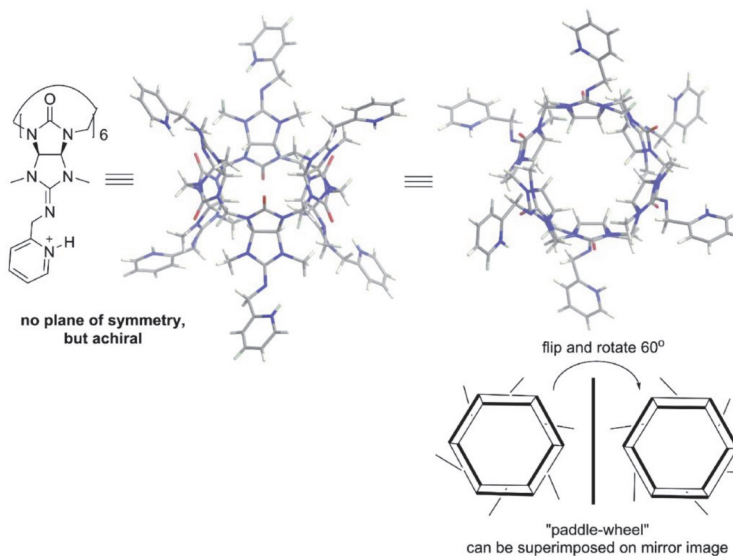


Figure 9. Drawing and crystal structure of protonated picolyl-azabambusuril [44] and cartoon of its “paddle-wheel” configuration.

The alkyl-azabambusuril crystal structure [44] revealed its “paddle-wheel”-like configuration. The unidirectional orientation of the imine double bonds in azabambusuril (Figure 9, right side), reflects high diastereoselectivity during their formation. Curiously, in spite of the desymmetrization

of bambusuril monomer, alkyl-azabambusuril is achiral, as its mirror image can be superimposed by flipping and rotating this “paddle-wheel” (Figure 9). Nevertheless, in the future chiral bambusurils could be made from nonuniformly substituted monomers.

As one can see, HCs have many options for the incorporation of stereogenic atoms into their structure, and several of them have been prepared in enantiopure form with high yield and in a single macrocyclization step [45–47]. Chiral (*S,S*)- or (*R,R*)-cyclohexano-hemicucurbit[6,8]urils (cycHC) are derived from enantiopure cyclohexa-1,2-diylurea [45,47] (Figure 10A), and biotin[6]uril from the vitamin biotin [46] (Figure 11).

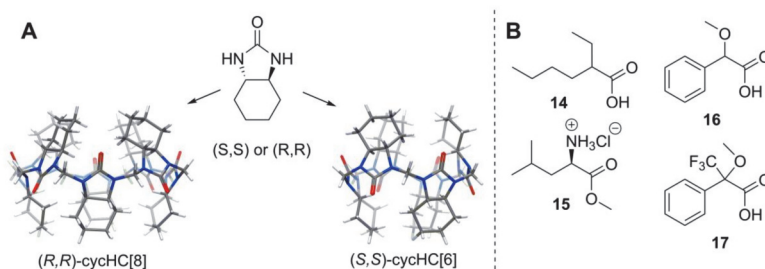


Figure 10. (A) Structure of cyclohexa-1,2-diylurea and crystal structure of chiral cycHCs [45,47]; (B) chiral guests whose binding was studied with cycHCs [47].

Enantiopure (*S,S*)-cycHC[6] binding ability has been tested on some chiral compounds shown in Figure 10B. Association constants determined by DOSY NMR in CDCl_3 were quite low and remained in the range 10^1 – 10^2 M^{-1} . The (*R,R*)-cycHC[6] [45] showed a preference for binding of (*R*)-**16** and (*R,R*)-cycHC[8] [47] for (*S*)-**16**, with a $K_{(R)}/K_{(S)}$ value of 1.4 and $K_{(S)}/K_{(R)}$ of 2.0, respectively. Interestingly, the guest **17**, whose acidity and also association constant was higher than those of **16**, bound to (*R,R*)-cycHC[8] nonstereoselectively. No crystal structures of these complexes were obtained; therefore, the position of the guests is not fully disclosed.

Nevertheless, a tentative binding mode of guests to cycHCs was proposed based on ion-mobility MS of cycHC[6] complexes with Na^+ and anions, accompanied by DFT calculations of neutral molecules and anions [48]. Anions form inclusion complexes with cycHCs, and undissociated carboxylic acids form external complexes through hydrogen bonding with the urea carbonyl group. (Figure 11A).

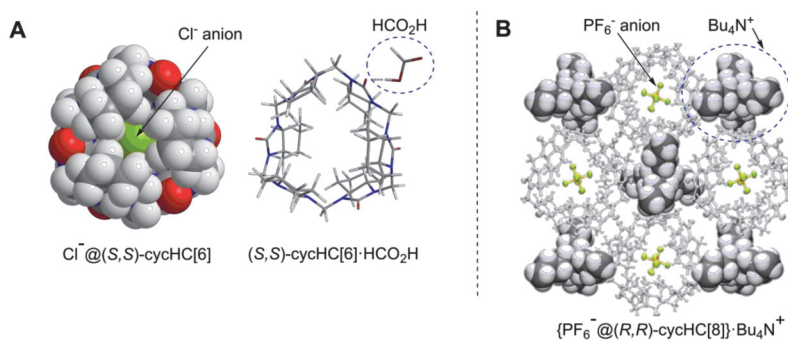


Figure 11. (A) Minimum energy geometry of inclusion complex of $\text{Cl}^- @(\text{S,S})\text{-cycHC}[6]$ and external complex of $(\text{S,S})\text{-cycHC}[6] \cdot \text{HCO}_2\text{H}$ [48]; (B) crystal structure of $(\text{PF}_6^- @(\text{R,R})\text{-cycHC}[8]) \cdot \text{Bu}_4\text{N}^+$ [49].
Published by The Royal Society of Chemistry.

The crystal structure of the tetrabutylammonium hexafluorophosphate complex with (*R,R*)-cycHC[8] (Figure 11B) [49] confirmed the previous hypotheses that an anion can be encapsulated and that the cation forms an external complex with this host.

Another enantiopure member of single-bridged CBs is biotin[6]juril [46] (Figure 12), but so far, only its binding to achiral anions has been studied [50,51], and no reports on its stereoselective applications have been presented yet.

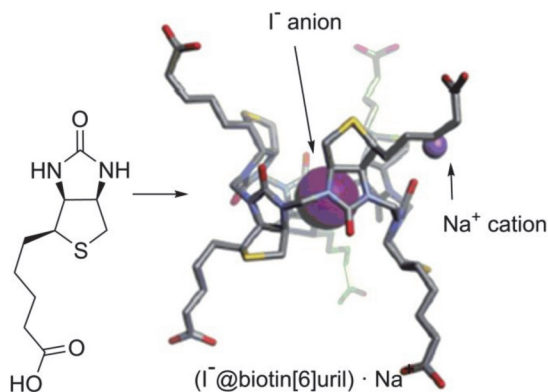


Figure 12. Biotin structure and crystal structure of the $(\text{I}^- @ \text{biotin}[6]\text{juril}) \cdot \text{Na}^+$ complex [46].

Noteworthy is the diastereoselectivity of biotin[6]juril formation. Biotin is the most unsymmetrical urea monomer that has been used for making CB-type macrocycles. It does not have any symmetry elements in its structure, and therefore, the possibility of the formation of nine diastereomeric six-membered HCs exists. In spite of that, only a single diastereomer was formed during biotin condensation with formaldehyde [46]. This is the result of the dynamic formation of methylene bridges, which drives equilibrium toward the formation of the thermodynamically most favorable macrocycle.

From the examples above, one can see that several chiral hosts are known in the CB family, though their chiral recognition properties are barely studied, and their applications are awaiting.

3. Breaking Symmetry through Complex Formation with Achiral Compounds

The symmetry of achiral CBs might also be broken through complexation. The majority of studies in the field of CB chemistry are associated with binding affinity and their applications. Here, just some references to reviews are given [24,25]. Depending on the application, different non-covalent interactions become important. In the solid state [26,27,52], some examples exist, where achiral ligands can cause spontaneous resolution during crystallization and right- or left-handed chiral crystals are produced with equal probability. Examples where chiral helices have been formed with CB complexes are presented in this section.

The first helical structure formed upon complexation of the achiral ligand with CB was reported by Kim et al. [53]. A helix was constructed based on ammonium cation-dipole interaction between a guest and CB and silver cation-dipole interaction between pseudorotaxanes. A polyrotaxane chain was formed from CB[6], *N,N'*-bis(3-pyridylmethyl)-1,5-diaminopentane and AgNO_3 . The crystal structure had an equal number of right- and left-handed helices, so it was racemic. (Figure 13, on the left). Later, along with several achiral polyrotaxanes, another helical racemic polyrotaxane was reported by Kim's group [54]. In that, a silver ion was exchanged with a cadmium ion, and as a result, a longer helical pitch was formed (Figure 13, on the right).

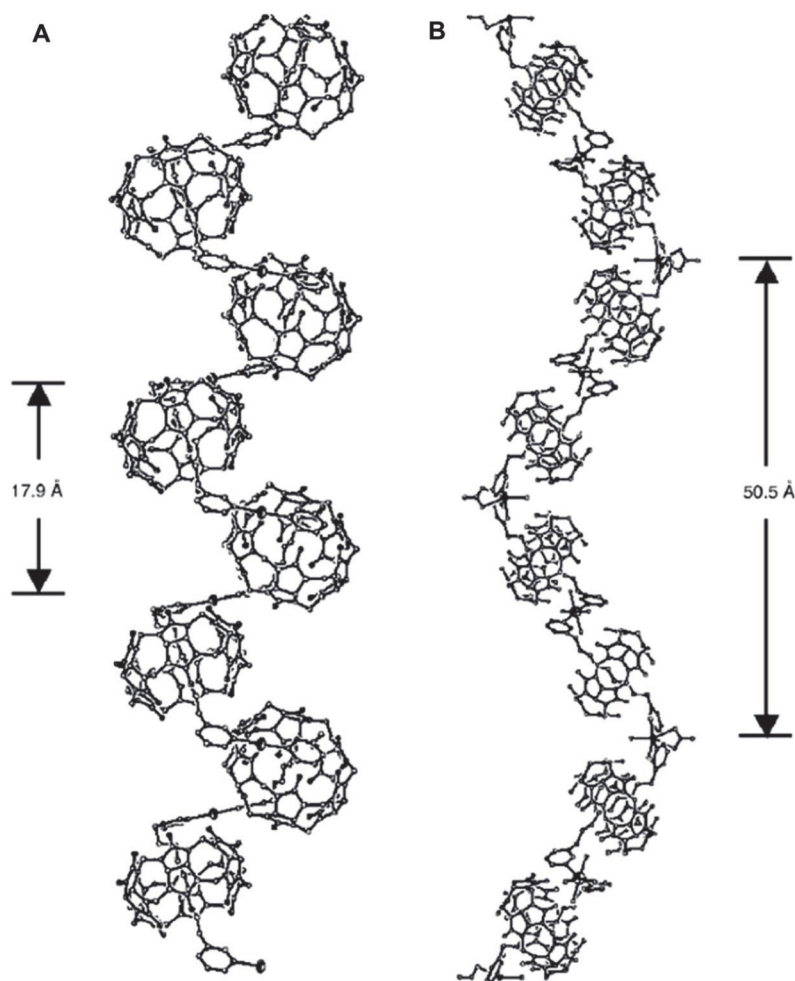


Figure 13. CB[6] polyrotaxane formed from CB[6] (A) *N,N'*-bis(3-pyridylmethyl)-1,5-diaminopentane and AgNO_3 [53] (B) or $\text{Cd}(\text{NO}_3)_2$ [54]; reproduced from [54].

Solid phase complexes with both handed helical networks of polyrotaxane were also shown by Xue and Liu et al., upon complex formation from *N,N'*-bis(2-pyridylmethyl)-1,6-hexanediamine, tetramethyl-CB[6] and AgNO_3 . In the reported structure, CBs are aligned, as the dumbbell of rotaxane, which is constructed from substituted hexanediamine, taking a helical conformation. The authors state that the source of conformational chirality is the linkage of two 2-pyridylmethyl moieties with the silver ion [55].

Helical solid-state structures might be constructed also without pseudorotaxane formation. The network of CBs in Figure 14 is built through cation-dipole interaction and halogen bonding. CB[6] sodium cationic units are connected with copper(II) anionic complexes, the $[\text{Cu}(3,5\text{-diiodosalicylate})(8\text{-hydroxyquinoline-5-sulfonate})]^{2-}$ [56] (Figure 14A). Right- and left-handed helices were both incorporated into a racemic crystal structure. Further, Chen, Liu, Yamauchi et al. [56] noted that upon exchange of iodo-ligand $[\text{Cu}(3\text{-iodobenzoate})(8\text{-hydroxyquinoline-5-sulfonate})\text{Cl}]^{2-}$ was formed, which had all CB-chains organized into homochiral helix (Figure 14B).

The research group of Tao and Liu [57] reported the formation of a pair of homochiral 1-D-helical coordination polymers of CB[5] with Dy^{3+} upon crystallization in the presence of achiral hydroquinone (Figure 15). The interaction between hydroquinone and CB through π -H-C and π - π stacking might direct the formation of a chiral helix.

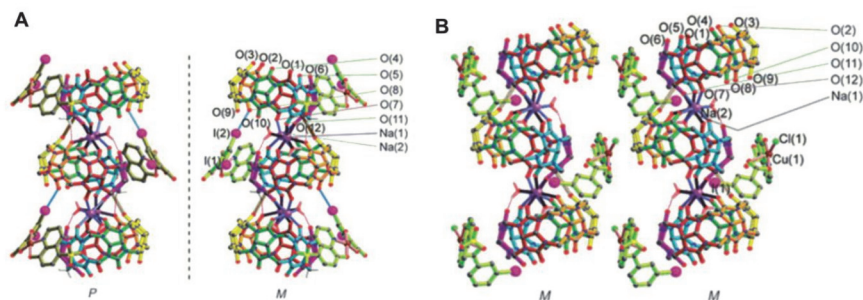


Figure 14. (A) Racemic $[\text{CB}[6]\text{Na}_2\text{-Cu}(3,5\text{-diiodosalicylate})(8\text{-hydroxyquinoline-5-sulfonate})]$; (B) homochiral $[\text{CB}[6]\text{Na}_2\text{-Cu}(3\text{-iodobenzoate})(8\text{-hydroxyquinoline-5-sulfonate})\text{Cl}]$. Reproduced from [56].

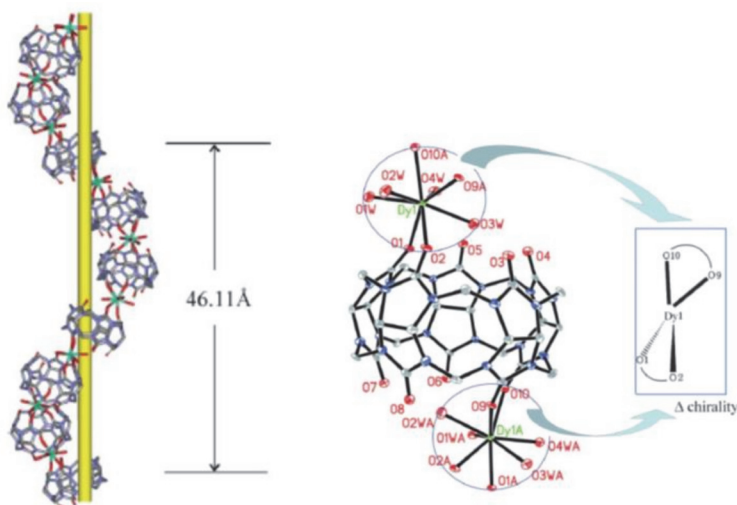


Figure 15. Right-handed *P*-helix and network structure of $(\text{CB}[5]\text{Dy}(\text{H}_2\text{O})_4\text{CB}[5])^{3+}$ and hydroquinone, crystallized in space group $P6_1$ [57], reproduced from [57] with permission from The Royal Society of Chemistry.

In the crystal structure with a *P*-helix, two carbonyl groups of CB[5] are coordinated to Dy^{3+} and as every Dy^{3+} is connected with two CB[5] molecules; also, Dy^{3+} is chiral and has the Δ -configuration. The authors attempted also a measurement of circular dichroism (CD) of single crystal, but unfortunately could not detect a reliable CD signal. The absolute configuration was assigned by single crystal diffraction analysis through the Flack parameter. Intriguingly, randomly performed crystallizations showed that two clusters crystallized in the space group $P6_5$, whereas the other six clusters crystallized in the space group $P6_1$. In other words, the sample in the present case had undergone spontaneous resolution with an enantiomeric excess value of 50% [57]. Formation

of similar helical networks has also been observed with heavy lanthanides like Er^{3+} , Yb^{3+} or Lu^{3+} , but not with light lanthanides [58].

The given examples of helical polyrotaxanes show that upon understanding the supramolecular interactions of CBs with guests and with the suitable interplay between participating species, one can obtain chiral material. On the other hand, helical networks with CBs are relatively rare, compared with solid-state structures of coordination polymers made by the incorporation of various CBs. Therefore, one could state that induction of chirality in the solid state with CBs has been the result of good luck, and further research is required to develop an understanding for directed design.

In addition to the formation of helices from CB units, one can utilize larger homologues of CBs as a confined space, in which the helix can be fitted. Tao et al. [59] have shown that CB[8] is large enough to fold a long-hydrocarbon guest into a helix conformation within its cavity (Figure 16). The asymmetric unit of CB[8] pseudorotaxanes contained both the right- and left-handed helical guests in equal occupancy in its structure.

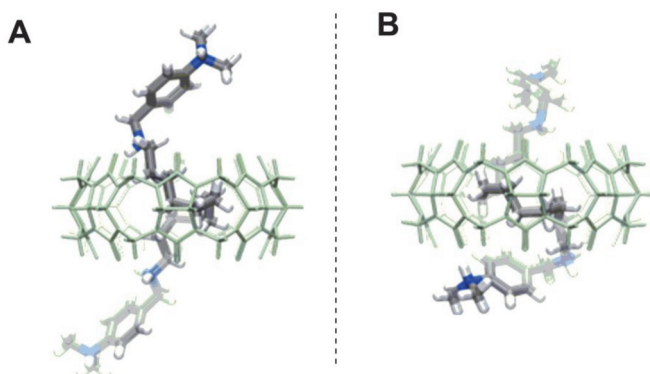


Figure 16. *N,N'*-bis(4-dimethylaminobenzyl)-dodecane-1,12-diamine folded inside of the CB[8] (A) into a right-handed helix; (B) into a left-handed helix [59].

One can see that CBs can be involved in the formation of chiral helical structures, but so far, stereoselectivity of this process has not been directed. Hopefully, future methods for homochiral and stereoselective helix formation will be developed, for example through seeding or by some chiral stimulus.

4. Breaking Symmetry through Complex Formation with Chiral Compounds

It is clear that upon complexation with an enantiomerically pure guest, the entire host-guest complex becomes chiral. The situation becomes more intriguing if such a supramolecular complex can be applied in further chirogenesis or enantiodiscrimination [60,61].

One of the most reliable methods to detect chirality is CD. Cucurbiturils' carbonyl-group UV-absorbance is below 250 nm and coincides with the cut-off region of the many organic solvents, therefore the signal of a chiral guest is often used for interaction studies. One of the parameters that reflects chirality, the concentration independent value of the *g*-factor, is a good measure of chirality sensing. Inoue and Kim et al. [62] have shown that the *g*-factor of chiral charge transfer dyad **18** can be affected by complexation with CB[8] (Figure 17).

One step further from the creation of a chiral complex of CB through binding with a chiral guest is the compilation of a ternary system that can show stereoselectivity. The very first and very comprehensive study in this direction was done by the group of Inoue and Kim [63]. They investigated a number of ternary systems and found that the CB[6] complex with (*R*)-2-methylpiperazine is especially selective toward complexation with (*S*)-2-methylbutylamine ($K = 15,000 \pm 3000 \text{ M}^{-1}$)

if compared with the complex between (S)-2-methylpiperazine with (S)-2-methylbutylamine ($K = 800 \pm 100 \text{ M}^{-1}$) (Figure 18). A matched enantiomer is bound with 19-times greater affinity than the mismatched enantiomer. It was claimed to be the highest enantioselectivity ever reported for a supramolecular system derived from an achiral host. To explain such a selectivity, an analogy to the commander–sergeant–soldier [64] system was exploited. Binding to CBs is governed by the hydrophobic effect related to the guest’s ability to enter the CBs’ cavity. Double-charged methylpiperazine is designated as a soldier, and it is weakly bound to CB at portals; it cannot enter the cavity, but can attract two CBs, causing aggregation of the CB-methylpiperazine complex. Aggregation can be minimized at a concentration below 0.3 mM. CB is designated as the sergeant, and its role is to mediate the formation of diastereomeric complexes between two ammonium compounds. 2-Methylbutylamine is the commander, as its binding controls the formation of the final complex. The mismatching enantiomer of 2-methylbutylamine induces an unfavorable change of enthalpy, leading to an endothermic reaction, which is explained by the unfavorable change in the geometry of the bound methylpiperazine. The matching enantiomer of 2-methylbutylamine, on the other hand, does not disturb the complex between CB and bound methylpiperazine and is therefore overall strongly favored, and its binding leads eventually to disaggregation of the CB complex. In addition, in this work, selectivity toward diastereomeric dipeptides was shown [63].

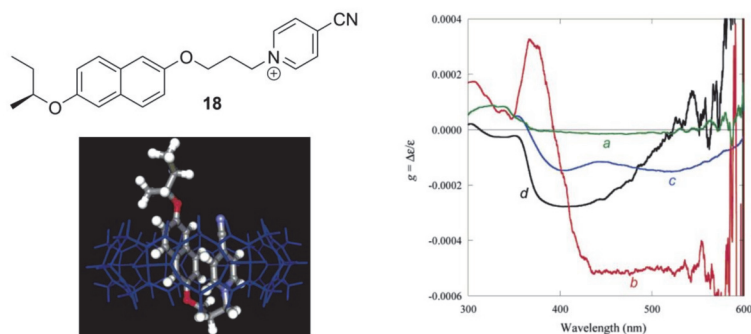


Figure 17. Structure of the charge-transfer dyad **18**; **18**@CB[8] complex 3D model and g-factor graph for: (a) the folded monomer in acetonitrile at 25 °C; (b) the head-to-tail dimer of **18** in CH_2Cl_2 at -95 °C; (c) the folded conformation in CB[8] in D_2O at 25 °C; (d) the inclusion complex with α -CD in H_2O at 25 °C. Reprinted from [62].

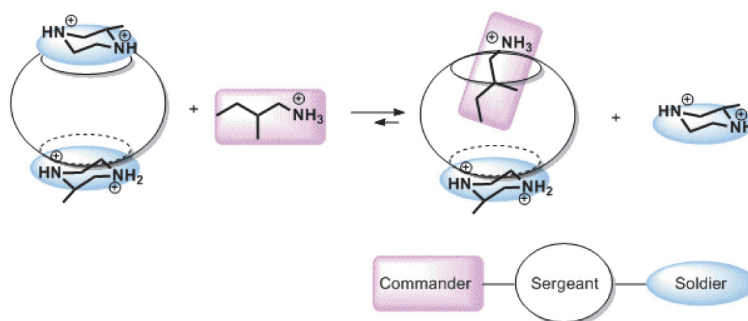


Figure 18. Representation of the complexation pathway in a ternary supramolecular system of CB[6], (S)-2-methylpiperazine and 2-methylbutylamine, with outstanding chiral selectivity [63].

The most recent study on a ternary system with two chiral compounds and CB[7] was published by Day et al. [65]. They observed that chiroptical properties of chiral organic salts can be affected by the formation of CB complexes. The most illustrative example of the effect of CB[7] is the change in the CD signal of diastereomeric pairs of chiral (*S*)-ammonium-2-benzyloxycyclopentane (*R*- or *S*-ABC⁺) salts with hydrogen tartrate (*L*- or *D*-HT[−]) (Figure 15). The additional absorption band is induced in the signal of one diastereomer (*S*-ABC@CB7·*D*-HT, the positive CD signal), as the other diastereomer signal retains the same λ_{\max} (*S*-ABC@CB7·*L*-HT, negative CD band) (Figure 19A). CB[7] has the same influence with respect to enantiomeric ammonium tartrate salts, and the sign of the Cotton effect is dictated by the chiral salt itself and is opposite for the signal for the enantiomeric pairs (Figure 19B).

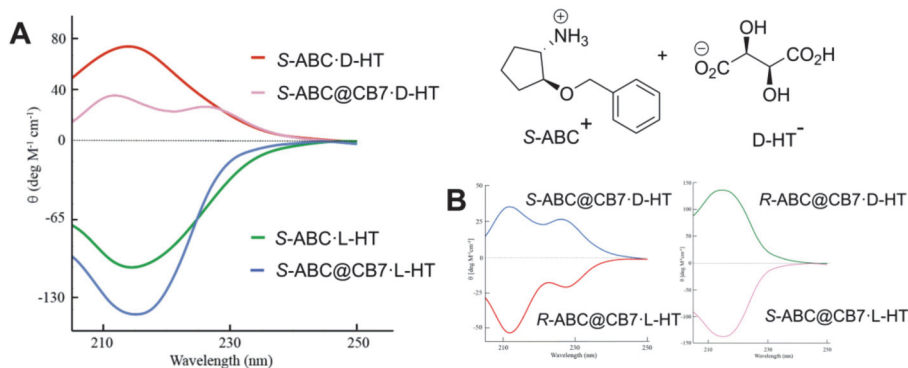


Figure 19. (A) CD signals for (*S*)-ammonium-2-benzyloxycyclopentane salt with *D*- and *L*-hydrogen tartrate and with and without CB[7]; (B) CD signal of two enantiomeric pairs of ternary complexes [65]. HT, hydrogen tartrate; (*S*)-ammonium-2-benzyloxycyclopentane (*S*-ABC⁺).

Based on the phenomena that chiral compounds can induce CD signal upon complexation with achiral molecules and that CB[8] forms a complex with two aromatic guests, Biedermann and Nau [66,67] developed a wonderful analytical method for the detection of chiral amino acids, peptides, proteins and aromatic drugs (Figure 20). Some examples of the application of this method are outlined in Figure 20B. One can follow the formation of some particular chiral product that chemoselectively forms a complex with a CB[8] sensor. In this sensor CB[8] acts as a host and fluorescent dye, for instance dimethyldiazaperopyrenium (MDPP), serves as a signaling unit. For example, during enzymatic hydrolysis of racemic glycyl-phenylalanine dipeptide (Gly-*D*/*L*-Phe), only one enantiomer is digested, and *L*-phenylalanine (*L*-Phe) is formed, while the Gly-*D*-Phe dipeptide remains intact. The binding constant of *L*-Phe ($450 \times 10^3 \text{ M}^{-1}$) to supramolecular sensor MDPP@CB[8] is much higher, compared with binding of Gly-*D*-Phe ($7 \times 10^3 \text{ M}^{-1}$) dipeptide; therefore, the [*L*-Phe·MDPP@CB[8]] complex is mainly formed, and *L*-Phe can be sensed through the CD signal of the ternary complex (Figure 20B, top). It is also remarkable that the kinetics of the enzyme reaction can be monitored by following the formation of a single enantiomer. Hippuryl-phenylalanine dipeptide hydrolysis kinetics, which was determined through the CD signal of the CB[8]-sensor system, coincides with conventionally measured UV-outcome, but in the first method, one can directly monitor enantioselectivity of the reaction and assign absolute configuration of the product.

In addition to chiral sensing applications, CBs have also been engaged in enantioselective supramolecular catalysis. Scherman and Herrmann et al. [68] showed that the CB[8] complex with a copper salt of a chiral amino acid can function as a chiral nanoreactor (Figure 21). The Diels-Alder reaction in the presence of CB[8], *L*-tryptophan and Cu²⁺ gave cycloaddition product in enantiomeric excess (*ee*) of 73% compared with *ee* 31% from the reaction without CB. A catalytic system utilizing *N*- α -methyl-*L*-tryptophan as a chiral inducer gave the product in the presence of CB[8] in an *ee* of 92%

and without CB[8] in an *ee* of 72%. As a result, for the first time, it was shown that CB can increase enantioselectivity in the catalysis.

There are also fascinating examples of diastereoselective photocycloaddition reactions catalyzed by complexation with CBs, but as this topic has just been recently reviewed, it is not covered herein [28].

The presented examples show that there are outstanding approaches already proven to be possible, and noteworthy input has been made by studying complexation of chiral compounds with CBs. In addition to the examples described above, in Tables 1–4 is outlined a collection of chiral guests, whose complexation with CBs has been studied.

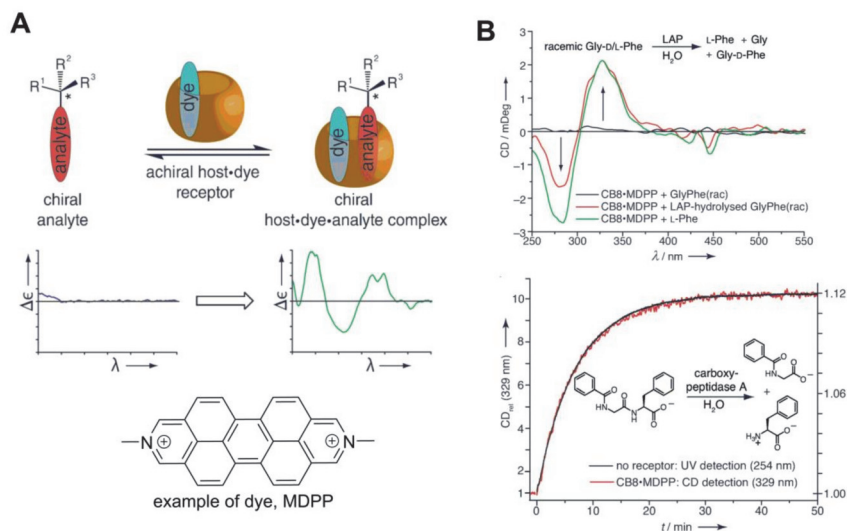


Figure 20. (A) Principle of the supramolecular chirality sensing system with CB[8]; (B) examples of the application of this sensing system: (top) CD spectra of CB[8]:MDPP (20 μM) in the presence of racemic Gly-D/L-Phe, before and after its enzymatic hydrolysis by leucine aminopeptidase (LAP) at pH 7.8; (bottom) kinetic trace for the hydrolysis of hippuryl-Phe (160 μM) by carboxypeptidase A at pH 7.8. The reaction progress was monitored by CD (329 nm) in the presence of MDPP@CB8 (20 μM, red line) and, as a control, directly by UV-Vis spectroscopy (254 nm, black line). Reprinted with permission from [66]). MDPP, dimethyldiazaperopyrenium.

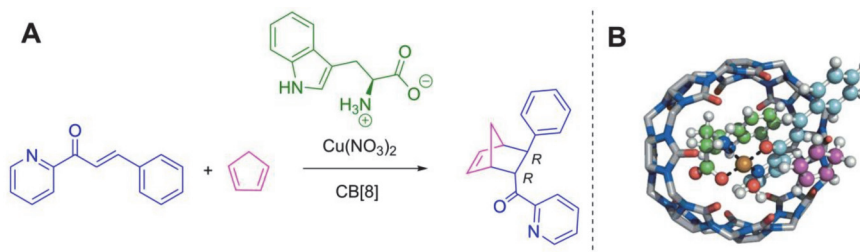


Figure 21. (A) Diels-Alder reaction catalyzed in a CB-nanoreactor; (B) lowest energy geometry of the complex of Cu²⁺, H₂O, tryptophan, azachalcone and CB[8] with cyclopentadiene approaching in the endo direction [68].

Table 1. Carbohydrates as guests for CBs (G, guest; H, Host; Ref, reference).

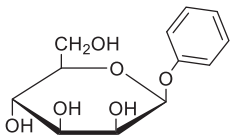
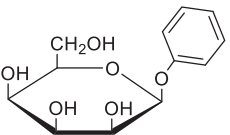
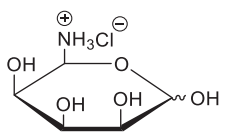
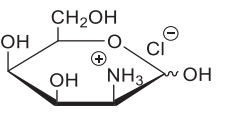
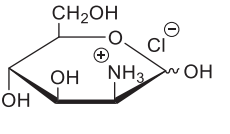
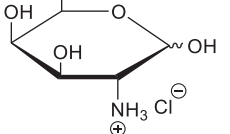
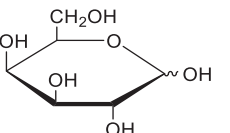
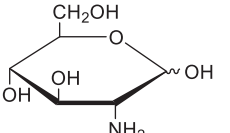
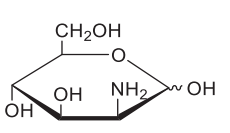
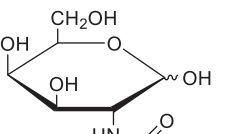
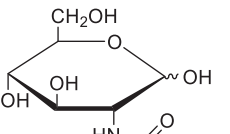
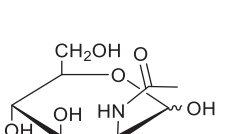
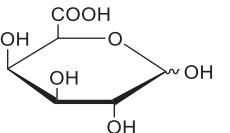
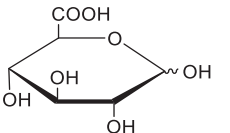
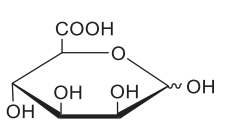
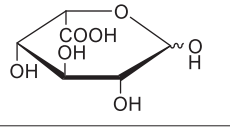
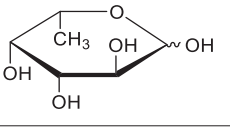
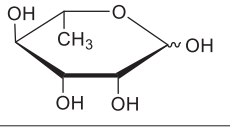
Legend	Structure of Guest, Name of Host and Reference Number		
G			
H	CB[8]	CB[8]	CB[7]
Ref.	[66]	[66]	[69]
G			
H		CB[7]	
Ref.		[69]	
G			
H		CB[7]	
Ref.		[70]	
G			
H		CB[7]	
Ref.		[70]	
G			
H		CB[7]	
Ref.		70	
G			
H		CB[7]	
Ref.		[70]	

Table 2. Pharmaceuticals as guests for CBs.

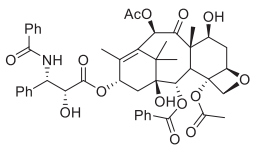
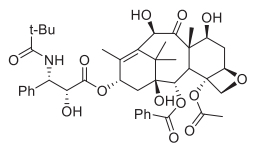
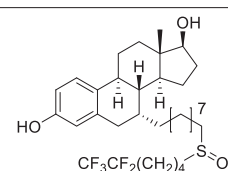
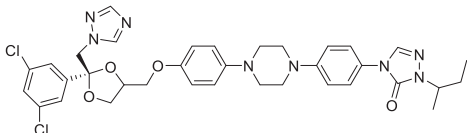
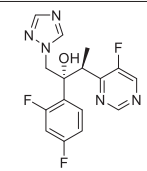
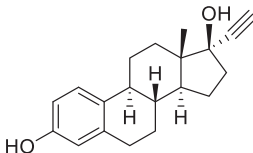
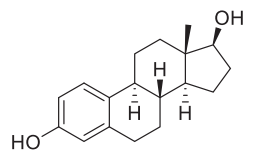
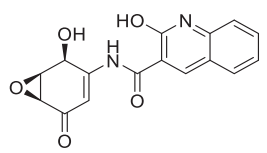
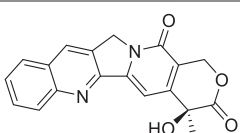
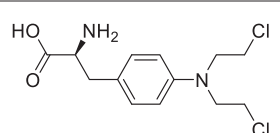
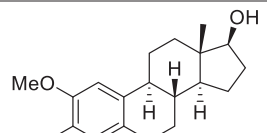
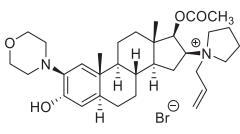
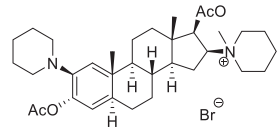
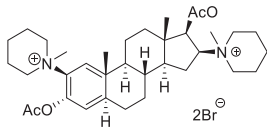
Legend	Structure of Guest, Name of Host and Reference Number		
G			
	Paclitaxel	Docetaxel	Fulvestrant
H	Acyclic CB		
Ref.	[71]		
G			
	Itraconazole	Voriconazole	
H	Acyclic CB		
Ref.	[71]		
G			
	α -ethynylestradiol	Estradiol	PBS 1086
H	Acyclic CB		
Ref.	[71–73]		
G			
	S-camptothecin	Melphalan	2-methoxyestradiol
H	Acyclic CB, CB[7], CB[8]	Acyclic CB	Acyclic CB
Ref.	[71–77]	[71–73]	[73]
G			
	Rocuronium	Vecuronium	Pancuronium
H	Acyclic CB		
Ref.	[78]		

Table 2. Cont.

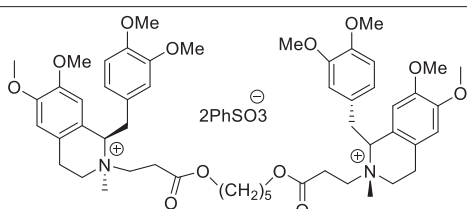
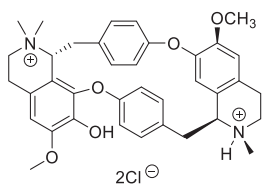
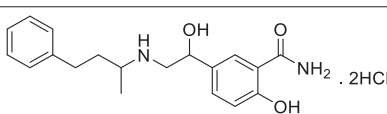
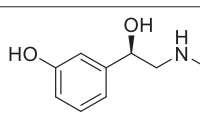
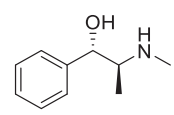
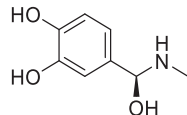
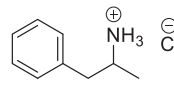
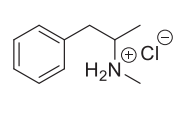
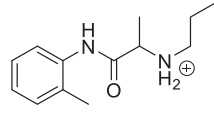
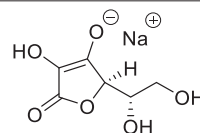
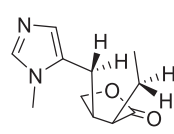
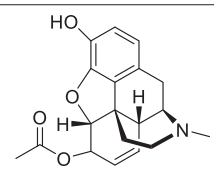
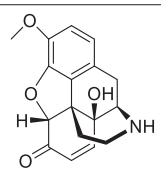
Legend	Structure of Guest, Name of Host and Reference Number		
G			
	Cisatracurium		Tubocurarine
H	Acyclic CB		
Ref.	[78]		
G			
	Labetalol		Phenylephrine
H	CB[7]		CB[6], Acyclic CB
Ref.	[79]		[80]
G			
	Pseudoephedrine	Adrenaline	Amphetamine hydrochloride
H	CB[6], Acyclic CB	CB[6]	CB[7]
Ref.	[80]	[81]	[82]
G			
	Methamphetamine hydrochloride	Prilocaine	Sodium ascorbate
H	CB[7]	CB[7]	CB[6]
Ref.	[82]	[83]	[84]
G			
	Pilocarpine	6-monoacetylmorphine	Noroxycodone

Table 2. Cont.

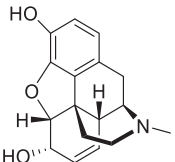
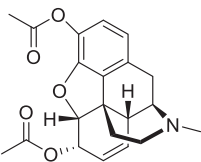
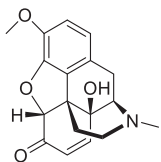
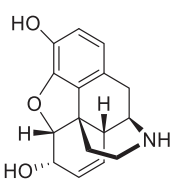
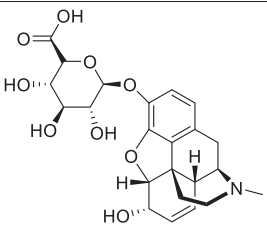
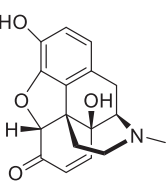
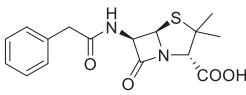
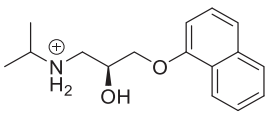
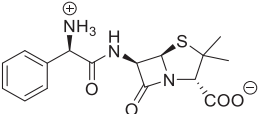
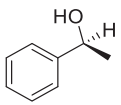
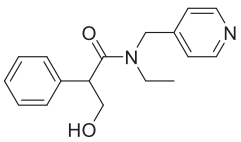
Legend	Structure of Guest, Name of Host and Reference Number		
H	CB[7]	Acyclic CB	Acyclic CB
Ref.	[85]	[86]	[86]
G			
	Morphine	Heroin	Oxycodone
H	Acyclic CB		
Ref.	[86]		
G			
	Normorphine	Morphine-6-glucuronide	Oxymorphone
H	Acyclic CB		
Ref.	[86]		
G			
	Penicillin G	(S)-propranolol	Ampicillin
H	CB[8]		
Ref.	[66]		
G			
	(S)-1-phenylethanol	Tropicamide	
H	CB[8]	CB[7], CB[8]	
Ref.	[66]	[87]	

Table 3. Amino acids, amino derivatives and peptides as guests for CBs.

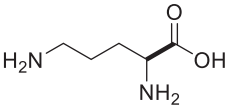
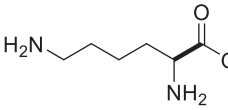
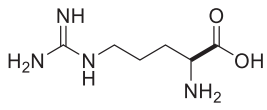
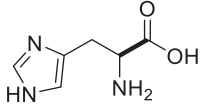
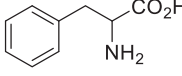
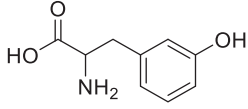
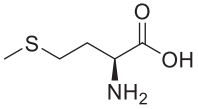
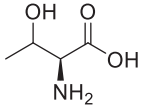
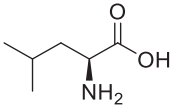
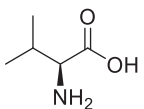
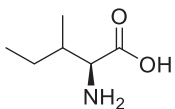
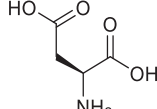
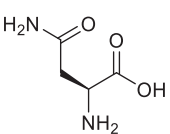
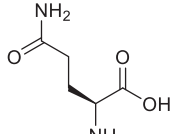
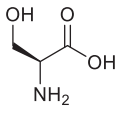
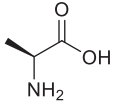
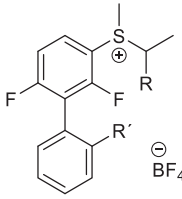
Legend	Structure of Guest, Name of Host and Reference Number		
G			
H	CB[6], Acyclic CB	CB[6], Acyclic, CB[7], iCB[7]	CB[6], Acyclic, CB[7], iCB[7]
Ref.	[88]	[82,89–92]	[82,89–92]
G			
H	CB[6], CB[7], CB[8], iCB[7]	CB[6], CB[7], CB[8], iCB[7]	CB[6], CB[7], CB[8], iCB[7]
Ref.	[82,89,91,93,94]	[89,91–96]	[89,92–94]
G			
H	iCB[7], CB[6]	iCB[7]	iCB[7]
Ref.	[91,97]	[91]	[91]
G			
H	iCB[7], CB[7]	iCB[7], CB[7]	CB[7]
Ref.	[91,92]	[91,92]	[92]
G			
H		CB[7]	
Ref.		[92]	
G			R = H, CH ₃ ; R' = CH ₃ , Cl
H	CB[7]	CB[8]	
Ref.	[92]	[98]	

Table 3. Cont.

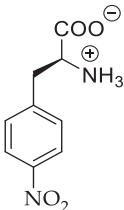
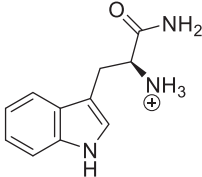
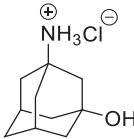
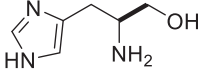
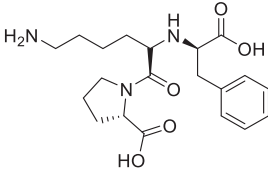
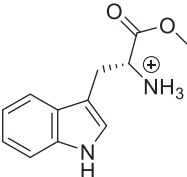
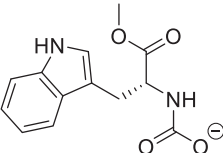
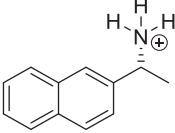
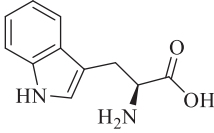
Legend	Structure of Guest, Name of Host and Reference Number		
G			
H	CB[7]		
Ref.	[66]		
G			
H	CB[6], Acyclic CB	CB[6], Acyclic CB	CB[8]
Ref.	[88]	[88]	[94]
G			
H	CB[8]	CB[7], CB[6]	CB[6], CB[8], iCB[7]
Ref.	[94]	[99]	[91,94,100,101]
G	Phe-Gly Phe-Ala Phe-Val Gly-Ala Asp-Phe Hippuryl-Phe	TrpPro Trp-OMe NAc-Trp Aspartame NAcTrp-NH2 Trp(Pro)6-NH2 Trp(Gly)6-NH2	Trp(Ala)6-NH2 Trp(Val)6-NH2 Trp(Leu)6-NH2 Trp(Asp)6-NH2 Trp(Glu)6-NH2 5-F-Trp(Gly)6-NH2 5-F-Trp(Asn)6-NH2
H	CB[8]		
Ref.	[66]		
G	Phe-Gly-Gly Gly-Phe-Gly Gly-Gly-Phe Gly-Gly-Trp-Gly-Gly	His-Gly-Gly Gly-His-Gly Gly-Gly-His Gly-Gly-Tyr Tyr-Gly-Gly	Gly-Tyr Gly-Trp Gly-Gly
H	CB[8]	CB[8]	CB[6]
Ref.	[102]	[102]	[103]
G	Gly-Tyr-Gly	Trp-Gly-Gly	Gly-Gly-Trp
H	CB[8]	CB[8]	CB[8]
Ref.	[102,104]	[94,102,104]	[94,102]

Table 3. Cont.

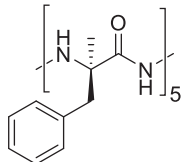
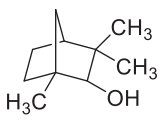
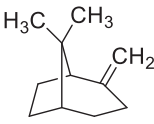
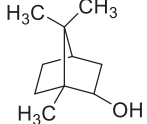
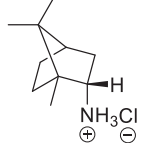
Legend	Structure of Guest, Name of Host and Reference Number		
G		Thr-Gly-Ala-Phe-Met Thr-Gly-Ala-AMPhe-Met	Phe-Leu Phe-Met-NH ₂ Phe-Leu-NH ₂ Thr-Gly-Ala-Phe-Leu Thr-Gly-Ala-Phe-Met-NH ₂ Thr-Gly-Ala-Phe-Leu-NH ₂ Thr-Gly-Ser-Phe-Met-NH ₂ Thr-Gly-Gly-Phe-Met-NH ₂ Thr-Gly-DAla-Phe-Met-NH ₂
H	CB[8]	CB[7]	CB[7]
Ref.	[105]	[106]	[96]
G	Gly-Phe		
H	CB[8], CB[6]		
Ref.	[51,88]		

Table 4. Terpenes as guests for CBs.

Legend	Structure of Guest, Name of Host and Reference Number			
G				
H	CB[7], CB[8]	CB[7]	CB[7]	CB[7]
Ref.	[74,107]	[107]	[107]	[108]

5. Conclusions

Cucurbituril chemistry has undergone remarkable growth in recent years. Applications of CB-type hosts have gained considerable attention due to CBs' outstanding binding ability and influence on the optical signal of dyes. However, studies on chiral sensing have emerged just recently, even though the first results in studies on the influence of CBs on supramolecular chirality appeared more than a decade ago. One can see that CB-type hosts are rich in means of symmetry breaking, which leads to induction of chirality. In addition, the synthesis of some chiral and enantiopure CB-type hosts have been developed, though the utilization of the created chiral systems is still obscure. Outstanding examples for the induction of supramolecular chirality from achiral building blocks and for the formation of helices in the solid state have been shown. Further on, the first elegant applications of the phenomena that CBs do form complexes with chiral guests and can induce specific chiroptical and catalytic properties are available. In addition, there are examples of stereoselective binding between diastereomers and cis–trans isomers, the selectivity of which is driven by the confined space inside the cucurbiturils. Based on that, the foundation for the emergence of new supramolecular systems, whose selectivity can be directed by external stimuli and that can be applied for chirality sensing and enantioselective applications, exists and should be encouraged.

Acknowledgments: The authors thank Sandra Kaabel for fruitful discussion and illustrations. The writing of this paper was supported by the Estonian Ministry of Education and Research through Grant PUT692.

Author Contributions: Both authors contributed substantially to the work reported.

Conflicts of Interest: The authors declare no conflict of interest.

References

1. Freeman, W.A.; Mock, W.L.; Shih, N.Y. Cucurbituril. *J. Am. Chem. Soc.* **1981**, *103*, 7367–7368. [[CrossRef](#)]
2. Flinn, A.; Hough, G.C.; Stoddart, J.F.; Williams, D.J. Decamethylcucurbit[5]uril. *Angew. Chem. Int. Ed.* **1992**, *31*, 1475–1477. [[CrossRef](#)]
3. Kim, J.; Jung, I.-S.; Kim, S.-Y.; Lee, E.; Kang, J.-K.; Sakamoto, S.; Yamaguchi, K.; Kim, K. New Cucurbituril Homologues: Syntheses, Isolation, Characterization, and X-ray Crystal Structures of Cucurbit[*n*]uril (*n* = 5, 7, and 8). *J. Am. Chem. Soc.* **2000**, *122*, 540–541. [[CrossRef](#)]
4. Day, A.; Arnold, A.P.; Blanch, R.J.; Snushall, B. Controlling Factors in the Synthesis of Cucurbituril and Its Homologues. *J. Org. Chem.* **2001**, *66*, 8094–8100. [[CrossRef](#)] [[PubMed](#)]
5. Aav, R.; Kaabel, S.; Fomitšenko, M. Cucurbiturils: Synthesis, Structures, Formation Mechanisms, and Nomenclature. In *Comprehensive Supramolecular Chemistry II*; Atwood, J.L., Ed.; Elsevier: Oxford, UK, 2017; Volume 3, pp. 203–220, ISBN 978-0-12-803199-5.
6. Lisbjerg, M.; Pittelkow, M. Hemicucurbit[*n*]urils. In *Comprehensive Supramolecular Chemistry II*; Atwood, J.L., Ed.; Elsevier: Oxford, UK, 2017; Volume 3, pp. 221–236, ISBN 978-0-12-803199-5.
7. Ganapati, S.; Isaacs, L. Acyclic Cucurbit[*n*]uril-type Receptors: Preparation, Molecular Recognition Properties and Biological Applications. *Isr. J. Chem.* **2018**, in print. [[CrossRef](#)]
8. Andersen, N.N.; Lisbjerg, M.; Eriksen, K.; Pittelkow, M. Hemicucurbit[*n*]urils and Their Derivatives—Synthesis and Applications. *Isr. J. Chem.* **2018**, in print. [[CrossRef](#)]
9. Masson, E.; Raeisi, M.; Kotturi, K. Kinetics Inside, Outside and Through Cucurbiturils. *Isr. J. Chem.* **2018**, in print. [[CrossRef](#)]
10. Ouari, O.; Bardelang, D. Nitroxide Radicals with Cucurbit[*n*]urils and Other Cavitands. *Isr. J. Chem.* **2018**, in print. [[CrossRef](#)]
11. Shen, J.; Dearden, D.V. Recent Progress in Gas Phase Cucurbit[*n*]uril Chemistry. *Isr. J. Chem.* **2018**, in print. [[CrossRef](#)]
12. Kaifer, A.E. Portal Effects on the Stability of Cucurbituril Complexes. *Isr. J. Chem.* **2018**, in print. [[CrossRef](#)]
13. Hou, C.; Zeng, X.; Gao, Y.; Qiao, S.; Zhang, X.; Xu, J.; Liu, J. Cucurbituril As A Versatile Tool to Tune the Functions of Proteins. *Isr. J. Chem.* **2018**, in print. [[CrossRef](#)]
14. Kaabel, S.; Aav, R. Templating Effects in the Dynamic Chemistry of Cucurbiturils and Hemicucurbiturils. *Isr. J. Chem.* **2018**, in print. [[CrossRef](#)]
15. Wiemann, M.; Jonkheijm, P. Stimuli-Responsive Cucurbit[*n*]uril-Mediated Host-Guest Complexes on Surfaces. *Isr. J. Chem.* **2018**, in print. [[CrossRef](#)]
16. Vícha, R.; Jelínková, K.; Rouchal, M. Cucurbit[*n*]urils-related Multitopic Supramolecular Components: Design, Properties, and Perspectives. *Isr. J. Chem.* **2018**, in print. [[CrossRef](#)]
17. Koc, A.; Tuncel, D. Supramolecular Assemblies of Cucurbiturils with Photoactive, π -conjugated Chromophores. *Isr. J. Chem.* **2018**, in print. [[CrossRef](#)]
18. Robinson-Duggon, J.; Pérez-Mora, F.; Dibona-Villanueva, L.; Fuentealba, D. Potential Applications of Cucurbit[*n*]urils Inclusion Complexes in Photodynamic Therapy. *Isr. J. Chem.* **2018**, in print. [[CrossRef](#)]
19. Barooah, N.; Khurana, R.; Bhasikuttan, A.C.; Mohanty, J. Stimuli-responsive Supra-biomolecular Nanoassemblies of Cucurbit[7]uril with Bovine Serum Albumin: Drug Delivery and Sensor Applications. *Isr. J. Chem.* **2018**. [[CrossRef](#)]
20. Macartney, D.H. Cucurbit[*n*]uril Host-Guest Complexes of Acids, Photoacids, and Super Photoacids. *Isr. J. Chem.* **2018**. [[CrossRef](#)]
21. Masson, E.; Ling, X.; Joseph, R.; Kyeremeh-Mensah, L.; Lu, X. Cucurbituril chemistry: A tale of supramolecular success. *RSC Adv.* **2012**, *2*, 1213–1247. [[CrossRef](#)]
22. Tomas, L.; Vladimir, S. Bambusuril Anion Receptors. *Isr. J. Chem.* **2018**, in print. [[CrossRef](#)]
23. Reany, O.; Amar, M.; Ehud, K. Hetero-Bambusurils. *Isr. J. Chem.* **2018**, in print. [[CrossRef](#)]
24. Barrow, S.J.; Kaser, S.; Rowland, M.J.; del Barrio, J.; Scherman, O.A. Cucurbituril-Based Molecular Recognition. *Chem. Rev.* **2015**, *115*, 12320–12406. [[CrossRef](#)] [[PubMed](#)]
25. Sinn, S.; Biedermann, F. Chemical Sensors Based on Cucurbit[*n*]uril Macrocycles. *Isr. J. Chem.* **2018**, *58*. [[CrossRef](#)]
26. Ni, X.-L.; Xiao, X.; Cong, H.; Liang, L.-L.; Cheng, K.; Cheng, X.-J.; Ji, N.-N.; Zhu, Q.-J.; Xue, S.-F.; Tao, Z. Cucurbit[*n*]uril-based coordination chemistry: From simple coordination complexes to novel poly-dimensional coordination polymers. *Chem. Soc. Rev.* **2013**, *42*, 9480–9508. [[CrossRef](#)] [[PubMed](#)]

27. Ni, X.-L.; Xiao, X.; Cong, H.; Zhu, Q.-J.; Xue, S.-F.; Tao, Z. Self-Assemblies Based on the “Outer-Surface Interactions” of Cucurbit[n]urils: New Opportunities for Supramolecular Architectures and Materials. *Acc. Chem. Res.* **2014**, *47*, 1386–1395. [[CrossRef](#)] [[PubMed](#)]
28. Pattabiraman, M.; Sivaguru, J.; Ramamurthy, V. Cucurbiturils as Reaction Containers for Photocycloaddition of Olefins. *Isr. J. Chem.* **2017**, *57*, in print. [[CrossRef](#)]
29. Mandadapu, V.; Day, A.I.; Ghanem, A. Cucurbituril: Chiral Applications. *Chirality* **2014**, *26*, 712–723. [[CrossRef](#)] [[PubMed](#)]
30. Huang, W.-H.; Zavalij, P.Y.; Isaacs, L. Chiral Recognition inside a Chiral Cucurbituril. *Angew. Chem. Int. Ed.* **2007**, *46*, 7425–7427. [[CrossRef](#)] [[PubMed](#)]
31. Kozerski, L.; Hansen, P.E. Aggregation of amphiphilic molecules in water. I. α -phenylethylamine: ^1H and ^{13}C NMR study. *J. Phys. Org. Chem.* **1991**, *4*, 58–66. [[CrossRef](#)]
32. Parve, O.; Reile, I.; Parve, J.; Kasvandik, S.; Kudrjašova, M.; Tamp, S.; Metsala, A.; Villo, L.; Pehk, T.; Jarvet, J.; et al. An NMR and MD Modeling Insight into Nucleation of 1,2-Alkanediols: Selective Crystallization of Lipase-Catalytically Resolved Enantiomers from the Reaction Mixtures. *J. Org. Chem.* **2013**, *78*, 12795–12801. [[CrossRef](#)] [[PubMed](#)]
33. Huang, W.-H.; Zavalij, P.Y.; Isaacs, L. Metal-Ion-Induced Folding and Dimerization of a Glycoluril Decamer in Water. *Org. Lett.* **2009**, *11*, 3918–3921. [[CrossRef](#)] [[PubMed](#)]
34. Cheng, X.-J.; Liang, L.-L.; Chen, K.; Ji, N.-N.; Xiao, X.; Zhang, J.-X.; Zhang, Y.-Q.; Xue, S.-F.; Zhu, Q.-J.; Ni, X.-L.; et al. Twisted Cucurbit[14]uril. *Angew. Chem. Int. Ed.* **2013**, *52*, 7252–7255. [[CrossRef](#)] [[PubMed](#)]
35. Qiu, S.-C.; Chen, K.; Wang, Y.; Hua, Z.; Li, F.; Huang, Y.; Tao, Z.; Zhang, Y.; Wei, G. Crystal structure analysis of twisted cucurbit [14]uril conformations. *Inorg. Chem. Commun.* **2017**, *86*, 49–53. [[CrossRef](#)]
36. Li, Q.; Qiu, S.-C.; Zhang, J.; Chen, K.; Huang, Y.; Xiao, X.; Zhang, Y.; Li, F.; Zhang, Y.-Q.; Xue, S.-F.; et al. Twisted Cucurbit[n]urils. *Org. Lett.* **2016**, *18*, 4020–4023. [[CrossRef](#)] [[PubMed](#)]
37. Lu, X.; Isaacs, L. Synthesis and Recognition Properties of Enantiomerically Pure Acyclic Cucurbit[n]uril-Type Molecular Containers. *Org. Lett.* **2015**, *17*, 4038–4041. [[CrossRef](#)] [[PubMed](#)]
38. Cao, L.; Hettiarachchi, G.; Briken, V.; Isaacs, L. Cucurbit[7]uril Containers for Targeted Delivery of Oxaliplatin to Cancer Cells. *Angew. Chem. Int. Ed.* **2013**, *52*, 12033–12037. [[CrossRef](#)] [[PubMed](#)]
39. Chen, J.; Liu, Y.; Mao, D.; Ma, D. Acyclic cucurbit[n]uril conjugated dextran for drug encapsulation and bioimaging. *Chem. Commun.* **2017**, *53*, 8739–8742. [[CrossRef](#)] [[PubMed](#)]
40. Herges, R. Topology in Chemistry: Designing Möbius Molecules. *Chem. Rev.* **2006**, *106*, 4820–4842. [[CrossRef](#)] [[PubMed](#)]
41. Li, Q.; Qiu, S.-C.; Chen, K.; Zhang, Y.; Wang, R.; Huang, Y.; Tao, Z.; Zhu, Q.-J.; Liu, J.-X. Encapsulation of alkyldiammonium ions within two different cavities of twisted cucurbit[14]uril. *Chem. Commun.* **2016**, *52*, 2589–2592. [[CrossRef](#)] [[PubMed](#)]
42. Miyahara, Y.; Goto, K.; Oka, M.; Inazu, T. Remarkably Facile Ring-Size Control in Macrocyclization: Synthesis of Hemicucurbit[6]uril and Hemicucurbit[12]uril. *Angew. Chem. Int. Ed.* **2004**, *43*, 5019–5022. [[CrossRef](#)] [[PubMed](#)]
43. Svec, J.; Necas, M.; Sindelar, V. Bambus[6]uril. *Angew. Chem. Int. Ed.* **2010**, *49*, 2378–2381. [[CrossRef](#)] [[PubMed](#)]
44. Singh, M.; Solel, E.; Keinan, E.; Reany, O. Aza-Bambusurils En Route to Anion Transporters. *Chem. Eur. J.* **2016**, *22*, 8848–8854. [[CrossRef](#)] [[PubMed](#)]
45. Aav, R.; Shmatova, E.; Reile, I.; Borissova, M.; Topić, F.; Rissanen, K. New Chiral Cyclohexylhemicucurbit[6]uril. *Org. Lett.* **2013**, *15*, 3786–3789. [[CrossRef](#)] [[PubMed](#)]
46. Lisbjerg, M.; Jessen, B.M.; Rasmussen, B.; Nielsen, B.E.; Madsen, A.Ø.; Pittelkow, M. Discovery of a cyclic 6 + 6 hexamer of D-biotin and formaldehyde. *Chem. Sci.* **2014**, *5*, 2647–2650. [[CrossRef](#)]
47. Prigorchenko, E.; Öeren, M.; Kaabel, S.; Fomitšenko, M.; Reile, I.; Järving, I.; Tamm, T.; Topić, F.; Rissanen, K.; Aav, R. Template-controlled synthesis of chiral cyclohexylhemicucurbit[8]uril. *Chem. Commun.* **2015**, *51*, 10921–10924. [[CrossRef](#)] [[PubMed](#)]
48. Öeren, M.; Shmatova, E.; Tamm, T.; Aav, R. Computational and ion mobility MS study of (all-S)-cyclohexylhemicucurbit[6]uril structure and complexes. *Phys. Chem. Chem. Phys.* **2014**, *16*, 19198–19205. [[CrossRef](#)] [[PubMed](#)]
49. Kaabel, S.; Adamson, J.; Topić, F.; Kiesilä, A.; Kalenius, E.; Öeren, M.; Reimund, M.; Prigorchenko, E.; Lõokene, A.; Reich, H.J.; et al. Chiral hemicucurbit[8]uril as an anion receptor: Selectivity to size, shape and charge distribution. *Chem. Sci.* **2017**, *8*, 2184–2190. [[CrossRef](#)] [[PubMed](#)]

50. Lisbjerg, M.; Nielsen, B.E.; Milhøj, B.O.; Sauer, S.P.A.; Pittelkow, M. Anion binding by biotin[6]uril in water. *Org. Biomol. Chem.* **2014**, *13*, 369–373. [CrossRef] [PubMed]
51. Lisbjerg, M.; Valkenier, H.; Jessen, B.M.; Al-Kerdi, H.; Davis, A.P.; Pittelkow, M. Biotin[6]uril Esters: Chloride-Selective Transmembrane Anion Carriers Employing C–H···Anion Interactions. *J. Am. Chem. Soc.* **2015**, *137*, 4948–4951. [CrossRef] [PubMed]
52. Leong, W.L.; Vittal, J.J. One-Dimensional Coordination Polymers: Complexity and Diversity in Structures, Properties, and Applications. *Chem. Rev.* **2011**, *111*, 688–764. [CrossRef] [PubMed]
53. Whang, D.; Kim, K. Helical polyrotaxane: Cucurbituril ‘beads’ threaded onto a helical one-dimensional coordination polymer. *Chem. Commun.* **1997**, 2361–2362. [CrossRef]
54. Park, K.-M.; Whang, D.; Lee, E.; Heo, J.; Kim, K. Transition Metal Ion Directed Supramolecular Assembly of One- and Two-Dimensional Polyrotaxanes Incorporating Cucurbituril. *Chem. Eur. J.* **2002**, *8*, 498–508. [CrossRef]
55. Zeng, J.-P.; Cong, H.; Chen, K.; Xue, S.-F.; Zhang, Y.-Q.; Zhu, Q.-J.; Liu, J.-X.; Tao, Z. A Novel Strategy to Assemble Achiral Ligands to Chiral Helical Polyrotaxane Structures. *Inorg. Chem.* **2011**, *50*, 6521–6525. [CrossRef] [PubMed]
56. Zhang, F.; Yajima, T.; Li, Y.-Z.; Xu, G.-Z.; Chen, H.-L.; Liu, Q.-T.; Yamauchi, O. Iodine-Assisted Assembly of Helical Coordination Polymers of Cucurbituril and Asymmetric Copper(II) Complexes. *Angew. Chem. Int. Ed.* **2005**, *44*, 3402–3407. [CrossRef] [PubMed]
57. Chen, K.; Hu, Y.-F.; Xiao, X.; Xue, S.-F.; Tao, Z.; Zhang, Y.-Q.; Zhu, Q.-J.; Liu, J.-X. Homochiral 1D-helical coordination polymers from achiral cucurbit[5]uril: Hydroquinone-induced spontaneous resolution. *RSC Adv.* **2012**, *2*, 3217–3220. [CrossRef]
58. Chen, K.; Liang, L.-L.; Liu, H.-J.; Zhang, Y.-Q.; Xue, S.-F.; Tao, Z.; Xiao, X.; Zhu, Q.-J.; Lindoy, L.F.; Wei, G. Hydroquinone-assisted assembly of coordination polymers from lanthanides and cucurbit[5]uril. *CrystEngComm* **2012**, *14*, 7994–7999. [CrossRef]
59. Xiao, X.; Liu, J.-X.; Fan, Z.-F.; Chen, K.; Zhu, Q.-J.; Xue, S.-F.; Tao, Z. Chirality from achiral components: N,N′-bis(4-dimethylaminobenzyl)dodecane-1,12-diammonium in cucurbit[8]uril. *Chem. Commun.* **2010**, *46*, 3741–3743. [CrossRef] [PubMed]
60. Hembury, G.A.; Borovkov, V.V.; Inoue, Y. Chirality-Sensing Supramolecular Systems. *Chem. Rev.* **2008**, *108*, 1–73. [CrossRef] [PubMed]
61. Liu, M.; Zhang, L.; Wang, T. Supramolecular Chirality in Self-Assembled Systems. *Chem. Rev.* **2015**, *115*, 7304–7397. [CrossRef] [PubMed]
62. Mori, T.; Ko, Y.H.; Kim, K.; Inoue, Y. Circular Dichroism of Intra- and Intermolecular Charge-Transfer Complexes. Enhancement of Anisotropy Factors by Dimer Formation and by Confinement. *J. Org. Chem.* **2006**, *71*, 3232–3247. [CrossRef] [PubMed]
63. Rekharsky, M.V.; Yamamura, H.; Inoue, C.; Kawai, M.; Osaka, I.; Arakawa, R.; Shiba, K.; Sato, A.; Ko, Y.H.; Selvapalam, N.; et al. Chiral Recognition in Cucurbituril Cavities. *J. Am. Chem. Soc.* **2006**, *128*, 14871–14880. [CrossRef] [PubMed]
64. Green, M.M.; Reidy, M.P.; Johnson, R.D.; Darling, G.; O’Leary, D.J.; Willson, G. Macromolecular stereochemistry: The out-of-proportion influence of optically active comonomers on the conformational characteristics of polyisocyanates. The sergeants and soldiers experiment. *J. Am. Chem. Soc.* **1989**, *111*, 6452–6454. [CrossRef]
65. Wu, W.; Cronin, M.P.; Wallace, L.; Day, A.I. An Exploration of Induced Supramolecular Chirality Through Association of Chiral Ammonium Ions and Tartrates with the Achiral Host Cucurbit[7]uril. *Isr. J. Chem.* **2018**, *58*, in print. [CrossRef]
66. Biedermann, F.; Nau, W.M. Noncovalent Chirality Sensing Ensembles for the Detection and Reaction Monitoring of Amino Acids, Peptides, Proteins, and Aromatic Drugs. *Angew. Chem. Int. Ed.* **2014**, *53*, 5694–5699. [CrossRef] [PubMed]
67. Nau, W.; Biedermann, F. A Method for Detecting a Chiral Analyte. Patent DE102013021899A1, 2015. Available online: <https://patents.google.com/patent/DE102013021899A1/en> (accessed on 2 February 2018).
68. Zheng, L.; Sonzini, S.; Ambarwati, M.; Rosta, E.; Scherman, O.A.; Herrmann, A. Turning Cucurbit[8]uril into a Supramolecular Nanoreactor for Asymmetric Catalysis. *Angew. Chem. Int. Ed.* **2015**, *54*, 13007–13011. [CrossRef] [PubMed]

69. Jang, Y.; Natarajan, R.; Ko, Y.H.; Kim, K. Cucurbit[7]uril: A High-Affinity Host for Encapsulation of Amino Saccharides and Supramolecular Stabilization of Their α -Anomers in Water. *Angew. Chem. Int. Ed.* **2014**, *53*, 1003–1007. [[CrossRef](#)] [[PubMed](#)]
70. Lee, H.H.L.; Kim, H.I. Supramolecular Analysis of Monosaccharide Derivatives Using Cucurbit[7]uril and Electrospray Ionization Tandem Mass Spectrometry. *Isr. J. Chem.* **2018**, in print. [[CrossRef](#)]
71. Zhang, B.; Isaacs, L. Acyclic Cucurbit[*n*]uril-type Molecular Containers: Influence of Aromatic Walls on their Function as Solubilizing Excipients for Insoluble Drugs. *J. Med. Chem.* **2014**, *57*, 9554–9563. [[CrossRef](#)] [[PubMed](#)]
72. Gilberg, L.; Zhang, B.; Zavalij, P.Y.; Sindelar, V.; Isaacs, L. Acyclic cucurbit[*n*]uril-type molecular containers: Influence of glycoluril oligomer length on their function as solubilizing agents. *Org. Biomol. Chem.* **2015**, *13*, 4041–4050. [[CrossRef](#)] [[PubMed](#)]
73. Sigwalt, D.; Moncelet, D.; Falcinelli, S.; Mandadapu, V.; Zavalij, P.Y.; Day, A.; Briken, V.; Isaacs, L. Acyclic Cucurbit[*n*]uril-Type Molecular Containers: Influence of Linker Length on Their Function as Solubilizing Agents. *ChemMedChem* **2016**, *11*, 980–989. [[CrossRef](#)] [[PubMed](#)]
74. Romero, M.A.; González-Delgado, J.A.; Mendoza, J.; Arteaga, J.F.; Basilio, N.; Pischel, U. Terpenes Show Nanomolar Affinity and Selective Binding with Cucurbit[8]uril. *Isr. J. Chem.* **2018**, in print. [[CrossRef](#)]
75. Gavvala, K.; Sengupta, A.; Hazra, P. Modulation of Photophysics and pKa Shift of the Anti-cancer Drug Camptothecin in the Nanocavities of Supramolecular Hosts. *ChemPhysChem* **2013**, *14*, 532–542. [[CrossRef](#)] [[PubMed](#)]
76. Dong, N.; Xue, S.-F.; Zhu, Q.-J.; Tao, Z.; Zhao, Y.; Yang, L.-X. Cucurbit[*n*]urils ($n = 7, 8$) binding of camptothecin and the effects on solubility and reactivity of the anticancer drug. *Supramol. Chem.* **2008**, *20*, 663–671. [[CrossRef](#)]
77. Yang, X.; Wang, Z.; Niu, Y.; Chen, X.; Lee, S.M.Y.; Wang, R. Influence of supramolecular encapsulation of camptothecin by cucurbit[7]uril: Reduced toxicity and preserved anti-cancer activity. *Med. Chem. Comm.* **2016**, *7*, 1392–1397. [[CrossRef](#)]
78. Ma, D.; Zhang, B.; Hoffmann, U.; Sundrup, M.G.; Eikermann, M.; Isaacs, L. Acyclic Cucurbit[*n*]uril-Type Molecular Containers Bind Neuromuscular Blocking Agents In Vitro and Reverse Neuromuscular Block In Vivo. *Angew. Chem. Int. Ed.* **2012**, *51*, 11358–11362. [[CrossRef](#)] [[PubMed](#)]
79. Li, C.; Feng, J.; Ju, H. Supramolecular interaction of labetalol with cucurbit[7]uril for its sensitive fluorescence detection. *Analyst* **2014**, *140*, 230–235. [[CrossRef](#)] [[PubMed](#)]
80. Minami, T.; Esipenko, N.A.; Akdeniz, A.; Zhang, B.; Isaacs, L.; Anzenbacher, P. Multianalyte Sensing of Addictive Over-the-Counter (OTC) Drugs. *J. Am. Chem. Soc.* **2013**, *135*, 15238–15243. [[CrossRef](#)] [[PubMed](#)]
81. Danylyuk, O.; Fedin, V.P.; Sashuk, V. Kinetic trapping of the host–guest association intermediate and its transformation into a thermodynamic inclusion complex. *Chem. Commun.* **2013**, *49*, 1859–1861. [[CrossRef](#)] [[PubMed](#)]
82. Jang, Y.; Jang, M.; Kim, H.; Lee, S.J.; Jin, E.; Koo, J.Y.; Hwang, I.-C.; Kim, Y.; Ko, Y.H.; Hwang, I.; et al. Point-of-Use Detection of Amphetamine-Type Stimulants with Host-Molecule-Functionalized Organic Transistors. *Chem* **2017**, *3*, 641–651. [[CrossRef](#)]
83. Wyman, I.W.; Macartney, D.H. Host–guest complexations of local anaesthetics by cucurbit[7]uril in aqueous solution. *Org. Biomol. Chem.* **2010**, *8*, 247–252. [[CrossRef](#)] [[PubMed](#)]
84. Pandey, S.; Soni, V.K.; Choudhary, G.; Sharma, P.R.; Sharma, R.K. Understanding behaviour of vitamin-C guest binding with the cucurbit[6]uril host. *Supramol. Chem.* **2017**, *29*, 387–394. [[CrossRef](#)]
85. Saleh, N.; Al-Handawi, M.B.; Al-Kaabi, L.; Ali, L.; Salman Ashraf, S.; Thiemann, T.; al-Hindawi, B.; Meetani, M. Intermolecular interactions between cucurbit[7]uril and pilocarpine. *Int. J. Pharm.* **2014**, *460*, 53–62. [[CrossRef](#)] [[PubMed](#)]
86. Shcherbakova, E.G.; Zhang, B.; Gozem, S.; Minami, T.; Zavalij, P.Y.; Pushina, M.; Isaacs, L.D.; Anzenbacher, P. Supramolecular Sensors for Opiates and Their Metabolites. *J. Am. Chem. Soc.* **2017**, *139*, 14954–14960. [[CrossRef](#)] [[PubMed](#)]
87. Saleh, N.; Meetani, M.A.; Al-Kaabi, L.; Ghosh, I.; Nau, W.M. Effect of cucurbit[*n*]urils on tropicamide and potential application in ocular drug delivery. *Supramol. Chem.* **2011**, *23*, 650–656. [[CrossRef](#)]
88. Minami, T.; Esipenko, N.A.; Zhang, B.; Isaacs, L.; Anzenbacher, P. “Turn-on” fluorescent sensor array for basic amino acids in water. *Chem. Commun.* **2014**, *50*, 61–63. [[CrossRef](#)] [[PubMed](#)]
89. Lee, J.W.; Lee, H.H.L.; Ko, Y.H.; Kim, K.; Kim, H.I. Deciphering the Specific High-Affinity Binding of Cucurbit[7]uril to Amino Acids in Water. *J. Phys. Chem. B* **2015**, *119*, 4628–4636. [[CrossRef](#)] [[PubMed](#)]

90. Bailey, D.M.; Hennig, A.; Uzunova, V.D.; Nau, W.M. Supramolecular Tandem Enzyme Assays for Multiparameter Sensor Arrays and Enantiomeric Excess Determination of Amino Acids. *Chem. Eur. J.* **2008**, *14*, 6069–6077. [[CrossRef](#)] [[PubMed](#)]
91. Gao, Z.-Z.; Kan, J.-L.; Chen, L.-X.; Bai, D.; Wang, H.-Y.; Tao, Z.; Xiao, X. Binding and Selectivity of Essential Amino Acid Guests to the Inverted Cucurbit[7]uril Host. *ACS Omega* **2017**, *2*, 5633–5640. [[CrossRef](#)]
92. Kovalenko, E.; Vilaseca, M.; Díaz-Lobo, M.; Masliy, A.N.; Vicent, C.; Fedin, V.P. Supramolecular Adducts of Cucurbit[7]uril and Amino Acids in the Gas Phase. *J. Am. Soc. Mass Spectrom.* **2016**, *27*, 265–276. [[CrossRef](#)] [[PubMed](#)]
93. Hang, C.; Tau, L.-L.; Yu, Y.-H.; Yang, F.; Du, Y.; Xue, S.-F.; Tao, Z. Molecular Recognition of Amino acid by Cucurbiturils. *Acta Chim. Sin.* **2006**, *64*, 989–996.
94. Bush, M.E.; Bouley, N.D.; Urbach, A.R. Charge-Mediated Recognition of N-Terminal Tryptophan in Aqueous Solution by a Synthetic Host. *J. Am. Chem. Soc.* **2005**, *127*, 14511–14517. [[CrossRef](#)] [[PubMed](#)]
95. Liu, S.; Ruspic, C.; Mukhopadhyay, P.; Chakrabarti, S.; Zavalij, P.Y.; Isaacs, L. The Cucurbit[*n*]uril Family: Prime Components for Self-Sorting Systems. *J. Am. Chem. Soc.* **2005**, *127*, 15959–15967. [[CrossRef](#)] [[PubMed](#)]
96. Ghale, G.; Ramalingam, V.; Urbach, A.R.; Nau, W.M. Determining Protease Substrate Selectivity and Inhibition by Label-Free Supramolecular Tandem Enzyme Assays. *J. Am. Chem. Soc.* **2011**, *133*, 7528–7535. [[CrossRef](#)] [[PubMed](#)]
97. Thuéry, P. Supramolecular assemblies built from lanthanide ammoniocarboxylates and cucurbit[6]uril. *CrystEngComm* **2012**, *14*, 8128–8136. [[CrossRef](#)]
98. Joseph, R.; Masson, E. Cucurbit[8]uril recognition of rapidly interconverting diastereomers. *Supramol. Chem.* **2014**, *26*, 632–641. [[CrossRef](#)]
99. Tang, H.; Fuentealba, D.; Ko, Y.H.; Selvapalam, N.; Kim, K.; Bohne, C. Guest Binding Dynamics with Cucurbit[7]uril in the Presence of Cations. *J. Am. Chem. Soc.* **2011**, *133*, 20623–20633. [[CrossRef](#)] [[PubMed](#)]
100. Danylyuk, O.; Fedin, V.P. Solid-State Supramolecular Assemblies of Tryptophan and Tryptamine with Cucurbit[6]uril. *Cryst. Growth Des.* **2012**, *12*, 550–555. [[CrossRef](#)]
101. Ling, Y.; Wang, W.; Kaifer, A.E. A new cucurbit[8]uril-based fluorescent receptor for indole derivatives. *Chem. Commun.* **2007**, 610–612. [[CrossRef](#)] [[PubMed](#)]
102. Heitmann, L.M.; Taylor, A.B.; Hart, P.J.; Urbach, A.R. Sequence-specific recognition and cooperative dimerization of n-terminal aromatic peptides in aqueous solution by a synthetic host. *J. Am. Chem. Soc.* **2006**, *128*, 12574–12581. [[CrossRef](#)] [[PubMed](#)]
103. Danylyuk, O. Exploring cucurbit[6]uril–peptide interactions in the solid state: Crystal structure of cucurbit[6]uril complexes with glycol-containing dipeptides. *CrystEngComm* **2017**, *19*, 3892–3897. [[CrossRef](#)]
104. Biedermann, F.; Rauwald, U.; Cziferszky, M.; Williams, K.A.; Gann, L.D.; Guo, B.Y.; Urbach, A.R.; Bielawski, C.W.; Scherman, O.A. Benzobis(imidazolium)–Cucurbit[8]uril Complexes for Binding and Sensing Aromatic Compounds in Aqueous Solution. *Chem. Eur. J.* **2010**, *16*, 13716–13722. [[CrossRef](#)] [[PubMed](#)]
105. Sonzini, S.; Ryan, S.T.J.; Scherman, O.A. Supramolecular dimerisation of middle-chain Phe pentapeptides via CB[8] host–guest homoternary complex formation. *Chem. Commun.* **2013**, *49*, 8779–8781. [[CrossRef](#)] [[PubMed](#)]
106. Logsdon, L.A.; Urbach, A.R. Sequence-Specific Inhibition of a Nonspecific Protease. *J. Am. Chem. Soc.* **2013**, *135*, 11414–11416. [[CrossRef](#)] [[PubMed](#)]
107. Romero, M.A.; Basilio, N.; Moro, A.J.; Domingues, M.; González-Delgado, J.A.; Arteaga, J.F.; Pischel, U. Photocaged Competitor Guests: A General Approach Toward Light-Activated Cargo Release from Cucurbiturils. *Chem. Eur. J.* **2017**, *23*, 13105–13111. [[CrossRef](#)] [[PubMed](#)]
108. Cao, L.; Isaacs, L. Absolute and relative binding affinity of cucurbit[7]uril towards a series of cationic guests. *Supramol. Chem.* **2014**, *26*, 251–258. [[CrossRef](#)]



Appendix 2

Publication II

K. A. Mishra, J. Adamson, M. Öeren, S. Kaabel, M. Fomitšenko, R. Aav, 'Dynamic Chiral Cyclohexanohemicucurbit[12]uril'. *Chemical Communications*, **2020**, 56 (93), 14645–14648.

Reprinted with permission from Royal Society of Chemistry.



Dynamic chiral cyclohexanohemicucurbit[12]uril †‡

 Cite this: *Chem. Commun.*, 2020, 56, 14645

 Kamini A. Mishra, ^a Jasper Adamson, ^b Mario Öeren, ^c Sandra Kaabel, ^{ad} Maria Fomitšenko ^a and Riina Aav ^{*a}

 Received 12th October 2020,
Accepted 29th October 2020

DOI: 10.1039/d0cc06817a

rsc.li/chemcomm

NMR spectroscopy and DFT modeling studies of chiral cyclohexanohemicucurbit[12]uril indicate that the macrocycle adopts a concave octagonal shape with two distinct conformational flexibilities in solution. Methylene bridge flipping occurs at temperatures above 265 K, while urea monomers rotate at temperatures above 308 K, resulting in the loss of confined space within the macrocycle.

Dynamic molecules capable of adopting distinct shapes in response to external stimuli have driven the development of molecular machines in supramolecular chemistry.¹ Of great importance in this field is the ability to control and direct interactions which can be achieved within the confined spaces of macrocycle cavities. Large macrocycles able to repeatedly undergo significant conformational changes while retaining their molecular integrity have attracted particular interest.^{2,3}

Several macrocycles that differ considerably in conformation from their smaller counterparts have been reported. Cyclodextrins (CDs) containing more than 9 glucose units, referred to as large-ring CDs (LR-CDs),⁴ can assume a helical folding arrangement, *e.g.*, the 26-membered CD.^{5–9} LR-CDs with 14 units have been shown to adopt a conformation that resembles a concave polygon.^{10,11} Large pillar[*n*]arenes, where *n* = 8–10, containing up to 10 monomers in their structures, also adopt concave polygon shapes.¹² Giant calix[*n*]arenes with up to 90 phenolic subunits have been described;¹³ however, calix[16]arene is the largest calix[*n*]arene with

a known conformation. It has the shape of two superimposed Celtic torcs.¹⁴ The largest reported cucurbituril (CB) contains 15 monomers.¹⁵ CBs with up to 10 monomers display a tubular shape, while homologs with 13 or more monomers are locked into a twisted conformation.^{15–18} Hemicucurbiturils (HCs) are single-bridged CB analogues.¹⁹ HC[12], which is formed by the condensation of ethylene urea and formaldehyde and has a highly flexible geometry in solution phase, is the only known 12-membered HC analog.²⁰ The second-largest known HC is the 8-membered, chiral cyclohexanohemicucurbit[8]uril, **cycHC[8]**,^{21–24} which adopts a tubular shape. Despite detection by mass-spectrometry of cycHCs possessing up to 15 members^{23,24} and norbornahemicucurbiturils having up to 8 members,²⁵ only smaller homologs have been isolated, namely **cycHC[6]**s,^{21,26–29} bambus[*n*]urils, where *n* = 4 or 6,^{30–35} and biotin[6]urils.^{35–38} These smaller 6-membered homologs adopt a relatively rigid conformation with well-defined cavity shapes.

Herein, we describe the synthesis and isolation of the first enantiopure cyclohexanohemicucurbit[12]uril (**cycHC[12]**) and detail its conformational dynamics *via* NMR spectroscopy coupled with density functional theory (DFT) calculations (Fig. 1).

Our findings show that the macrocycle adopts a concave octagon conformation in toluene at low temperatures, while elevated temperatures result in the activation of two dynamic mechanisms: the bridge flip and the monomer flip. Although **cycHC[12]** was previously identified by UV-HPLC in a crude reaction mixture,^{23,24} it was not isolated. We have found that subjecting an isolated macrocycle (**cycHC[8]**) or the monomer (cyclohexa-1,2-diyurea) to acidic conditions, in the presence of heptafluorobutyric acid (see S2, ESI† for details) leads to the formation of longer oligomers and larger macrocycles. The developed procedure produced **cycHC[12]** with a 1% yield, which permitted elucidation of its shape and conformational dynamics by ¹H NMR and DFT. Unfortunately, our attempts to obtain single crystals of **cycHC[12]** from various solvents have been unsuccessful.

^a Department of Chemistry and Biotechnology, Tallinn University of Technology, Akadeemia tee 15, 12618 Tallinn, Estonia. E-mail: riina.aav@taltech.ee

^b Chemical Physics Laboratory, National Institute of Chemical Physics and Biophysics, Akadeemia tee 23, 12618 Tallinn, Estonia

^c Optibrium Limited, F5-6 Blenheim House, Denny End Road, Cambridge, CB25 9PB, UK

^d Department of Chemistry, McGill University, 801 Sherbrooke Street West, H3A 0B8, Montreal, Quebec, Canada

† Dedicated to the memory of late Prof. Hans J. Reich.

‡ Electronic supplementary information (ESI) available: Synthesis, isolation, characterization of **cycHC[12]** by HRMS, 1D and 2D NMR, VT-NMR, conformational dynamics analysis, DFT calculations is described. See DOI: 10.1039/d0cc06817a



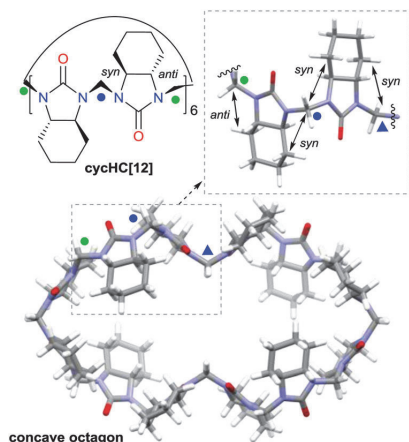


Fig. 1 Chemical structure of **cycHC[12]** and the lowest energy DFT-modelled (BP86/SVP) structure of **cycHC[12]**. Blue and green dots represent *syn*- and *anti*-methylene bridge configurations, respectively. The blue triangle represents the *syn* bridge directed inside the cavity.

Due to the alternating orientations of the cyclohexanomonomers in HCs, the methylene bridges have two possible configurations: *syn* or *anti*. The *syn*- and *anti*-configuration describes the mutual orientation of the bridge and its nearest neighboring cyclohexano carbon skeleton – bridges that are pointed toward the same direction as the cyclohexano skeleton are designated as *syn*. In contrast, those pointed at opposite sides are designated as *anti* (Fig. 1). These distinct bridges, marked by blue and green colored marks (dots or triangles), are shown in Fig. 1–3. Smaller chiral homologs of cycHCs are known to adopt a barrel-shaped conformation with distinct *syn*- or *anti*-oriented bridges in a one-to-one ratio seen in their NMR analysis.^{21,27} Thus, a similarly regular 12-gon shape was initially expected for the new chiral **cycHC[12]** macrocycle (Fig. 2, on the right). However, NMR analysis of **cycHC[12]** in toluene at 265 K did not support a highly symmetric regular 12-gon conformation (Fig. 3). The experimental 1D and 2D NMR spectra of **cycHC[12]** instead showed the presence of three non-equal urea groups (α , β , and γ) and four methylene bridges (B1, B2, B3, and B4), indicating the existence of two perpendicular axes of C_2 symmetry

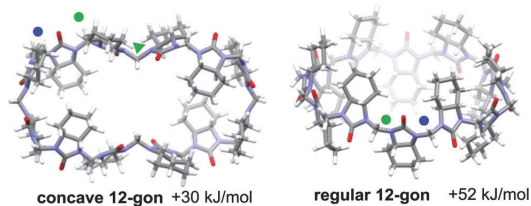


Fig. 2 DFT-modeled structures of **cycHC[12]** (BP86/SVP) higher energy conformers. Blue and green dots represent *syn*- and *anti*-methylene bridge configurations, respectively. The green triangle indicates the *anti*-bridge directed inside the cavity.

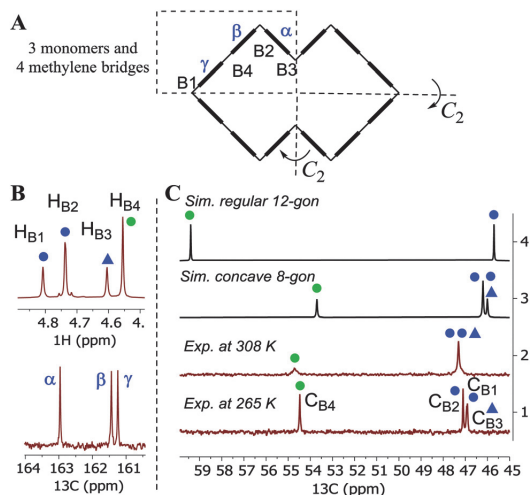


Fig. 3 (A) Symmetry of **cycHC[12]** and the position of symmetry-related monomers (α , β , γ). (B) NMR spectra of **cycHC[12]** bridge protons H_{B1} – H_{B4} (upper) and carbonyl carbons (lower) in *d*-toluene. (C) Stacked ^{13}C -NMR spectra of bridge carbons C_{B1} – C_{B4} : (1) experimental at 265 K, (2) experimental at 308 K, (3) simulated for concave octagon, and (4) simulated for regular 12-gon (see simulation details in S20, ESI ‡). Blue and green dots designate *syn* (B1 and B2) and *anti* (B4) bridge configurations. The blue triangles represent *syn*-configuration bridges, which are directed inside the cavity (B3).

that divide the structure into four symmetry-related parts (Fig. 3A and B). These structural features, supported by NMR data, suggest a concave polygon conformation, with two methylene bridges flipped towards the center of the cavity (Fig. 1, designated with a triangle).

DFT (BP86/SVP) modeling was used to rationalize the NMR results and investigate the potential **cycHC[12]** conformers. Three initial geometries were selected, the first based on the barrel-like geometry of smaller homologs and the second and third, concave polygons based on the symmetry revealed by the NMR results. The difference between the two concave structures is the configuration of their inwards-pointing methylene groups. The concave octagon conformer has a *syn*-oriented inner bridge marked by the blue triangle (Fig. 1), and the concave 12-gon has an *anti*-oriented inner bridge, marked by the green triangle in (Fig. 2). Of the three optimized structures, the concave octagon conformer is the most prevalent, as it is 52 and 30 kJ mol^{-1} lower in energy than the regular and concave 12-gon conformers (see S18, ESI ‡) respectively. Furthermore, the chemical shifts predicted for the concave octagon conformer (Fig. 3C, spectrum 3) are in good agreement with the experimental values (Fig. 3C, spectrum 1), strongly supporting the presence of this **cycHC[12]** conformation at 265 K. The calculated ^{13}C chemical shifts of the regular 12-gon conformation (45.7 and 59.4 ppm) (Fig. 3C, spectrum 4) deviate significantly from the experimental **cycHC[12]** spectra. They more closely resemble those of the barrel-shaped **cycHC[8]** methylene bridges in similar chiral environments (46.88 ppm and 56.04 ppm)



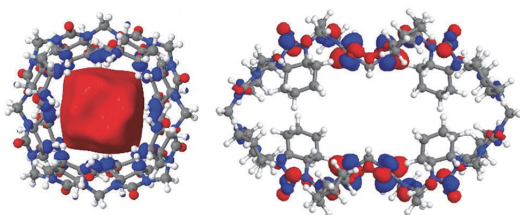


Fig. 4 LUMO of **cycHC[8]** and **cycHC[12]** concave octagons.

(see S20, ESI[†]). In the **cycHC[12]** experimental ¹³C NMR spectra, the *anti*-configuration bridge carbons C_{B4} resonate at a higher frequency (54.48 ppm) than the C_{B3} bridge carbons, which are turned inside the cavity and therefore adopt a *syn* configuration. The latter bridges resonate in a similar range (46.91–47.10 ppm) as the *syn*-oriented bridges C_{B1} and C_{B2} (Fig. 1 and 2). This results from the orientation of C_{B3} into the cavity, causing its electronic environment, and thus its NMR shielding, to resemble the C_{B1} and C_{B2} bridges. In addition, calculations with a higher level of theory, LC-TPSS/aug-pVTZ, were performed to increase the accuracy of the calculated chemical shifts. The addition of long-range corrections made the structures more compact, but the resulting chemical shift values had a greater deviation from the experimental results compared to BP86/SVP (see Table S7, ESI[†]). The deviation is due to the compression of **cycHC[12]**, but this is probably not a good representation of the experimental geometry due to the lack of explicit solvent molecules.³⁹

Interestingly, the rotation of the two methylene bridges into the cavity induces a conformational change that strongly affects the localization of the frontier orbitals, concentrating the lowest unoccupied molecular orbital (LUMO) on the urea monomers rather than inside the cavity as observed for **cycHC[8]** and all smaller HCs^{28,40} (Fig. 4 and S21, ESI[†]).

Variable temperature (VT) ¹H-NMR spectra show the merging of the H_{B1} signal with the H_{B2} signal and the H_{B3} signal with the

H_{B4} signal in pairs between 265 K and 308 K (Fig. 5B, stacked spectra 1 and 6). We suggest this arises from the onset of a dynamic exchange, whereby bridges B1 and B2 and bridges B3 and B4 exchange their magnetic environments in response to the conformational changes of the macrocycle. The merging of the H_{B1} signal with the H_{B2} signal and the H_{B3} signal with the H_{B4} signal both arise from the same conformational changes in the macrocycle. The bridge flip motion can be best explained as a flip of the B3 bridge outwards and the B4 bridge inwards, which simultaneously exchanges the magnetic environments of the B1 and B2 bridge moieties (Fig. 5A). This process reduces the distance between opposing C_{B4} methylene bridges from 18 Å to 7 Å while increasing the distance between C_{B3} bridges. At 265 K, the dynamic exchange is slow, and all bridge environments give separate signals in the ¹H NMR spectrum; however, above the coalescence temperature (308 K), the conformations are in fast exchange in the NMR timescale on an 800 MHz spectrometer, resulting in the signals merging (Fig. 5B stacked spectra 6–10).

At temperatures above 308 K, the two resulting proton signals coalesce, indicating an additional mode of dynamic exchange. We hypothesize that this results from the free rotation of the monomers (Fig. 5B stacked spectra 6–10 and Fig. 5C), averaging the magnetic environments of the *syn*- and *anti*-configurations and the inwards and outwards orientations of the bridges. We refer to the second dynamic exchange as the monomer flip. For this process, slow and fast exchange processes are represented by the 308 K and 348 K spectra, respectively (Fig. 5B), and the individual rate constants are available in Table S3 (ESI[†]). We undertook line shape analysis of the VT ¹H NMR spectra (see Tables S2 and S3 in ESI[†] for fitting details) to derive the activation enthalpy, entropy, and Gibbs free energy values associated with both of the dynamic exchanges (Table 1 and S12, S13, ESI[†]). At lower temperatures, the activation Gibbs free energy for the bridge flip is lower than for the monomer flip, which agrees with the monomer flip

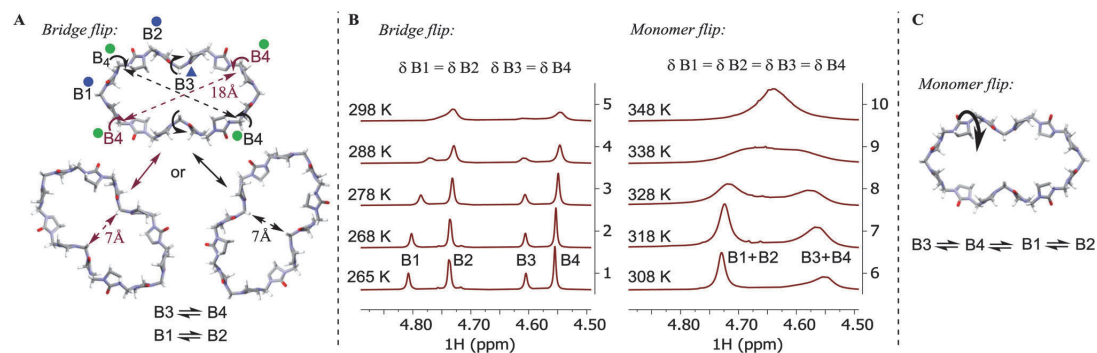


Fig. 5 (A) Illustration of the **cycHC[12]** bridge flip mechanism. Dotted arrows designate bridge moieties that move in relation to the center of the macrocycle. Solid arrows designate conformers in equilibrium. Curved arrows designate the conformational flip. Blue and green dots designate *syn*- and *anti*-bridge configurations, respectively. The triangle represents the bridges directed into the cavity. (B) Evolution of ¹H NMR bridge signals at temperatures from 265 K to 348 K showing the (a) methylene bridge flip and the (b) urea monomer flip. (C) Illustration of monomer flip at higher temperatures at which all bridge signals undergo NMR chemical exchange. On structures cyclohexano groups are omitted for clarity.



Table 1 Activation enthalpy, entropy, and Gibbs free energy values for the **cycHC[12]** bridge flip and the monomer flip at 298 K. Notes on the errors in the values are presented in ESI. Values are reported in kJ mol⁻¹

Bridge flip			Monomer flip		
ΔH^\ddagger	$T\Delta S^\ddagger$	ΔG^\ddagger	ΔH^\ddagger	$T\Delta S^\ddagger$	ΔG^\ddagger
38.5 ± 6.1	-25.5 ± 6.3	64.0 ± 8.8	59.9 ± 1.1	-6.6 ± 1.0	66.6 ± 1.5

process having a higher coalescence temperature. It is evident that the bridge flip is more strongly governed by the activation entropy, which we suggest originates from the macrocycle changing its size considerably due to this process.

In conclusion, we have synthesized, isolated, and characterized the conformation of the largest substituted HC homolog to date. **CycHC[12]** contains 12 monomers and resembles a concave octagon at 265 K, as revealed by solution NMR analysis and DFT calculations. VT ¹H NMR analysis provides evidence for two dynamic processes at elevated temperatures: a bridge flip and a monomer flip. These dynamic processes have not been observed for the **cycHC[8]** macrocycle due to its small size. We propose that the dynamic characteristics of **cycHC[12]** would allow it to bind larger species and adapt its structure for a guest molecule by taking advantage of the change in cavity diameter of nearly 1 nm.

The authors would like to acknowledge Oliver Paberits and Karin Kreekman for experimental assistance. We also thank the Estonian MER (Grant No. PRG399 and PSG400), the ERDF (CoE 3.2.0101.08-0017, CoE 2014-2020.4.01.15-0013, and CoE TK134), and H2020-FETOPEN (828779 (INITIO)) for financial support.

Conflicts of interest

There are no conflicts of interest to declare.

Notes and references

- V. Balzani, A. Crechi, F. M. Raymo and J. F. Stoddart, *Angew. Chem., Int. Ed.*, 2000, **39**, 3348–3391.
- L. Cronin, P. A. McGregor, S. Parsons, S. Teat, R. O. Gould, V. A. White, N. J. Long and N. Robertson, *Inorg. Chem.*, 2004, **43**, 8023–8029.
- X. Chi, G. Yu, L. Shao, J. Chen and F. Huang, *J. Am. Chem. Soc.*, 2016, **138**, 3168–3174.
- W. Saenger, J. Jacob, K. Gessler, T. Steiner, D. Hoffmann, H. Sanbe, K. Koizumi, S. M. Smith and T. Takaha, *Chem. Rev.*, 1998, **98**, 1787–1802.
- K. Gessler, I. Usón, T. Takaha, N. Krauss, S. M. Smith, S. Okada, G. M. Sheldrick and W. Saenger, *Proc. Natl. Acad. Sci. U. S. A.*, 1999, **96**, 4246–4251.
- H. Taira, H. Nagase, T. Endo and H. Ueda, *J. Inclusion Phenom. Macrocyclic Chem.*, 2006, **56**, 23–28.
- M. G. Gotsev and P. M. Ivanov, *ARKIVOC*, 2007, **13**, 167–189.
- K. I. Assaf, D. Gabel, W. Zimmermann and W. M. Nau, *Org. Biomol. Chem.*, 2016, **14**, 7702–7706.
- C. Sonnendecker, S. Thürmann, C. Przybylski, F. D. Zitzmann, N. Heinke, Y. Krauke, K. Monks, A. A. Robitzki, D. Belder and W. Zimmermann, *Angew. Chem., Int. Ed.*, 2019, **58**, 6411–6414.
- K. Harata, T. Endo, H. Ueda and T. Nagai, *Supramol. Chem.*, 1998, **9**, 143–150.
- J. Jacob, K. Gessler, D. Hoffmann, H. Sanbe, K. Koizumi, S. M. Smith, T. Takaha and W. Saenger, *Angew. Chem., Int. Ed.*, 1998, **37**, 605–609.
- X.-B. Hu, Z. Chen, L. Chen, L. Zhang, J.-L. Hou and Z.-T. Li, *Chem. Commun.*, 2012, **48**, 10999–11001.
- V. Guérineau, M. Rollet, S. Viel, B. Lepoittevin, L. Costa, P. Saint-Aguet, R. Laurent, P. Roger, D. Gignes, C. Martini and V. Huc, *Nat. Commun.*, 2019, **10**, 1–14.
- C. Bavoux, R. Baudry, I. Dumazet-Bonnamour, R. Lamartine and M. Perrin, *J. Inclusion Phenom. Macrocyclic Chem.*, 2001, **40**, 221–224.
- Q. Li, S.-C. Qiu, J. Zhang, K. Chen, Y. Huang, X. Xiao, Y. Zhang, F. Li, Y.-Q. Zhang, S.-F. Xue, Q.-J. Zhu, Z. Tao, L. F. Lindoy and G. Wei, *Org. Lett.*, 2016, **18**, 4020–4023.
- J. Kim, I.-S. Jung, S.-Y. Kim, E. Lee, J.-K. Kang, S. Sakamoto, K. Yamaguchi and K. Kim, *J. Am. Chem. Soc.*, 2000, **122**, 540–541.
- W.-H. Huang, S. Liu, P. Y. Zavalij and L. Isaacs, *J. Am. Chem. Soc.*, 2006, **128**, 14744–14745.
- X.-J. Cheng, L.-L. Liang, K. Chen, N.-N. Ji, X. Xiao, J.-X. Zhang, Y.-Q. Zhang, S.-F. Xue, Q.-J. Zhu, X.-L. Ni and Z. Tao, *Angew. Chem., Int. Ed.*, 2013, **52**, 7252–7255.
- N. N. Andersen, M. Lisbjerg, K. Eriksen and M. Pittelkow, *Isr. J. Chem.*, 2018, **58**, 435–448.
- Y. Miyahara, K. Goto, M. Oka and T. Inazu, *Angew. Chem., Int. Ed.*, 2004, **43**, 5019–5022.
- E. Prigorchenko, M. Oeren, S. Kaabel, M. Fomitsenko, I. Reile, I. Järving, T. Tamm, F. Topic, K. Rissanen and R. Aav, *Chem. Commun.*, 2015, **51**, 10921–10924.
- S. Kaabel, J. Adamson, F. Topić, A. Kiesilä, E. Kalenius, M. Öeren, M. Reimund, E. Prigorchenko, A. Löökene, H. J. Reich, K. Rissanen and R. Aav, *Chem. Sci.*, 2017, **8**, 2184–2190.
- M. Fomitsenko, E. Shmatova, M. Öeren, I. Järving and R. Aav, *Supramol. Chem.*, 2014, **26**, 698–703.
- S. Kaabel, R. S. Stein, M. Fomitsenko, I. Järving, T. Friščić and R. Aav, *Angew. Chem., Int. Ed.*, 2019, **58**, 6230–6234.
- T. Fiala and V. Sindelar, *Synlett*, 2013, **24**, 2443–2445.
- Y. Li, L. Li, Y. Zhu, X. Meng and A. Wu, *Cryst. Growth Des.*, 2009, **9**, 4255–4257.
- R. Aav, E. Shmatova, I. Reile, M. Borissova, F. Topić and K. Rissanen, *Org. Lett.*, 2013, **15**, 3786–3789.
- M. Öeren, E. Shmatova, T. Tamm and R. Aav, *Phys. Chem. Chem. Phys.*, 2014, **16**, 19198–19205.
- E. Prigorchenko, S. Kaabel, T. Narva, A. Baškir, M. Fomitsenko, J. Adamson, I. Järving, K. Rissanen, T. Tamm and R. Aav, *Chem. Commun.*, 2019, **55**, 9307–9310.
- O. Reany, A. Mohite and E. Keinan, *Isr. J. Chem.*, 2018, **58**, 449–460.
- T. Lizal and V. Sindelar, *Isr. J. Chem.*, 2018, **58**, 326–333.
- J. Svec, M. Necas and V. Sindelar, *Angew. Chem., Int. Ed.*, 2010, **49**, 2378–2381.
- M. A. Yawer, V. Havel and V. Sindelar, *Angew. Chem., Int. Ed.*, 2015, **54**, 276–279.
- V. Havel, M. Babiak and V. Sindelar, *Chem. – Eur. J.*, 2017, **23**, 8963–8968.
- V. Havel, J. Svec, M. Wimmerova, M. Dusek, M. Pojarova and V. Sindelar, *Org. Lett.*, 2011, **13**, 4000–4003.
- M. Lisbjerg, B. M. Jessen, B. E. Nielsen, A. Ø. Madsen and M. Pittelkow, *Chem. Sci.*, 2014, **5**, 2647–2650.
- M. Lisbjerg, B. E. Nielsen, B. O. Mülhøj, S. P. A. Sauer and M. Pittelkow, *Org. Biomol. Chem.*, 2015, **13**, 369–373.
- M. Lisbjerg, H. Valkenier, B. M. Jessen, H. Al-Kerdi, A. P. Davis and M. Pittelkow, *J. Am. Chem. Soc.*, 2015, **137**, 4948–4951.
- M. A. Iron, *J. Chem. Theory Comput.*, 2017, **13**, 5798–5819.
- T. F. G. G. Cova, S. C. C. Nunes, A. J. M. Valente, T. M. V. D. Pinho e Melo and A. A. C. C. Pais, *J. Mol. Liq.*, 2017, **242**, 640–652.



Appendix 3

Publication III

T. Shalima, **K. A. Mishra**, S. Kaabel, L. Ustrnul, S. Bartkova, K. Tõnsuaadu, I. Heinmaa, R. Aav, 'Cyclohexanohemicucurbit[8]uril Inclusion Complexes with Heterocycles and Selective Extraction of Sulfur Compounds from Water'. *Frontiers in Chemistry*, **2021**, *9*, 1036.

Reprinted with permission from Frontiers in Chemistry Open Access License Agreement rules.



Cyclohexanohemicucurbit[8]uril Inclusion Complexes With Heterocycles and Selective Extraction of Sulfur Compounds From Water

Tatsiana Shalima¹, Kamini A. Mishra¹, Sandra Kaabel², Lukas Ustrnul¹, Simona Bartkova¹, Kaia Tõnsuaadu³, Ivo Heinmaa⁴ and Riina Aav^{1*}

¹Department of Chemistry and Biotechnology, School of Science, Tallinn University of Technology, Tallinn, Estonia, ²Department of Chemistry, McGill University, Montreal, QC, Canada, ³Laboratory of Inorganic Materials, School of Engineering, Institute of Materials and Environmental Technology, Tallinn University of Technology, Tallinn, Estonia, ⁴Laboratory of Chemical Physics, National Institute of Chemical Physics and Biophysics, Tallinn, Estonia

Solid-phase extraction that utilizes selective macrocyclic receptors can serve as a useful tool for removal of chemical wastes. Hemicucurbiturils are known to form inclusion complexes with suitably sized anions; however, their use in selective binding of non-charged species is still very limited. In this study, we found that cyclohexanohemicucurbit [8]uril encapsulates five- and six-membered sulfur- and oxygen-containing unsubstituted heterocycles, which is investigated by single-crystal X-ray diffraction, NMR spectroscopy, isothermal titration calorimetry, and thermogravimetry. The macrocycle acts as a promising selective sorption material for the extraction of sulfur heterocycles, such as 1,3-dithiolane and α -lipoic acid, from water.

Keywords: Hemicucurbituril, solid-phase extraction, heterocycles, inclusion complex, lipoic acid, sorbent recycling, SC-XRD, MAS NMR

OPEN ACCESS

Edited by:

Cally Jo Elizabeth Haynes,
University College London,
United Kingdom

Reviewed by:

Khaleel Assaf,
Al-Balqa Applied University, Jordan
Paula M. Marcos,
University of Lisbon, Portugal

*Correspondence:

Riina Aav
riina.aav@taltech.ee

Specialty section:

This article was submitted to
Supramolecular Chemistry,
a section of the journal
Frontiers in Chemistry

Received: 30 September 2021

Accepted: 04 November 2021

Published: 03 December 2021

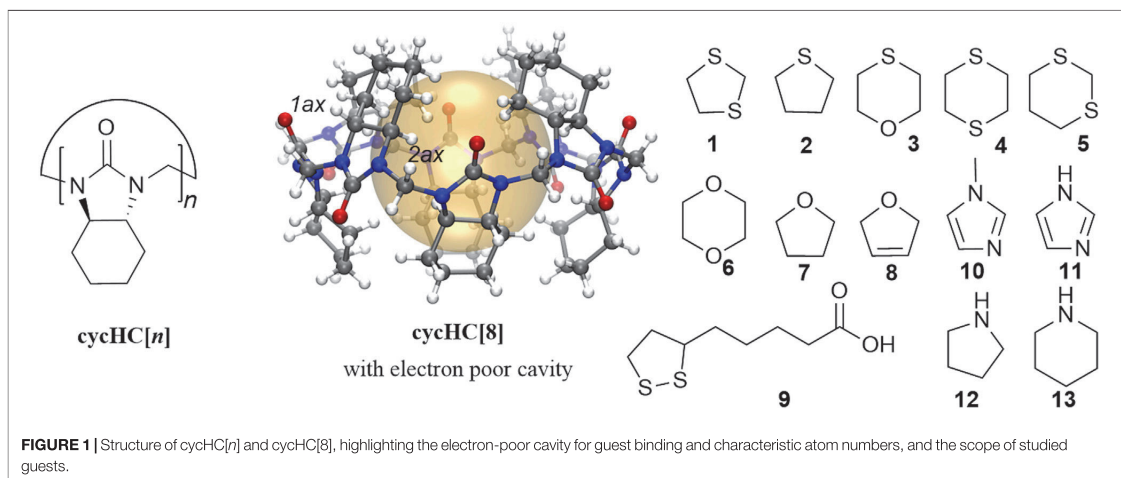
Citation:

Shalima T, Mishra KA, Kaabel S,
Ustrnul L, Bartkova S, Tõnsuaadu K,
Heinmaa I and Aav R (2021)
Cyclohexanohemicucurbit[8]uril
Inclusion Complexes With
Heterocycles and Selective Extraction
of Sulfur Compounds From Water.
Front. Chem. 9:786746.
doi: 10.3389/fchem.2021.786746

INTRODUCTION

Hemicucurbiturils, formed in templated single-step oligomerization reactions (Kaabel and Aav, 2018), are single-bridged cucurbituril-type macrocycles (Andersen et al., 2018; Lizal and Sindelar, 2018; Xi et al., 2018) that bear an electron-deficient hydrophobic cavity. The latter grants these macrocycles the ability to encapsulate anions (Buschmann et al., 2005; Cucolea et al., 2016; Kaabel et al., 2017; Assaf and Nau, 2018; Reany et al., 2018; Vázquez and Sindelar, 2018; Andersen et al., 2019; Kandrnálová et al., 2019; Valkenier et al., 2019; Maršálek and Šindelář, 2020); in addition, the formation of complexes with acids and some neutral species has been reported in the previous work. In particular, unsubstituted hemicucurbit[*n*]urils (*n* = 6, 12) bind phenol derivatives (Jin et al., 2016a; 2016b) and ferrocene (Jin et al., 2017), and cyclohexanohemicucurbit[*n*]urils cycHC [*n*] (*n* = 6, 8, 12) (Li et al., 2009; Aav et al., 2013; Prigorchenko et al., 2015, 2019; Mishra et al., 2020) form external complexes with both inorganic and organic acids (Öeren et al., 2014; Ustrnul et al., 2019, 2021). We envisioned that heterocycles 1–13 have relatively high electron densities compared to carbocycles and may therefore be able to occupy space within the eight-membered cycHC[8] (Figure 1).

S-heterocycles are compounds of interest as these substances are bioactive (Rezanka et al., 2006; Lamberth et al., 2015) and may contribute to the distinct aromas of food (Mottram and Mottram, 2002; Mahadevan and Farmer, 2006; Schoenauer and Schieberle, 2018), and heterocycle 2 is added as an odorant to the natural gas. Unsubstituted S-containing heterocycles, such as 1,3-dithiolane 1 and



1,4-thioxane **3**, are found in meat (Garbusov et al., 1976) and around chemical warfare dumping sites where they are formed due to the degradation of mustard gas (Røen et al., 2010; Magnusson et al., 2016; Vanninen et al., 2020). Bioactive α -lipoic acid **9** exhibits antioxidant properties (Rochette et al., 2013; Salehi et al., 2019), and to date, cyclodextrins have been used to enhance its solubility and bioavailability (Lin-Hui et al., 1995; Maeda et al., 2010; Takahashi et al., 2011; Ikuta et al., 2013; Racz et al., 2013; Caira et al., 2017; Celebioglu and Uyar, 2019). Carbon-based materials are used for solid-phase extraction (SPE) of S-heterocycles from water (Lees et al., 2017; Jöul et al., 2018); however, such systems are designed to non-selectively retain all non-polar to moderately polar components.

In this study, we report that cycHC[8] encapsulates neutral electron-rich heterocycles containing sulfur and oxygen atoms and acts as a selective sorbent material for suitably sized S-heterocycles. Complexation was characterized by ^1H NMR titration and isothermal titration calorimetry (ITC), single-crystal X-ray diffraction (SC-XRD), ^{13}C solid-state CPMAS NMR (ssNMR), and thermogravimetric analysis (TGA) and applied in SPE.

MATERIALS AND METHODS

Materials, Reagents, and Solvents

All reagents and solvents were purchased from commercial suppliers. Ultrapure water for sample preparation in ITC and extraction studies was obtained by means of Milli-Q[®] IQ 7003/05/10/15. Macrocyclic host compounds (cycHC[*n*]) were synthesized in our laboratory according to the procedures described in the literature (Aav et al., 2013; Prigorchenko et al., 2015; Kaabel et al., 2019).

Binding of Heterocycles in Solid State

Single crystals of the host-guest complexes were obtained from saturated cycHC[8] solutions in methanol by adding 20 μL of the

respective guest compound. SC-XRD data were collected at 123 K on a Rigaku Compact HomeLab diffractometer, equipped with a Saturn 944 HG CCD detector and an Oxford Cryostream cooling system using monochromatic Cu- $K\alpha$ radiation (1.54178 Å) from a MicroMax[™]-003 sealed tube microfocus X-ray source. The crystallographic data are deposited with the Cambridge Crystallographic Data Centre (CCDC 2069875–2069879) and can be obtained free of charge *via* www.ccdc.cam.ac.uk/data_request/cif.

Complexation between 1,3-dithiolane and cycHC[*n*] upon SPE was investigated by simultaneous thermogravimetry and differential thermal analysis coupled with evolved gas mass spectrometric analysis (TG-DTA/EGA-MS). The measurements were performed in the apparatus consisting of a Setaram SetSys-Evo 1600 thermal analyzer and a Pfeiffer OmniStar quadrupole mass spectrometer. Additionally, binding of 1,3-dithiolane and α -lipoic acid by cycHC[*n*] was characterized with ^{13}C ssNMR spectroscopy. The solid complexes were obtained *via* ball milling of cycHC[8] with the respective guest in the presence of a small amount of water. The ssNMR spectra were acquired on a Bruker Avance II spectrometer at 14.1 T magnetic field (^{13}C resonance frequency 150.91 MHz) using a home-built MAS probe for $25 \times 4\text{-mm}$ Si_3N_4 rotors.

Binding of Heterocycles in Solution

Complexation-induced shifts of cycHC[8] were studied by ^1H NMR spectroscopy in 3 mM CD_3OD solution upon addition of 60 eq. of the respective guest compound. Association constants for the complexation with 1,3-dithiolane, 1,4-thioxane, and 1,4-dioxane were determined by ^1H NMR titration. ^1H NMR (400 MHz) spectra in solution were recorded on a Bruker Avance III spectrometer. Thermodynamic measurements by ITC were performed on a MicroCal PEAQ-ITC calorimeter using a 200- μL calorimetric cell and a 40- μL syringe.

Characterization of the Sorbents

Prior to analysis and further extraction experiments, cycHC[*n*] were milled in an FTS-1000 shaker mill at 30 Hz frequency by using a 14-ml ZrO₂-coated grinding jar charged with 3 × 7-mm ZrO₂ milling balls for 30 min. Surface area analysis of the milled cycHC[*n*] was performed on a KELVIN 1040/1042 Sorptometer at 150°C with N₂ as an adsorptive gas and He as a carrier gas. The obtained data were processed by Kelvin 1042 V3.12 software. Microscopic investigation of cycHC[*n*] particle sizes and their distribution was carried out before and after milling. Solid samples were examined by using an Olympus BX61 microscope. The acquired images were further analyzed by CellProfiler (version 4.0.3) software (Carpenter et al., 2006; McQuin et al., 2018).

Extraction of Heterocycles From Aqueous Solutions

SPE was performed for 0.4–2.7 mM aqueous solutions of heterocyclic guests. A solid sorbent [5 or 20 M excess of cycHC[*n*] or powdered silicarbon TH90 special, Aktivkohle, taken in the equivalent amount by weight/extraction performance to that of the macrocyclic host] was dispersed in the guest solution and rotated for 30–60 min on a Vortex-Genie 2 mixer or Stuart magnetic stirrer. The heterogeneous mixture was further separated by using either a Hettich Universal 32R centrifuge or RC membrane syringe filters, and the liquid phase was analyzed for the guest content by HPLC or UV spectrophotometry. HPLC determination was performed on an Agilent 1200 Series HPLC system equipped with a multiple wavelength detector (MWD), Macherey-Nagel Nucleoshell RP18 column (150 × 3.0 mm, 2.7 μm), or Phenomenex Kinetex XB-C18 column (150 × 4.6 mm, 2.6 μm). UV absorption was measured by using a Jasco V-730 dual beam spectrophotometer and Varian Cary 50 UV-vis spectrophotometer in 10 mm quartz cuvettes. Mettler Toledo AB204-2 analytical balances (precision 0.1 mg) and Radwag MYA 11.4Y microbalances (precision 0.006 mg) were used in sample preparation.

Reusability of cycHC[8] was investigated by comparing its removal efficiency after four sorption–desorption cycles. The sorption step was performed analogously to the extraction procedure. The desorption step included rinsing the material with water, drying for 6 h at 110–120°C in the oven, followed by additional drying for 3 h under vacuum. The dried macrocycle was milled according to the general procedure and utilized in the subsequent cycle.

RESULTS AND DISCUSSION

SC-XRD of Inclusion Complexes

A series of compatibly sized electron-rich S-, O-, and N-heterocyclic compounds were crystallized *via* slow evaporation, and compounds **1**, **3**, **6**, **7**, and **8** formed inclusion complexes with cycHC[8] upon co-crystallization (Figure 2 and Supplementary Materials S4–S13). The N-containing heterocycles, **12** and **13**, and the largest explored guest, **4**, did not yield crystals of inclusion complexes with cycHC[8]. Packing of **1** and **3** inclusion complexes with cycHC[8] gave rise to isomorphous (*Z'* = 4) crystal structures (Supplementary

Materials S10,11), in an arrangement previously unrecorded for cycHC[8] inclusion complexes. The packing of complexes involving O-containing smaller heterocycles **6**, **7**, and **8** appears to be mainly directed by hydrogen bonding interactions with methanol such that the resulting crystal structures are isomorphous to each other (Supplementary Materials S6–S8) and the previously published methanol solvate of cycHC[8] (Prigorchenko et al., 2015). The smaller guest molecules **6**, **7**, and **8** had a total site occupancy limited to 50–75% of the resolved disorder components. The remaining electron density map exhibited no clear features, making it impossible to resolve whether the diffuse component of the guest disorder also includes partial substitutional disorder from methanol. In contrast, the position of the larger S-containing guests, **1** and **3**, is more conserved within the respective crystal structures (Supplementary Materials S12,13) with almost no diffuse component observed, indicating that these guests have fewer orientations available within cycHC[8]. Notably, analyzing the disorder models of all inclusion complexes reveals a similarity throughout, namely, where guests are oriented with heteroatoms close to the portals of cycHC[8] (Figure 2 and Supplementary Materials S6–S13). In several structures, heterocycles are located at a suitable distance (2.7–2.8 Å) from a methanol molecule at the portal of cycHC[8] and can therefore potentially accept hydrogen bonds *via* the portals of the macrocycle. This process would explain the observed conservation of this type of guest orientation motif. The guest molecules are tightly enwrapped within cycHC[8], especially the largest S-containing compounds, **1** and **3**, that fill close to 70% of the cavity volume (Figure 2, complexes D and E), indicating that guest binding and release must be accompanied by opening and closing of the host portals. Similar conformational dynamics of cycHC[8] have been previously observed and computationally described in the binding of large anionic guests (Kaabel et al., 2017).

¹H NMR and ITC Binding Studies in Solution

Furthermore, we evaluated host-guest complex formation in CD3OD solution. Inclusion complex formation was followed by an observed chemical shift change of cycHC[8] proton H2ax (Figure 1 and Supplementary Materials S14, S15) positioned inside the cavity. Our screening study revealed that S-containing five-membered heterocycles **1** and **2** caused larger chemical shift changes of 0.064 and 0.048 ppm, respectively, compared to the six-membered heterocycles **3**, **4**, **5**, and **6**. A negligible shift was observed for **7**, while no shift was observed for **8** or the N-heterocycles **10** and **11**. Signals of **9** overlapped with the characteristic cycHC[8] signal, and, therefore, its encapsulation could not be evaluated by ¹H NMR. Nevertheless, all chemical shift changes were relatively small compared to those that occurred upon binding of anions (Kaabel et al., 2017). The binding of **1**, **3**, and **6** was further evaluated by ¹H NMR titration (Figures 3A,B). The guest binding in methanol followed the order of log*P* values (Supplementary Materials S48) and agreed with our screening study; the strongest binding was shown for **1**, followed by **3** and **6**, with values of *K* = 7.9 ± 0.2 M⁻¹, 2.18 ± 0.04 M⁻¹, and 1.77 ± 0.04 M⁻¹, respectively (Supplementary Materials S16–S22) for the 1:1 binding model.

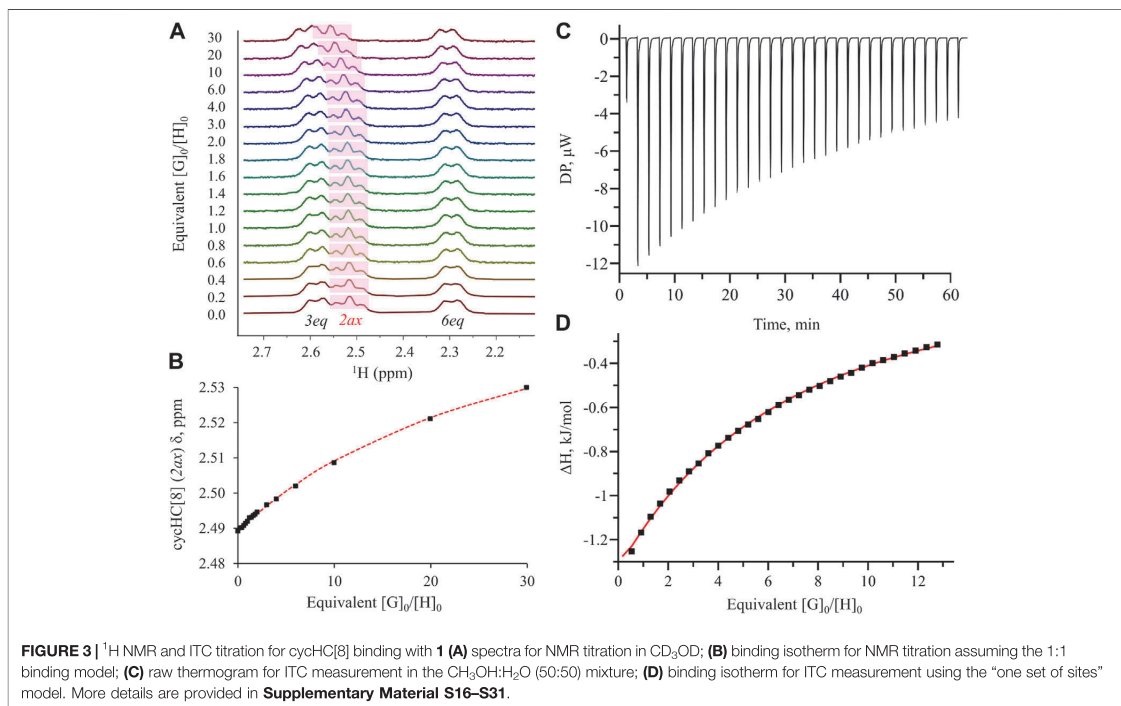
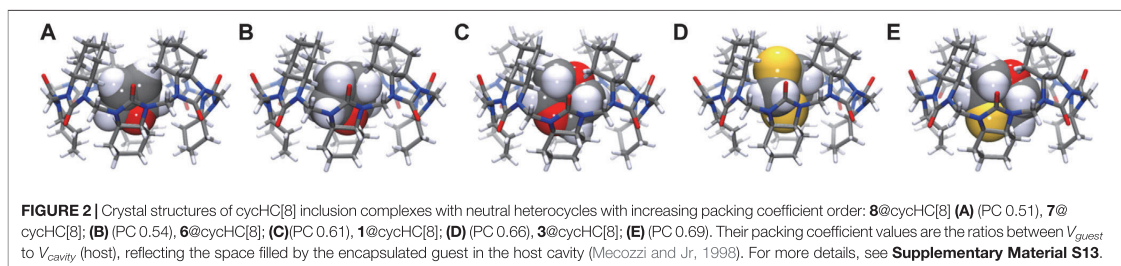


TABLE 1 | Thermodynamic parameters from ITC measurements for complexation of guests **1**, **3**, and **6** with cycHC[8] for the 1:1 binding model. All energy values are given in kJ/mol.

No.	Guest	Solvent	ΔH°	$-T\Delta S^\circ$	ΔG°	K_a, M_{-1}
1	1	CH_3OH	-9.8 ± 0.6	3.6	-6.2	13.1 ± 0.8
2	1	$\text{CH}_3\text{OH}:\text{H}_2\text{O}$ (50:50)	-20.4 ± 0.9	10.2	-10.2	65.6 ± 2.5
3	3	CH_3OH	-13.7 ± 1.2	11.4	-2.3	2.5 ± 0.2
4	3	$\text{CH}_3\text{OH}:\text{H}_2\text{O}$ (50:50)	-42.9 ± 3.9	39.6	-3.3	3.7 ± 0.3

The thermodynamic characteristics of binding were collected by ITC (Figures 3C,D; Table 1 and Supplementary Materials S23–S31). Binding of **6** with cycHC[8] in methanol was too weak

to be determined by ITC; however, K values for S-heterocycles **1** and **3** were in agreement with NMR data, showing the strongest binding for guest **1** (Table 1, lines 1 and 3). The binding of both guests in

methanol was enthalpically favorable and entropically unfavorable. A similar binding character was observed upon the binding of chaotropic anions to cycHC[8] in protic media (Kaabel et al., 2017). Although chaotropicity is mainly attributed to ionic species, chaotrope-like organic molecules have been reported in studies of crystalline hydrates (Dobrzyccki et al., 2019). The chaotropic character (Assaf and Nau, 2018) is most strongly exhibited in aqueous media, and higher solvent polarity can enhance binding to the hydrophobic host. Therefore, we further studied the binding of **1** and **3** in mixtures of CH₃OH and H₂O (Supplementary Materials S25–S27,S29). In the presence of water, binding of the guests was indeed stronger, increasing the association constant of **1** from 13 M⁻¹ in CH₃OH to a value of 66 M⁻¹ in the 1:1 CH₃OH:H₂O (50:50) mixture (Table 1, lines 1–2). For the bulkier and less hydrophobic guest **3**, the observed increase in the association constant was smaller (Table 1, lines 3–4). Binding enthalpy was strongly increased in the presence of water, accompanied by a rise in the entropic penalty for both guests (Table 1). Any further increase in the proportion of water proved impossible due to the limited solubility of cycHC[8].

Characterization of Solid cycHC[*n*] and SPE Experiments

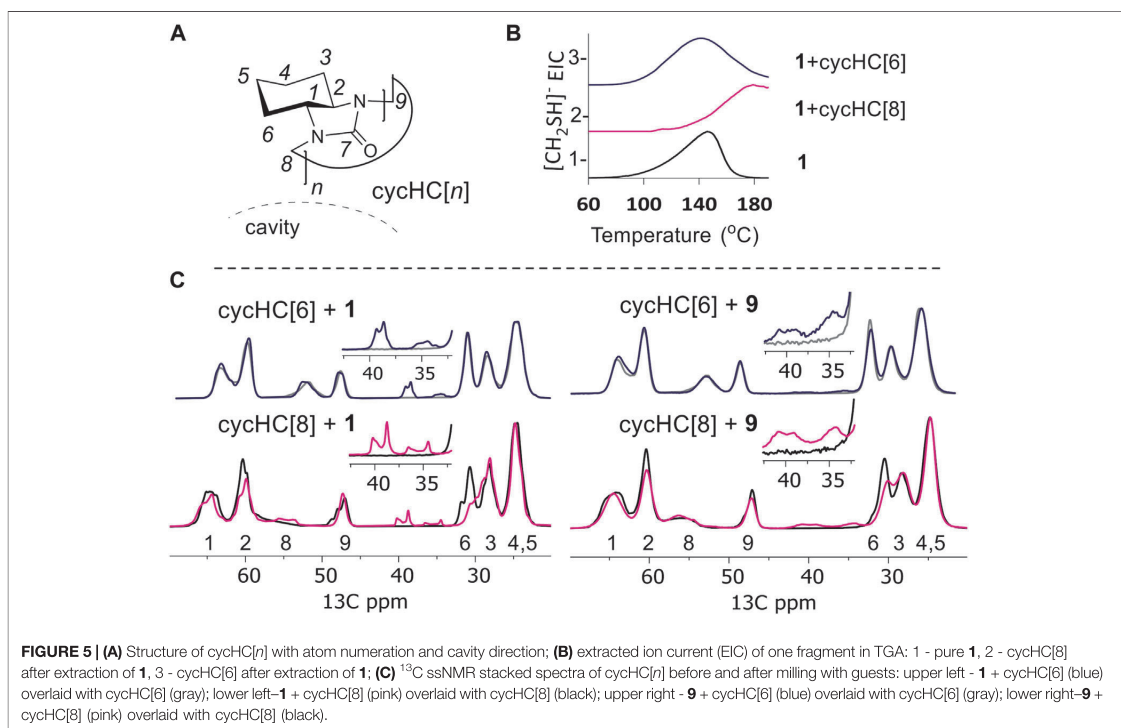
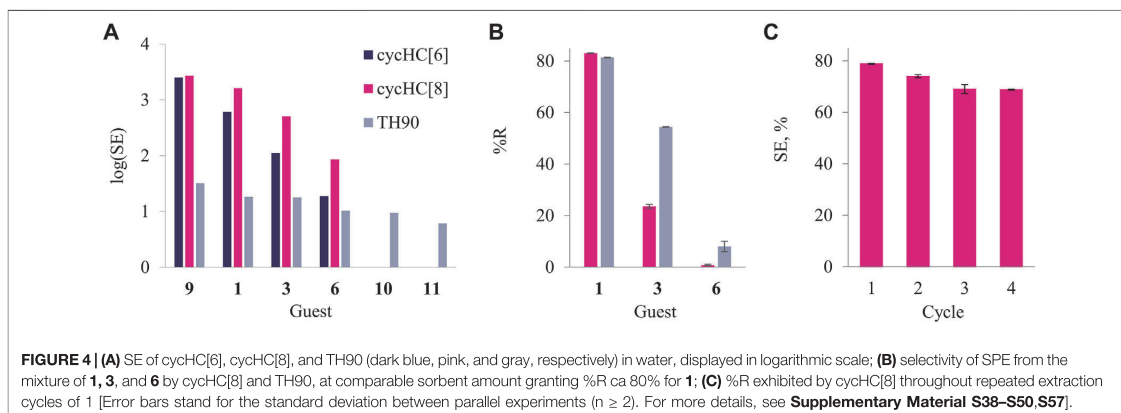
The low water solubility of the hydrophobic cycHC[8] and its ability to form inclusion complexes prompted us to investigate whether cycHC[8] can be used for the sorption of heterocycles from water *via* SPE. In parallel with cycHC[8], powdered silicarbon (TH90) and cycHC[6] were used. The cycHC[6] consists of the same monomers, so the hydrophobic properties of the outer surface are very similar to those of cycHC[8], but its cavity is much smaller (35 Å³) (Prigorchenko et al., 2015), and thus, it cannot accommodate the heterocycles studied. Hence, cycHC[6] served as an analog for differentiation between external physisorption and inclusion complex formation during extraction. The commonly used activated carbon-based sorbent TH90 was chosen as a reference to evaluate the efficiency and selectivity of sorption. The cycHC[*n*] compounds were milled before their use in extraction; microscopy studies and image analysis of the cycHC[*n*] showed that milling led to a relatively uniform particle size of 5 μm (Supplementary Materials S32–35). The Brunauer–Emmett–Teller (BET) analysis of cycHC[*n*] by N₂ adsorption–desorption (Supplementary Materials S36,37) found the available surface area to be relatively similar for both cycHC[6] and cycHC[8] with values of 6.03 m²/g and 9.02 m²/g, respectively; therefore, the cycHC[*n*] homologs are expected to have similar extraction efficiencies. In contrast, the surface area of commercially available TH90 is much larger (ca. 1000 m²/g), which allows us to predict higher extraction efficiency per weight.

SPE was performed for heterocycles **1**, **3**, **6**, **9**, **10**, and **11** by stirring the dispersed solid sorbent in an aqueous solution of each guest; the change in the guest concentration upon extraction was then determined (Supplementary Materials S47,48). The cycHC[*n*] demonstrated negligible removal of O-containing **6**, as well as N-containing **10** and **11**. The larger cycHC[8] proved to efficiently extract the S-containing **1** (78%) and moderately remove **3** (25%), while cycHC[6] was considerably less efficient at removing these guests, with a 16% extraction value for **1** and only 3% value for **3**.

As expected, TH90 acts as a non-selective adsorbent, and taken in the same ratio of guest to sorbent (by weight), it removes over 50% of all of the studied heterocycles from water. Sorption efficiency (*SE*) was expressed as the mass of the sorbed guest (μg) per cm² of the respective sorbent surface area and converted into logarithmic scale. The latter demonstrates that cycHC[*n*] possess higher affinity toward hydrophobic S-containing heterocycles, while TH90 exhibits roughly the same performance independently of the guest nature (Figure 4A). Furthermore, we evaluated sorption selectivity using a mixture of guests **1**, **3**, and **6**, and the amount of sorbent (cycHC[8] and TH90) providing ca. 80% removal percentage (%R) for guest **1** (Supplementary Materials S49, S50). Both sorbents showed low sorption of the least hydrophobic guest **6**, although TH90 proved to remove ca. 10 times more than cycHC[8]. More importantly, over two times difference was observed between the affinity of two S-heterocycles **1** and **3**; cycHC[8] is 2.3 times more selective than TH90 (Figure 4B and Supplementary Material S50); in addition, cycHC[8] sorbent is reusable after binding of **1**. A simple washing and drying procedure, followed by milling, allows the reactivation of the sorbent's surface for future use without significant loss in binding efficiency for at least four cycles (Figure 4C and Supplementary Materials S57–58).

TGA and ¹³C ssNMR Studies

The formation of inclusion complexes in the cycHC[8] sorbent after SPE of **1** was confirmed by TGA, by identifying the formation of the characteristic fragmentation product [CH₂SH]⁺ (*m/z* 47) of **1** when bound to cycHC[*n*] sorbents and in pure form (see Supplementary Material S51 for details). The evolution profiles for pure **1** and its complex with cycHC[6] (Figure 5B) occur at similar temperatures of 148°C and 138°C, respectively, indicating that no inclusion complexes form with the smaller macrocycle. Furthermore, the complex with cycHC[8] releases the characteristic degradation product at a significantly higher temperature, 189°C, indicating additional interactions between cycHC[8] and one which impact higher thermal stability to **1** (Figure 5B and Supplementary Material S51). SPE of the largest and most hydrophobic guest in this study, **9**, leads to similar efficiency of extraction by cycHC[6] and cycHC[8], with %R values of 46 and 78%, respectively (Supplementary Materials S47,48), which may indicate a different binding behavior of **9** to cycHC[*n*] in comparison to **1**. To better understand the interaction of guests **1** and **9** with cycHC[8] and cycHC[6], we investigated complex formation using ¹³C ssNMR spectroscopy (Figure 5C and Supplementary Materials S52–56). Recently, complex formation *via* mechanochemical agitation of cucurbit[7]uril was followed by ssNMR (Dračinský et al., 2021). Powders obtained by liquid-assisted grinding of cycHC[*n*] with the guest in the presence of water served as the model for binding during the extraction process at the solute–solid interphase. Figure 5C illustrates the changes induced upon binding of **1** with cycHC[8] and cycHC[6] (Supplementary Materials S53,54). The most significant change after milling is observed in the ¹³C signal of carbons 2 and 6, pointing inside the cavity of cycHC[8] (Figure 5C lower left and Supplementary Material S54). Intensities of these signals are decreased and the chemical shift in position 6 changed from



30.6 to 29.8 ppm, evidencing the formation of inclusion complex **1**@cycHC[8]. In contrast, the spectra of **1** milled with cycHC[6] do not evidence such changes (**Figure 5C** upper left and **Supplementary Material S53**), confirming that physisorption on the surface of cycHC[n] does not have a significant effect on sorbent ssNMR shifts. In an analogous experiment with **9** (**Figure 5C** right and **Supplementary Materials S54–S56**)

similar trends can be observed, that is, a change in the signal intensities of carbons 2 and 6 of cycHC[8], accompanied by a slight chemical shift change at carbon 6 (**Figure 5C** lower right) and no change in the spectrum of cycHC[6] (**Figure 5C** upper right). Thus, the prominent selectivity of cycHC[8] toward binding of five-membered S-heterocycles **1** and **9** is explained by inclusion complex formation during SPE. Unfortunately, no

enantioselectivity was observed during extraction of stereoisomers of **9** (Supplementary Material S48).

CONCLUSION

Encapsulation of five- and six-membered electron-rich heterocyclic guests by cycHC[8] is mostly related to their size, which must be complementary with the host cavity, and the hydrophobic effect is one of the driving forces of the interaction. From the binding studies of **1** and **3** with cycHC[8] in methanol and a methanol–water mixture, complex formation was found to be even more favorable in the presence of water and the thermodynamic characteristics resembled the binding of chaotropic anions. We showed that cycHC[8] can serve as a selective solid sorbent material for SPE of sulfur heterocycles from aqueous solutions; in addition, cycHC[8] was successfully applied for selective extraction of **1** and **9**. The ssNMR, TGA, and comparative extraction by homologous cycHC[6] and commonly used TH90 revealed that prominent selectivity of cycHC[8] toward binding of five-membered S-heterocycles is driven by inclusion complex formation. Design of advanced material with increased surface area would enhance the extraction performance even further. Crucially, the solid cycHC[8] sorbent material can be reused, which makes it a candidate for applications in selective SPE systems or the removal of pollutants and other target compounds from water, based on molecular recognition properties.

DATA AVAILABILITY STATEMENT

The datasets presented in this study can be found in Supplementary Material.

REFERENCES

- Aav, R., Shmatova, E., Reile, I., Borissova, M., Topić, F., and Rissanen, K. (2013). New Chiral Cyclohexylhemicurbit[6]uril. *Org. Lett.* 15, 3786–3789. doi:10.1021/ol401766a
- Andersen, N. N., Eriksen, K., Lisbjerg, M., Ottesen, M. E., Milhøj, B. O., Sauer, S. P. A., et al. (2019). Entropy/Enthalpy Compensation in Anion Binding: Biotin[6]uril and Biotin-L-Sulfoxide[6]uril Reveal Strong Solvent Dependency. *J. Org. Chem.* 84, 2577–2584. doi:10.1021/acs.joc.8b02797
- Andersen, N. N., Lisbjerg, M., Eriksen, K., and Pittelkow, M. (2018). Hemicurbit[n]urils and Their Derivatives - Synthesis and Applications. *Isr. J. Chem.* 58, 435–448. doi:10.1002/ijch.201700129
- Assaf, K. I., and Nau, W. M. (2018). The Chaotropic Effect as an Assembly Motif in Chemistry. *Angew. Chem. Int. Ed.* 57, 13968–13981. doi:10.1002/anie.201804597
- Buschmann, H.-J., Cleve, E., and Schollmeyer, E. (2005). Hemicurbit[6]uril, a Selective Ligand for the Complexation of Anions in Aqueous Solution. *Inorg. Chem. Commun.* 8, 125–127. doi:10.1016/j.inoche.2004.11.020
- Caira, M., Bourne, S., and Mzondo, B. (2017). Encapsulation of the Antioxidant R-(+)- α -Lipoic Acid in Permethylated α - and β -Cyclodextrins: Thermal and X-ray Structural Characterization of the 1:1 Inclusion Complexes. *Molecules* 22, 866. doi:10.3390/molecules22060866
- Carpenter, A. E., Jones, T. R., Lamprecht, M. R., Clarke, C., Kang, I., Friman, O., et al. (2006). CellProfiler: Image Analysis Software for Identifying and

AUTHOR CONTRIBUTIONS

RA contributed to conceptualization and idea of the research; TS and KM synthesized cycHC[n]; SK accomplished crystallization and SC-XRD studies; TS, KM, and SK performed ^1H NMR screening and titrations; KM and LU fulfilled ITC measurements; TS and KM investigated SPE; SB carried out microscopic characterization of cycHC[n]; KT was responsible for TGA; TS and IH conducted ^{13}C ssNMR experiments. The manuscript was written via contribution of all authors.

FUNDING

This work was supported by the Estonian Research Council Grants (PRG399, MOBJD556, and MOBJD592), the European Regional Development Fund (CoE 2014-2020.4.01.15-0013 and CoE TK134), and H2020- FETOPEN 828779 (INITIO).

ACKNOWLEDGMENTS

The authors would like to thank Elina Suut and Jagadeesh Varma Nallaparaju for the synthesis of cycHC[n], Dr. Heidi Lees and Piia Jõul for providing the S-containing heterocyclic compounds used for crystallization and extraction experiments, and Mai Uibu for BET analysis.

SUPPLEMENTARY MATERIAL

The Supplementary Material for this article can be found online at: <https://www.frontiersin.org/articles/10.3389/fchem.2021.786746/full#supplementary-material>

Quantifying Cell Phenotypes. *Genome Biol.* 7, R100. doi:10.1186/gb-2006-7-10-r100

Celebioglu, A., and Uyar, T. (2019). Encapsulation and Stabilization of α -Lipoic Acid in Cyclodextrin Inclusion Complex Electrospun Nanofibers: Antioxidant and Fast-Dissolving α -Lipoic Acid/Cyclodextrin Nanofibrous Webs. *J. Agric. Food Chem.* 67, 13093–13107. doi:10.1021/acs.jafc.9b05580

Cuculea, E. I., Buschmann, H.-J., and Muthiac, L. (2016). Hemicurbiturils as Receptors in Extraction and Transport of Some Amino Acids. *Supramolecular Chem.* 28, 727–732. doi:10.1080/10610278.2015.1121267

Dobrzycki, L., Socha, P., Ciesielski, A., Boese, R., and Cyrański, M. K. (2019). Formation of Crystalline Hydrates of Nonionic Chaotropes and Kosmotropes: Case of Piperidine. *Cryst. Growth Des.* 19, 1005–1020. doi:10.1021/acs.cgd.8b01548

Dražinský, M., Hurtado, C. S., Masson, E., and Kaleta, J. (2021). Stuffed Pumpkins: Mechanochemical Synthesis of Host-Guest Complexes with Cucurbit[7]uril. *Chem. Commun.* 57, 2132–2135. doi:10.1039/D1CC00240F

Garbusov, V., Rehfeld, G., Wölm, G., Golovnja, R. V., and Rothe, M. (1976). Volatile Sulfur Compounds Contributing to Meat Flavour. Part I. Components Identified in Boiled Meat. *Nahrung* 20, 235–241. doi:10.1002/food.19760200302

Ikuta, N., Sugiyama, H., Shimosegawa, H., Nakane, R., Ishida, Y., Uekaji, Y., et al. (2013). Analysis of the Enhanced Stability of R(+)-Alpha Lipoic Acid by the Complex Formation with Cyclodextrins. *Ijms* 14, 3639–3655. doi:10.3390/ijms14023639

Jin, X.-Y., Wang, F., Cong, H., and Tao, Z. (2016a). Host-guest Interactions between Hemicurbiturils and a Hydroxyl-Substituted Schiff Base. *J. Incl. Phenom. Macrocycl. Chem.* 86, 249–254. doi:10.1007/s10847-016-0659-3

- Jin, X.-Y., Wang, F., Cong, H., and Tao, Z. (2016b). Host-guest Interactions of Hemicucurbiturils with Aminophenols. *J. Incl. Phenom. Macrocycl. Chem.* 86, 241–248. doi:10.1007/s10847-016-0653-9
- Jin, X.-Y., Zhao, J.-L., Wang, F., Cong, H., and Tao, Z. (2017). Formation of an Interaction Complex of Hemicucurbit[6]uril and Ferrocene. *J. Organomet. Chem.* 846, 1–5. doi:10.1016/j.jorganchem.2017.05.053
- Jöul, P., Vaher, M., and Kuhlinskaja, M. (2018). Evaluation of Carbon Aerogel-Based Solid-phase Extraction Sorbent for the Analysis of Sulfur Mustard Degradation Products in Environmental Water Samples. *Chemosphere* 198, 460–468. doi:10.1016/j.chemosphere.2018.01.157
- Kaabel, S., and Aav, R. (2018). Templating Effects in the Dynamic Chemistry of Cucurbiturils and Hemicucurbiturils. *Isr. J. Chem.* 58, 296–313. doi:10.1002/ijch.201700106
- Kaabel, S., Adamson, J., Topić, F., Kiesilä, A., Kalenius, E., Öeren, M., et al. (2017). Chiral Hemicucurbit[8]uril as an Anion Receptor: Selectivity to Size, Shape and Charge Distribution. *Chem. Sci.* 8, 2184–2190. doi:10.1039/c6sc05058a
- Kaabel, S., Stein, R. S., Fomitsenko, M., Järving, I., Friščič, T., and Aav, R. (2019). Size-Control by Anion Templating in Mechanochemical Synthesis of Hemicucurbiturils in the Solid State. *Angew. Chem. Int. Ed.* 58, 6230–6234. doi:10.1002/anie.201813431
- Kandrnálová, M., Kokan, Z., Havel, V., Nečas, M., and Šindlář, V. (2019). Hypervalent Iodine Based Reversible Covalent Bond in Rotaxane Synthesis. *Angew. Chem. Int. Ed.* 58, 18182–18185. doi:10.1002/anie.201908953
- Lamberth, C., Walter, H., Kessabi, F. M., Quaranta, L., Beaudegnies, R., Trah, S., et al. (2015). The Significance of Organosulfur Compounds in Crop Protection: Current Examples from Fungicide Research. *Phosphorus, Sulfur, Silicon Relat. Elem.* 190, 1225–1235. doi:10.1080/10426507.2014.984033
- Lees, H., Vaher, M., and Kaljurand, M. (2017). Development and Comparison of HPLC and MEKC Methods for the Analysis of Cyclic Sulfur Mustard Degradation Products. *Electrophoresis* 38, 1075–1082. doi:10.1002/elps.201600418
- Li, Y., Li, L., Zhu, Y., Meng, X., and Wu, A. (2009). Solvent Effect on Pseudopolymorphism of Hemicyclohexylcucurbit[6]uril. *Cryst. Growth Des.* 9, 4255–4257. doi:10.1021/cg9007262
- Lin-Hui, T., Zheng-Zhi, P., and Ying, Y. (1995). Inclusion Complexes of α - and β -Cyclodextrin with α -lipoic Acid. *J. Incl. Phenom. Macrocycl. Chem.* 23, 119–126. doi:10.1007/BF00707889
- Lizal, T., and Sindelar, V. (2018). Bambusuril Anion Receptors. *Isr. J. Chem.* 58, 326–333. doi:10.1002/ijch.201700111
- Maeda, H., Onodera, T., and Nakayama, H. (2010). Inclusion Complex of α -lipoic Acid and Modified Cyclodextrins. *J. Incl. Phenom. Macrocycl. Chem.* 68, 201–206. doi:10.1007/s10847-010-9767-7
- Magnusson, R., Nordlander, T., and Östin, A. (2016). Development of a Dynamic Headspace Gas Chromatography-Mass Spectrometry Method for On-Site Analysis of Sulfur Mustard Degradation Products in Sediments. *J. Chromatogr. A* 1429, 40–52. doi:10.1016/j.chroma.2015.12.009
- Mahadevan, K., and Farmer, L. (2006). Key Odor Impact Compounds in Three Yeast Extract Pastes. *J. Agric. Food Chem.* 54, 7242–7250. doi:10.1021/jf061102x
- Maršálek, K., and Šindlář, V. (2020). Monofunctionalized Bambus[6]urils and Their Conjugates with Crown Ethers for Liquid-Liquid Extraction of Inorganic Salts. *Org. Lett.* 22, 1633–1637. doi:10.1021/acs.orglett.0c00216
- McQuin, C., Goodman, A., Chernyshev, V., Kamensky, L., Cimini, B. A., Karhohs, K. W., et al. (2018). CellProfiler 3.0: Next-Generation Image Processing for Biology. *Plos Biol.* 16, e2005970. doi:10.1371/journal.pbio.2005970
- Mecozzi, S., and Jr, J. R. (1998). The 55 % Solution: A Formula for Molecular Recognition in the Liquid State. *Chem. Eur. J.* 4, 1016–1022. doi:10.1002/(SICI)1521-3765(19980615)4:6<1016:AID-CHEM1016>3.0.CO;2-B
- Mishra, K. A., Adamson, J., Öeren, M., Kaabel, S., Fomitsenko, M., and Aav, R. (2020). Dynamic Chiral Cyclohexanohemicucurbit[12]uril. *Chem. Commun.* 56, 14645–14648. doi:10.1039/D0CC06817A
- Mottram, D. S., and Mottram, H. R. (2002). An Overview of the Contribution of Sulfur-Containing Compounds to the Aroma in Heated Foods. In *ACS Symposium Series, Heteroatomic Aroma Compound*. Editors G. A. Reineccius and T. A. Reineccius 826, 73–92. doi:10.1021/bk-2002-0826.ch004
- Öeren, M., Shmatova, E., Tamm, T., and Aav, R. (2014). Computational and Ion Mobility MS Study of (All-S)-Cyclohexylhemicucurbit[6]uril Structure and Complexes. *Phys. Chem. Chem. Phys.* 16, 19198–19205. doi:10.1039/C4CP02202E
- Prigorchenko, E., Kaabel, S., Narva, T., Baškir, A., Fomitsenko, M., Adamson, J., et al. (2019). Formation and Trapping of the Thermodynamically Unfavoured Inverted-Hemicucurbit[6]uril. *Chem. Commun.* 55, 9307–9310. doi:10.1039/C9CC04990H
- Prigorchenko, E., Öeren, M., Kaabel, S., Fomitsenko, M., Reile, I., Järving, I., et al. (2015). Template-controlled Synthesis of Chiral Cyclohexylhemicucurbit[8]uril. *Chem. Commun.* 51, 10921–10924. doi:10.1039/c5cc04101e
- Racz, C.-P., Santa, S., Tomoaia-Cotisel, M., Borodi, G., Kacsó, I., Pirna, A., et al. (2013). Inclusion of α -lipoic Acid in β -cyclodextrin. Physical-Chemical and Structural Characterization. *J. Incl. Phenom. Macrocycl. Chem.* 76, 193–199. doi:10.1007/s10847-012-0191-z
- Reany, O., Mohite, A., and Keinan, E. (2018). Hetero-Bambusurils. *Isr. J. Chem.* 58, 449–460. doi:10.1002/ijch.201700138
- Rezanka, T., Sobotka, M., Spizek, J., and Sigler, K. (2006). Pharmacologically Active Sulfur-Containing Compounds. *Aiamec* 5, 187–224. doi:10.2174/187152106776359002
- Rochette, L., Ghibu, S., Richard, C., Zeller, M., Cottin, Y., and Vergely, C. (2013). Direct and Indirect Antioxidant Properties of α -lipoic Acid and Therapeutic Potential. *Mol. Nutr. Food Res.* 57, 114–125. doi:10.1002/mnfr.201200608
- Roen, B. T., Unneberg, E., Törnnes, J. A., and Lundanes, E. (2010). Headspace-trap Gas Chromatography-Mass Spectrometry for Determination of sulphur Mustard and Related Compounds in Soil. *J. Chromatogr. A* 1217, 2171–2178. doi:10.1016/j.chroma.2010.01.088
- Salehi, B., Berkay Yilmaz, Y., Antika, G., Boyunegmez Tumer, T., Fawzi Mahomoodally, M., Lobine, D., et al. (2019). Insights on the Use of α -Lipoic Acid for Therapeutic Purposes. *Biomolecules* 9, 356. doi:10.3390/biom9080356
- Schoenauer, S., and Schieberle, P. (2018). Structure-Odor Correlations in Homologous Series of Mercapto Furans and Mercapto Thiophenes Synthesized by Changing the Structural Motifs of the Key Coffee Odorant Furan-2-Ylmethanethiol. *J. Agric. Food Chem.* 66, 4189–4199. doi:10.1021/acs.jafc.8b00857
- Takahashi, H., Bungo, Y., and Mikuni, K. (2011). The Aqueous Solubility and Thermal Stability of α -Lipoic Acid Are Enhanced by Cyclodextrin. *Biosci. Biotechnol. Biochem.* 75, 633–637. doi:10.1271/bbb.100596
- Ustrnul, L., Burankova, T., Öeren, M., Juhhimenko, K., Ilmarinen, J., Siilak, K., et al. (2021). Binding between Cyclohexanohemicucurbit[*n*]urils and Polar Organic Guests. *Front. Chem.* 9, 468. doi:10.3389/fchem.2021.701028
- Ustrnul, L., Kaabel, S., Burankova, T., Martónova, J., Adamson, J., Konrad, N., et al. (2019). Supramolecular Chirogenesis in Zinc Porphyrins by Enantiopure Hemicucurbit[*n*]urils (N = 6, 8). *Chem. Commun.* 55, 14434–14437. doi:10.1039/c9cc07150d
- Valkenier, H., Akrawi, O., Jurček, P., Sleziačková, K., Lizal, T., Bartík, K., et al. (2019). Fluorinated Bambusurils as Highly Effective and Selective Transmembrane Cl⁻/HCO₃⁻ Antiporters. *Chem* 5, 429–444. doi:10.1016/j.chempr.2018.11.008
- Vanninen, P., Östin, A., Beldowski, J., Pedersen, E. A., Söderström, M., Szubska, M., et al. (2020). Exposure Status of Sea-Dumped Chemical Warfare Agents in the Baltic Sea. *Mar. Environ. Res.* 161, 105112. doi:10.1016/j.marenvres.2020.105112
- Vázquez, J., and Sindelar, V. (2018). Supramolecular Binding and Release of Sulfide and Hydrosulfide Anions in Water. *Chem. Commun.* 54, 5859–5862. doi:10.1039/C8CC00470F
- Xi, Y., Man, C., Fang, W., Xian-Yi, J., Hang, C., and Zhu, T. (2018). Development of a Sub-group of the Cucurbituril Family, Hemicucurbiturils: Synthesis and Supramolecular Chemistry. *Mini-rev. Org. Chem.* 15, 274–282.

Conflict of Interest: The authors declare that the research was conducted in the absence of any commercial or financial relationships that could be construed as a potential conflict of interest.

Publisher's Note: All claims expressed in this article are solely those of the authors and do not necessarily represent those of their affiliated organizations, or those of the publisher, the editors, and the reviewers. Any product that may be evaluated in this article, or claim that may be made by its manufacturer, is not guaranteed or endorsed by the publisher.

Copyright © 2021 Shalima, Mishra, Kaabel, Ustrnul, Bartkova, Tõnsuaadu, Heinmaa and Aav. This is an open-access article distributed under the terms of the Creative Commons Attribution License (CC BY). The use, distribution or reproduction in other forums is permitted, provided the original author(s) and the copyright owner(s) are credited and that the original publication in this journal is cited, in accordance with accepted academic practice. No use, distribution or reproduction is permitted which does not comply with these terms.

Appendix 4

Publication IV

T. Dalidovich, **K. A. Mishra**, T. Shalima, M. Kudrjašova, D. G. Kananovich, R. Aav, 'Mechanochemical Synthesis of Amides with Uronium-based Coupling Reagents: A Method for Hexa-amidation of Biotin[6]uril'. *ACS Sustainable Chemistry & Engineering*, **2020**, *8* (41), 15703–15715.

Reprinted with permission. Copyright © 2020, American Chemical of Chemistry.

Mechanochemical Synthesis of Amides with Uronium-Based Coupling Reagents: A Method for Hexa-amidation of Biotin[6]uril

Tatsiana Dalidovich, Kamini A. Mishra, Tatsiana Shalima, Marina Kudrjašova, Dzmitry G. Kananovich,* and Riina Aav*

Cite This: *ACS Sustainable Chem. Eng.* 2020, 8, 15703–15715

Read Online

ACCESS |



Metrics & More



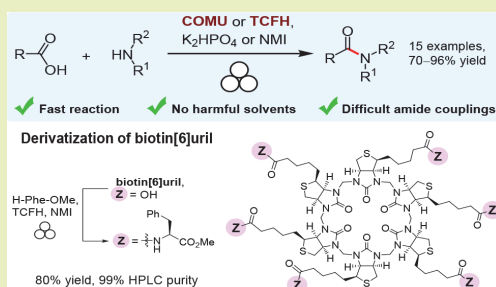
Article Recommendations



Supporting Information

ABSTRACT: Solvent-free, atom-efficient, and mechanochemically activated reactions have emerged as a synthetic strategy for sustainable chemistry. Herein we report a new mechanochemical approach for the amide coupling of carboxylic acids and amines, mediated by combination of (1-cyano-2-ethoxy-2-oxoethylideneaminoxy)-dimethylaminomorpholinocarbenium hexafluorophosphate (COMU) or *N,N,N',N'*-tetramethylchloroformamidinium hexafluorophosphate (TCFH) and K_2HPO_4 . The method delivers a range of amides in high yields (70–96%) and fast reaction rates. The reaction protocol is mild, keeps stereochemical integrity of the adjacent to carbonyl stereocenters, and streamlines isolation procedure for solid amide products. Minimal waste is generated due to the absence of bulk solvent. We show that K_2HPO_4 plays a dual role, acting as a base and a precursor of reactive acyl phosphate species. Amide bonds from hindered carboxylic acids and low-nucleophilic amines can be assembled within 90 minutes by using TCFH in combination with K_2HPO_4 or *N*-methylimidazole. The developed mechanochemical liquid-assisted amidation protocols were successfully applied to the challenging couplings of all six carboxylate functions of biotin[6]uril macrocycle with phenylalanine methyl ester, resulting in 80% yield of highly pure hexa-amide-biotin[6]uril. In addition, fast and high-yielding synthesis of peptides and versatile amide compounds can be performed in a safe and environmentally benign manner, as verified by green metrics.

KEYWORDS: mechanochemistry, solvent-free chemistry, amides, peptides, amide coupling reagents, macrocycle, hemicucurbituril, green metrics



INTRODUCTION

The amide bond is widespread in both natural compounds and artificial materials. It occurs in molecules fundamental to life, such as peptides and proteins, as well as in synthetic polymers and in a massive array of pharmaceuticals. In fact, amide preparation from carboxylic acids and amines represents the most frequently applied chemical transformation in drug production and comprises about 25% of the current medicinal chemistry synthetic toolbox.¹ As a consequence of its wide usage, the development of sustainable amidation methods was listed among the top green chemistry research priorities by the American Chemical Society Green Chemistry Pharmaceutical Roundtable (ACS GCIPR) in 2007² and has been retained in the recent revision.³ Although direct condensation of carboxylic acids and amines with water as a single byproduct can be considered a “green” landmark in the field, it remains impractical because of the process’s harsh reaction conditions ($T > 100\text{ }^\circ\text{C}$) and limited substrate scope.^{4–6} A robust method of amide synthesis commonly requires prior activation of a carboxylic function to replace OH with a better leaving group.^{7–9} Notably, this is also the case in biosynthetic

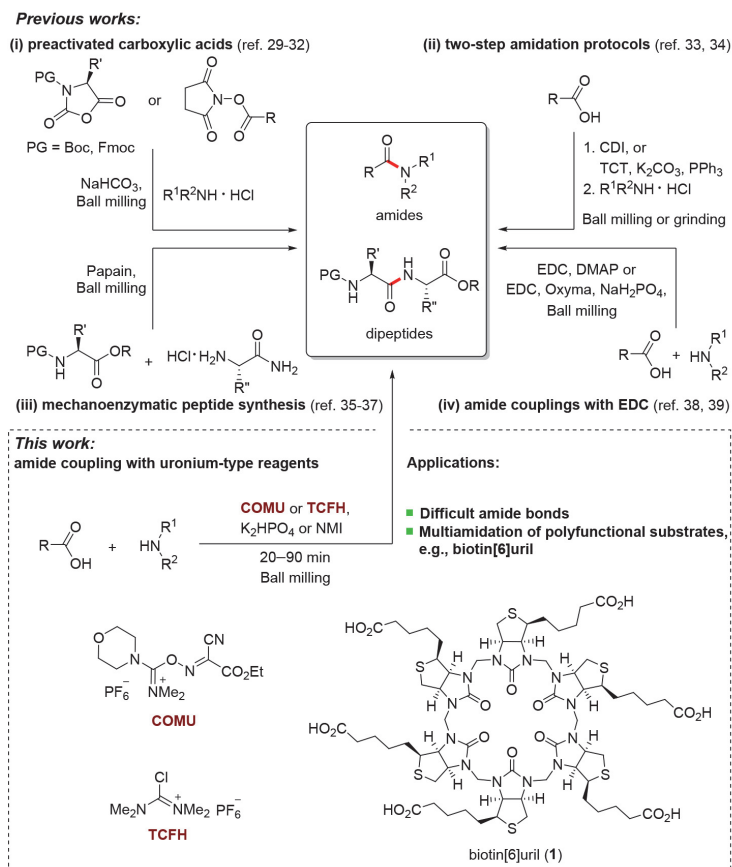
pathways, including the translation process and nonribosomal enzymatic transformations.^{10–13} For laboratory and industrial use, vast numbers of amide coupling reagents, performing in situ activation of carboxylic acid, have been developed in the quest for faster, milder, and high-yielding amidation protocols.^{14,15} The low atom economy of these reagents and accompanying safety issues are their major drawbacks, which has incited the development of alternative approaches.^{16–19} Important advancements have thus far followed traditional solution-based approaches; however, solvent is actually responsible for 80–90% of mass consumption in a typical chemical process and also plays a major role in overall toxicity.²⁰ In this way, solvent greatly outperforms the contributions of reagents themselves. Hazardous solvents like

Received: July 30, 2020

Revised: September 11, 2020

Published: October 6, 2020



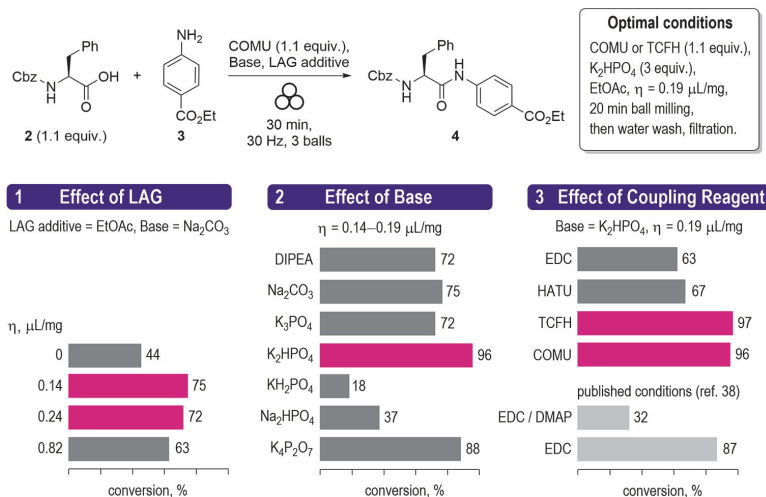
Scheme 1. Overview of the State-of-Art Mechanochemical Amidation Approaches and Outline of the Current Work^{29–39}

DMF and DCM are preferred in industrial amide synthesis, reinforcing both environmental and safety concerns.^{17,21} Therefore, the application of solvent-free techniques represents an efficient way to improve the overall process mass intensity and to prevent generation of hazardous waste. Recent advances in mechanochemistry and its related fields have established solvent-free reactions as environmentally friendly tools to perform chemical transformations that are no less efficient than the conventional solution-based chemistry.^{22–25}

In the area of amide synthesis, the benefits of solvent-free techniques have not remained unnoticed and have been previously demonstrated in numerous studies (Scheme 1).^{26–28} For example, mechanochemical synthesis of various amides and peptides has been performed from a series of activated carboxylic acid derivatives, such as *N*-carboxyanhydrides,^{29,30} *N*-hydroxysuccinimide esters,³¹ and *N*-acyl benzotriazoles,³² *N*-Acyl imidazoles³³ and acyloxytriazine esters³⁴ have been produced mechanochemically from carboxylic acids prior to reacting with amines. Notably, even papain enzyme can catalyze the formation of peptides from the corresponding amino acid building blocks under solvent-free conditions.^{35–37} In addition, direct coupling of amines with carboxylic acid has

been demonstrated by using 1-ethyl-3-(3-(dimethylamino)propyl)carbodiimide (EDC) as a coupling reagent.^{38,39} In general, EDC-mediated transformations have shown remarkably short reaction times (typically within 10–30 min), high yields, and simple workup protocols.

Following these prominent earlier contributions,^{26–39} we aimed to further expand the scope and synthetic utility of the mechanochemical amidation methods. The current research was impelled by three objectives: First, most of the amide coupling reagents are simply not efficient enough for a range of substrates,⁸ which require expansion of the established one-step mechanochemical amidation protocols beyond the previously applied EDC; for that purpose, in this work we mapped the coupling efficiency of uronium-type reagents (COMU and TCFH, Scheme 1) on several carboxylic acid/amine pairs. Second, the scope of previously published mechanochemical approaches was evaluated based mainly on peptide synthesis, while the challenging couplings of sterically hindered carboxylic acids and low nucleophilicity amines remained virtually unproven. Here we demonstrate that such difficult amide bonds can also be assembled under solvent-free conditions. Implementation of the two objectives mentioned

Scheme 2. Optimization Experiments^{4a}

^{4a}Conversion of 3 into 4 according to ¹H NMR analysis of the crude reaction mixtures.

above was required as a prerequisite for the third objective as our ultimate goal. Chiral hemicarbiturils^{40–45} are oligomeric macrocycles and are made efficiently from uniformly functionalized monomers. Nevertheless, in spite of their relatively step-efficient synthesis, their postmodifications might be challenging. Therefore, we chose carboxyl-group bearing hemicarbituril, the biotin[6]uril^{46–48} for demonstrating applicability of mechanochemistry for uniform derivatization of oligomeric macrocycles. Despite the apparent ease of such a transformation, it also presented a substantial challenge: The 6-fold stepwise amidation of carboxylate groups in **1** is inevitably accompanied by accumulation of the “failed” under-functionalized products if incomplete coupling occurs at each step. Limited solubility of **1** in the common organic solvents dictates additional practical inconvenience of the traditional solution chemistry; in fact, only dipolar aprotic solvents like DMF can be used. Here we showed that application of solvent-free techniques, additionally reinforced with the reactive uronium-type amide coupling reagents, allows the desired functionalization of **1** in a high-yielding, scalable, and sustainable manner, avoiding harmful solvents or significant reagent excess.

RESULTS AND DISCUSSION

Development of Mechanochemical Amidations with Uronium-Type Reagents. At the outset, amide coupling of Cbz-protected L-phenylalanine (**2**) and ethyl 4-aminobenzoate (benzocaine, **3**), mediated by COMU as a representative “green” uronium-type amide coupling reagent,^{49–51} was selected as a model process (Scheme 2). We aimed to screen and compare the results of various reaction conditions, including the evaluation of coupling efficiency for different coupling reagents beyond the COMU itself, to reveal the most promising hits in terms of product yield and green chemistry requirements. The choice of aromatic amine **3** was dictated by its reduced nucleophilicity in comparison with aliphatic amines, additionally attenuated by an electron-withdrawing ethoxycarbonyl group. We expected that suppressed reactivity

of **3** in the carbonyl addition reactions would facilitate more reliable differentiation of various coupling conditions. Use of phenylalanine derivative **2** as coupling counterpart provided an additional opportunity to examine the resistance α -stereocenter toward its possible epimerization, as commonly encountered in peptide synthesis.^{9,15}

The test reactions were run in a Form-Tech Scientific FTS1000 shaker mill operating at 30 Hz by using 14 mL zirconia-coated milling jars, 3 × 7 mm zirconia milling balls and typical solid reactants loading around 0.3–0.4 g (including 0.2 mmol of amine **3** as a limiting substrate). After 30 min of milling time, a sample of the crude reaction mixture was treated with CDCl₃, followed by separation of insoluble inorganic materials. The conversion of amine **3** into amide **4** was determined by ¹H NMR analysis (see the Supporting Information for the details). The amide coupling reagent, base, and amount of liquid additive needed to assist the grinding process (Scheme 2) were identified as the three most crucial parameters affecting the yield of amide **4**, as described below.

The addition of a small volume of liquid constitutes an efficient method to enhance the performance of solvent-free mechanochemical reactions, known as liquid-assisted grinding (LAG).^{22,24} The ratio of the volume of liquid (μL) added to the amount of solid present (mg) is denoted as η ($\mu\text{L}/\text{mg}$).⁵² A value of $\eta = 0$ generally corresponds to dry grinding, but in a typical LAG process, η is usually between 0 and 1.²⁴ Although LAG cannot be described as a totally solvent-free technique, it requires a minimal amount of liquid, which is especially advantageous if a green solvent is used. Among the latter,^{20,53,54} ethyl acetate appears to be the most promising and chemically compatible candidate to act as a LAG additive in COMU-mediated amide coupling. In our experiments (Scheme 2, Chart 1), the addition of ethyl acetate indeed showed a pronounced effect on the yield of amide **4**, generated in the mixture of solid reactants **2** and **3**, with COMU reagent and sodium carbonate (ca. 10 equiv) as a base. Although dry grinding provided a rather modest outcome (44% conversion),

LAG resulted in a markedly improved reaction performance, with the optimal η value in a range of 0.14–0.24 $\mu\text{L}/\text{mg}$, while the further increase of η led to slightly diminished conversion values.

The choice of base is also important in amide coupling. State-of-the-art solution approaches commonly apply non-nucleophilic tertiary amines, e.g., *N,N*-diisopropylethylamine (DIPEA).¹⁵ However, the use of cheap and nontoxic inorganic salts, e.g., NaHCO_3 , K_2CO_3 , and NaH_2PO_4 ,^{29,31,34,39} insoluble in common organic solvents, can be considered as an additional advantage of mechanochemical reactions. In our hands (Scheme 2, Chart 2), replacement of DIPEA with Na_2CO_3 gave similar conversion values (72 vs 75%). For further process optimization, a range of readily available phosphate salts, with notably distinct pK_a values, were screened. Among them, potassium pyrophosphate $\text{K}_4\text{P}_2\text{O}_7$ and dipotassium phosphate K_2HPO_4 provided the best outcomes, especially the latter (96% conversion). Generally, the performance of phosphate salts does not correlate with Brønsted basicity of the respective anions. Although the poor outcome with KH_2PO_4 (only 18% conversion) in comparison with K_2HPO_4 (96%) could be probably connected with the significantly reduced base strength of the former (respective pK_a values 2.12 vs 7.21; the pK_a of RCO_2H is typically about 4–5 in aqueous media),⁵⁵ much more basic K_3PO_4 (pK_a 12.32) also afforded amide 4 with reduced efficiency (72%). Surprisingly, the counteraction effect (Na^+ vs K^+) also had a prominent impact on reaction outcome (37 vs 96%, for Na_2HPO_4 and K_2HPO_4 , respectively). These results clearly indicate that the effect of an inorganic base on a solid-state reaction is more intricate than trivial proton transfer.

Finally, amide coupling reagents are essential for attaining high yields. The selection of coupling reagent was governed by considering chemical (substrate scope, reactivity), safety, and environmental issues. Uronium salts are advantageous because of their prominent reactivity and efficient reaction rates,^{8,14} but the most commonly applied triazole-based reagents, such as HBTU and HATU, possess dangerous explosive properties⁵⁶ and pose significant health risks.⁵⁷ COMU was introduced as a safe and “greener” replacement.^{49,50,58} To our delight, COMU also noticeably exceeded the coupling efficiencies of HATU and EDC in our experiments (Scheme 2, Chart 3), delivering a high 96% conversion. TCFH can be considered as an even more reactive alternative with better atom economy, affording a high 97% yield of amide 4 within only 10 min.

The mechanochemical amidation with COMU/ K_2HPO_4 was also rapid, reaching the maximal conversion within 20 min (Figure 1; see the Supporting Information for further detail), far surpassing the rate of the solution-based process (in DMF-d_7 , Figure 1). The latter reached the maximal 70% conversion after approximately 20 h (see the Supporting Information). Concurrently, about 30% of COMU reagent degraded due to its well-known hydrolytic instability in DMF solutions, which is often referred as the main disadvantage of COMU.^{59,60} Evidently, this drawback can be fully eliminated under solvent-free conditions.

After achieving these results in the optimization experiments, we formulated the optimal experimental procedure as follows: COMU or TCFH (1.1 equiv) as coupling reagents, K_2HPO_4 (3 equiv) as base, ethyl acetate as LAG additive, and 20 min milling time. The amount of solid base (3 equiv) was adjusted to keep η within the optimal range ($\sim 0.2 \mu\text{L}/\text{mg}$), but not less than 2 equiv was required according to the

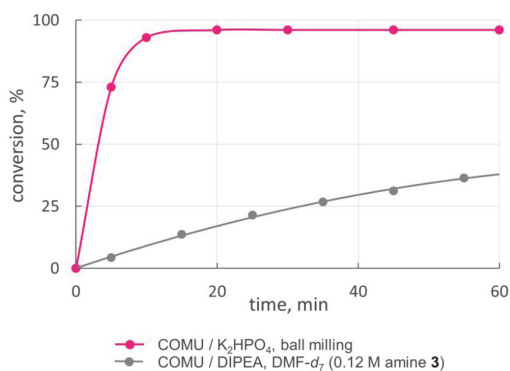


Figure 1. Accumulation of amide 4 over time in mechanochemical (purple) and solvent-based (gray) reactions.

reaction stoichiometry. Furthermore, an additional equivalent of K_2HPO_4 was required to release free amine when the ammonium salt was used as the starting material. Isolation of pure amide 4 was achieved with a high 96% yield by simple water wash and filtration since all byproducts are water-soluble. No detectable racemization of the chiral center in 4 occurred during the synthesis, as was established by the chiral-phase HPLC chromatography (see the Supporting Information).

Green Chemistry Metrics Comparison. The advantages and drawbacks of the developed mechanochemical amidation methods were further revealed and compared with the solution-based reaction by analyzing the respective green metrics (Table 1). The metrics were calculated and assessed by marking them with red, orange, or green flags by following the Clark’s unified metrics toolkit (see the Supporting Information).⁶¹ Atom economy (AE), reaction mass efficiency (RME), and process mass intensity (PMI) are defined as follows:⁶¹

$$\text{AE} = \frac{\text{molecular weight of product}}{\text{total molecular weight of reactants}} \times 100 \quad (1)$$


$$\text{RME} = \frac{\text{mass of isolated product}}{\text{total mass of reactants}} \times 100 \quad (2)$$

$$\text{PMI} = \frac{\text{total mass in a process}}{\text{mass of product}} \quad (3)$$

First, isolated yields and product purity were much better in mechanochemical reactions, due to the higher conversion and more facile isolation procedure discussed above. Atom economy was a bit higher for the TCFH-mediated reaction because of the lower molecular weight of TCFH. RME reflects both product yield and atom economy issues and was lower for the solution-based reaction. Comparison of PMI values clearly shows that mechanochemical reactions produce far less waste. Excluding mass-extensive workup procedures, solvent occupied 84% of PMI for the solution-based reaction and only about 15% (LAG additive) for the mechanochemical conditions. Furthermore, sustainable solvents like water and ethyl acetate were used in the latter, in contrast with toxic DMF.

To determine the safety risks, a combination of physical, health, and environmental threats must be assessed, which can be done with the help of MSDS⁶² and further available safety data.⁵⁶ DMF, for instance, is a flammable (H226), acute toxic

Table 1. Comparison of Green Metrics for Mechanochemical and Solution-Based Amidation Reactions



Metrics	Mechanochemistry		Solution ^a
	COMU / K ₂ HPO ₄	TCFH / K ₂ HPO ₄	COMU / DIPEA in DMF
Yield (%) ^b	96	92	70
Atom economy (%) ^c	50	60	50
RME (%)	46	53	35
PMI (total), including:	196.3	203.7	1464.7
PMI (reactants)	3.4	3.1	3.7
PMI (solvent)	0.6	0.6	18.9
PMI (work-up)	192.3	200	1442.2 ^d
Solvent choice	EtOAc, water	EtOAc, water	DMF
Work-up, isolation	filtration	filtration	chromatography
Health and safety			
Main hazard statements ^e	H302, H312	H360	H226, 312, 332, 360

^aFollowing the published protocol, see ref 51. ^bYield of isolated product. ^cIncluding coupling reagent. ^dExcluding column chromatography. ^eSee the [Supporting Information](#) for additional safety data.

(H312, 332), as well as a reproductive toxin (H360) and can thus be cited as the main hazard contributor for the solution-based process, which therefore received a red flag. For the mechanochemical reactions, the TCFH-mediated process was given a red flag due to the production of tetramethylurea byproduct (reproductive toxin, H360). In contrast, exothermic decomposition with a thermal onset of 127 °C can be considered as the main hazard of COMU, according to a recent study.⁵⁶ However, this property enables an orange flag since the temperature increase inside of the milling jar has not been examined. On the basis of the literature reports on temperature monitoring during the milling,^{63,64} we could expect that the temperature increase during the milling stays lower than the thermal onset of COMU. To conclude, although the developed mechanochemical amidation conditions cannot be considered totally safe, the risks are minimal because of its room-temperature operation and relatively low amount of produced waste, as opposed to the solution-based reaction (see the [Supporting Information](#) for additional safety considerations).

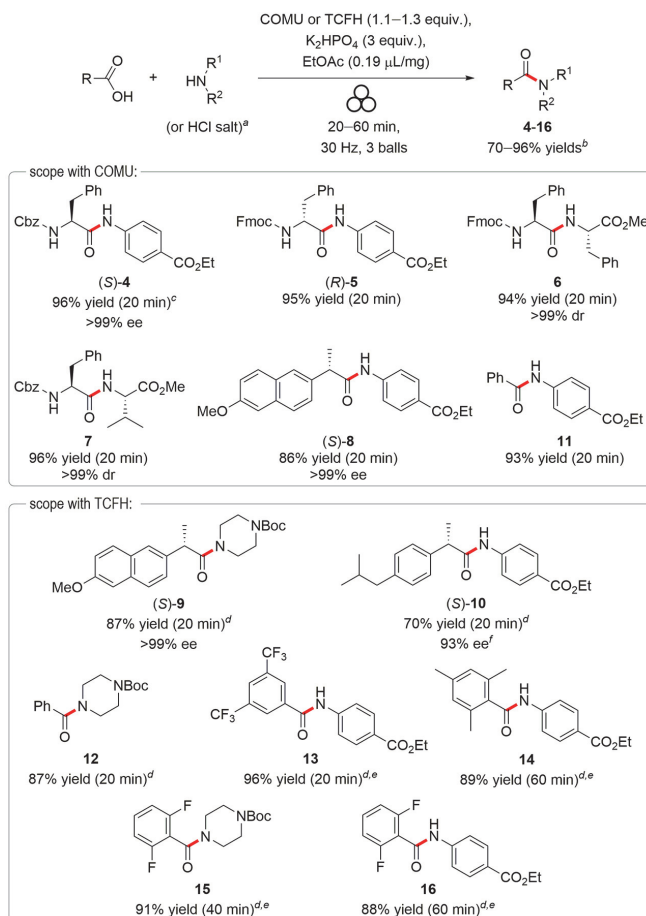
Substrate Scope for Mapping Reactivity with COMU and TCFH. Having established the optimal conditions, substrate scope, and limitations was briefly examined on a range of amine and acid coupling partners ([Scheme 3](#)).

The substrate scope included, besides others, N- and C-protected amino acids and pharmaceutically relevant starting materials, e.g., (S)-naproxen, (S)-ibuprofen, benzocaine 3, and N-Boc-protected piperazine. In addition to the foremost example of Cbz-masked amide (S)-4 comprehensively described above, its Fmoc-protected analogue (R)-5 was obtained in a high 95% yield by using the COMU-mediated reaction. Following the same protocol, dipeptides 6 and 7 with sterically hindered amino acid residues (phenylalanine and valine) were flawlessly prepared in high yields. No detectable epimerization of the stereocenters was noted in these cases. Coupling of (S)-(+)-6-methoxy- α -methyl-2-naphthaleneacetic acid [(S)-naproxen] with amine 3 provided a more demanding

test for stereochemical integrity, since 2-arylpropionic acids are prone to easy epimerization.^{65–68} Amide product (S)-8 was obtained from (S)-naproxen with a high 86% yield and excellent stereochemical purity (>99% ee). This was also the case in the TCFH-mediated reaction, which showed high reactivity and a subtle amount of epimerization for (S)-9. However, amidation of (S)-ibuprofen (98% ee) produced (S)-10 with slightly degraded optical purity (93–94% ee). Crude amides 10, 12, and 15 appeared as oils immediately following the milling, which eventually enabled a chromatographic isolation for these cases (see the [Supporting Information](#)).

One advantage of TCFH- over COMU-mediated amide coupling is the higher reactivity of the former reagent, which makes it more suitable for less reactive substrates. This property was explicitly revealed during the amidation of sterically hindered *ortho*-substituted benzoic acids. Thus, coupling of benzoic acid with benzocaine 3 proceeded well under the COMU-mediated protocol, furnishing amide 11 in a 93% yield after 20 min of milling time. Conversely, 2,4,6-trimethylbenzoic acid under the same conditions produced only 22% of target amide 14, without any further improvement, even when a longer milling time (up to 60 min) was applied. After the brief optimization studies (see the [Supporting Information](#)), we found that a slight excess (1.3 equiv) of more reactive TCFH and at least 60 min of milling time are required to attain a high 89% yield of 14. Moreover, chromatographic purification of 14 was necessary to separate mesitoic anhydride impurity. Diminished reactivity was also observed for 2,6-difluorobenzoic acid, furnishing amides 15 and 16 in reactions with N-Boc piperazine and low nucleophilicity amine 3 in acceptable yields after milling times of 40 and 60 min, respectively. However, coupling of the same amines with benzoic and 3,5-bis(trifluoromethyl)benzoic acids proceeded flawlessly, producing amides 12 and 13 with excellent yields and brief reaction times.

Activating Effect of Phosphate Salts. During the optimization studies, the enhancement of yields with

Scheme 3. Substrate Scope for Mechanochemical Amidation with COMU/K₂HPO₄ and TCFH/K₂HPO₄ Systems

^aAmine hydrochloride salt was used for preparation of peptides **6** and **7**. ^bYields of isolated products. ^cObtained in 92% yield and >99% ee with TCFH. ^dIsolated by column chromatography. ^eWith 1.3 equiv of TCFH. ^fObtained with 94% ee with COMU.

dipotassium phosphate and potassium pyrophosphate was especially notable (Scheme 2, Chart 2). We speculated that phosphate salts could additionally contribute to the activation of the carboxyl substrate **2** via the formation of acyl phosphate intermediates containing a “high-energy” phosphoester bond, prone to easy nucleophilic amine attack.^{69,70} Interestingly, the same pathway is also involved in the ATP-dependent biosynthesis of amide bond-containing biomolecules.¹¹ The plausibility of our assumption is further supported by existing literature showing that acyl phosphates can be indeed generated in solution by the dicyclohexylcarbodiimide (DCC)-mediated coupling of carboxylic acids with phosphate salts.^{71–73} To confirm the credibility of our hypothesis, mechanochemical synthesis of acyl phosphates from carboxylic acids and phosphate salts, mediated by COMU and TCFH, was attempted.

As expected, 20 min of ball milling of COMU (1.1 equiv) with acetic acid (1 equiv) and K₂HPO₄ (3 equiv) yielded 60%

of acetyl phosphate **17**, which was confirmed by NMR analysis of the freshly obtained reaction mixture in D₂O solution (Figure 2). Acetyl phosphate **17** displayed a singlet signal at $\delta = -2.1$ ppm in ³¹P NMR, which rapidly disappeared after the addition of morpholine, both in D₂O solution and in the solid state (see the Supporting Information). In the ¹³C NMR spectrum, carbonyl group **17** showed a doublet signal at $\delta = 168.1$ ppm ($J_{\text{CP}} = 8.8$ Hz), due to its coupling with the neighboring phosphorus.⁶⁹ Significantly lower yields of **17** were attained with K₃PO₄ or with TCFH as coupling reagent (Figure 2). The reaction of acetic acid with K₄P₂O₇ produced acetyl pyrophosphate **18** in a 50% yield, according to ³¹P NMR analysis. As a result of the nonequivalence of phosphorus atoms in **18**, a pair of doublet signals appeared in ³¹P NMR, at $\delta = -5.0$ and -17.9 ppm ($d, J_{\text{PP}} = 21.7$ Hz), thus confirming its structure.⁷¹ As an extra example, the generation of acyl phosphate **19** (50% yield, $\delta = -7.6$ ppm in ³¹P NMR) was also

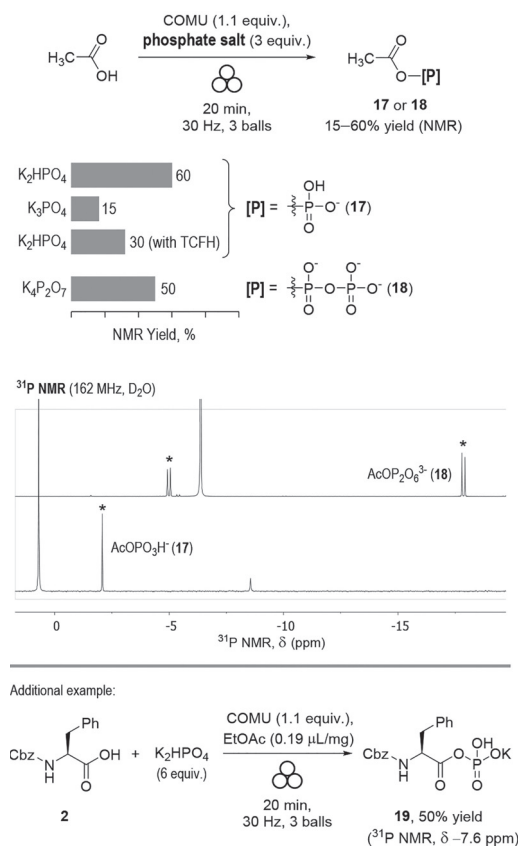
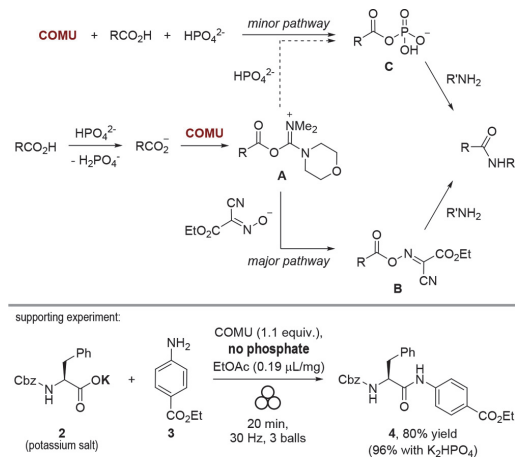


Figure 2. Mechanochemical generation of acyl phosphates **17**, **19**, and acetyl pyrophosphate **18**. Signals of **17** and **18** in the traces of ^{31}P NMR spectra are marked with asterisks. Other signals belong to inorganic phosphates (see the Supporting Information).

successful from Cbz-masked phenylalanine **2**, which was similar to the acetic acid outcome.

These results clearly indicate that generation of acyl phosphates can indeed take place in these newly developed mechanochemical amidation approaches and could account for the observed enhanced efficiency of K_2HPO_4 and $\text{K}_4\text{P}_2\text{O}_7$ additives. To evaluate the contribution of the acyl phosphate pathway (Scheme 4, via intermediate **C**) against the manifested activated ester pathway (via intermediates **A** and **B**),^{50,74} the following experiment was undertaken. Amide coupling reaction of potassium salt of **2** with amine **3** without the phosphate salt additive afforded amide **4** in 80% yield, 16% lower than that obtained with K_2HPO_4 . It was concluded from these results that in the amidation reaction leading to **4**, K_2HPO_4 acts primarily as a base performing the deprotonation of **2**, but it also contributes at least 16% to the formation of amide **4** via acyl phosphate **19**. This estimation correlates well with the results of other optimization experiments (Scheme 2, Chart 2). For example, K_3PO_4 produced a rather low 15% yield of acetyl phosphate **17** (Figure 2), which also agrees with the lower conversion to amide **4** in the comparison with K_2HPO_4 .

Scheme 4. Plausible Mechanistic Pathways Leading to Amide Product

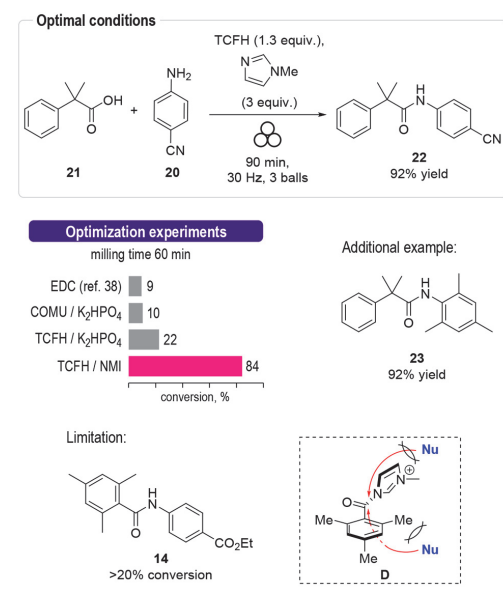


The acyl phosphate pathway probably contributes less in the case of the more reactive TCFH reagent, which also produced a rather low 30% yield of **17** (Figure 2). The exact mechanistic sequence leading to acyl phosphates **C** from COMU, RCO_2H , and K_2HPO_4 remains unclear but may include the reaction of acyl uronium intermediate **A** with HPO_4^{2-} anion (Scheme 4) or, alternatively, the initial formation of uronium phosphate⁷⁵ by the reaction of COMU with K_2HPO_4 .

Challenging Amide Bond Formation. As shown above, the coupling of low nucleophilic amine **3** with sterically hindered mesitoic acid could be efficiently mediated by the TCFH/ K_2HPO_4 reagent system (Scheme 3). In accordance with existing literature,^{65,76} we selected the coupling of electron-deficient 4-aminobenzonitrile **20** with 2-methyl-2-phenylpropanoic acid **21** (Scheme 5), an even more arduous way to test the performance of mechanochemical amidation protocols. A brief screening of various coupling conditions was undertaken, and conversion to amide product **22** was determined by ^1H NMR analysis after 60 min of milling time (Scheme 5).

The use of EDC alone,³⁸ or the COMU/ K_2HPO_4 system, yielded only a low $\sim 10\%$ conversion. Combination of TCFH and K_2HPO_4 delivered a noticeably better outcome but still failed to raise the conversion above 22%. According to the recent study of Beutner et al.,⁶⁵ a combination of *N*-methylimidazole (NMI) and TCFH reagent provided a high yield of **22** in solution, due to in situ generation of reactive *N*-acyl imidazolium ions. To our gratification, the same combination of reagents also worked well under the solvent-free conditions, affording respectable 84% conversion after a 60-min reaction time. Finally, a slight excess (1.3 equiv) of TCFH reagent, along with a bit longer milling time (90 min), allowed us to obtain pure amide **22** in 92% isolated yield after an aqueous workup (see the Supporting Information). Following the same reaction protocol, the coupling of **21** with sterically hindered 2,4,6-trimethylaniline was performed and furnished corresponding amide **23** with a 92% yield. Notably, high yields of amides **22** and **23** were attained in a rather efficient reaction time of 1.5 h, in significant contrast with the solution-based reaction (21 h for amide **22**).⁶⁵

Scheme 5. Mechanochemical Coupling of Hindered Carboxylic Acids and Poor Nucleophilic Amines

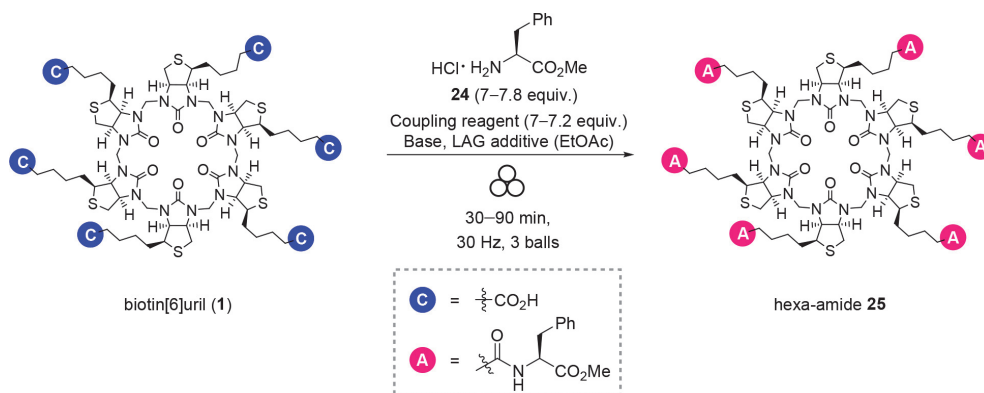


Surprisingly, the same highly reactive combination of reagents failed to render amide **14** from mesitoic acid with yields exceeding 20%. This was also the case in the CD₃CN solution (see the [Supporting Information](#)). We found that the reaction was stopped due to the formation of sterically bulky and therefore nonplanar *N*-acyl imidazolium **D**, which in contrast to the analogous species produced from benzoic acid was totally inert toward the subsequent reaction with amine **3** (see the [Supporting Information](#) for further details). The inertness of **D** could be explained by the efficient steric shielding of the carbonyl group with both neighboring mesityl and imidazolyl moieties, preventing attack of a nucleophile

along the Bürgi–Dunitz trajectory (Scheme 5). This stands in sharp contrast to the successful TCFH/K₂HPO₄-mediated transformation, where the less sterically crowded intermediate species are expected to form (e.g. mesityl chloride, uronium, or phosphate).

Amide Coupling of Biotin[6]uril. As a part of our ongoing efforts toward the development of new chiral supramolecular receptors,^{42,77–81} we needed an expedient synthetic procedure for derivatization of biotin[6]uril (**1**),⁴⁶ easily available in multigram quantities by HCl-catalyzed condensation of formaldehyde with D-biotin. The starting macrocyclic molecule, notable for its anion binding properties, common for the cucurbituril family,^{41,82–85} satisfies six carboxylic functions, which could be conveniently coupled with various amines, thus providing facile access to a library of diversely functionalized chiral macrocyclic receptors. Although amide coupling of carboxylates in **1** might appear simple, unencumbered by any steric or electronic influence, full amidation of **1** is challenging because it proceeds via six consecutive steps. For example, if a high 97% yield were produced during each step, then the fully functionalized product would eventually generate only a (0.97)⁶·100% = 83% yield, while the rest of the produced material would contain a set of “failed” under-functionalized molecules, thus necessitating time-consuming, laborious, and mass-inefficient chromatographic purification. The situation resembles the synthesis of oligopeptides and oligonucleotides, in which an extremely high coupling efficiency (>99% per coupling step) is required to attain reasonable yields and high purity of long-chain oligomers, and it is customarily achieved by using an excess of highly reactive coupling reagents.⁵⁸ The low solubility of **1** in the environmentally benign and volatile organic solvents, compatible with the conventional amidation protocols (e.g., ethyl acetate), constitutes an additional restriction of the solution-based chemistry. We believed that the high coupling efficiency observed under the solvent-free conditions would allow us to perform the desired functionalization in a high-yielding, and scalable manner without using an excess of reagents, toxic solvents, or laborious purification.

As a convenient model reaction for this study, we selected the amide coupling of **1** with methyl ester of phenylalanine **24**

Scheme 6. Derivatization of Biotin[6]uril (**1**)⁴⁴

⁴⁴Via six-fold amidation with L-phenylalanine methyl ester (**24**).

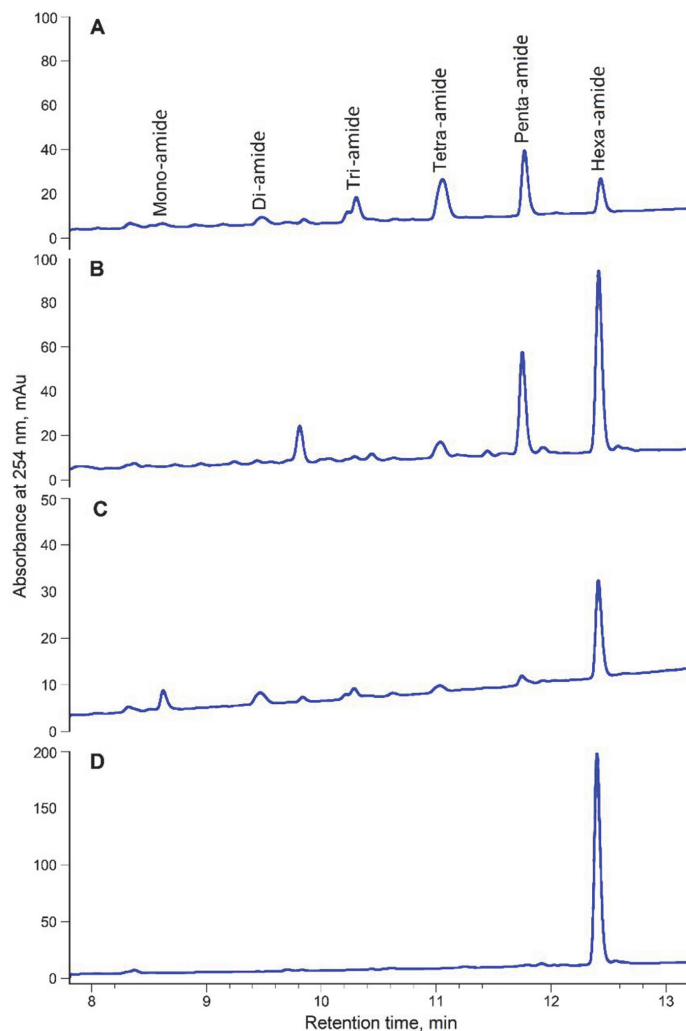


Figure 3. Derivatization of biotin[6]uril **1** via amide coupling with phenylalanine methyl ester **24**. Traces of HPLC chromatograms for the selected reaction mixtures: (A) COMU/K₂HPO₄; (B) EDC/DMAP; (C) TCFH/NMI; (D) TCFH/NMI with EtOAc as LAG additive.

(used as HCl salt, see Scheme 6). At its outset, this task required us to explore the performance of different amide coupling conditions. Only a slight excess of amine **24** and a coupling reagent (7–7.8 equiv, which is 1.16–1.3 equiv per CO₂H group of **1**) were applied in the optimization experiments. It was expected that more reactive combinations of reagents would deliver higher yields of hexa-amide product **25**. On the basis of our previous findings, the order of coupling efficiency for the different reagent systems can be roughly plotted as follows: EDC \sim COMU/K₂HPO₄ < TCFH/K₂HPO₄ \ll TCFH/NMI. Although such generalizations must be made with care since the coupling performance is substrate-dependent^{8,86} and exceptions are possible, e.g., case of amide

14 above, this preliminary reactivity plot provided a helpful guide.

Outcomes of the test reactions were analyzed by HPLC (Figure 3, see the Supporting Information for further detail) and quantified by calculating HPLC area percentage for the hexa-amide product **25** (S_{rel} , Table 2), relative to under-functionalized compounds.

These initial experiments (Table 2, entries 1–4) clearly indicated that complete hexafunctionalization of **1** is difficult to perform. Thus, both the COMU and TCFH/K₂HPO₄ systems produced a mixture of phenylalanine-derivatized biotin[6]urils, containing all possible products from mono- to hexa-amide **25**, with the latter displaying a rather low 16% contribution (entries 1 and 2; Figure 3A). The use of EDC/DMAP

Table 2. Amide Coupling of Biotin[6]uril **1** with Phenylalanine Methyl Ester **24**

Entry	Reaction conditions ^a	Liquid chemicals (additives, solvents)	η , $\mu\text{L}/\text{mg}$	Time, min	S_{rel} % ^b	
1	COMU/ K_2HPO_4	EtOAc	0.19	90	16	
2	TCFH/ K_2HPO_4	EtOAc	0.19	90	16	
3	EDC/DMAP ^c	CH_3NO_2	0.25	90	55	
4	TCFH/NMI	NMI	0.29	90	52	
5	ball milling	TCFH/NMI ^d	NMI	0.32	60	86
6		TCFH/NMI ^d /NaCl ^e	NMI	0.16	60	73
7		TCFH/NMI ^d	NMI, DMF	0.53	60	97
8		TCFH/NMI ^d	NMI, heptane	0.64	60	84
9		TCFH/NMI ^d	NMI, EtOAc	0.64	60	98
10	slurry stirring	TCFH/NMI ^d	NMI, EtOAc	0.64	60	95
11	solution (DMF)	HATU, DIPEA	DIPEA, DMF	2.1	60	68
12		TCFH, NMI ^d	NMI, DMF	2.4	60	98

^aReaction conditions: biotin[6]uril (50–70 mg, 0.03–0.05 mmol), **24** (7 equiv), coupling reagent (7 equiv), and base (18 equiv), unless other specified. ^bHPLC area percentage of hexa-amide **25**, relative to other amide products. ^c12 equiv of DMAP was used, following the published procedure; see ref 38. ^dWith 7.2 equiv of TCFH, 7.8 equiv of **24**, and 21 equiv of NMI. ^eNaCl was used as grinding additive.

combination (entry 3),³⁸ was more successful in this case, primarily producing a mixture of penta- and hexa-amides (Figure 3B). The highly reactive TCFH/NMI combination (entry 4) generated hexa-amide **25** as its main reaction product, but it was noticeably contaminated with under-functionalized compounds (52% HPLC area, Figure 3C).

Notably, at least 90 min of milling had to be applied, since samples taken after 30 and 60 min still showed incomplete conversion (see the Supporting Information). Although the FTS1000 shaker mill could hypothetically achieve a long milling time, we considered any time longer than 1.5 h as impractical; therefore, our next goal was to adjust the reaction parameters accordingly, in order to reach at least 90% conversion within a 1.5 h reaction time.

Applying a slightly greater excess of TCFH (1.2 equiv per carboxylate) and NMI (3.5 equiv per carboxylate) noticeably improved the yield of target product **25** (86% HPLC area, entry 5) and also shortened the reaction time. For further improvement, a screening of optimal η and LAG additive was performed. Since NMI is a liquid and liquid tetramethylurea is produced, the addition of solid NaCl was attempted to reduce the initial η to 0.16 $\mu\text{L}/\text{mg}$. However, this distinctly reduced the yield of the product (73% HPLC area, entry 6). In contrast, the addition of a few drops (ca. 35–50 μL) of solvent noticeably improved the outcome (entries 7–9) and was best when polar solvents like DMF or EtOAc were added (entries 7 and 9). These results clearly indicate that the nature of LAG additive plays an important role³⁹ and can substantially increase reaction rate, a probable result of the favorable interactions of the polar reactants with the mobile surface layers of LAG additive and improved mass transfer.²⁴ The outcome with EtOAc was especially remarkable, providing **25** with the best purity (98% HPLC area, Figure 3D). Since the reaction mixture visibly liquefied as the reaction progressed (due to the generation of tetramethylurea), slurry stirring was also tried instead of ball milling (entry 10) and resulted in a slightly reduced coupling efficiency.

Solution-based amide couplings were performed in DMF (entries 11 and 12) for the comparison with mechano-synthesis. Homogeneous solutions were obtained with an amount of solvent (ca. 0.5 mL) comparable to the weight of solid reactants (ca. 0.24 g), which kept η at around 2 $\mu\text{L}/\text{mg}$. In the DMF solution, HATU was another frequently used and highly reactive uronium-based amide coupling reagent that produced

a rather modest outcome (entry 11). Conversely, the coupling efficiency of the TCFH/NMI combination in DMF solution (entry 12) was virtually the same as that in DMF-free transformation to a solid state (entry 9). Importantly, a bulk amount of harmful solvent was fully avoided in the latter.

Under the optimal reaction conditions (entry 9), desired hexa-amide product **25** was isolated in a nearly quantitative yield and 95% HPLC purity (relative to all other peaks) after a simple water wash and filtration. The purity of product was further increased (99% according to HPLC) by following a simple purification protocol (filtration of chloroform solution via Celite, and then precipitation with hexane from EtOAc solution [see the Supporting Information]). The same amide coupling reaction was also successful at loadings that were 3 times higher (150 mg of **1** per milling jar, 300 mg total), creating **25** in 80% isolated yield and 99% HPLC purity, albeit with a longer milling time (90 min).

CONCLUSIONS

In conclusion, we have developed an efficient mechanochemical protocol for the direct synthesis of amides from carboxylic acids and amines by employing uronium-type amide coupling reagents (COMU and TCFH) and K_2HPO_4 as a base. The reaction protocols demonstrated fast reaction rates (typically within 20 min), generally high yields, an absence of noticeable epimerization for stereogenic centers adjacent to carbonyl group, and a simple isolation procedure for solid amide products. In addition to faster rates of solvent-free amide couplings in contrast to the solution-based protocols, the absence of solvent eliminated reagent compatibility issues, e.g., COMU and DMF, greatly reduced the amount of waste generated and significantly attenuated safety risks. The dual role of K_2HPO_4 as both base and activating reagent for a carboxylic acid substrate was also manifested. The rapid formation (within 60–90 min) of amide products was observed for even challenging coupling partners, such as sterically hindered carboxylic acids and poor nucleophilic amines, within the TCFH/ K_2HPO_4 and TCFH/NMI reagent systems. However, the full amidation of polyfunctionalized substrates, e.g., biotin[6]uril, was found to be especially challenging, even though the single amide bond itself is not difficult to form. Highly reactive coupling conditions (TCFH/NMI), prolonged reaction times (60–90 min), and suitable LAG additives (EtOAc) are essential for producing hexa-amide

25 in high yield and purity. This efficient and environmentally benign synthetic methodology is useful for the preparation of analogues of a new supramolecular host, **25**, as well as for the synthesis of peptides and amides, which could be used in various fields of applied chemistry.

■ ASSOCIATED CONTENT

Supporting Information

The Supporting Information is available free of charge at <https://pubs.acs.org/doi/10.1021/acssuschemeng.0c05558>.

Detailed information about experimental methods, additional data for characterizations of products, kinetics and mechanistic studies, ^1H and ^{13}C NMR spectra, HPLC chromatograms, and green chemistry metrics (PDF)

■ AUTHOR INFORMATION

Corresponding Authors

Dzmitry G. Kananovich – Tallinn University of Technology, School of Science, Department of Chemistry and Biotechnology, 12618 Tallinn, Estonia; Email: dzmitry.kananovich@taltech.ee

Riina Aav – Tallinn University of Technology, School of Science, Department of Chemistry and Biotechnology, 12618 Tallinn, Estonia; orcid.org/0000-0001-6571-7596; Email: riina.aav@taltech.ee

Authors

Tatsiana Dalidovich – Tallinn University of Technology, School of Science, Department of Chemistry and Biotechnology, 12618 Tallinn, Estonia

Kamini A. Mishra – Tallinn University of Technology, School of Science, Department of Chemistry and Biotechnology, 12618 Tallinn, Estonia; orcid.org/0000-0001-5512-2767

Tatsiana Shalima – Tallinn University of Technology, School of Science, Department of Chemistry and Biotechnology, 12618 Tallinn, Estonia

Marina Kudrjašova – Tallinn University of Technology, School of Science, Department of Chemistry and Biotechnology, 12618 Tallinn, Estonia

Complete contact information is available at <https://pubs.acs.org/doi/10.1021/acssuschemeng.0c05558>

Funding

The research was supported by the European Union's H2020-FETOPEN grant 828779 (INITIO). Funding from the Estonian Research Council grant PRG399 and support from COST Action CA18112 "Mechanochemistry for Sustainable Industry" and the ERDF CoE in Molecular Cell Engineering 2014-2020.4.01.15-0013 are gratefully acknowledged.

Notes

The authors declare no competing financial interest.

■ ACKNOWLEDGMENTS

We are grateful to Prof. Nicholas Gathergood for infusing us with his passion for green chemistry and the popularization of green metrics during his work at Tallinn University of Technology (2015–2019). Additionally, we acknowledge Dr. Alexander-Mati Müürisepp (TalTech) for measuring IR spectra.

■ ABBREVIATIONS

AE, atom economy; CDI, *N,N'*-carbonyldiimidazole; COMU, (1-cyano-2-ethoxy-2-oxoethylideneaminoxy)dimethylamino-morpholinocarbenium hexafluorophosphate; DCC, dicyclohexylcarbodiimide; DCM, dichloromethane; DIPEA, *N,N*-diisopropylethylamine; DMAP, 4-dimethylaminopyridine; DMF, *N,N*-dimethylformamide; EDC, 1-ethyl-3-(3-(dimethylamino)propyl) carbodiimide; HATU, hexafluorophosphate azabenzotriazole tetramethyl uronium; HBTU, hexafluorophosphate benzotriazole tetramethyl uronium; HPLC, high-performance liquid chromatography; LAG, liquid-assisted grinding; MSDS, material safety data sheet; NMI, *N*-methylimidazole; Oxyma, ethyl cyanohydroxyiminoacetate; PMI, process mass intensity; RME, reaction mass efficiency; TCFH, *N,N,N',N'*-tetramethylchloroformamidinium hexafluorophosphate; TCT, 2,4,6-trichloro-1,3,5-triazine

■ REFERENCES

- (1) Boström, J.; Brown, D. G.; Young, R. J.; Keserü, G. M. Expanding the Medicinal Chemistry Synthetic Toolbox. *Nat. Rev. Drug Discovery* **2018**, *17*, 709–727.
- (2) Constable, D. J. C.; Dunn, P. J.; Hayler, J. D.; Humphrey, G. R.; Leazer, J. L., Jr.; Linderman, R. J.; Lorenz, K.; Manley, J.; Pearlman, B. A.; Wells, A.; et al. Key Green Chemistry Research Areas – a Perspective from Pharmaceutical Manufacturers. *Green Chem.* **2007**, *9*, 411–420.
- (3) Bryan, M. C.; Dunn, P. J.; Entwistle, D.; Gallou, F.; Koenig, S. G.; Hayler, J. D.; Hickey, M. R.; Hughes, S.; Kopach, M. E.; Moine, G.; Richardson, P.; Roschangar, F.; Steven, A.; Weiberth, F. J. Key Green Chemistry Research Areas from a Pharmaceutical Manufacturers' Perspective Revisited. *Green Chem.* **2018**, *20*, 5082–5103.
- (4) Dalu, F.; Scorciapino, M. A.; Cara, C.; Luridiana, A.; Musinu, A.; Casu, M.; Secci, F.; Cannas, C. A Catalyst-Free, Waste-Less Ethanol-Based Solvothermal Synthesis of Amides. *Green Chem.* **2018**, *20*, 375–381.
- (5) Charville, H.; Jackson, D. A.; Hodges, G.; Whiting, A.; Wilson, M. R. The Uncatalyzed Direct Amide Formation Reaction – Mechanism Studies and the Key Role of Carboxylic Acid H-Bonding. *Eur. J. Org. Chem.* **2011**, *2011*, 5981–5990.
- (6) Gelens, E.; Smeets, L.; Sliedregt, L. A. J. M.; van Steen, B. J.; Kruse, C. G.; Leurs, R.; Orru, R. V. A. An Atom Efficient and Solvent-Free Synthesis of Structurally Diverse Amides Using Microwaves. *Tetrahedron Lett.* **2005**, *46*, 3751–3754.
- (7) Dunetz, J. R.; Magano, J.; Weisenburger, G. A. Large-Scale Applications of Amide Coupling Reagents for the Synthesis of Pharmaceuticals. *Org. Process Res. Dev.* **2016**, *20*, 140–177.
- (8) Valeur, E.; Bradley, M. Amide Bond Formation: Beyond the Myth of Coupling Reagents. *Chem. Soc. Rev.* **2009**, *38*, 606–631.
- (9) Montalbetti, C. A. G. N.; Falque, V. Amide Bond Formation and Peptide Coupling. *Tetrahedron* **2005**, *61*, 10827–10852.
- (10) Trobro, S.; Åqvist, J. Mechanism of Peptide Bond Synthesis on the Ribosome. *Proc. Natl. Acad. Sci. U. S. A.* **2005**, *102*, 12395–12400.
- (11) Goswami, A.; Van Lanen, S. G. Enzymatic Strategies and Biocatalysts for Amide Bond Formation: Tricks of the Trade Outside of the Ribosome. *Mol. Biosyst.* **2015**, *11*, 338–353.
- (12) Philpott, H. K.; Thomas, P. J.; Tew, D.; Fuerst, D. E.; Lovelock, S. L. A Versatile Biosynthetic Approach to Amide Bond Formation. *Green Chem.* **2018**, *20*, 3426–3431.
- (13) Petchey, M. R.; Grogan, G. Enzyme-Catalysed Synthesis of Secondary and Tertiary Amides. *Adv. Synth. Catal.* **2019**, *361*, 3895–3914.
- (14) El-Faham, A.; Albericio, F. Peptide Coupling Reagents, More than a Letter Soup. *Chem. Rev.* **2011**, *111*, 6557–6602.
- (15) Han, S.-Y.; Kim, Y.-A. Recent Development of Peptide Coupling Reagents in Organic Synthesis. *Tetrahedron* **2004**, *60*, 2447–2467.

- (16) de Figueiredo, R. M.; Suppo, J.-S.; Campagne, J.-M. Nonclassical Routes for Amide Bond Formation. *Chem. Rev.* **2016**, *116*, 12029–12122.
- (17) Sabatini, M. T.; Boulton, L. T.; Sneddon, H. F.; Sheppard, T. D. A Green Chemistry Perspective on Catalytic Amide Bond Formation. *Nat. Catal.* **2019**, *2*, 10–17.
- (18) Pattabiraman, V. R.; Bode, J. W. Rethinking Amide Bond Synthesis. *Nature* **2011**, *480*, 471–479.
- (19) Massolo, E.; Pirolo, M.; Benaglia, M. Amide Bond Formation Strategies: Latest Advances on a Dateless Transformation. *Eur. J. Org. Chem.* **2020**, *2020*, 4641.
- (20) Constable, D. J. C.; Jimenez-Gonzalez, C.; Henderson, R. K. Perspective on Solvent Use in the Pharmaceutical Industry. *Org. Process Res. Dev.* **2007**, *11*, 133–137.
- (21) MacMillan, D. S.; Murray, J.; Sneddon, H. F.; Jamieson, C.; Watson, A. J. B. Evaluation of Alternative Solvents in Common Amide Coupling Reactions: Replacement of Dichloromethane and *N,N*-Dimethylformamide. *Green Chem.* **2013**, *15*, 596–600.
- (22) Do, J.-L.; Friščić, T. Chemistry 2.0: Developing a New, Solvent-Free System of Chemical Synthesis Based on Mechanochemistry. *Synlett* **2017**, *28*, 2066–2092.
- (23) James, S. L.; Adams, C. J.; Bolm, C.; Braga, D.; Collier, P.; Friščić, T.; Grepioni, F.; Harris, K. D. M.; Hyett, G.; Jones, W.; Krebs, A.; Mack, J.; Maini, L.; Orpen, A. G.; Parkin, I. P.; Shearouse, W. C.; Steed, J. W.; Waddell, D. C. Mechanochemistry: Opportunities for New and Cleaner Synthesis. *Chem. Soc. Rev.* **2012**, *41*, 413–447.
- (24) Do, J.-L.; Friščić, T. Mechanochemistry: A Force of Synthesis. *ACS Cent. Sci.* **2017**, *3*, 13–19.
- (25) Hernández, J. G.; Bolm, C. Altering Product Selectivity by Mechanochemistry. *J. Org. Chem.* **2017**, *82*, 4007–4019.
- (26) Margetić, D.; Štrukil, V. Carbon–Nitrogen Bond-Formation Reactions. *Mechanochemical Organic Synthesis* **2016**, 141–233.
- (27) Kaupp, G.; Schmeyers, J.; Boy, J. Quantitative Solid-State Reactions of Amines with Carbonyl Compounds and Isothiocyanates. *Tetrahedron* **2000**, *56*, 6899–6911.
- (28) Cao, Q.; Crawford, D. E.; Shi, C.; James, S. L. Greener Dye Synthesis: Continuous, Solvent-Free Synthesis of Commodity Perylene Diimides by Twin-Screw Extrusion. *Angew. Chem., Int. Ed.* **2020**, *59*, 4478–4483.
- (29) Declercq, V.; Nun, P.; Martinez, J.; Lamaty, F. Solvent-Free Synthesis of Peptides. *Angew. Chem., Int. Ed.* **2009**, *48*, 9318–9321.
- (30) Hernández, J. G.; Juaristi, E. Green Synthesis of $\alpha\beta$ - and $\beta\beta$ -Dipeptides under Solvent-Free Conditions. *J. Org. Chem.* **2010**, *75*, 7107–7111.
- (31) Bonnamour, J.; Métro, T.-X.; Martinez, J.; Lamaty, F. Environmentally Benign Peptide Synthesis Using Liquid-Assisted Ball-Milling: Application to the Synthesis of Leu-Enkephalin. *Green Chem.* **2013**, *15*, 1116–1120.
- (32) Gonnet, L.; Tintillier, T.; Venturini, N.; Konnert, L.; Hernandez, J.-F.; Lamaty, F.; Laconde, G.; Martinez, J.; Colacino, E. *N*-Acyl Benzotriazole Derivatives for the Synthesis of Dipeptides and Tripeptides and Peptide Biotinylation by Mechanochemistry. *ACS Sustainable Chem. Eng.* **2017**, *5*, 2936–2941.
- (33) Métro, T.-X.; Bonnamour, J.; Reidon, T.; Sarpoulet, J.; Martinez, J.; Lamaty, F. Mechanochemistry of Amides in the Total Absence of Organic Solvent from Reaction to Product Recovery. *Chem. Commun.* **2012**, *48*, 11781–11783.
- (34) Duangkamol, C.; Jaita, S.; Wangngae, S.; Phakhodee, W.; Pattararapan, M. An Efficient Mechanochemical Synthesis of Amides and Dipeptides Using 2,4,6-Trichloro-1,3,5-Triazine and PPh_3 . *RSC Adv.* **2015**, *5*, 52624–52628.
- (35) Hernández, J. G.; Ardila-Fierro, K. J.; Crawford, D.; James, S. L.; Bolm, C. Mechanoenzymatic Peptide and Amide Bond Formation. *Green Chem.* **2017**, *19*, 2620–2625.
- (36) Ardila-Fierro, K. J.; Crawford, D. E.; Körner, A.; James, S. L.; Bolm, C.; Hernández, J. G. Papain-Catalysed Mechanochemical Synthesis of Oligopeptides by Milling and Twin-Screw Extrusion: Application in the Julia–Colonna Enantioselective Epoxidation. *Green Chem.* **2018**, *20*, 1262–1269.
- (37) Bolm, C.; Hernández, J. G. From Synthesis of Amino Acids and Peptides to Enzymatic Catalysis: A Bottom-Up Approach in Mechanochemistry. *ChemSusChem* **2018**, *11*, 1410–1420.
- (38) Štrukil, V.; Bartolec, B.; Portada, T.; Đilović, I.; Halasz, L.; Margetić, D. One-Pot Mechanochemistry of Aromatic Amides and Dipeptides from Carboxylic Acids and Amines. *Chem. Commun.* **2012**, *48*, 12100–12102.
- (39) Porte, V.; Thioly, M.; Pigoux, T.; Métro, T.-X.; Martinez, J.; Lamaty, F. Peptide Mechanochemistry by Direct Coupling of *N*-Protected α -Amino Acids with Amino Esters. *Eur. J. Org. Chem.* **2016**, *2016*, 3505–3508.
- (40) Kaabel, S.; Aav, R. Templating Effects in the Dynamic Chemistry of Cucurbiturils and Hemicucurbiturils. *Isr. J. Chem.* **2018**, *58*, 296–313.
- (41) Andersen, N. N.; Lisbjerg, M.; Eriksen, K.; Pittelkow, M. Hemicucurbit[n]Urils and Their Derivatives – Synthesis and Applications. *Isr. J. Chem.* **2018**, *58*, 435–448.
- (42) Kaabel, S.; Stein, R. S.; Fomitšenko, M.; Järving, I.; Friščić, T.; Aav, R. Size-Control by Anion Templating in Mechanochemical Synthesis of Hemicucurbiturils in the Solid State. *Angew. Chem., Int. Ed.* **2019**, *58*, 6230–6234.
- (43) Mohite, A. R.; Reany, O. Inherently Chiral Bambus[4]Urils. *J. Org. Chem.* **2020**, *85*, 9190–9200.
- (44) Sokolov, J.; Sindelář, V. Chiral Bambusurils for Enantioselective Recognition of Carboxylate Anion Guests. *Chem. - Eur. J.* **2018**, *24*, 15482–15485.
- (45) Sokolov, J.; Štefek, A.; Sindelář, V. Functionalized Chiral Bambusurils: Synthesis and Host-Guest Interactions with Chiral Carboxylates. *ChemPlusChem* **2020**, *85*, 1307–1314.
- (46) Lisbjerg, M.; Jessen, B. M.; Rasmussen, B.; Nielsen, B. E.; Madsen, A. Ø.; Pittelkow, M. Discovery of a Cyclic 6 + 6 Hexamer of D-Biotin and Formaldehyde. *Chem. Sci.* **2014**, *5*, 2647–2650.
- (47) Lisbjerg, M.; Nielsen, B. E.; Milhøj, B. O.; Sauer, S. P. A.; Pittelkow, M. Anion Binding by Biotin[6]Urils in Water. *Org. Biomol. Chem.* **2015**, *13*, 369–373.
- (48) Lisbjerg, M.; Valkenier, H.; Jessen, B. M.; Al-Kerdi, H.; Davis, A. P.; Pittelkow, M. Biotin[6]Urils: Chloride-Selective Transmembrane Anion Carriers Employing C–H···Anion Interactions. *J. Am. Chem. Soc.* **2015**, *137*, 4948–4951.
- (49) El-Faham, A.; Funosas, R. S.; Prohens, R.; Albericio, F. COMU: A Safer and More Effective Replacement for Benzotriazole-Based Uronium Coupling Reagents. *Chem. - Eur. J.* **2009**, *15*, 9404–9416.
- (50) El-Faham, A.; Subirós-Funosas, R.; Albericio, F. A Novel Family of Onium Salts Based Upon Isonitroso Meldrum's Acid Proves Useful as Peptide Coupling Reagents. *Eur. J. Org. Chem.* **2010**, *2010*, 3641–3649.
- (51) El-Faham, A.; Albericio, F. COMU: A Third Generation of Uronium-Type Coupling Reagents. *J. Pept. Sci.* **2010**, *16*, 6–9.
- (52) Friščić, T.; Childs, S. L.; Rizvi, S. A. A.; Jones, W. The Role of Solvent in Mechanochemical and Sonochemical Cocrysal Formation: A Solubility-Based Approach for Predicting Cocrysalisation Outcome. *CrystEngComm* **2009**, *11*, 418–426.
- (53) Prat, D.; Hayler, J.; Wells, A. A Survey of Solvent Selection Guides. *Green Chem.* **2014**, *16*, 4546–4551.
- (54) Prat, D.; Wells, A.; Hayler, J.; Sneddon, H.; McElroy, C. R.; Abou-Shehadeh, S.; Dunn, P. J. CHEM21 Selection Guide of Classical- and Less Classical-Solvents. *Green Chem.* **2016**, *18*, 288–296.
- (55) Lundblad, R. L.; Macdonald, F., Eds. *Handbook of Biochemistry and Molecular Biology*; CRC Press: Boca Raton, FL, 2010.
- (56) Sperry, J. B.; Minter, C. J.; Tao, J.; Johnson, R.; Duzguner, R.; Hawksworth, M.; Oke, S.; Richardson, P. F.; Barnhart, R.; Bill, D. R.; Giusto, R. A.; Weaver, J. D. Thermal Stability Assessment of Peptide Coupling Reagents Commonly Used in Pharmaceutical Manufacturing. *Org. Process Res. Dev.* **2018**, *22*, 1262–1275.
- (57) McKnelly, K. J.; Sokol, W.; Nowick, J. S. Anaphylaxis Induced by Peptide Coupling Agents: Lessons Learned from Repeated Exposure to HATU, HBTU, and HCTU. *J. Org. Chem.* **2020**, *85*, 1764–1768.

- (58) Isidro-Llobet, A.; Kenworthy, M. N.; Mukherjee, S.; Kopach, M. E.; Wegner, K.; Gallou, F.; Smith, A. G.; Roschangar, F. Sustainability Challenges in Peptide Synthesis and Purification: From R&D to Production. *J. Org. Chem.* **2019**, *84*, 4615–4628.
- (59) Subirós-Funosas, R.; Nieto-Rodríguez, L.; Jensen, K. J.; Albericio, F. COMU: Scope and Limitations of the Latest Innovation in Peptide Acyl Transfer Reagents. *J. Pept. Sci.* **2013**, *19*, 408–414.
- (60) Kumar, A.; Jad, Y. E.; de la Torre, B. G.; El-Faham, A.; Albericio, F. Re-Evaluating the Stability of COMU in Different Solvents. *J. Pept. Sci.* **2017**, *23*, 763–768.
- (61) McElroy, C. R.; Constantinou, A.; Jones, L. C.; Summerton, L.; Clark, J. H. Towards a Holistic Approach to Metrics for the 21st Century Pharmaceutical Industry. *Green Chem.* **2015**, *17*, 3111–3121.
- (62) SDS Search and Product Safety Center. <https://www.sigmaldrich.com/safety-center.html> (accessed on 15 July 2020).
- (63) Cindro, N.; Tireli, M.; Karadeniz, B.; Mrla, T.; Užarevič, K. Investigations of Thermally Controlled Mechanochemical Milling Reactions. *ACS Sustainable Chem. Eng.* **2019**, *7*, 16301–16309.
- (64) Schmidt, R.; Martin Scholze, H.; Stolle, A. Temperature Progression in a Mixer Ball Mill. *Int. J. Ind. Chem.* **2016**, *7*, 181–186.
- (65) Beutner, G. L.; Young, I. S.; Davies, M. L.; Hickey, M. R.; Park, H.; Stevens, J. M.; Ye, Q. TCFH–NMI: Direct Access to *N*-Acyl Imidazoliums for Challenging Amide Bond Formations. *Org. Lett.* **2018**, *20*, 4218–4222.
- (66) Lopez, F. J.; Ferriño, S. A.; Reyes, M. S.; Román, R. Asymmetric Transformation of the Second Kind of Racemic Naproxen. *Tetrahedron: Asymmetry* **1997**, *8*, 2497–2500.
- (67) Blasco, M. A.; Gröger, H. Organocatalytic Racemization of α -Aryl Propionates in the Presence of Water. *Synth. Commun.* **2013**, *43*, 9–15.
- (68) Chen, C.-S.; Chen, T.; Shieh, W.-R. Metabolic Stereoisomeric Inversion of 2-Arylpropionic Acids. On the Mechanism of Ibuprofen Epimerization in Rats. *Biochim. Biophys. Acta, Gen. Subj.* **1990**, *1033*, 1–6.
- (69) Gao, X.; Deng, H.; Tang, G.; Liu, Y.; Xu, P.; Zhao, Y. Intermolecular Phosphoryl Transfer of *N*-Phosphoryl Amino Acids. *Eur. J. Org. Chem.* **2011**, *2011*, 3220–3228.
- (70) Di Sabato, G.; Jencks, W. P. Mechanism and Catalysis of Reactions of Acyl Phosphates. I. Nucleophilic Reactions. *J. Am. Chem. Soc.* **1961**, *83*, 4393–4400.
- (71) Kluger, R.; Huang, Z. Acyl Pyrophosphates: Activated Analogs of Pyrophosphate Monoesters Permitting New Designs for Inactivation of Targeted Enzymes. *J. Am. Chem. Soc.* **1991**, *113*, 5124–5125.
- (72) Biron, J.-P.; Pascal, R. Amino Acid *N*-Carboxyanhydrides: Activated Peptide Monomers Behaving as Phosphate-Activating Agents in Aqueous Solution. *J. Am. Chem. Soc.* **2004**, *126*, 9198–9199.
- (73) Leman, L. J.; Orgel, L. E.; Ghadiri, M. R. Amino Acid Dependent Formation of Phosphate Anhydrides in Water Mediated by Carbonyl Sulfide. *J. Am. Chem. Soc.* **2006**, *128*, 20–21.
- (74) Twibanire, J. K.; Grindley, T. B. Efficient and Controllably Selective Preparation of Esters Using Uronium-Based Coupling Agents. *Org. Lett.* **2011**, *13*, 2988–2991.
- (75) Xiong, B.; Hu, C.; Gu, J.; Yang, C.; Zhang, P.; Liu, Y.; Tang, K. Efficient and Controllable Esterification of P(O)-OH Compounds Using Uronium-Based Salts. *ChemistrySelect* **2017**, *2*, 3376–3380.
- (76) Larrivéé-Aboussafy, C.; Jones, B. P.; Price, K. E.; Hardink, M. A.; McLaughlin, R. W.; Lillie, B. M.; Hawkins, J. M.; Vaidyanathan, R. DBU Catalysis of *N,N'*-Carbonyldiimidazole-Mediated Amidations. *Org. Lett.* **2010**, *12*, 324–327.
- (77) Aav, R.; Shmatova, E.; Reile, I.; Borissova, M.; Topić, F.; Rissanen, K. New Chiral Cyclohexylhemicucurbit[6]Urils. *Org. Lett.* **2013**, *15*, 3786–3789.
- (78) Prigorchenko, E.; Öeren, M.; Kaabel, S.; Fomitšenko, M.; Reile, I.; Järving, I.; Tamm, T.; Topić, F.; Rissanen, K.; Aav, R. Template-Controlled Synthesis of Chiral Cyclohexylhemicucurbit[8]Urils. *Chem. Commun.* **2015**, *51*, 10921–10924.
- (79) Kaabel, S.; Adamson, J.; Topić, F.; Kiesilä, A.; Kalenius, E.; Öeren, M.; Reimund, M.; Prigorchenko, E.; Löökene, A.; Reich, H. J.; Rissanen, K.; Aav, R. Chiral Hemicucurbit[8]Urils as an Anion Receptor: Selectivity to Size, Shape and Charge Distribution. *Chem. Sci.* **2017**, *8*, 2184–2190.
- (80) Prigorchenko, E.; Kaabel, S.; Narva, T.; Baškiri, A.; Fomitšenko, M.; Adamson, J.; Järving, I.; Rissanen, K.; Tamm, T.; Aav, R. Formation and Trapping of the Thermodynamically Unfavoured Inverted-Hemicucurbit[6]Urils. *Chem. Commun.* **2019**, *55*, 9307–9310.
- (81) Ustrnul, L.; Kaabel, S.; Burankova, T.; Martõnova, J.; Adamson, J.; Konrad, N.; Burk, P.; Borovkov, V.; Aav, R. Supramolecular Chirogenesis in Zinc Porphyrins by Enantiopure Hemicucurbit[n]-Urils ($n = 6, 8$). *Chem. Commun.* **2019**, *55*, 14434–14437.
- (82) Yawer, M. A.; Havel, V.; Sindelar, V. A Bambusuril Macrocycle That Binds Anions in Water with High Affinity and Selectivity. *Angew. Chem., Int. Ed.* **2015**, *54*, 276–279.
- (83) Lizal, T.; Sindelar, V. Bambusuril Anion Receptors. *Isr. J. Chem.* **2018**, *58*, 326–333.
- (84) Masson, E.; Ling, X.; Joseph, R.; Kyeremeh-Mensah, L.; Lu, X. Cucurbituril Chemistry: A Tale of Supramolecular Success. *RSC Adv.* **2012**, *2*, 1213–1247.
- (85) Aav, R.; Kaabel, S.; Fomitšenko, M. Cucurbiturils: Synthesis, Structures, Formation Mechanisms, and Nomenclature; In *Comprehensive Supramolecular Chemistry II*; Atwood, J. L., Ed.; Elsevier: Oxford, 2017; pp 203–220. DOI: 10.1016/B978-0-12-409547-2.12514-4.
- (86) Hachmann, J.; Lebl, M. Search for Optimal Coupling Reagent in Multiple Peptide Synthesizer. *Biopolymers* **2006**, *84*, 340–347.

Curriculum vitae

Personal data

Name: Kamini Atindrakumar Mishra
Date of birth: 02.05.1992
Place of birth: Maharashtra, India
Citizenship: Indian

Contact data

E-mail: kamini_mishra@outlook.com

Education and degree awarded

2016-2022 Tallinn University of Technology, Ph.D
2014-2016 Department of Chemistry, University of Mumbai, India, M.Sc.
2011-2014 Birla College of Science, Commerce, and Arts, Mumbai, India, B.Sc.
2009-2011 K M. Agrawal College, Mumbai, India, High School

Language competence

English Fluent
German Beginner

Professional employment

2016-2021 Tallinn University of Technology, Department of Chemistry and Biotechnology, PhD Student and Early-Stage Researcher

Honors and awards

2020 Research paper of the year in the field of Natural and Exact and Health Sciences in Tallinn University of Technology-Dalidovich *et al.*, *ACS Sustainable Chemistry & Engineering*, 2020, 8, 15703–15715.

2011-2016 Inspire (SHE) Scholarship, Ministry of Science and Technology, Government of India

Elulookirjeldus

Isikuandmed

Nimi: Kamini Atindrakumar Mishra
Sünniaeg: 02.05.1992
Sünnikoht: Maharashtra, India
Kodakondsus: Indian

Kontaktandmed

E-post: kamini_mishra@outlook.com

Hariduskäik

2016-2022 Tallinna Tehnikaülikool, Ph.D.
2014-2016 Department of Chemistry, University of
Mumbai, India, M.Sc.
2011-2014 Birla College of Science, Commerce, and Arts,
Mumbai, India, B.Sc.
2009-2011 K M. Agrawal College, Mumbai, India, High
School

Keelteoskus

Inglise keel kõrgtase
Saksa keel algtase

Teenistuskäik

2016-2021 Tallinna Tehnikaülikool, Keemia ja
Biotehnoloogia instituut, doktorant-
nooremteadur

Teaduspreemiad ja tunnustused

2020 Tallinna Tehnikaülikooli Loodus-, täppis- ja
terviseteaduste valdkonna parim
teadusartikkel- Dalidovich *et al.*, *ACS
Sustainable Chemistry & Engineering*, 2020, 8,
15703–15715.

2011-2016 Inspire (SHE) Scholarship, Ministry of Science
and Technology, Government of India

ISSN 2585-6901 (PDF)
ISBN 978-9949-83-832-5 (PDF)